Dispersing Carbon Nanotubes: Towards Molecular Understanding

Ricardo M. Ferreira Fernandes

This Ph.D. thesis was completed under the Thesis Co-supervision Agreement between KTH Royal Institute of Technology and the University of Porto.

KTH Royal Institute of Technology
School of Chemical Science and Engineering
Department of Chemistry
Applied Physical Chemistry
SE-100 44 Stockholm, Sweden

University of Porto
Faculty of Sciences
Department of Chemistry and Biochemistry
Rua do Campo Alegre
4169-007 Porto, Portugal

TRITA CHE Report 2015:60

ISSN 1654-1081

ISNB 978-91-7595-713-5

Akademisk avhandling som med tillstånd av KTH i Stockholm framlägges till offentlig granskning för avläggande av teknisk doktorsexamen torsdag den 26 November kl 10:00 i sal F3, KTH, Lindstedtsvägen 26, Stockholm. Avhandlingen försvaras på engelska.

Fakultetsopponent: Prof. Philippe Poulin, Centre de Recherche Paul Pascal – CNRS, Bordeaux, France.

To my family

nanos gigantum humeris insidentes

Bernard of Chartres

Abstract

Carbon nanotubes (CNTs) exhibit unique and fascinating intrinsic electrical, optical, thermal or mechanical properties, that lead to a plethora of potential applications in composite materials, electronics, energy storage, medicine, among others. However, the manipulation of nanotubes is not trivial and there are significant difficulties to overcome before achieving their full potential in applications. Because of their high aspect ratio and strong tube-to-tube van der Waals interactions, nanotubes form bundles and ropes that are difficult to disperse in liquids. In this thesis, the topic of dispersing carbon nanotubes in water was addressed by several experimental methods such as nuclear magnetic resonance (NMR) diffusometry and light/electron microcopy. The main goal was to obtain molecular information on how the dispersants interact with carbon nanotubes.

In dispersions of single-walled carbon nanotubes (SWNTs) in water, only a small fraction of the polymeric dispersant (Pluronic F127) was shown to be adsorbed at the NT surface. Regarding dynamic features, the residence time of F127 on the SWNT surface was measured to be in the order of hundred milliseconds, and the lateral diffusion coefficient of the polymer along the nanotube surface proved to be an order of magnitude slower than that in the solution. The surface coverage of SWNTs by F127 was also investigated and the competitive adsorption of F127 and the protein bovine serum albumin, BSA, was assessed. F127 was found to bind stronger to the CNT surface than BSA does.

Low molecular weight dispersants, viz. surfactants, were also investigated. Using carefully controlled conditions for the sonication and centrifugation steps, reproducible sigmoidal dispersibility curves were obtained, that exhibited an interesting variation with molecular properties of the surfactants. Various metrics that quantify the ability of different surfactants to disperse CNTs were obtained. In particular, the concentration of surfactant required to attain maximal dispersibility depends linearly on alkyl chain length, which indicates that the CNT-surfactant association, although hydrophobic in nature, is different from a micellization process. No correlation between dispersibility and the critical micellization concentration, *cmc,* of the surfactants was found. For gemini surfactants of the *n*-s-*n* type with spacer length s and hydrophobic tail length *n*, the dispersibility of multiwalled carbon nanotubes (MWNTs) also followed sigmoidal curves that were compared to those obtained with single-tailed homologues. The increase in spacer length caused an increase in the dispersion efficiency. The observations indicate a loose type of monolayer adsorption rather than the formation of micelle-like aggregates on the nanotube surface. With the future goal of embedding nanotubes in liquid crystal (LC) phases and thereby creating nanocomposites, the effect of the spacer length on the thermotropic behavior of the gemini 12-s-12 surfactant was investigated. Different mesophases were observed and a non-monotonic effect of the

spacer length was found and rationalized within a model of the surfactant packing in the solid state.

The relative binding strength of simple surfactants to CNTs was assessed by the amount of F127 they displace from the CNT surface upon addition. Anionic surfactants were found to replace more F127, which was interpreted as a sign of stronger binding to CNT. The data collected for all surfactants showed a good correlation with their *critical dispersibility concentration* that suggests the existence of a surface coverage threshold for dispersing nanotubes.

On the macroscopic scale, the formation of weakly bound CNT aggregates in homogeneous dispersions was found to be induced by vortex-shaking. These aggregates could quickly and easily be re-dispersed by mild sonication. This counterintuitive behavior was related to the type of dispersant used and of the duration of mechanical agitation and was explained as a result of loose coverage by the dispersant.

Keywords: carbon nanotubes, dispersion, surfactants, polymers, adsorption, liquid crystals, nuclear magnetic resonance, self-diffusion.

Sammanfattning

Kolnanorör (CNTs) uppvisar unika och fascinerande elektriska, optiska, termiska samt mekaniska egenskaper som kan leda till en uppsjö av potentiella tillämpningar inom kompositmaterial, elektronik, energilagring, medicin, etc. Det är emellertid inte trivialt hur dessa kolnanorör bör behandlas, det finns betydande hinder att övervinna innan man kan uppnå dess fulla potential inom de olika tillämpningsområdena. På grund av deras starka van der Waals-interaktioner bildar nanorör hårt bundna aggregat som är svåra att dispergera i vätskor. I denna avhandling berörs detta område, dispergering av kolnanorör i vatten, med flera experimentella metoder, bl.a. kärnmagnetisk resonans (NMR) diffusometri och ljus- och elektronmikroskopi. Huvudsyftet har varit att få molekylär information rörande hur olika dispergeringsmedel interagerar med kolnanorör.

I dispersioner av enkel-väggs kolnanorör (SWNT) i vatten, kunde det påvisas att endast en liten del av det polymera dispergeringsmedlet (Pluronic F127) adsorberar på kolnanorörens yta. Beträffande dynamiska egenskaper så uppmättes uppehållstiden för F127 på SWNT till att vara i storleksordningen hundra millisekunder samt den laterala diffusionskoefficienten av F127 längs ytan en storleksordning långsammare än den i vattenlösning. Hur stor del av SWNTs yta som var täckt av F127 undersöktes också. Genom att studera den konkurrerande adsorptionen mellan F127 och proteinet bovint serumalbumin (BSA), bedömdes det att F127 binder starkare än BSA till ytan.

Lågmolekylära dispergeringsmedel, s.k. surfaktanter, undersöktes med noga kontrollerade ultraljuds- och centrifugeringssteg. Utifrån dessa kunde reproducerbara sigmoidala dispergeringsskurvor erhållas, vilka uppvisade ett intressant beroende av tensidernas molekylära egenskaper. Olika mått på de olika ytaktiva ämnenas förmågan att dispergera CNT kunde därmed erhållas. I synnerhet visade det sig att koncentrationen som krävs för att uppnå maximal mängd dispergerade nanorör berodde linjärt på alkylkedjelängd hos surfaktanterna. Detta tyder på att interaktionen mellan CNT och surfaktanten, även om den är av hydrofob karaktär, är annorlunda än den som återfinns vid en micellisering. Inget samband mellan mängden dispergerade nanorör och den kritiska micelliseringskoncentrationen (*cmc*) av de surfaktanterna kunde påträffas. För tvillingsurfaktanter av *n-s-n* typ, där *s* är längden mellan svansarna och *n* är längden på de hydrofoba svansarna, var dispergeringsskurvorna för flerväggiga kolnanorör (MWNTs) också sigmoidala och kunde därmed jämföras med de som erhölls med enkelsvansade homologer. Det kunde observeras att en ökande *s* orsakade en ökning av dispergeringsmedlets effektivitet, vilket indikerar en svag monoskiktsadsorption snarare än micelliknande aggregering på kolnanorörsytan. Med det framtida målet att dispergera nanorör i flytande kristaller (LC), undersöktes effekten av längden *s* på det termotropa beteendet hos tvillingsurfaktanter av typen 12-s-12. Det kunde

iaktas olika mesofaser och en icke-monoton effekt av *s* hittades, vilket förklarades av en modell som beskriver den fasta fasens ytaktiva packning.

Den relativa bindningsstyrkan mellan de enkla surfaktanter och CNTs uppskattades genom den mängd av F127 som de avlägsnar från CNTs yta när de tillsätts dispersionen. Anjontensider visade sig avlägsna störst mängd F127, vilket tolkades som ett tecken på dess starkare bindning till CNT. Sammanfattningsvis kunde ses en god korrelation mellan den relativa bindningsstyrkan och tensidernas s. k. kritiska dispergeringskoncentration, vilket tyder på förekomsten av en sorts täckningströskel för surfaktanters förmåga att dispergera kolnanorören.

På makroskopisk skala, kunde bildandet av svaga kolnanorörsaggregat i homogena dispersioner visa sig induceras av virvelsblandning. Dessa aggregat kunde dock snabbt och enkelt återdispergeras genom en mild ultraljudsbehandling. Detta omvända beteende kunde relateras till den typ av dispergeringsmedel som användes samt till hur länge den mekaniska omrörningen pågick och förklarades som ett resultat av en relativt svag interaktion mellan dispergeringsmedlet och kolnanorören.

Nyckelord: kolnanorör, dispersion, ytaktiva ämnen, polymerer, adsorption, vätskekristaller, kärnmagnetisk resonans, självdiffusion.

Resumo

Os nanotubos de carbono (CNTs) combinam num só material propriedades elétricas, óticas, térmicas e mecânicas únicas, que potenciam uma enorme diversidade de aplicações, desde materiais compósitos, à eletrónica molecular, ao armazenamento de energia até à nanomedicina. No entanto, devido às fortes interações de van der Waals que estabelecem entre si, os CNTs agregam-se em pequenos aglomerados, o que dificulta a sua dispersão em líquidos e posterior manipulação. Neste trabalho, com o objetivo principal de compreender a nível molecular as interações não-covalentes estabelecidas entre os CNTs e os respetivos dispersantes, estudou-se a dispersão de CNTs em água utilizando diferentes dispersantes (baixa e alta massa molecular) através de várias técnicas experimentais, tais como a ressonância magnética nuclear (RMN) de auto-difusão e microscopia de luz/eletrónica.

Para dispersões aquosas de nanotubos de carbono de parede única (SWNT), foi demonstrado que apenas uma pequena fração do dispersante polimérico (Pluronic F127) está adsorvido à superfície do CNT. Relativamente à dinâmica do polímero adsorvido no nanotubo, verificou-se que o tempo de residência do F127 na superfície do SWNT é da ordem de centenas de milissegundos, e o coeficiente de difusão lateral do polímero ao longo da superfície do nanotubo é uma ordem de grandeza mais lenta do que em solução. A cobertura da superfície de CNTs pelo F127 foi investigada e a adsorção competitiva entre o F127 e a proteína de albumina de soro bovino (BSA) foi também avaliada. Verificou-se que o polímero F127 se liga mais fortemente à superfície do SWNT do que a BSA.

A capacidade de dispersantes de baixa massa molar, i.e. tensioativos, para dispersar CNTs em água foi também estudada. Utilizando condições rigorosamente controladas nos passos de ultrasonicação e centrifugação, obtiveram-se curvas de dispersibilidade de CNTs em função da concentração de dispersante que apresentam um perfil sigmoidal, o que permitiu extrair novos parâmetros que caracterizam a capacidade de dispersão dos diferentes tensioativos. Determinou-se assim a concentração mínima de tensioativo necessária para que ocorra dispersão de CNTs, designada *concentração de dispersibilidade crítica* (*cdc*). Adicionalmente, verificou-se que a dispersibilidade máxima de CNT varia linearmente com o comprimento da cadeia alquílica do tensioactivo, o que indica que a associação CNT-tensioativo, embora de natureza hidrofóbica, é diferente do processo de micelização. Não se observou correlação entre a dispersibilidade e a concentração micelar crítica (*cmc*) dos tensioativos.

Para tensioativos gemini do tipo *n*-s-*n*, com espaçador s e comprimento da cadeia alquílica *n*, a dispersibilidade de nanotubos de carbono de parede múltipla (MWNT) em água, segue também uma curva sigmoidal; os resultados foram criticamente comparados com a dispersibilidade de MWNTs promovida pelos respetivos tensioativos homólogos de cadeia simples. Verifica-se que o aumento do

comprimento do espaçador s conduz a um aumento na eficiência de dispersão, o que indica que a adsorção do tensioativo ocorre na forma de uma monocamada desorganizada não-compacta, em vez da formação de agregados micelares na superfície do nanotubo. Adicionalmente, com o objetivo futuro da incorporação de CNTs em cristais líquidos, criando-se assim um nanocompósito, o efeito do comprimento do espaçador s no comportamento termotrópico da família de tensioativos gemini 12-s-12 foi investigado. Diferentes mesofases foram observadas e verificou-se um efeito não monótono do comprimento do espaçador, que foi interpretado de acordo com um modelo de empacotamento do tensioactivo no estado sólido.

A afinidade de diferentes tensioativos para a superfície dos nanotubos de carbono foi avaliada através da monitorização da fração de F127 deslocada da superfície do CNT após adição do respetivo tensioativo. Verifica-se que os tensioativos aniónicos substituem mais F127, o que foi interpretado como evidência de uma maior afinidade para com a superfície do CNT. Os dados recolhidos de todos os tensoativos mostraram uma boa correlação com a sua concentração de dispersibilidade crítica (*cdc*), o que sugere a existência de um limiar de cobertura da superfície para que ocorra dispersão de nanotubos.

À escala macroscópica, verifica-se que a agregação de CNTs dispersos em água é induzida pela aplicação de agitação do tipo vórtex. Estes agregados são rapidamente re-dispersos pela aplicação de ultrasonicação suave. Diferentes dispersantes foram avaliados e os resultados foram interpretados como consequência de uma menor ou maior extensão da cobertura da superfície do CNT.

Palavras-chave: nanotubos de carbono, dispersão, tensioativos, polímeros, adsorção, cristais líquidos, ressonância magnética nuclear, auto-difusão.

List of papers

I. **Lateral diffusion of dispersing molecules on nanotubes as probed by NMR**

Ricardo M.F. Fernandes, Matat Buzaglo, Michael Shtein, Ilan Pri Bar, Oren Regev, Eduardo F. Marques and István Furó

J Phys Chem C, **2014**, 118, 582–589

II. **Surface coverage and competitive adsorption on carbon nanotubes**

Ricardo M.F. Fernandes, Matat Buzaglo, Oren Regev, Eduardo F. Marques and István Furó

J Phys Chem C, **2015**, 119, 22190–22197

III. **Dispersing carbon nanotubes with ionic surfactants under controlled conditions: comparisons and insight**

Ricardo M.F. Fernandes, Bárbara Abreu, Bárbara Claro, Matat Buzaglo, Oren Regev, István Furó and Eduardo F. Marques

Langmuir, **2015**, 31, 10955-10965

IV. **Assessing surfactant binding to carbon nanotubes via competitive adsorption: binding strength and critical coverage**

Ricardo M.F. Fernandes, Jing Dai, Oren Regev, Eduardo F. Marques and István Furó

Manuscript

V. **Mechanical agitation induces aggregation of pre-dispersed carbon nanotubes**

Ricardo M.F. Fernandes, Matat Buzaglo, Oren Regev, István Furó and Eduardo F. Marques

Manuscript

VI. **Gemini surfactants as dispersants of multiwalled carbon nanotubes: a systematic study on the role of molecular structure**

Jessica Rocha, Ricardo M.F. Fernandes, Oren Regev, István Furó and Eduardo F. Marques

Submitted for publication

VII. **Strong spacer length effects on the thermal behavior and mesophase formation by gemini surfactants**

Ricardo M.F. Fernandes, Yujie Wang, Pedro B. Tavares, Sandra C.C. Nunes, Alberto A.C.C. Pais and Eduardo F. Marques

Manuscript

The author contribution to the appended papers

I. Prepared all the samples, performed all the NMR experiments and data analysis. Participated in the writing of the manuscript.

II. Participated in the planning, performed all the experimental work, data analysis and participated in the writing of the manuscript.

III. Participated in the planning, instructing and performed part of the experimental work. Contributed in the data analysis and writing of the manuscript.

IV. Planning, performed the majority of the experimental work and data analysis. Participated in the writing of the manuscript.

V. Planning, performed the majority of the experimental work and participated in the writing of the manuscript.

VI. Planning and part of the experimental work; contributed to the writing of the manuscript.

VII. Performed part of the experimental work and contributed to the writing of the manuscript.

Other papers of the author not included in this thesis:

Enhanced interfacial properties of novel amino acid-derived surfactants: Effects of headgroup chemistry and of alkyl chain length and unsaturation

Rodrigo O. Brito, Sandra G. Silva, Ricardo M.F. Fernandes, Eduardo F. Marques, José Enrique-Borges and M. Luísa C. do Vale

Colloids Surf B **2011**, 86, 65-70.

Serine-Based Bis-quat Gemini Surfactants: Synthesis and Micellization Properties

Sandra G. Silva, Ricardo M.F. Fernandes, Eduardo F. Marques and M. Luísa C. do Vale

Eur J Org Chem **2012**, 2, 345-352.

Table of contents

1. Introduction

1.1. Carbon nanotubes

The discovery of carbon nanostructures such as the fullerenes (in comparison, point-like and thereby zero dimensional 0D), carbon nanotubes (1D) and graphene (2D), strongly contributed to the development of nanoscience and nanotechnology.[1] Within these nanostructures, carbon nanotubes appeared as candidates for a plethora of applications. In the next subsections the structure and properties of carbon nanotubes will be described, followed by a brief overview of the nanotubes synthesis. In the last part of this section the different approaches to disperse nanotubes will be discussed with particular emphasis on the dispersion in water using surfactants and polymers.

1.1.1. Structure and properties

Structure

Carbon nanotubes (CNTs) constitute a rather new allotrope of carbon, having been given renewed attention in 1991 by Iijima.[2] In the nanotube lattice, each carbon atom is bound to three other atoms, forming a sp^2 hybridized hexagon network.[3] The carbon atoms are connected by three σ bonds. In addition, a π system is formed by electrons accommodated in the non-hybridized p orbitals of adjacent carbon atoms in the lattice.[3-5] Moreover, the electrons that are participating in the aromatic π system can act as charge carriers, and hence make nanotubes electrically conductive.[6]

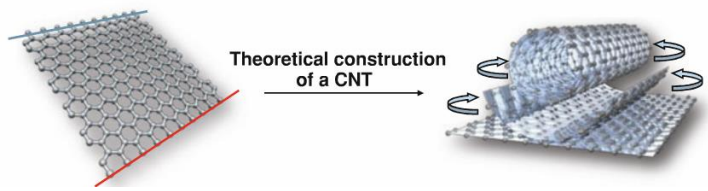

Figure 1. Theoretical roll-up of a carbon nanotube from a graphene sheet. Reprinted with permission from Springer-Verlag.[7]

CNTs can be easily visualized by the roll up of a graphene sheet (the single atomic layer that constitutes graphite) into a hollow cylinder with the hexagonal rings seamlessly fused (Figure 1). The number of graphene sheets that compose the nanotube wall is used to classify the type of CNTs. Therefore, CNTs fall in two major categories, designated as 1) single-walled carbon nanotubes (SWNTs)—formed by one rolled-up layer of graphene; and 2) multiwalled carbon nanotubes (MWNTs)—composed by several (two or more) layers.

The dimensions of SWNTs and MWNTs are similar in terms of length, L (in favorable cases, up to hundreds of μm). However, as expected, the two types differ

considerably in their diameter, *d*. Typically, for SWNTs *d* is in the range of 0.7−2 nm. MWNTs present higher *d* values, which is dependent on the number of graphene layers that comprises the nanotube. The separation between the layers in the MWNT is typically 0.34 nm (same range as that for graphite). Thus, considering a MWNT with an inner diameter *d*≈2 nm and outer diameter *d*=20 nm, it will be formed by 53 coaxial tubes. Moreover, MWNT samples are typically composed by nanotubes with different number of concentric layers; thereby *d* is rather polydisperse.[6, 8]

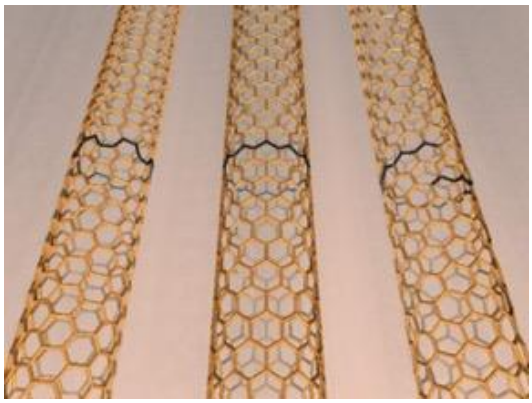

Figure 2. Three SWNT with different structures. Armchair (left), zigzag (center) and chiral (right). Reprinted with permission from the authors.[9]

Considering a SWNT, rolling up of the graphene sheet into a cylinder may produce nanotube structures with different diameters and topologies. Figure 2 summarizes the three general structures formed: armchair, zigzag and chiral. These structures differ from each other as concerning the direction (with respect to the bond angles within the sheet) of the axis of the hypothetical cylinder around which the sheet is rolled up.

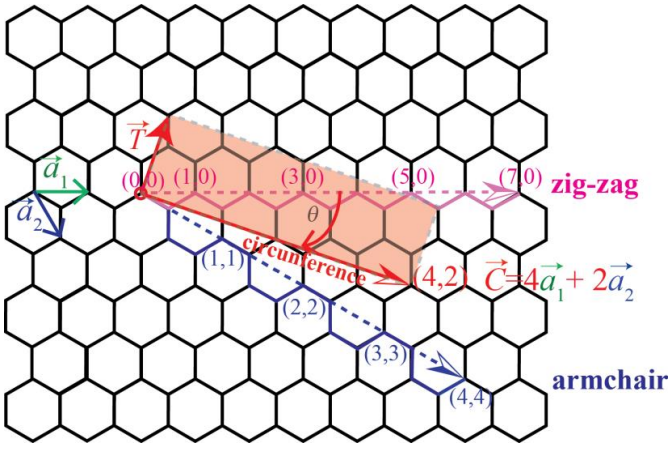

Figure 3. Graphene honeycomb lattice with the lattice real space unit vectors vector ($\vec{a_1}$, $\vec{a_2}$) which defines the chiral vector $\vec{C}=4\vec{a_1}+\vec{a_2}$ of the (4,2) tube, and characterizes the circumference *C* of the tube. The red rectangle represents the unit cell of the (4,2) SWNT, defined by the translational vector T. The chiral angle θ is defined between a1 and *C*. The zigzag and the armchair patterns are highlighted.

The simplest way to quantify the structure of an individual SWNT is using a vector model (Hamada indices).[6-8] As shown in Figure 3, using the graphene lattice real space unit vectors ($\vec{a_1}$, $\vec{a_2}$) and a pair (n, m) of integers one can characterize the nanotube structure by the chiral vector $\vec{C}$:

$$\vec{C} = n\vec{a}_1 + m\vec{a}_2 \tag{1.1}$$

In the carbon nanotubes, the graphene sheet is rolled-up in such a way that the $\vec{C}$ chiral vector becomes the circumference $|\vec{C}|$ of the nanotube. Therefore, the diameter of the nanotube can be easily calculated by:

$$d = \frac{|\vec{C}|}{\pi} = \frac{a\sqrt{n^2 + nm + m^2}}{\pi} \tag{1.2}$$

where $a = |\vec{a}_1| = |\vec{a}_2| \approx$ 0.249 nm. The orientation of the hexagonal rings in the honeycomb lattice relative to the nanotube axis is defined by the chiral angle θ, which is defined as the angle between $\vec{a}_1$ and $\vec{C}$, calculated according to:[10]

$$\theta = \arctan(\sqrt{3}m/(2n+m)) \tag{1.3}$$

Due to hexagonal symmetry of the graphene sheet, the chiral angle varies between 0º to 30º. Figure 3 shows that the chiral angle is 0º to zigzag nanotubes and 30º to armchair nanotubes. Armchair and zigzag nanotubes are characterized by a high symmetry and they do not have any enantiomeric pair, i.e. the mirror image is superimposable with the original structure. For chiral nanotubes, a specific (n,m) SWNT has two enantiomers.[6, 7]

In summary, nanotubes are described by the pair of indices (n,m). These two numbers allow the calculation of the nanotube diameter and the chiral angle θ. It is expected that nanotubes with different chirality (n,m) display different properties as is described in the next section.

Properties

Nanotubes are characterized by the high L/d aspect ratio, achieving in most cases lengths 10^3 times (or more) larger than the diameter.[11] Because of the high aspect ratio L/d, CNTs are commonly designated as quasi-one-dimensional materials. Therefore, it is not surprising that their properties are strongly direction-dependent, i.e. anisotropic. The σ and π bonds established between the carbon atoms in the hexagonal lattice, combined with the high aspect ratio and the nanometer-size of the nanotubes confers to this carbon allotrope unique electric, optical, mechanical and thermal properties.

The electronic properties of CNTs arise due to the confinement of electrons in the nanotube.[6] Moreover, depending on the structure, CNTs can be metallic, like copper, or semiconducting, like silicon.[12] Band gap calculations predict that metallic nanotubes fulfil the condition:

$$(n - m) = 3q \tag{1.4}$$

where q is an integer. Therefore, all armchair nanotubes are metallic (e.g. 4-4=3q, q=0). Moreover, this equation implies that for each of the two other general nanotube classes (zig-zag and chiral), 1/3 are metallic and 2/3 are semiconducting. Additionally, the curvature of the graphene sheet into nanotube introduces some strain in the bond angles (i.e. carbon atoms are pyramidalized in the nanotube structure) and the π orbitals are slightly misaligned.[3] Consequently, the curvature effect shifts metallic non-armchair tubes towards semiconducting, but since the size of the gap is rather small at room temperature, these tubes in practice display metallic behavior.[6, 7]

Carbon nanotubes absorb light in a broad wavelength range, from UV to near-infrared, with absorbance strongly dependent on wavelength. Absorption by individual SWNT at discrete wavelengths is determined by the van Hove singularities, corresponding to electronic transitions between different states. Because of the 1D geometry of CNTs, electrons are located in discrete energy bands, and only certain transitions are permitted leading to discrete peaks in the spectra.[6]

The band gap energies in the nanotubes are related to the peaks in the optical absorption spectra, because both are connected to the density of the electronic states. Since the structure of the nanotube dictates the density of electronic states, the absorption peaks (van Hove singularities) can be used to determine the nanotube structure. Transitions indexed as by E_{11}^{S}, E_{22}^{S}, E_{11}^{M}, etc where the subscripts refer to the electronic energy bands and superscripts represent metallic (*M*) or semiconducting (*S*) tubes. The metallic E_{11}^{M}, transitions arise in the UV-vis region from 350-620 nm, overlapping at some extent with the E_{11}^{S}. Despite the theoretical possibility to determine the different types of nanotubes in a sample by optical absorption, in practice the overlap between the absorption bands frequently hampers this. Moreover, the bundling of nanotubes, generally, broadens and slightly red-shifts the peaks, making identification even more difficult.[6, 7]

It is well established that CNTs are the stiffest and strongest material produced so far.[12] The strong sp^2 C=C bonds in the CNT lattice confer to it high mechanical resistance. Axial tensile tests reported values around 1000 GPa for the tensile modulus[13, 14], roughly 5 times higher than that for steel. In terms of tensile strength, nanotubes can achieve 63 GPa, a value approximately 50 times higher than that for steel. However, under compression nanotubes can buckle relatively easily.[6, 12] Measurements of the radial elasticity suggest that van der Waals forces can deform

two adjacent nanotubes and that the radial tensile modulus is in the order of 30 GPa.[15-17]

Crystalline carbon presents the highest thermal conductivities, *k*, of all known materials.[12] Calculations of an isolated (10,10) nanotube predicted a value of *k*=6600 $W \cdot m^{-1} \cdot K^{-1}$ at room temperature (for sake of comparison, for copper *k*=400 $W \cdot m^{-1} \cdot K^{-1}$).[18] Experimental studies on SWNT have given values varying from 2000-10,000 $W \cdot m^{-1} \cdot K^{-1}$ at room temperature. Thermal conductivity of CNTs, like to the other properties, is anisotropic. It is extremely high along the nanotube axis, however, the radial thermal conductivity is order of magnitudes lower.[19]

Thus far, it was elucidated that nanotubes with different structures display different properties. However, to explore the full potential of nanotubes properties, it is important to have them in their individual state, and not in mats, bundles and ropes (see Figure 4). Additionally, it is also necessary to develop synthetic processes to produce them in bigger scales. In the next section, the methodologies to synthesize nanotubes will be briefly described.

1.1.2. Synthesis

Carbon nanotubes can be visualized by rolling up graphene sheets into a hollow cylinder. However, CNTs are in reality grown using other approaches. Thus far, there are three main ways to produce CNTs: *arc discharge*, *visible light vaporization* and *chemical vapor deposition* (CVD) which are briefly outlined below; for additional details the reader is referred to a number of textbooks.[1, 6, 8, 10, 12]

In the arc discharge method, the ends of two graphite rods are placed close to one another under reduced pressure. The chamber is usually filled with an inert gas like helium (or argon) at a pressure around 0.7 atm. An electric arc is established between the graphite rods which increases the temperature in the surface enough to sublimate carbon. A deposit (soot) formed on the cathode contains then CNTs. With no metal catalyst, the nanotubes generated are MWNTs; introducing catalyst SWNTs are formed. This method is easy to set up and operate and quite inexpensive. However, the CNT yield is low and an extra purification step is necessary.[6]

In the visible light vaporization method (using a laser or a solar furnace as source) light is focused at high intensity on a graphite block placed in a chamber filled with He or Ar at a reduced pressure. The solid graphite is then converted into small vaporized particles. By providing a suitable temperature gradient in the system by an inert gas flow, those particles are collected and upon collision recombine into nanotubes. A catalyst can be introduced to tune the type of CNT that is formed. This process is not easy to scale up, the cost is quite high and is difficult to operate. On the other hand, the yield of nanotubes formed is around 50% and the nanotubes produced have low defect density.[6]

In the CVD method, multiple carbon based materials (e.g. C_2H_4, C_2H_2, CO) can be used as the source of carbon during the growth of CNTs. Basically, the CVD is a

thermal reaction where a catalyst (e.g. nickel, cobalt, iron) is used to break down the source molecules and feed the growth of the nanotube. In contrast to the previous methods, in CVD the presence of catalyst is mandatory. Typically, the temperature involved is rather low.[6]

The CVD method produces SWNTs with a relatively high yield, which makes this method a good candidate to manufacture nanotubes in industrial quantities. Therefore, this method is one of the most studied (e.g. combination of different catalysts with different hydrocarbons at different pressures). Among the variants of CVD method, the two most important processes to produce high purity SWNTs are HiPCO® and CoMoCAT®. In HiPCO (High-Pressure Carbon Monoxide Process), SWNT are grown by the thermal decomposition of iron pentacarbonyl, $Fe(CO)_5$, in a flow of CO at high pressures and temperatures.[20] In CoMoCAT (Cobalt-Molybdenium Catalysis), CNTs are grown on a silica support with Co:Mo immobilized, by CO disproportionation (decomposition into C and CO_2).[21]

The development of the methods for CNT synthesis is still a hot topic where tailoring the processes in order to obtain a particular type of CNT is much sought after. Typically, different approaches produce a mixture of nanotubes with different chiralities rather than a unique chirality. Thus, processes to separate the different types of nanotubes are still needed.

1.1.3. Functionalization and dispersion of nanotubes – overview

As it was mentioned, the properties of the nanotubes are dictated by the structure of the material. However, current synthetic methodologies cannot produce a particular type of CNT with a specific chirality. Instead, clusters of nanotubes with different chiralities and diameters are produced all together. Furthermore, all production methods yield CNTs in the form of bundles (Figure 4) due to the strong tube-to-tube van der Waals interaction, which makes the hydrophobic nanotubes virtually insoluble in common liquids. Therefore, in order to get the full potential of the nanotube applications, two major drawbacks need to be overcome: 1) dispersion in a solvent and 2) efficient separation according to the chirality.[3, 5, 22, 23]

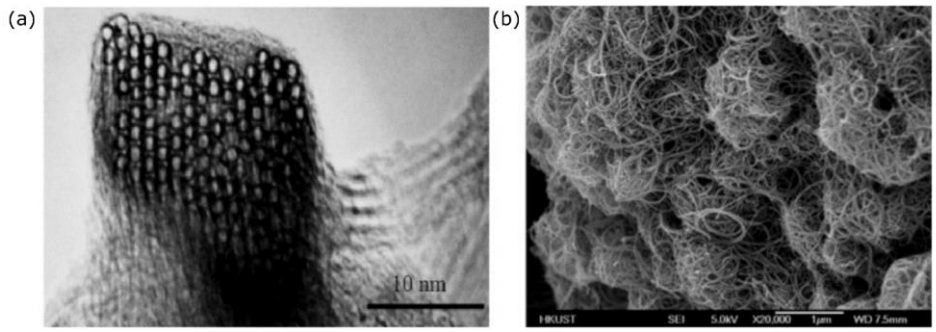

Figure 4. a) TEM image of a SWNT bundle (reproduced with permission from the American Association for the Advancement of Science[24]); b) SEM Image of entangled MWNT agglomerates (reproduced with permission from Elsevier [25]).

Because the terminologies “solubilization” and “dispersion” of nanotubes are used ambiguously in the literature, the term “dispersion” must be clarified. For nanotubes distributed homogeneously in a solvent the term dispersion is more accurate because carbon nanotubes do not form true thermodynamically stable “solutions” but more likely are metastable. Henceforth, within this thesis the terms dispersion and dispersibility are used.[26]

Up to now, three main pathways have been explored to disperse nanotubes in liquid medium: 1) in organic solvents; 2) by covalently functionalize and 3) by noncovalently functionalize the CNT. The three methods to disperse CNTs are briefly discussed below. The noncovalent functionalization of CNTs in water is discussed in more detail in section 1.1.4.

Organic solvents

The use of organic solvents is one of the possible approaches to separate and disperse nanotubes in liquid medium. Carbon nanotubes are hydrophobic, thus it is expected that organic solvents wet CNTs. However, CNTs are only dispersed in a rather limited number of solvents, such as *N*-methyl-2-pyrrolidone (NMP), *N*,*N*-dimethylformamide (DMF), o-dichlorobenzene and chloroform.[5, 22, 27, 28]

Coleman and coworkers, based on thermodynamic considerations, proposed that organic solvents would spontaneously disperse nanotubes if the Gibbs energy of mixing, ΔG_{mix}, is negative.[29-33] Typically, dissolution is driven by the entropy of mixing ΔS_{mix}. However, the CNTs are extremely large and thereby the entropy of mixing, ΔS_{mix}, is small and is generally not sufficient to overcome the positive enthalpy of mixing, ΔH_{mix} (due to strong attraction between nanotubes). Therefore, nanotubes will be dispersed when ΔH_{mix} is negative. It is known that ΔH_{mix} can be approximated by the Hildebrand–Scatchard equation. Hence, dispersion of CNTs will be facilitated when the Hildebrand solubility parameter of the solvent matches that of CNT (the solute).[32]

Bergin *et al* investigated the dispersibility of nanotubes in several solvents.[30] The solubility of nanotubes was analyzed both under the Hildebrand and Hansen parameters. The authors showed that solvents with surface energies very close to the surface energy of graphite (40 $mJ \cdot m^{-2}$) tend to successfully disperse CNTs. However, this does not mean that all solvents with surface tension equal to 40 $mJ \cdot m^{-2}$ will successfully disperse nanotubes. Thus, surface energy solubility parameters connected with Hansen parameters were developed. However, despite advances in modeling, a deeper understanding of nanotube behavior in organic solvents is still needed.[7, 30]

Covalent functionalization

Dispersibility can be affected by covalently attaching hydrophilic groups to the nanotube surface. Those groups are going to 1) interact with the solvent enhancing the dispersibility of nanotube and 2) enhance the repulsion between the nanotubes hence diminishing the cohesion between them. The main drawback of this approach is that chemical bonding with the CNT wall changes the carbon sp^2 hybridization state to sp^3. Moreover, during this process often harsh chemical conditions are used (e.g. high acidity) that can introduce structural defects in the nanotube wall. Consequently, this approach is less attractive due to the loss of CNTs properties that are extremely dependent on the sp^2 hybridization (particularly, the electrical and optical properties).[5, 34]

Noncovalent functionalization

Among the several methods to disperse carbon nanotubes, noncovalent functionalization is widespread. They are based on having some molecules (like surfactants and polymers) physically adsorbed to the CNT surface. In contrast to covalent functionalization, no chemical reactions take place in the nanotube walls. Hence, the sp^2 hybridization of carbon atoms is kept intact and the π system is not disrupted. Moreover, different molecules may adsorb differently to CNTs with different chirality. Thus, noncovalent methods open the possibility to sort CNTs using techniques such as electrophoresis,[35, 36] density gradient ultracentrifugation[37], or gel chromatography.[38] In section 1.1.4. noncovalent functionalization of CNTs in water will be discussed further.

1.1.4. Dispersibility and colloidal stabilization of CNTs in water

Since water is non-toxic, and performs as solvent in many industrial processes, it is important to study the dispersibility and stabilization of non-covalently functionalized CNTs in water (see above). In this methodology, ultrasonication is used to create temporarily a gap in the nanotubes bundle (overcoming the tube-to-tube attractive interactions). The dispersant molecules with affinity to the nanotube adsorb at the pristine surfaces provided by sonication and ultimately, prevent reaggregation of the nanotube. This process of exfoliation is known as the unzipping mechanism (Figure 5),[39] where the high local shear forces produced by ultrasonication open gaps at the ends of nanotubes bundles (Figure 5 b). These gaps become new available sites where surfactant may adsorb, preventing nanotube reaggregation (Figure 5 c). Due to the turbulent regime of the system during sonication, the opening-up of the gap proceeds randomly yet continuously. The surfactant coverage is built up along the opened sections of the gap either by surface diffusion or bulk diffusion within the solvent phase until a nanotube can be completely separated from the bundle (Figure 5 d). This mechanism describes the exfoliation process in general. However, the microscopic picture of the CNT

exfoliation is more complex. In general, efficient dispersion of nanotubes requires that the dispersants have 1) an anchoring part that attaches to the CNT surface, and 2) a stabilizing part that interacts favorably with water.

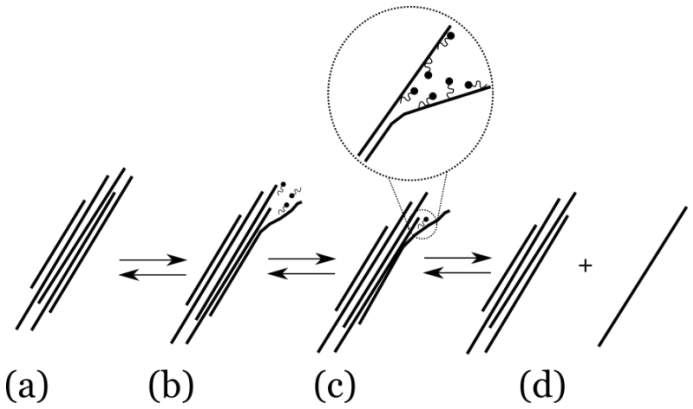

Figure 5. The unzipping mechanism of exfoliation: (a) a bundle of CNTs; (b) high local shear forces open a gap at the bundle end; (c) surfactant molecules adsorb in the new area created, and prevent nanotube reaggregation. The opening progresses along the nanotube length, akin to unzipping; (d) a nanotube coated by surfactant is released and remains dispersed in solution.

Pristine carbon nanotubes lack charge or permanent dipole moment. Therefore, no strong molecular interactions are expected to occur with water dipoles, which makes nanotubes virtually insoluble in water. Moreover, the lack of interaction with water results in a hydrophobic surface, characterized by a possible entropically unfavorable orientation of water molecules adjacent to the surface. This phenomenon is general for all hydrophobic molecules and moieties. Therefore, when a hydrophobic surface and a hydrophobic moiety are coming together, the entropically unfavorable organized water is released to the bulk, thereby reducing the total Gibbs energy of the system.[40] The hydrophobic interaction is the driving force to adsorption on the nanotube surface. Indeed molecules with hydrophobic moieties, such as surfactants, block co-polymers and proteins have been exploited to disperse nanotubes.[5, 41-45]

In addition to hydrophobic interaction, another important molecular interaction exists between aromatic molecules, i.e. the so-called π−π interaction.[46] Since nanotubes are aromatic these interactions can also lead to adsorption on the nanotube surfaces.[5, 34, 47]

Adsorption of molecules to CNTs is a prerequisite to disperse them, yet not enough *per se*. In order to keep nanotubes apart after sonication, it is also important to create a repulsive barrier that prevents their re-aggregation.

Noncharged molecules, such as block copolymers and nonionic surfactants, are also known to effectively disperse carbon nanotubes. In this case the repulsive barrier for the nanotube dispersibility arises from steric stabilization.[48] In this process the hydrophobic part of the polymer (or surfactant) adsorbs on the nanotube

while the hydrophilic part produces a layer that will be strongly hydrated and expands out and away the nanotube surface towards the solvent to gain configurational entropy. When nanotubes coated with the dispersant approach each other the adsorbed layers produce a strong repulsion due two main effects: 1) reduction of the configurational entropy of the hydrated moieties leading to an increase in the Gibbs energy of the system and 2) unfavorable mixing of the adsorbed layers due to osmotic repulsion.[49, 50]

For charged species, this may be the electrostatic repulsion. Ionic surfactants adsorbed on carbon nanotubes confer in effect charge to the nanotube and, with a diffuse layer of counterions, dress the nanotubes in an electrical double layer. The diffusive nature of the counterions creates a measurable surface charge, quantified as zeta potential, ζ.[23, 49] The repulsive interactions between the electrical double layers stabilize the nanotube dispersion. The effect of the mutually opposing electrostatic and van der Waals potential energy barriers is summarized in the DLVO theory, which predicts the colloidal stability of the dispersions.[49,51] Conversely, the ζ potential gives information about the binding of surfactant to the CNT surface.[52]

The DLVO theory only takes into account the attractive van der Waals and repulsive double layer interactions. However, steric forces, hydrodynamic forces, and hydration forces *inter alia* are not considered by the theory.[40]

Thus far, the type of interactions established between dispersants and CNTs and the stabilization mechanism (electrostatic and steric) was presented. The combinations of these factors for each dispersant molecule are the key features to control the nanotube dispersion in water. In the following two subsections, I will discuss the ability of different dispersants (both surfactants and polymers) to disperse CNTs, and detail the different mechanisms of interaction and the possible configuration/model of the dispersant around the CNT.

CNTs dispersibility by surfactants

Due to their amphiphilic structure, surfactants adsorb at interfaces, modifying properties such as surface tension, wettability and surface charge of the interface.[53] These properties play an important role in the dispersibility and stabilization of nanotubes in water. In addition, at a critical concentration, surfactants self-assemble in mesoscopic structures, e.g. micelles. The properties and the bulk phase behavior of surfactants in water will be described in more detail in the section 1.2.1.

Surfactants with different chemical structure are expected to adsorb and disperse nanotubes to a different extent. A large number of works in the literature address this question.[5,22,23,34,41,42,54-64] However, due to the widely different conditions of sample preparation and the variation of the properties of pristine nanotubes used, the results from different works can typically not be compared.[63] This makes it difficult to safely discern trends.

In an early report Bandyopadhyaya *et al.* tested several surfactants to disperse SWNTs.[64] Later, Smalley and coworkers also reported the use of surfactants to disperse as-produced HiPCO SWNTs.[42] Among the ionic surfactants, it was reported that the surfactant sodium dodecyl benzene sulfonate (SDBS) gives the most well resolved (absorption and fluorescence) spectra and, thereby, most individual SWNTs. Islam and coworkers carried out a systematic study of sodium dodecyl sulfate (SDS), SDBS and TritonX-100, showing that SDBS and Tx-100 are more effective in dispersing SWNTs. The authors suggested that surfactants with benzene rings will enhance the dispersibility of the SWNT due to π−π stacking interactions.[41] Other studies have also indicated that surfactants with aromatic moieties present higher capability to disperse CNTs.[47, 57, 65] Additionally, bile salts are also reported as good nanotube dispersants.[54, 62, 66]

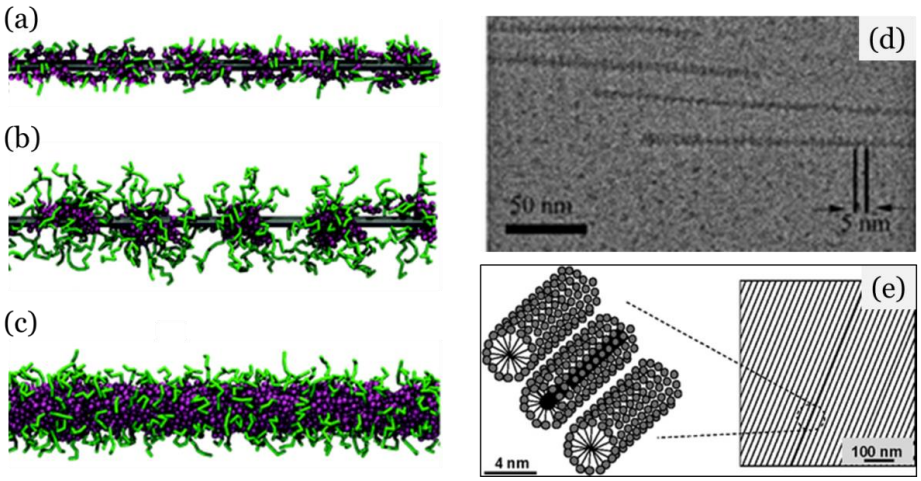

Figure 6. Different morphologies of surfactant aggregates adsorbed onto CNTs: (a) Langmuir type monolayer, (b) spherical micelles, (c) cylindrical micelle (hydrophobic tails are shown in magenta and hydrophilic headgroup in green); (d) cryo-TEM image of SWNT coated by spherical micelles of CTAB, and (e) schematic of nematically ordered cylindrical micelles CTAB embedding CTAB-coated SWNT, as imaged by cryo-TEM. Adapted from[56, 67, 68] with permission from The Royal Society of Chemistry.

Surfactants are expected to adsorb in some morphology onto the CNT surface. It remains difficult to assess this morphology, since the available methods are model-dependent and/or somewhat invasive. Yet, cryo-transmission electron microscopy (cryo-TEM), small-angle neutron scattering (SANS) and molecular dynamics simulations seem to provide some insight (Figure 6). SANS studies suggested a random adsorption of surfactant monolayer onto the CNT.[61] On the other hand, cryo-TEM observations shown both CTAB spherical micelles adsorbed on SWNTs (Figure 6 d)[67] and ordered arrays of CTAB cylindrical micelles embedding CTAB-coated SWNTs (Figure 6 e).[68] Molecular dynamics simulations pointed that weakly amphiphilic molecules may form a random monolayer (Figure 6a), whereas more hydrophobic surfactants form aggregates at the CNT surface (Figure 6 b-c). In

addition, simulations have shown that, in equilibrium, a dynamic balance between the surfactant in the free and adsorbed state is established.[56, 69]

Not only the chemical structure of the dispersants is important, but also the concentration of the dispersant is a key parameter in the CNT dispersibility in water. For instance, during exfoliation, the kinetics of the surfactant adsorption at the pristine surface in the gap opened up by sonication is dependent on the surfactant flux, which must depend on the surfactant concentration. In addition, the adsorption of surfactants onto a surface is also concentration-dependent.[53] Studies as a function of surfactant concentration, c_s, showed that the concentration of dispersed CNT, c_{CNT}, increases with c_s until a plateau is obtained.[59, 70] However, at even higher surfactant concentration, c_{CNT} decreases, due to the depletion effect caused by increasing concentration of free surfactant micelles in the dispersion.[63, 71-73] Moreover, it has been reported that micellization is not a prerequisite to disperse nanotubes.[74] Nevertheless, there is a lack of fundamental understanding of the adsorption isotherms that describe the adsorption of surfactants onto carbon nanotubes.[23]

Besides the surfactant concentration, the strength of the intermolecular interactions and the partition equilibrium established between the free surfactant in bulk and the adsorbed onto CNT are all important factors in the CNT dispersibility. However, comprehensive studies are scarce. A NMR diffusometry study shown that the residence time of ionic surfactants adsorbed onto the CNT surface, are below the NMR-accessible time scale (i.e. below the millisecond) which makes the calculation of the surfactant fraction adsorbed at nanotube difficult and prone to high uncertainties.[75] In this thesis, we investigate the effect of the chemical structure and the concentration of the surfactants on the dispersibility of CNTs in water and the surfactant binding strength to CNT surface.

CNTs dispersibility by synthetic and natural polymers

Up to now, both synthetic and natural polymers [45, 64, 76-92] have been used to disperse carbon nanotubes in water. Similar to surfactants, it is expected that one segment (or block) of the polymer interacts with the nanotube surface, whereas the other segment interacts with the solvent. However, due to the high molecular weight, polymer−nanotube interactions are likely to be somewhat different than surfactant−nanotube interactions. Thus, to describe polymer−nanotube interactions two main models have been proposed: the “polymer-wrapping” model[76] and the “loose adsorption” model.[93] The two models differ in the strength of attachment of the polymer to the nanotube. The polymer-wrapping suggests strong and specific polymer-nanotube interactions. On the other hand, the loose adsorption model assumes nonspecific interactions between the polymer and the nanotube, restricted to the adsorbing block (or end group).[94]

In the wrapping model, the polymer coats the nanotube by forming a helical structure in close contact with the nanotube surface.[76, 95-97] Molecular dynamics simulations indicated that polymers with flexible chains and bulky aromatic side groups (Polymethyl methacrylate and polystyrene) form a random interchain sheet (Figure 7 a).[98] On the other hand, polymers with stiff backbones tend to settle in a wrap around the nanotube with a helical configuration (Figure 7 b).[99, 100] As concerning biopolymers, single-stranded (ss) DNA has been referred to helically wrap SWNTs through π−π interactions between the nucleobases and the nanotube aromatic surface.[101] The resulting DNA-nanotube complex is stabilized in water due to interactions established with the hydrophilic (charged) groups of DNA. Additionally, ssDNA was reported to preferentially interact with SWNTs with a particular chirality.[102] Hence, using specific DNA sequences and adjusting the pH, it has been possible to separate SWNTs with different chirality.[103, 104]

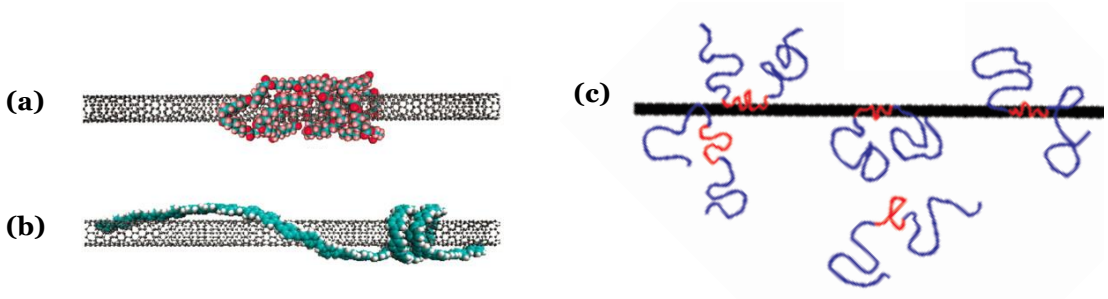

Figure 7. Depiction of the polymer configurations adsorbed on nanotube: (a) wrapping model with flexible chains;[98] (b) wrapping model with stiff backbones[100] and (c) loose adsorption model. Adapted with permission from [98, 100] © American Chemical Society.

The loose adsorption model is based on a weaker interaction between the polymer and the nanotube surface. In this model, the native conformation of polymer is not substantially changed. Typically, block copolymers tend to adopt this configuration around nanotubes, where the hydrophobic block acts as an anchor in the nanotube surface and the hydrophilic block expands towards the solvent (Figure 7 c).[44, 78, 79, 105] Experimental and simulation studies have shown that block copolymers adsorb to the nanotube surface through a non-wrapping mechanism.[44] Granite *et al* [78, 79] and others [106] used SANS to get some molecular insight in order to support this model. Indeed, SANS data shown that polymer chains are loosely adsorbed onto the nanotube surface. In addition, the dynamics of block copolymer (Pluronics F127)-CNT systems was investigated by NMR diffusometry, confirming an exchange between the adsorbed and free polymer in the bulk within the NMR time scale,[77] opening the door to additional NMR studies explored in this thesis.

Proteins are also known for his ability to disperse CNTs in water. Proteins are polymers of amino acids that can fold in so-called secondary structural motifs like α−helices, β−sheets and in less ordered loops, and then can have these motifs arranged in yet more complex (tertiary and quaternary) order. They present a large diversity of sizes and shapes. This feature is assumed to be related to the fact that

protein folding creates both hydrophobic pockets and hydrophilic regions, that is, an amphiphilic character. Hence, the hydrophobic pockets interact with the nanotube surface and the hydrophilic ones stabilize the nanotube in water by preventing reaggregation. In addition, proteins composed by amino acid residues containing aromatic rings (e.g. tryptophan, tyrosine, phenylalanine and histidine), may also interact with nanotubes through π−π interactions. Due to the complex structure, the models presented above are not straightforward to apply.[43, 88, 107] Calvaresi *et al* reports the interactions that control the binding of proteins to CNTs to be divided in four types: 1) van der Waals interactions (polarizability of groups in amino acid residues and π−π stacking), 2) hydrophobic interactions (an amino acid with a hydrophobic side chain tends to bind to the hydrophobic CNT surface), 3) amphiphilicity (i.e. amphiphilic residues behave similarly to surfactants) and 4) electrostatic interactions. Yet, it was found that proteins with similar content of individual amino acids bind CNTs to a different extent, which indicates that the secondary and tertiary structure also play an important role.[43]

One of the proteins widely used to disperse CNTs in water is the Bovine Serum Albumin (BSA). Thus, due to the complexity of protein-CNT interaction, BSA can be used as a model in order to understand and systematize the dispersibility of CNTs by proteins, which has relevant implications to biological and biomedical applications. Thus far, several works have been performed in order to understand the CNT exfoliation induced by BSA [87] and the effect of pH[83] on the dispersibility of CNTs. It has been reported that the electric charge and the conformation of protein affects the CNT dispersibility. In addition, NMR diffusion studies in the BSA-SWNT system have shown that only a small fraction of protein is bound to the nanotube and is in fast exchange (over the time scale of the diffusion NMR experiments) between the adsorbed and free state. In order to understand BSA-nanotube interactions better, adsorption studies have also been carried out.[108] In this thesis NMR diffusometry experiments employing BSA and Pluronics F127 to disperse CNTs were carried out with the goal to evaluate the adsorption competition between BSA and F127 to the CNT surface.

1.2. Soft matter

Soft matter comprises a large diversity of materials, such as surfactants, polymers, liquid crystals, colloids (e.g. foams, emulsions and gels) and other types of systems organized at the mesoscopic level. The term soft matter originates from the macroscopic mechanical properties. Soft matter can be characterized as a class of materials that yield a large response to a small perturbation. That means that a material is considered soft if it deforms easily (and typically in a plastic way) under an external stimulus (e.g. mechanical deformation, electric or magnetic field, etc).[109,110]

Soft materials consist of structural units that are much larger than atoms, and often have some degree of self-assembled ordering. Under certain conditions, many soft materials can be induced to flow. This is a consequence of the lack of the three-dimensional atomic organization that is found in a crystalline solid.[111] In terms of structure, these materials present molecular arrangements somewhere between those of a crystalline solid and a conventional liquid. Typically, soft materials are held together by weak intermolecular interactions (repulsive and attractive). From the viewpoint of kinetic energy, they present a molecular kinetic energy close to $k_B T$ and thus, their structure can be easily altered at relatively low temperatures.[110, 111]

In our everyday lives, soft matter is present everywhere, for instance in materials such as shampoo, toothpaste, cosmetic creams and food emulsions, like butter, ice-cream and mayonnaise. Additionally, advanced soft materials are also present in modern technologies such as liquid-crystal displays, paints and biomaterials for medical applications.

The combination of soft materials with hard materials (such as CNTs), is an important and relevant topic from both the fundamental and applied point of view. It is important to investigate the properties of soft and hard materials, firstly, individually and second, in combined forms. From a more fundamental point of view, we must understand the role of the molecular interactions in the hard−soft interface, in order to learn how to tune the desired properties of the final composite. For example, recent work has been published where nanotubes were combined with an elastomer, originating a new material that can be stretched up to 1320% with minimum change of the electrical resistance (about 5 %).[112] This superelastic conductor can be used, for instance, in artificial muscles or other superelastic electronic applications.

In the previous sections, the structure and properties of nanotubes were presented in detail. Before exploring any hard−soft combination, it is relevant to know the typical behavior of soft materials alone. Thus, in the following sections (1.2.1 up to 1.2.3), the soft materials that were explored in this thesis−surfactants, polymers and liquid crystals−will be described in more detail.

1.2.1. Surfactants

Surfactants are molecules composed of two parts with different affinities for a given solvent. The part with affinity to the solvent is designated as lyophilic, while the part insoluble in the solvent is called lyophobic. When the solvent is water, the parts are designated as hydrophilic and hydrophobic, respectively. The hydrophilic part is also called the polar headgroup and the hydrophobic part the tail (Figure 8 a). Surfactants are classified as amphiphiles because they contain both water-loving and oil-loving parts. The charge of the polar headgroup is typically used to classify the surfactant. The most common surfactants are cationic, anionic, zwitterionic and nonionic.[113]

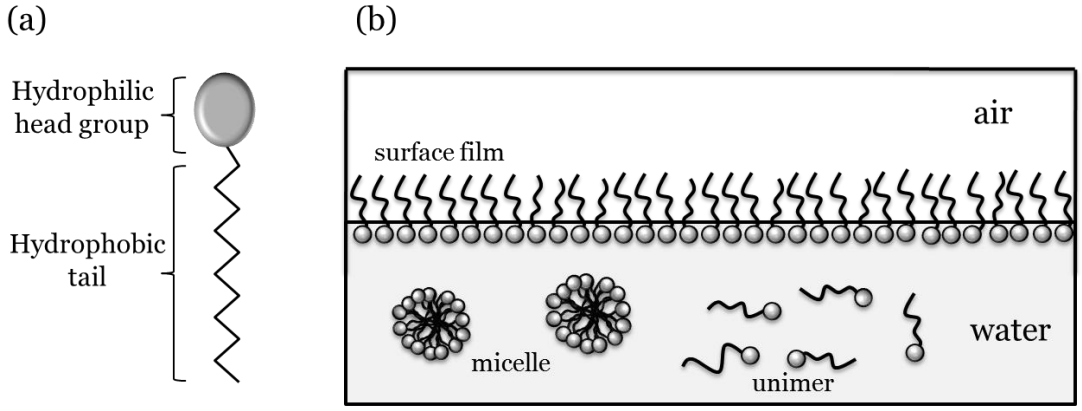

Figure 8. Schematic representation of a surfactant molecule (a) and surfactant behavior in water (b).

The amphiphilic character of the surfactant is the key role for the surfactant behavior in water. The solubility of surfactant in water is quite low, and surfactants are prone to self-assemble in water (or polar solvents) and adsorb at interfaces, lowering drastically the interfacial tension. Figure 8 b summarizes the surfactant behavior in water at low concentration.[114]

One of the main features of surfactants is the self-assembly property. The molecular interactions between the hydrophobic tail and water dipoles are not favorable; therefore, when a surfactant is solubilized, the water molecules form a "cage" that is extremely organized around the hydrophobic tail in order to minimize water-hydrocarbon interaction. This organization has a high entropic cost and is the driving force behind the hydrophobic effect.[40, 115] When two hydrocarbon chains are in close contact, the water that was organized around the hydrocarbon is released into the bulk, which leads to a global increase in the entropy of the system. Hence, association of surfactant unimers is entropically favorable and results in a lower Gibbs energy of the system. Indeed, when the unimer achieves a critical concentration in water, the surfactant self-assembles in micelles. This concentration is defined as the critical micelle concentration (*cmc*).[113-115]

Surfactants in water exhibit a rich phase behavior. Micellar solutions and liquid crystals (hexagonal, lamellar and cubic phases) are commonly found in the phase diagram as a function of surfactant concentration. Figure 9 displays the Fontell scheme, which represents a somewhat idealized sequence of self-organized structures as a function of surfactant concentration. A more quantitative description that rationalizes the packing of surfactants into different aggregates is given by the surfactant packing parameter (P_s) defined as the ratio

$$P_s = \frac{V_{hc}}{a_{hg} l_{hc}} \qquad (1.5)$$

of the volume of the hydrocarbon chain of the surfactant (V_{hc}) to the volume (a_{hg} l_{hc}) of a hypothetical cylinder defined by the effective area of the polar head group (a_{hg}) and the length of the fully extended hydrocarbon chain. Typically, P_s increases to the right in the Fontell scheme. When P_s is about 1/3 (corresponding to a surfactant with a geometric shape similar to a cone) the formation of micelles (L1) is favored; for P_s=1 lamellar phase (L_α) is preferred. In the case of P_s>1 the formation of reverse structures is preferred.

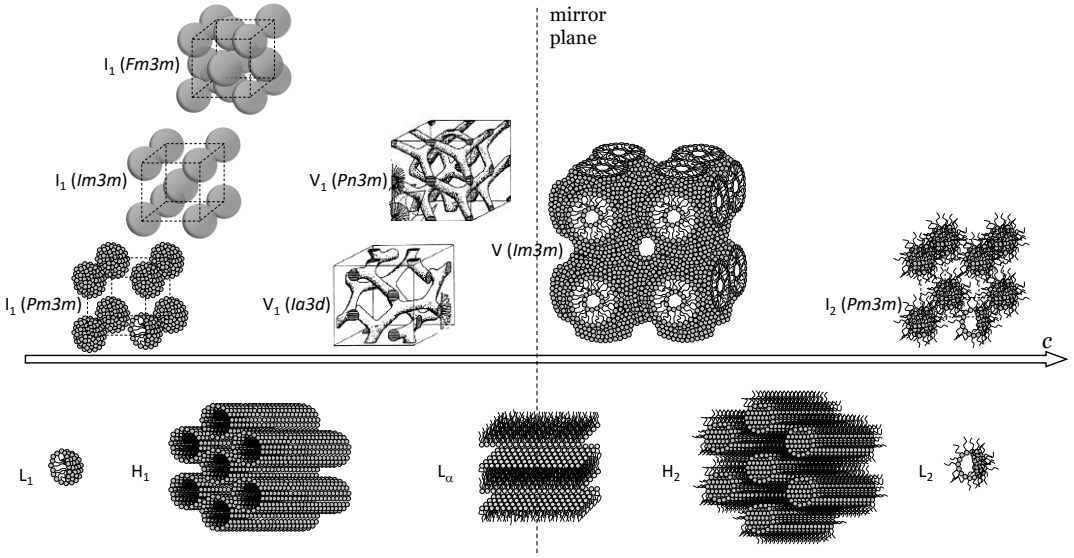

Figure 9. Fontel scheme showing the ideal dependence of mesophases with the concentration of the surfactant. Adapted with permission from Springer.[114]

1.2.2. Polymers

A polymer is a macromolecule that is built up by covalently linking smaller chemical units, referred as monomers. Polymers are commonly divided into biological and non-biological macromolecules. Biopolymers consist of nucleic acids, proteins and polysaccharides, while non-biological (i.e. synthetic) comprises common plastics and adhesives.[115] Polymer science is a vast area, comprising proteins, cellulose, silk, polystyrene, nylon, rubber, etc.[116] Within this section, the discussion will focus only on polymers in aqueous solution.

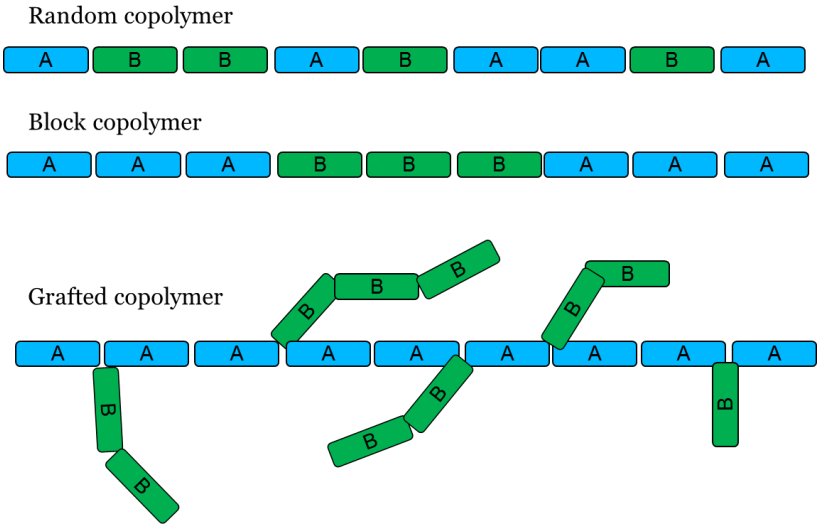

Figure 10. Copolymer classification according to composition.

Synthetic polymers are classified according to their structure and composition. As concerning the structure, a polymer can either be 1) linear, 2) branched or 3) cross linked (forming a network). Polymers are also classified according to composition. A polymer synthesized with more than one type of monomer is called a copolymer. Figure 10 shows how the monomers in the copolymer can be organized in different ways: 1) randomly, 2) distributed in blocks, or 3) one of the monomers can be grafted onto the backbone of the other polymer.[49] In block copolymers, the polymer chain consists of blocks of one repeating unit followed by one or more blocks of other repeating units. If any of the monomers carries a charged group, one can refer to the polymer as a polyelectrolyte.[49]

Block copolymers can be made of alternating hydrophilic and hydrophobic blocks, hence becoming amphiphilic. The most common block copolymers are of the poly(alkene oxide) type, where the hydrophilic segment is poly(ethylene oxide), PEO, and the hydrophobic segment is poly(propylene oxide), PPO. There are many possible combinations for PEO-PPO block copolymers. Among them, Pluronics, which have a general structure $(PEO)_x$-$(PPO)_y$-$(PEO)_x$, have gained high importance. Being amphiphilic, they can self-assemble in water at a critical micelle concentration; the size of the blocks, the proportion of PEO to PPO units and temperature are parameters that affect the *cmc*.[117] Pluronics also display a rich phase behavior exhibiting a large number of liquid crystalline phases.[115]

1.2.3. Thermotropic liquid crystals

Liquid crystalline (LC) phases combine order and mobility at molecular and supramolecular level. Due to this unique combination, such systems are sensitive to external (magnetic, electric, chemical or mechanical) stimuli by finding a new configuration of minimum energy. Hence, LC materials can be used, for instance, as

optoelectronic devices, temperature sensors, polarized light emitting materials and photoconductors.[118, 119]

The liquid-crystalline state is an intermediate state between the crystalline solid phase and the liquid phase. The molecules that originate liquid crystals are called mesogens and the liquid-crystalline phases are also named mesophases.[120] Typically liquid crystals fall into two main categories: 1) lyotropic liquid crystals, formed by the action of solvent due to unfavorable interaction with the solvophobic part of amphiphilic molecules; and 2) thermotropic liquid crystals, formed in the absence of solvent, only by the action of temperature.

In the case of thermotropic liquid crystals, upon heating the crystalline solid of the mesogenic compound, there is gradual introduction of some type of orientational and/or positional disorder of the molecules and hence formation of mesophases, before the totally disordered (isotropic) liquid state is reached.

The formation of thermotropic liquid crystal requires mesogens to be anisotropic in shape (i.e. molecular structure must be spatially different in one of the 3-D axis) or have an amphiphilic character. Typically, the shape of molecules that accomplish this requirements are rod-like (also called calamitic molecules) or disk-like. Due to their amphiphilic character, surfactants also form thermotropic liquid crystals. Figure 11 presents some typical mesogens.

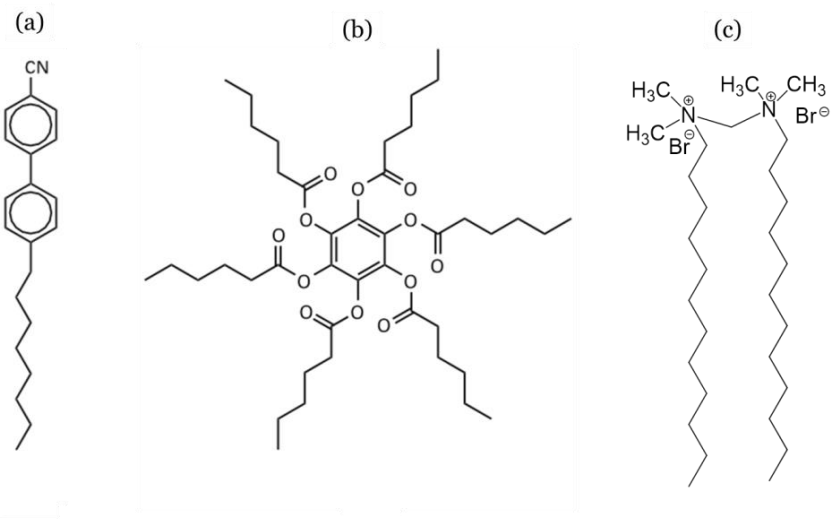

Figure 11. Molecular structure of typical mesogens forming liquid-crystalline phases: (a) calamitic molecule, (b) discotic molecule and (c) amphiphilic molecule (gemini surfactant).

The driving force of the formation of thermotropic liquid crystals is the anisotropic character of the molecules, viz. shape, charge, polarity and molecular geometry which results in the segregation in space into distinct microdomains producing long-range orientation and positional order.[118, 119]

In a liquid crystal, the molecular orientational order can be quantified by the order parameter *S*, described by means of a second Legendre polynomial: [121]

$$S = \left\langle \frac{3}{2}\cos^2\theta - \frac{1}{2} \right\rangle \tag{1.6}$$

where θ is the angle between the molecular axis of each mesogen and the unit vector $\hat{n}$ that points along the preferred average molecular orientation (Figure 12 a). The parameter *S* is 1 for perfectly ordered crystalline solids and 0 for liquids and gases. The *S* value ranges between 0.3 and 0.8 for typical liquid crystals. As expected, with increasing temperature, the order parameter *S* of the thermotropic liquid crystal decreases until zero when the phase is completely melted.

Mesogens form very different types of liquid crystals according to their shape and/or amphiphilicity. Rod-like mesogens (or calamitic molecules) typically form nematic phases, where molecules only have an average orientation in space and there is no positional order, i.e. molecular positions are not correlated in space. The order is thus only orientational, with the molecules presenting an average orientation in space (Figure 12 a). However, in some other structures, molecules can also have positional order like in the columnar phases (typically formed by discotic molecules) and smectic phases (typically formed by some amphiphiles), as shown in Figure 12 b and 12 c, respectively.

Disk-like mesogens can form nematic phases and more commonly columnar phases, due to the stacking of disks. Additionally, columnar phases may also have hexagonal, tetragonal and oblique order between different columns (Figure 12 b).

Smectic phases are organized in planar layers (Figure 12 c). The positional order within the layers is of short range, as opposed to layers in solid crystals. If the order is long-ranged, the phases are no longer considered pure liquid crystals, but slightly disordered solids.[111] The most simple smectic phase is the smectic A (SmA) and smectic C (SmC), where molecules are ordered in layers, but totally disordered in each plane, i.e. behaving like a liquid in the plane. However, molecules in the layer may also present positional order (e.g. SmB, SmI, SmF, SmE and SmH). These phases can be ordered by increasing degree of organization: (SmA) < (SmC) < (SmB) < (SmI) < (SmF) < (SmE) < (SmH). In the next page, the organization of the different smectic phases in the mesophase is described, also with reference to Figure 12c.[120]

- SmA — No positional order in the layers; $\hat{n}$ is perpendicular to the normal layer ($\hat{k}$).
- SmC — No position order in the layers; $\hat{n}$ is tilted to the normal layer ($\hat{k}$).
- SmB — In-plane hexagonal organization; $\hat{n}$ is perpendicular to the normal layer ($\hat{k}$).
- SmI — In-plane hexagonal organization; $\hat{n}$ is tilted to the normal layer ($\hat{k}$); molecules are tilted towards the apex of the hexagonal unit cell.
- SmF — In-plane hexagonal organization; $\hat{n}$ is tilted to the normal layer ($\hat{k}$); molecules are tilted towards the side of the hexagonal unit cell.
- SmE — Similar to SmB but with square organization in-plane.
- SmH — Similar to SmF but with square organization in-plane.

Typically, amphiphiles that commonly form smectic phases have a P_s close to 1 and the molecular shape is similar to a cylinder (e.g. double chained surfactants, gemini surfactants, bolaamphiphiles and catanionic surfactants).

In this thesis, the effect of the spacer length on the thermotropic behavior of the gemini 12-s-12 surfactants was investigated. The spacer length effect on gemini surfactants, which will change the P_s conferring a versatility that may be important for the choice of the liquid crystalline matrix to embed CNTs. This opens the door to a new hybrid material that will combine both the response of the LC and CNT to an external (magnetic, electric, chemical or mechanical) stimulus.

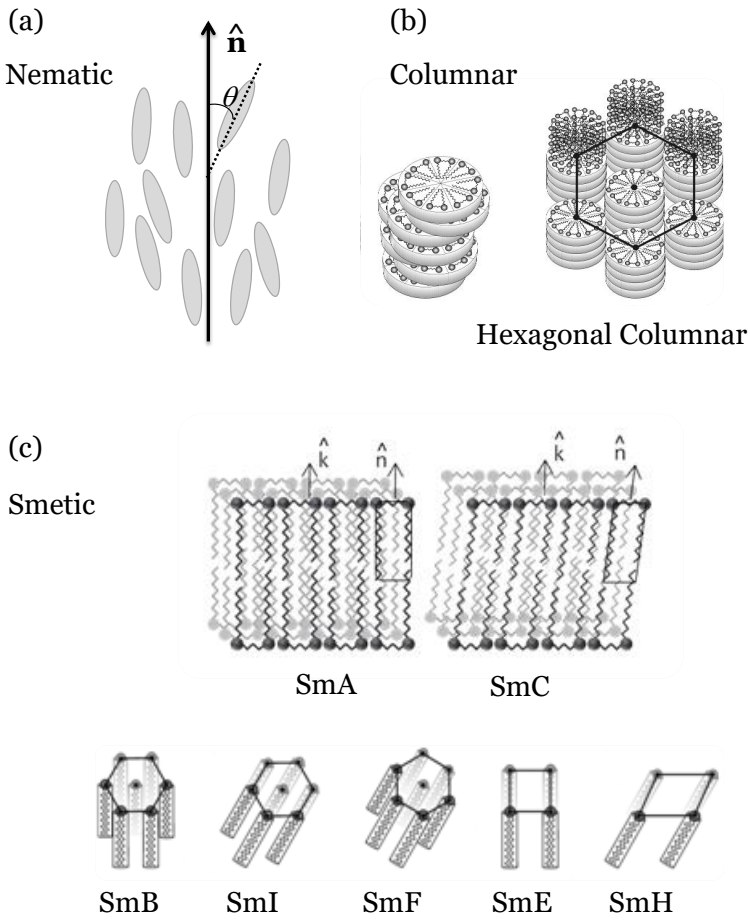

Figure 12. Schematic representation of thermotropic liquid crystal mesophases: (a) Nematic phase, where $\hat{n}$ is the vector that points along the preferred average molecular orientation and θ is the angle between the molecular axis of the mesogen and n is the bilayer director; (b) Stacking of disks forming an elongated rod and hexagonal columnar phases; (c) Smectic phases, where $\hat{k}$ stands for the vector normal to be bilayer and $\hat{n}$ is the bilayer director. Smectic phases B, I, F, E and H are shown as top views.

2. Experimental section

2.1. Methodology to prepare the CNTs dispersions

The CNT dispersions were prepared by first adding accurately a weighed amount of pristine nanotube powder to a vial, followed by the addition of (typically) 3 mL of dispersant solution. Exfoliation was then performed through a 3 mm tip sonicator, where the tip was immersed directly into the liquid, for a sufficiently long period (≈10 min). Non dispersed material assumed to consist of large remaining grains of non-exfoliated nanotubes, amorphous carbon and other impurities were removed by centrifugation. The concentration of CNT dispersed in the supernatant was quantified by a combined TGA/UV-vis methodology outlined below.

Sonication

The exfoliation process of nanotubes in surfactant solutions is rather intricate. As a high amplitude ultrasonic pressure wave propagates through a liquid medium, cavitation bubbles are created and, above a critical size, collapse and hot spots (with few thousands degrees Celsius and pressures of several tens of MPa) are generated. If the bubble collapses near a surface, a hydrodynamic microjet is built up in the liquid. This high-speed microjet creates high shear forces in the surrounding liquid medium. On other hand, if the bubble is unperturbed by a surface, a shock wave is generated during a symmetric collapse.[122] Nanotubes exfoliation is driven by the combination of both effects (shock waves and microjets), followed by the adsorption of dispersants that prevent CNT reaggregation (see unzipping mechanism Figure 5).

The effect of sonication on CNT dispersibility has been evaluated by several authors. Among other features, it was observed that a critical sonication threshold time exists for successfully opening all bundles and, provided that there is enough surfactant available, exfoliating all nanotubes.[123, 124] However, increasing the sonication time also increases CNT fragmentation.[63] Indeed, some reports state that nanotube exfoliation cannot happen without nanotube fragmentation.[125-127] Despite considerable effort, current knowledge on the most suitable and/or optimal experimental parameters, such as the time scale and energy density (i.e. the amount of acoustic energy transferred to a certain volume of liquid, herein expressed as $J \cdot mL^{-1}$) for de-bundling CNTs without considerable fragmentation, is still scarce. The difficulty to characterize the size distribution and homogeneity of dispersed CNT, together with difficulty to estimate the effective shear forces provided by sonication are the main causes for this shortcoming.[128]

In this thesis, in order to make sonication conditions easier to reproduce, the total energy transferred to the system was estimated by a calorimetric method. There, we assumed that the heat generated by ultrasound is proportional to the acoustic energy dissipated from which the power P transferred to the liquid was estimated as

$$P = mc_p\left(\frac{dT}{dt}\right) \qquad (2.1)$$

where m the mass of the water in our vial, c_p is the specific heat capacity of water and (dT/dt)is the rate of temperature increase as function of sonication time. For tip sonicaton, the power density (P/V) in the liquid was in the order of 1 W mL^{-1}. We observed that, with our available equipment (see below), bath sonication (where ultrasonication is applied indirectly through the walls of the sample container) delivers only a few % of the power density delivered by the tip sonication. However, since the bath was used during much longer (≈20 times) time the energy density ($J \cdot mL^{-1}$) transferred to the liquid was in the same order of magnitude as the tip.

For tip sonication a Bandelin Sonoplus Vb 2070 and a Qsonica Q-500 equipped with a 3 mm microtip was used. During the sonication process, the tip was always carefully placed in the center of the vial, always at the same position from the bottom in order to maximize the reproducibility of the sonication conditions. The tip was frequently polished, and the amplitude of vibration of the tip was set to 20-30% of maximum, in order to minimize surface erosion. The sonication time used varied between 8.5 to 10 min. An external bath, in thermal equilibrium with the processing vial, was used to dissipate the heat produced during the sonication and keeping the sample temperature stable. For bath sonication, an Elma Sonic (model S10, 30W, 37 kHz) sonicator was employed.

Centrifugation

After sonication, a centrifugation step is used to sediment any non-dispersed material. Typically, after sonication the nanotubes are in the form of individual nanotubes, small bundles and non-exfoliated macro-bundles. These CNT states have slightly different densities ρ and highly different L/d aspect ratios, which allows CNT separation based on g force and/or centrifugation time. [63] Indeed, using a density gradient ultracentrifugation it has been possible to separate nanotubes with different lengths.[129]

Nevertheless, mild centrifugation conditions (1-10 x 10^3 g) are usually sufficient to remove the large bundles of non-dispersed CNTs and leave individual nanotubes and small bundles in the dispersion.[52, 130] In this thesis the centrifugation was carried out at 4000 g during 20-30 min. After the centrifugation step ≈ 50% of the supernatant (≈1.5 mm above the precipitate line) was collected with a pipette and used in subsequent experiments.

CNT quantification

The quantification of CNTs dispersed in water is based on a thermogravimetric-spectroscopic approach.[131] In this methodology the exact concentration of the CNT dispersed in the liquid is quantified by thermogravimetric analysis (TGA) and

related to the optical density of the CNT dispersion. Because of the presence of CNT bundles with linear size comparable to wavelength, optical density may include both true absorbance and scattering.

In order to quantify the CNT concentration, an exact known volume V_s of the supernatant was freeze-dried for 24 hours resulting in a dry powder of mass m_s, composed by CNT and dispersant. Data yielded by thermogravimetric measurements were then used to provide the CNT concentration as

$$c_{CNT} = \left[\frac{m_s}{V_s} \times \left(1 - \frac{\phi_s}{\phi_d} \right) \right] \tag{2.2}$$

where ϕ_s is the TGA mass loss fraction in the dry supernatant and the ϕ_d is TGA mass loss fraction in neat dry surfactant. Hence, the ϕ_s/ϕ_d ratio accounts for incomplete surfactant decomposition in TGA. Measuring the optical density at λ=660 nm for same stock dispersion, one can estimate the apparent extinction coefficient ε_{660}. Once the ε_{660} is known, the CNT concentration of the subsequent samples can be estimated quickly and simply from the optical density. In other words, TGA experiments were used to calibrate ε_{660} to real CNT concentration. In order to ensure the maximum accuracy of the CNT concentration, a new calibration was performed every time that a different dispersant or new batch of nanotube was used.

2.2. Introduction to NMR

Nuclear magnetic resonance (NMR) spectroscopy is a noninvasive analytical technique used to obtain molecular information. It is a very versatile tool in terms of the methodology by which information is collected (e.g. chemical shift, spin relaxation, imaging, etc) and type of systems that can be studied (e.g. hard and soft materials). In NMR spectroscopy, the signal from NMR-active nuclei is measured and processed in order to get insight into, for instance, molecular or macromolecular structure, molecular dynamics, distribution of molecules and properties in biological tissues synthetic materials, etc. In this thesis, NMR was mainly used to measure the translational diffusion of molecules and understand aspects of molecular structure and dynamics of amphiphiles in contact with CNT.

2.2.1. NMR principles

Atoms are composed by a nucleus (made of protons and neutrons) embedded in a cloud of electrons. These particles (proton, neutron and electron) are, among other properties, characterized by an intrinsic angular momentum and an intrinsic magnetic moment that together are referred to as spin. Protons, neutrons and electrons are so-called fermions characterized by a spin quantum number I = 1/2.

The combination of the neutron spins and proton spins and motion of those particles within nuclei results in a nuclear spin I that, depending on the isotope, may take the value I=0, 1/2, 1, 3/2, 5/2 and higher. For instance, ^{1}H, ^{13}C, ^{15}N, ^{19}F, ^{29}Si, ^{31}P, ^{207}Pb have I = ½; ^{2}H and ^{14}N I=1; ^{23}Na and ^{35}Cl I=3/2; ^{17}O and ^{27}Al I= 5/2 while ^{12}C and ^{16}O lack nuclear spin (I=0). Only nuclei with $I\neq0$ are NMR-active, i.e. they interact with a magnetic field.[132]

The discrete states a nuclear spin can take are indexed by the magnetic quantum number m = -I, -I+1...I-1, I. In the absence of a magnetic field all spin states exhibit the same energy, that is, the system is degenerate. However, when an external magnetic field B_0 is applied, the degeneracy is lifted and the energy levels split. For a nuclear spin I=1/2, two states are possible, m=-1/2 and m=1/2. The energy associated with a spin state, E_m, is related to the external magnetic field B_0 as

$$E_m = -\mu_z B_0 \tag{2.4}$$

where μ_z is the z component of the nuclear magnetic moment μ of the nucleus:

$$\mu_z = \mathrm{m}\,\hbar\,\gamma \tag{2.5}$$

where $\hbar$ is the reduced Planck constant and γ is the gyromagnetic ratio, a parameter specific to each particular nucleus (element and isotope). It is this latter property that makes NMR element-specific. Combining equations 2.4 and 2.5, one can calculate the energy difference

$$\Delta E = \hbar\,\gamma\,B_0 \tag{2.6}$$

between the two states m=±1/2. Equation 2.6 shows that ΔE is proportional to the strength of the external magnetic field, B_0.

In thermal equilibrium, the distribution of an ensemble of nuclear spins between the two allowed energy states follows the Boltzmann distribution

$$\frac{N_{\mathrm{high}}}{N_{\mathrm{low}}} = e^{-\Delta E / k_{\mathrm{B}}T} \tag{2.7}$$

where N_{high} and N_{low} are the number of spins in the states with higher and lower energy, respectively, k_{B} the Boltzmann constant and T the absolute temperature. The Boltzmann distribution yields more spins at the lower energy level, and since in the two states the magnetic moments point oppositely to each other, the sample attains a net nuclear magnetization along the axis of the external magnetic field (z). The NMR signal is obtained by the perturbation of this net magnetization. Among other factors, the intensity of the NMR signal is proportional to the population difference (ΔN= N_{low} - N_{high}) between the two energy states. For an ensemble of ^{1}H spins at room temperature, and in a magnetic field with the strength of 11.7 T, the population difference, ΔN, is approximately 1 for every 10^4 spins. In other words, the net nuclear magnetization is very weak. It is for that reason that NMR is a very insensitive

technique hence requiring a large amount of sample (at least a few mg/mL) compared to other spectroscopic methods.

When the sample is affected by a time-dependent electromagnetic field characterized by a frequency

$$\nu_0 = \frac{\Delta E}{h} = \gamma B_0 / 2\pi \tag{2.8}$$

one can create transitions between the different spin states. The frequency ν_0 at this resonant condition is known as the Larmor frequency. Due to typically small energy difference between the involved states, the Larmor frequency falls in the radio range.

Basic features of NMR are usually visualized using the vector model, where the thermal equilibrium state of nuclei is represented by a vector M pointing in the same direction (z) as the external field B_0. For $I = 1/2$ nuclei that lack spin couplings, M depicting the net nuclear magnetization provides a suitable description, while for higher spins and with spin couplings, richer models may be needed. In the vector model, M is both (i) turned in different directions and (ii) is also left precessing around the direction of the external magnetic field. Regarding (i), it can be achieved by creating a circularly polarized magnetic field B_1 that oscillates with a frequency that matches the Larmor frequency. This requires a suitable coil placed around the sample. Having applied the magnetic field B_1 for a specific time period (summarized by the name radiofrequency or RF pulse), the magnetization vector M rotates away from its thermal equilibrium state along the z axis by a certain angle α. Specifically, if B_1 is applied as a pulse of duration $\pi/2\gamma B1$, the magnetization M is turned by 90°, i.e. the vector M initially aligned with z is tilted to x-y plane (also called the transverse plane). The power level of the RF pulse characterizes the strength of B_1, which affects the 90° pulse duration. The pulse duration is typically in the order of microseconds. Once the magnetization is tilted to the transverse plane, the magnetization is left precessing at the Larmor frequency around the direction of the field B_0. The precession induces a voltage in the coil previously used to generate the RF pulse, which in turn generates the so-called time-domain NMR signal, often termed the free induction decay (FID). The Fourier transformation of the FID provides the frequency-domain NMR spectrum.[132, 133]

Thus far, we have considered the effect of a RF pulse with its frequency exactly at Larmor frequency. However, virtually the same effect is obtained at off-resonance conditions, provided that the frequency of the pulse is sufficiently close to ν_0. The condition for this involves the inverse of duration to the 90° pulse. Hence, a short and strong 90° RF pulse can turn nuclear magnetization for spins characterized by Larmor frequencies over a reasonable range. This is important because nuclei in matter indeed experience different magnetic fields, which then results in different Larmor frequencies. This feature arises because electrons around the nuclei have the

capacity to contribute to the magnetic field that may either augment or diminish B_o. As a result, the local field is expressed as

$$B_{local} = (1-\sigma)B_o \tag{2.9}$$

where the dimensionless quantity σ is called the shielding constant. These differences in shielding are expressed in terms of chemical shift, where shielding values for particular molecules and particular sites in them are related to that experienced in some reference compound.

After having tilted the magnetization M to the x-y plane by a 90° RF pulse, the nuclear spins do not stay precessing there forever. Instead, the system returns to thermal equilibrium through a process called spin relaxation. There are two mutually independent relaxation processes involved, the longitudinal relaxation (characterized by a time constant T_1) and the transverse relaxation (with a time constant T_2). Longitudinal relaxation characterizes the return of the nuclear magnetization in the z direction (zero after a 90° RF pulse) to its thermal equilibrium value. Longitudinal relaxation is typically exponential with time t as multiples of T_1 in the exponent, e.g. it takes almost $5\times T_1$ for the magnetization to recover 99% of its equilibrium value.[133]

Transverse relaxation refers to the disappearance of magnetization in the x-y plane. Immediately, after the 90° RF pulse, the magnetization M in the x-y plane is large because of the strong phase coherence among the precessing spins. However, spins interact with each other, and each spin will experience a local field generated by the nearby spin. In liquids, the temporally and randomly fluctuating local field generated by a spin acts like a pulse, which tilts the magnetic moment of the adjacent spins away from their original direction. Thus, spins precess at different and randomly assigned average speed and, consequently and over time, the spins loose coherence and the net transverse magnetization decreases. Since molecular motions produce fluctuations in spin interactions, relaxation processes may inform about molecular dynamics.[133]

On the other hand, if the local fields are constant over time, such as in case of having an inhomogeneous magnetic field over the sample volume, the resulting decay of the transverse magnetization could be reversed using a method called spin echo. Erwin Hahn introduced it, having demonstrated that – through the application of an additional 180° pulse, after a delay τ – a spontaneous refocusing of the magnetization occurred at time 2τ. [134] A spin echo is analogous to a sound echo: the transverse magnetization is created by a RF 90° pulse, decays away, is reflected by a 180° pulse, and grows back to form an echo.[4]

Figure 13 displays the spin echo pulse sequence. A $90°_x$ RF pulse tilts the magnetization to the y axis into the transverse plane (x-y) where the magnetization starts to precess. Due to the presence of static local fields, different spins precess at different Larmor frequencies – and, as a result, the spins start to dephase (that is,

loose coherence), represented as the fanning out in Figure 13 c. After a period τ, a 180^{o}_{y} RF pulse is applied that inverts all magnetization vectors in the x-y plane. The magnetization vectors of the slow spins are now in the position previously occupied by the faster ones and vice versa. As the spins continue to precess, the fast ones are now behind the slow ones. As a result, the fan starts to close up and the signal, that is proportional to the vector sum of all components, grows. At time 2τ, the vectors will all be aligned along the y axis and the signal reaches its maximum value, to decrease thereafter again.[4]

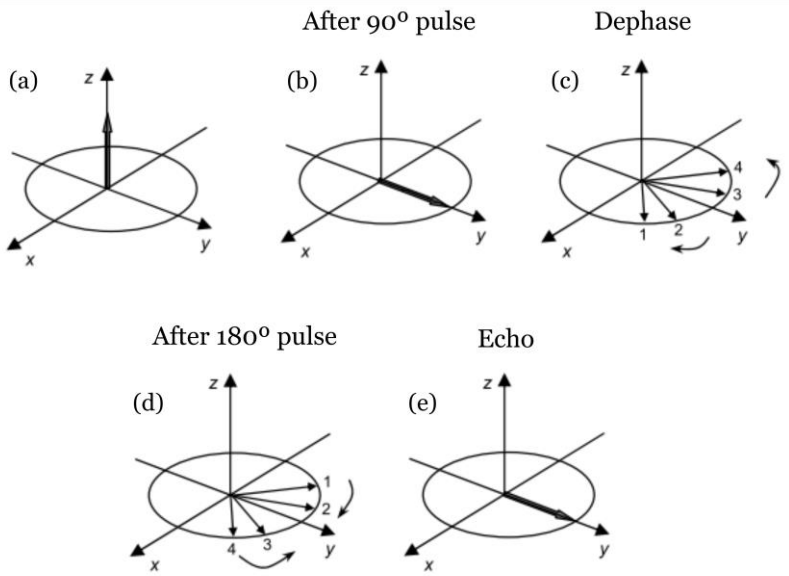

Figure 13. Spin echo pulse sequence. (a) magnetization in thermal equilibrium aligned with the external magnetic field B_o; (b) magnetization flipped into the transverse plane; (c) Some spins are precessing faster and some slower than others, thereby the magnetization fans out; (d) The 180^{o}_{y} RF pulse inverts the magnetization vectors in the transverse plane and the spins end up in mirror image positions with respect to the yz-plane; (e) The magnetization is refocused.

2.2.2. Diffusion NMR

Self-diffusion is the net result of the random thermally-induced motion of molecules or atoms in space. Translational diffusion is the basic mechanism by which molecules are distributed in solution and it plays a role in chemical reactions since the species have to meet before a reaction occurs. The probability of finding a molecule, initially at position r_o, at a position r after a time t follows a Gaussian distribution. In a homogeneous isotropic system, the width of this distribution is characterized by the self-diffusion coefficient D.[135, 136]

Considering a system without concentration or thermal gradients, the average displacement of the entities is zero. However, the mean square displacement $\langle r^2 \rangle$ for any individual entity over time t is not zero, but is given:

$$\left\langle r^2 \right\rangle = 6Dt \qquad (2.10)$$

which can be obtained after having considered random-walk statistics. For instance, water self-diffusion coefficient is in the order of 10^{-9} $m^2 \cdot s^{-1}$; hence the root mean square displacement $\sqrt{\langle r^2 \rangle}$ for water molecules during one second is only tens of microns. The self-diffusion coefficient is closely related to molecular size by the Stokes-Einstein equation:

$$D = \frac{k_B T}{6 \pi \eta r_s} \qquad (2.11)$$

where T the absolute temperature, η is the (micro)viscosity of the solvent and r_s is the Stokes (or hydrodynamic) radius. Therefore, the self-diffusion coefficient D is a parameter that provides information about the diffusing species and their surroundings, such as molecular interactions or self-assembly. In addition, studying the dependence of the displacement spectrum on the diffusion time permits one to extract information about the structure of the system (e.g. porous systems, liquid crystals, etc) through the effect of spatial limitations that those structures set for diffusing molecules. For some other systems, the diffusion time dependence allows one to follow the exchange between two sites with different diffusion coefficients (e.g. ligand binding to a macromolecule). Because of its noninvasive nature, NMR spectroscopy is an excellent tool for studying molecular dynamics in chemical and biological systems.[136]

Erwin Hahn, in his pioneering work about spin echo, pointed out that the echo amplitude would be influenced by the translational diffusion because of the resulting fluctuations of local magnetic field. [134] In the early times, the spin echo amplitude was measured in the presence of a static magnetic gradient in the B_0 field to measure diffusion. The limitations imposed by static gradients have been circumvented by Stejskal and Tanner[137] through the application of magnetic gradients as pulses in the spin echo sequence – yielding Pulsed Gradient Spin-Echo (PGSE) NMR.

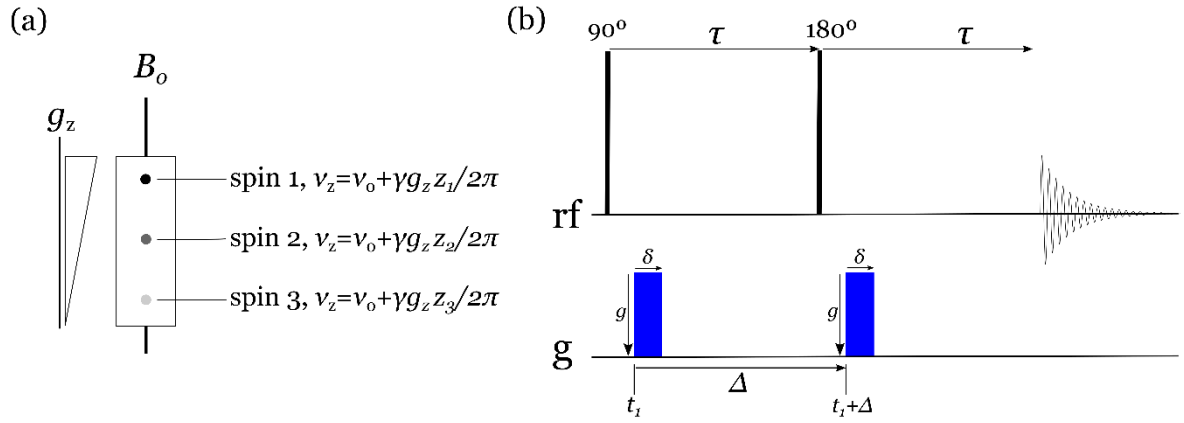

Figure 14. The principle of Pulsed Gradient Spin-Echo (PGSE) NMR experiments. (a) The spins are spatially labeled with a Larmor frequency that changes linearly with the magnitude of magnetic field; (b) The spin-echo based PGSE pulse sequence.

PGSE-NMR (Figure 14 b) is the most common pulse sequence used to measure translational diffusion. It employs two magnetic field gradient pulses during the dephasing and rephasing periods of a spin echo experiment The magnetic field gradient is defined as $g_i=\partial B_z/\partial i$ where i indexes the possible spatial directions x, y, and z; typically, one works with a linearly varying field that implies a constant magnetic field gradient along the sample. Usually, it is the gradient g_z that is explored, which implies that along the z axis the Larmor frequency of the spins changes linearly (Figure 14 a). The effect of the gradient during precession can be depicted as if the magnetization is twisted in a helix with axis z, where the precession angle of spins changes along the z axis according to the magnitude of the gradient or the duration of the gradient pulse.[136,138] The initial 90° RF pulse turns the magnetization to the transverse plane. During the first τ period and at time t_1, a gradient pulse of duration δ and magnitude g is applied. After the end of the first τ period, a 180° RF pulse is applied that has the effect of reversing the sign of the precession; in effect, it reverts the handedness of the helix mentioned above. At time t_1 +Δ, a second gradient pulse of equal magnitude and duration is applied. If the spins maintain their positions during the Δ period and thereby maintain also their Larmor frequency, the effects of the two applied gradient pulses cancel and all magnetization refocuses completely and provides maximum signal. On the other hand, if the spins have undergone some translational diffusion which changes their position during the time Δ, their Larmor frequency at the time of the two gradient pulses differ, which yields incomplete refocusing and an attenuation of the signal.[138]

In the pulsed gradient stimulated echo (PGSTE) pulse sequence, during the diffusion time Δ, the magnetization is stored along the z axis (Figure 15). The new concept of this pulse sequence is that the signal decay due to diffusion competes with longitudinal, rather than transverse relaxation. The use of this pulse sequence is particular advantageous for the study of the translational diffusion of larger molecules and aggregates, for which T_2 can be much shorter than T_1.[135, 138]

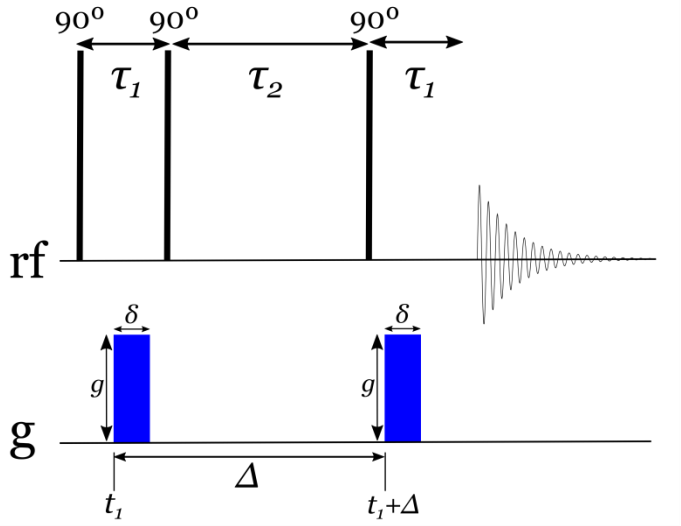

Figure 15. The Pulsed Gradient Stimulated-Echo PGSTE pulse sequence.

The attenuation of the NMR signal S due to the translational diffusion depends on three variables: the magnitude of the magnetic field gradient g, the pulse duration δ and the diffusion time Δ as summarized by the so-called Stejskal-Tanner equation [137]

$$\frac{S}{S_0} = e^{\left[-D(\gamma\delta g)^2 (\Delta-\delta/3)\right]} \qquad (2.12)$$

where S_0 is the signal without any gradient applied. Typically, translational diffusion is measured by recording the signal attenuation (S/S_0) as field g is increased. The diffusion time Δ can also be manipulated in order to observe the time dependence of diffusion, e.g. to study the restricted diffusion inside porous material or to follow exchange between sites.[136]

Experimental aspects

The majority of the ^{1}H NMR diffusometry experiments were carried out in Bruker Avance III spectrometer equipped with a standard-bore magnet providing a 500 MHz resonance for ^{1}H nuclei and a z-gradient probe Bruker DIFF30. The gradient pulses were provided by a Bruker GREAT 60 gradient amplifier. All the measurements were carried out at 20.0 °C and the gradient strength was calibrated by measuring the diffusion of ^{1}HDO in D2O (1.63×10^{-9} m^2·s^{-1}) at 20 °C. In order to be able to measure low volumes, Shigemi tubes were used.

2.3. Additional characterization techniques

2.3.1. Microscopy

Polarized light microscopy

For common observations of colloidal aggregates, regular non-polarized light is used. However, when anisotropic materials like liquid crystals are observed, one can exploit birefringence as a source of extra contrast. This requires linearly polarized light. Polarization is achieved by placing a polarizer filter along the optical path where the highly aligned structure of the filter interferes with the electric component of the electromagnetic radiation, and permits only waves with the electric field vector along one particular direction (polarization axis). When polarized light propagates through an anisotropic material, this direction is altered which can be evaluated by a second polarizer placed between the sample and the eyepiece of the microscope, typically in a way that the polarization axis is at 90º with respect to that of the first polarizer. Hence, the only light that crosses must have propagated in a region containing anisotropic and optically transparent material.[139]

Liquid crystalline phases are birefringent, and when analyzed in a microscope using polarized light, characteristic optical textures are observed. These textures arise from the birefringence phenomenon resulting from structural defects in the liquid crystalline-phase. Because the defects are intrinsic to the nature of the liquid crystalline phase, the texture observed is characteristic of that particular phase. Thus, through comparison of the observed image with a known characteristic texture, it is possible to assess a liquid crystalline phase. Figure 16 displays the fan shaped textures which enable the assignment of smectic phases A and C, respectively.

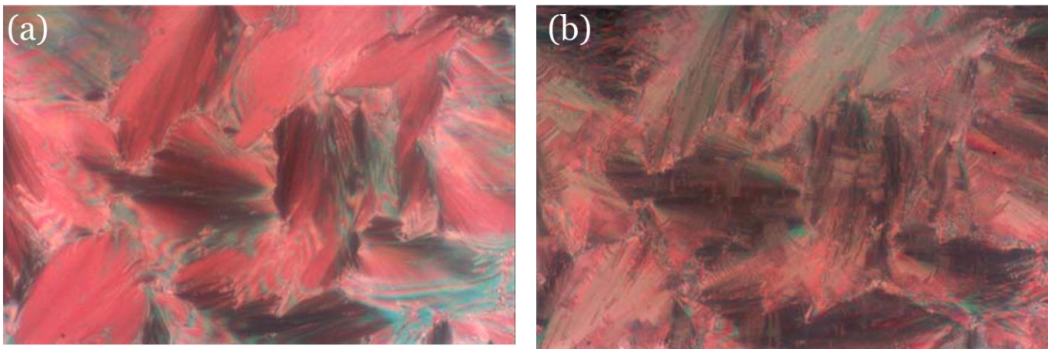

Figure 16. Optical textures observed in polarized light microscopy. (a) fan-shaped SmA texture; (b) Same sample area as (a), showing the transition to the broken fan-shaped texture with helix lines of the SmC phase. Reprinted with permission from Wiley-VCH.[120]

Differential interference contrast

The microscopic observation of some aggregates is sometimes not possible using simple light microscopy because of the lack of contrast between the aggregate and the surrounding medium (water). This problem can be circumvented by using the technique of differential interference contrast (DIC), that enhances the contrast. DIC is based on the principle of interferometry to gain information about the length of particular optical path. To do this, polarized light is manipulated to provide contrast between parts of the sample with different composition but similar refractive index or different thickness.[139]

In the DIC experiment, a polarized beam is split by the use of a Nomarski prims into two perpendicularly polarized mutually coherent beams which are spatially displaced at the sample plane, and recombined by a second Nomarski prism before observation. The orthogonal beams cross the sample in different regions, thereby they will experience different propagation conditions that influences their transmission. When the second Nomarski prism recombines the beams into one, interference will appear. This produces the appearance of a 3-D physical relief which corresponds to the variation of the optical density of the sample.

Experimental aspects

The microscopic observations were carried out using an Olympus BX51 polarized light microscope equipped with a differential interface contrast system. For the study of the thermotropic behavior of gemini surfactants, a Linkam TMHS heating stage controlled by a TP94 unit was used. For the observation of microscopic aggregates formed by nanotubes, the differential interface contrast mode was used together with an Olympus C-5060 Wide Zoom digital camera.

Cryo-Transmission Electron Microscopy

Electron microscopy allows direct observation of nanostructures due to its subnanometer compared to micrometer resolution in light microscopy. The limiting condition in light microscopy lies on the wavelength of visible light, but this obstacle can be overcome by using accelerated electrons instead of photons to visualize the sample. In order to control both focusing and magnification, the conventional optical lens system is replaced by electromagnetic lenses.[140] High-resolution electron microscopy requires high vacuum inside the microscopic chamber ($p < 10^{-5} - 10^{-6}$ Pa) in order to avoid interferences with the electron beam that interacts with the sample, which is a drawback for hydrated samples. Therefore, samples need to be either dried or vitrified (ultra-fast cooling) to reduce their vapor pressure. Drying is not an option in colloidal systems in which the liquid is essential for the formation of the structures (e.g., micelles or vesicles). Moreover, to prevent structural modification due to slow cooling (and subsequently formation of ice crystals) of

samples, (Figure 17) the sample is cooled extremely rapidly (1×10^5 K/s) and thereby vitrified, i.e., remains in amorphous state.

Cryo-TEM is an excellent tool to visualize nanostructures in liquid samples, provided that those can be properly vitrified.

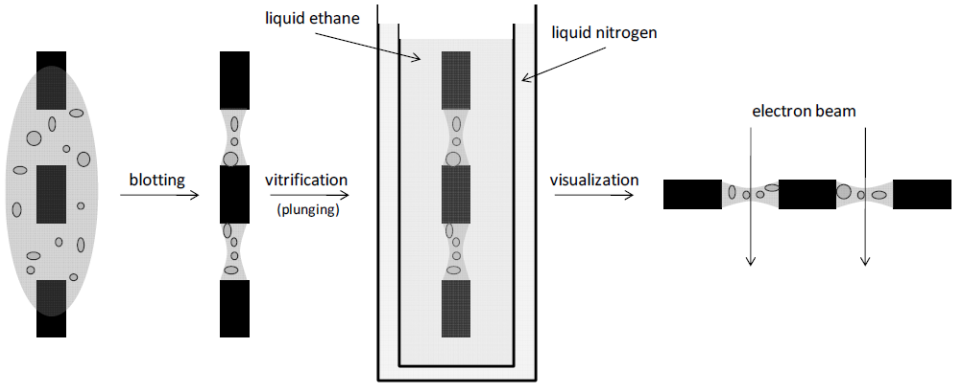

Figure 17. Schematic representation of the vitrification method used in cryo-TEM sample preparation. A drop (≈4 μL) of the sample is placed in a copper grid (represented as the black dashed region); the excess of liquid is blotted way, flowed by vitrification in liquid ethane. The sample is transferred to the TEM and visualized.

Experimental aspects

The sample support in cryo-TEM experiments is typically a copper grid, covered with a lacey polymer film. The specimens are prepared by dropping an aliquot (≈4 μL) of solution on the grid. Excess solution is blotted away with filter paper, resulting in a film that spans the holes of the polymer support, and whose thickness (>200nm) allows both a high cooling rate and a high transmission of the electron beam. The sample is then plunged into liquid ethane (≈92 K) in order to rapidly vitrify and then stored in to liquid nitrogen (< 77 K) before being transferred to a TEM (Tecnai 12, FEI) using a Gatan workstation and cryo-holder for imaging at 98K. The microscope was operated at 120 kV in low electron dose mode (to reduce radiation damage) and with a few micrometers under-focus to increase phase contrast. Images were recorded on a Gatan 794 CCD camera.

Cryo-Scanning Electron Microscopy

Scanning Electron Microscopy (SEM) produces images of a sample by scanning it with a high energy beam of electrons (primary beam). The interaction of electrons with the atoms in the sample yields secondary electrons that arise from those regions that are close to the sample surface. The secondary electrons are ejected from the valence shell of atoms. For these reasons, SEM provides information about sample topography and composition. The images obtained with SEM have a three dimensional appearance due to lateral and depth resolution, which is particularly useful to understand the morphology of any nano- or micro-structures present.[140]

Experimental aspects

The vitrification process for SEM is carried out by the immersion of the sample in nitrogen slush. The sample is fractured *in situ* and the solvent is sublimated, exposing the bulk structural details. If the sample is not electrically conductive, it needs to be sputter-coated with a thin conductive film (e.g. Au/Pd alloy) to drain the charge transferred by the primary electron beam. The images were acquired using a JEOL JSM 6301F SEM microscope equipped with a Gatan Alto 2500 cryo-preparation chamber.

2.3.2. X-ray diffraction

X-ray diffraction (XRD) is one of the most used techniques to characterize the structure of crystalline and liquid-crystalline materials. In common XRD diffractometers, X-ray are generated in a cathode ray tube where electrons are accelerated to bombard a metal target. As electrons plunge in the metal, they decelerate and generate a radiation with a continuous range of wavelengths called Bremsstrahlung. In addition, collision with an electron from the inner shell of the metal atom may eject an electron from the shell. Another electron of higher energy drops then into the vacancy, emitting the excess of energy as an X-ray photon of well-defined wavelength. If the electron falls into a *K* shell, the X-rays are classified as *K*-radiation.[4] The most common equipment uses copper as metal target, with CuK_α monochromatic radiation with a wavelength of $\lambda = 0.154$ nm. These X-rays are collimated and directed onto the sample. Electrons in the sample scatter the incoming X-rays in all directions. As the sample and detector are rotated, the intensity of the reflected X-rays is recorded. Depending in the structure of the sample, at certain angles constructive interference of the scattered X-rays occurs and a diffraction peak is observed.[141-143]

Crystalline materials are characterized by a periodic repetition of a structural unit. Figure 18 shows the representation of Bragg's law for a simple lattice crystal modulated as stacks of parallel planes of separation *d*. When wave 1 hits the point D on the surface of the plane, the extra path length traveled by wave 2 at a scattering angle θ is given by:

$$AC+BC = 2d \sin \theta \qquad (2.13)$$

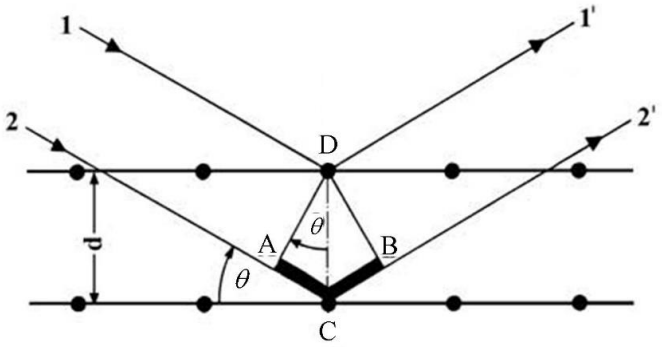

Figure 18. Schematic representation of Bragg's law of diffraction for parallel planes. *d* is the distance between the planes, θ is the diffraction angle and A, B, C and D are the points used to calculate the path length.

Constructive interference occurs (i.e. scattered waves are in phase) when the path length difference between the two waves is equal to an integer of the wavelength λ, i.e. (AC+BC) =nλ. Thus, equation 2.13 becomes:

$$n\lambda = 2d \sin\theta \qquad (2.14)$$

The equation above is known as Bragg's law. An XRD diffractogram usually presents the diffracted intensity, *I*, as a function of the scattering angle 2θ. Bragg reflection peaks occur when at certain angles the scattered waves are in phase. Bragg's law can also be expressed in terms of the modulus of the scattering vector *q* by

$$q = n\frac{2\pi}{d} \qquad (2.15)$$

where n is the order of the scattering peak. For the case of parallel planes, such as thermotropic smectic phases or lyotropic lamellar phases, *n* is a series of integers (1:2:3:4:5.). Table 1 presents the ratios of *q* values of the peaks in the diffractogram and the structural organization of the most common lyotropic liquid crystalline phases.[114]

Table 1 Ratios between q-values and the phase identity.

n	Lamellar	Hexagonal	Cubic (primitive)	Cubic Pn3m	cubic Fd3m	cubic Lm3m	cubic la3d
1	√1	√1	√1	√2	√3	√2	√6
2	√4	√3	√2	√3	√8	√4	√8
3	√9	√4	√3	√4	√11	√6	√14
4	√16	√7	√4	√6	√12	√8	√16
5	√25	√9	√5	√8	√16	√10	√20
6	√36	√12	√6	√9	√19	√12	√22

Experimental aspects

The X-ray powder diffraction spectra of the solid state gemini compounds were recorded at room temperature with a PANalytical X'Pert MPD diffractometer using the λ = 0.154 nm *K*α line of a Cu anode (Bragg–Brentano geometry) equipped with a X'Celerator detector. The spectra were obtained from 10 to 95° (2θ), using a step of 0.017° and 100 s/step.

2.3.3. Differential scanning calorimetry (DSC)

Differential scanning calorimetry (DSC) is a widely used technique for the thermal analysis of materials. This technique allows the quantification of the heat absorbed or released during a given physical or chemical process. The designation differential is due to the fact that the behavior of a sample is compared with a reference material which does not undergo any chemical or physical change during the analysis. The term scanning comes from the fact that the temperature of the sample and reference is increased or decreased in a controlled manner, to enable continuous measurement over a range of pre-determined temperatures.[144, 145]

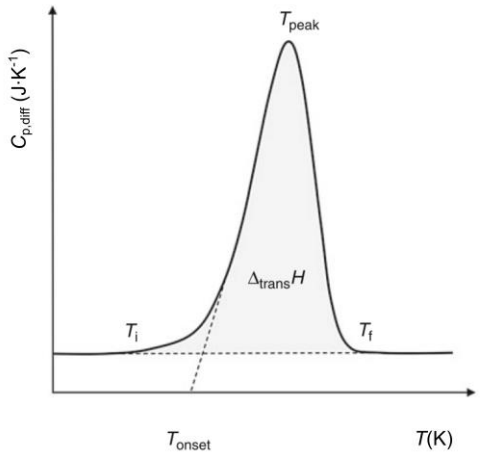

Figure 19. Representation of a thermogram with a first order transition and its parameters. Reprinted with permission from Springer.[114]

This technique provides a thermogram (Figure 19), which is usually a plot of the heat flow (or differential heat capacity) as function of temperature (or time). The thermogram analysis allows the determination of the enthalpy change during a physical process, e.g. a phase transition.[144, 145]

Experimental aspects

DSC scans were performed using a Setaram DSC141 differential calorimeter. The equipment was previously calibrated, both for temperature and energy, using benzoic acid, indium and tin as reference compounds. A mass of 6-12 mg of solid compound was weighed to Al crucibles, and an empty crucible was used as a reference. The heating-cooling cycles were performed at a scanning rate of 3 K min-1

in a temperature range of 20-250 °C, with nitrogen (p = 0.3 bar) used as sweeping fluid. Five independent essays were typically run for each compound, with at least one heating-cooling scan for each sample.

2.3.4. Thermogravimetric analysis (TGA)

Thermogravimetric analysis (TGA) is an experimental technique in which the mass of a sample is measured as a function of temperature or time. Typically the sample is heated at a constant rate or held at a constant temperature (isothermal measurement). The temperature range of the analysis will depend on the type of information required about the sample. Moreover, the atmosphere used in the TGA experiment plays an important role and can be reactive or inert. Changes of the atmosphere during the measurement are also possible. Mass changes occur when the sample loses material or reacts with the surrounding atmosphere.

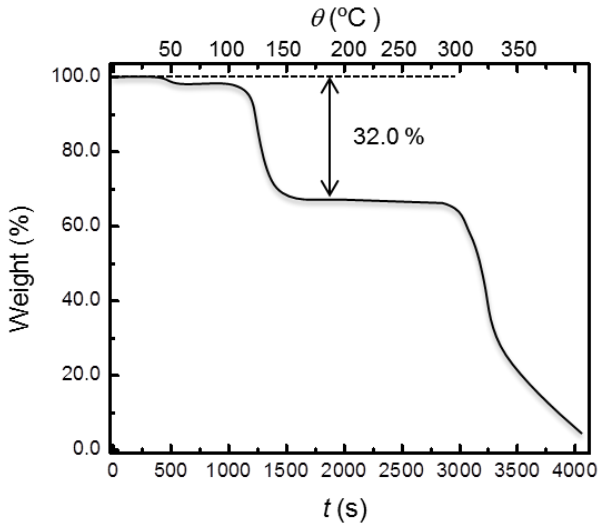

Figure 20. Thermogram from thermogravimetric analysis.

The output data from TGA is a thermogram (Figure 20), where the variation of mass is represented as a function of temperature (or time). Typically, when a thermogravimetric analysis of a mixture of different components is carried out, the most volatile components start to evaporate/sublimate or thermally decompose in gaseous products (if the products are not in the gas state no mass variation is detected). Therefore, if the components decompose at different temperatures with well-defined mass variations (steps), the composition of the mixture is easily determined.[146] The measurements can be carried out in air, nitrogen or other gases.

Experimental aspects

TGA measurements were carried out in a Mettler Toledo Star System (Mettler TGA/STDA851) under N_2 atmosphere at flow rate of 50 ml/min, for a heating rate of 10 ºC/min from 100 to 430 ºC. Aluminium crucibles of 100 µL of volume were used.

2.3.5. UV-vis

Ultraviolet-visible spectroscopy (UV-vis) refers to the absorption of electromagnetic radiation in the ultraviolet-visible spectral region. This type of spectroscopy corresponds to the electronic transitions of electrons in the molecular orbitals, which falls in the UV-vis region of electromagnetic spectrum. Molecules which contain π and non-bonding electrons can absorb photons with a given energy (i.e. wavelength in the UV-vis region) that matches the energy difference between the electron states. A spectrometer records the wavelength at which absorption occurs, together with the absorbance at each wavelength.

Because absorbance is proportional to concentration of absorbing molecules it is possible to carry out quantitative measurements of different analytes. Carbon nanotubes absorb in the UV-vis region as mentioned in the section 1.1.1 and shown in Figure 21. Because nanotubes may also scatter light, the term optical density (or apparent absorbance) is preferably used within this thesis instead of absorbance.

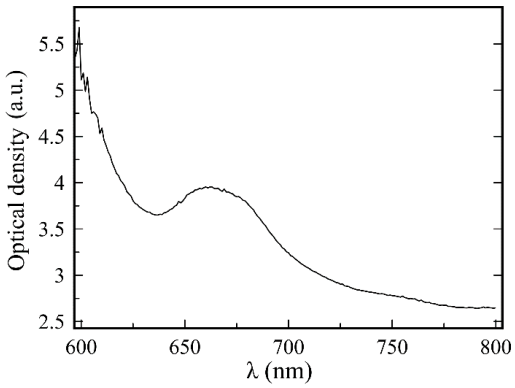

Figure 21. UV-Vis spectrum of a SWNT dispersion, stabilized by Pluronic F127 in water.

The Beer-Lambert law, which relates the apparent absorbance A of a liquid medium, having an optical path b and a extinction coefficient ε, with the concentration c according to

$$A = -\log T = \log \frac{I_0}{I} = \varepsilon b c \qquad (2.16)$$

where T is the transmittance, I_0 is the intensity of the incident light and I is the transmitted intensity. The amount of CNT dispersed in a given sample is determined by measuring the absorbance in relation to that of an aqueous dispersion with a known CNT concentration. Combining the TGA results with the UV-vis it is possible to calibrate the apparent extinction coefficient to mass.

Experimental aspects

The spectra were obtained using double beam (U- 2001 and Varian Cary 300 Bio) spectrometers. The dispersions were properly diluted to keep the apparent absorbance in a measurable range and absorbance was then recorded at λ = of 660 nm.

3. Summary of the research

In this chapter, a summary of the main results of this thesis is presented. We first explored the dispersibility of CNTs using high molecular-weight dispersants (namely, an amphiphilic polymer and a protein) where the exchange dynamics, the surface dynamics of the polymer onto the CNT surface, and the competitive adsorption of protein/polymer dispersants to the surface of nanotube were addressed (paper I and II). Additionally, a systematic study of the dispersibility of CNTs using low molecular-weight dispersants (surfactants) was investigated (paper III). The relative binding strength of the surfactant dispersants, and the effect of mechanical agitation on the dispersed CNTs were also subject to investigation (paper IV and V, respectively). In another study, the dispersibility of CNTs was evaluated using gemini surfactants, where the effect of the hydrophobicity of the surfactant (chain and spacer length) was explored (paper VI). Investigations on liquid crystal/CNT interactions were also attempted in this thesis. The thermotropic behavior of gemini surfactants in the absence of nanotubes was addressed (paper VII), and some exploratory work on gemini surfactant-CNT interactions was carried out.

3.1. Dispersibility and binding dynamics: high molecular-weight dispersants

In order to get a deeper insight into polymer-assisted CNT dispersions, we must follow the dynamics established between the dispersant and the nanotube at equilibrium. To fulfil this goal, NMR diffusometry was used, which allowed to quantify the fraction of dispersant adsorbed, to detect the surface displacement of dispersant on the CNT surface, and to assess the relative binding strength of polymer and protein (competitive adsorption) to the nanotube surface, as depicted in Figure 22.

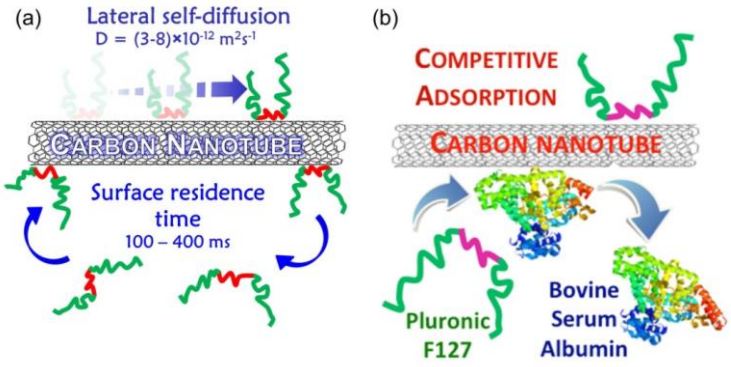

Figure 22. Main findings obtained for the dynamics established between the dispersant and the CNT by NMR diffusometry: (a) lateral diffusion of a triblock copolymer (Pluronics F127) onto the nanotube surface and the residence time; (b) competitive adsorption of dispersants onto the CNT surface where the relative binding strength is assessed.

3.1.1. Slow exchange and adsorbed polymer amount

The behavior of a triblock copolymer, Pluronics F127 $(PEO)_{97}$-$(PPO)_{69}$-$(PEO)_{97}$, on the SWNT surface was evaluated by NMR diffusometry. The diffusional decay of ^1H NMR methylene signal of F127 was found to be not single exponential, but instead have a more complex profile. Changing the diffusion time Δ allowed to conclude that F127 unimers were in slow exchange (within the NMR experimental time scale, Δ) between a slow- and a fast-diffusing site.

The two diffusing sites were identified as follows: 1) the fast decay corresponds to the free F127 unimer in solution and 2) the slow decay is assigned to the F127 bound to the SWNT surface. In order to extract the residence time, τ_{bound}, and the fraction of F127 adsorbed on the SWNT, fits of the diffusional decays at different Δ using the Kärger model were attempted.[147, 148] The data could not be fitted together, as shown in Figure 23 a, indicating the possibility of a distribution of residence times on the SWNT surface. The data were then fitted pairwise (Figure 23 b,c,d), by using those with shortest available diffusion times (Δ =10 and 20 ms) and those with the longer diffusion times (Δ=100, 200 and 500 ms). It was then possible to observe that the fitted residence times, τ_{bound}, get longer with the increasing diffusion times, with a distribution between 100 to 400 ms. In addition, the fraction of F127 adsorbed on nanotube is merely 6 – 8 % of the total F127 in the dispersion.

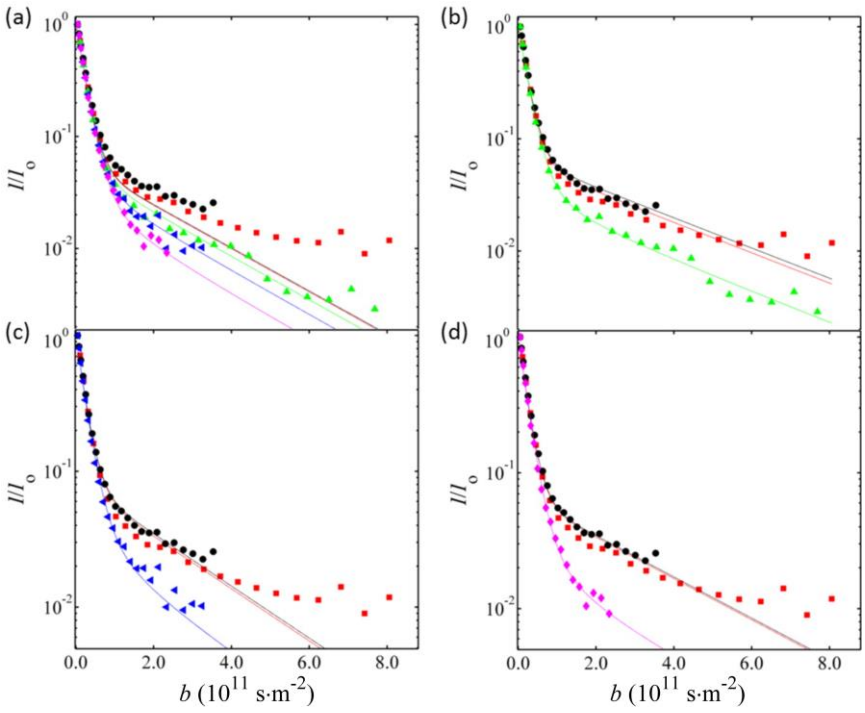

Figure 23. (a) Fitting the Kärger model simultaneously to all diffusion data collected with diffusion times ranging from 10 to 500 ms. In (b-d), the fits are to the data collected on one hand at the shortest diffusion times (Δ=10 ms, black symbols and Δ = 20 ms, red symbols) and on the other hand to data collected at one of the longer diffusion time (b) Δ = 100 ms, green (c) Δ = 250 ms, blue and (d) Δ = 500 ms, magenta.

3.1.2. Lateral diffusion and the wrapping/non-wrapping picture

Although the milliseconds time scale may be perceived as short in some context, it is still long as concerning conformational dynamics of the polymer. In particular, PEO and PPO chains are known to possess high flexibility and fast internal dynamics. This internal dynamics should permit the polymer to change its conformation also in relation to CNT, thus providing a mechanism for molecular displacement on the CNT surface. Therefore, the slow component in the diffusional decay is assigned to the polymer molecules diffusing on the nanotube surface. Taking into consideration that the lateral diffusion of polymer on nanotube axis is essentially one dimensional, the decay was fitted to 1-D isotropic diffusion.[136, 149] Despite some complications that can arise due to the orientation of nanotubes with the magnetic field, a lateral diffusion coefficient could be estimated, $D_{\text{lateral}} = (3\text{-}8) \times 10^{-12}$ m^2·s^{-1}. The depicted molecular picture (Figure 22 a), in this case, is consistent with a nonwrapping mode for the polymer-nanotube interaction.[78, 79, 150]

3.1.3. Surface coverage and competitive binding between polymer and protein

The binding affinity of dispersants to the CNT surface is closely related with the dispersibility and the kinetic stability of nanotubes in water. NMR diffusometry was used to assess the relative binding strength of different dispersants to SWNT surface, where F127-SWNT is used as a reference system. Diffusion NMR enables the quantification of the fraction of F127 that is bound to the SWNT and the fraction that is free in the bulk. Therefore, by adding a second dispersant to the system one can monitor how the fraction of adsorbed F127 changes. One can compare directly the binding strength of the second added dispersant, and check 1) if that dispersant replaces or not F127, 2) to which extent it does so (if at all) and 3) how the replacement changes with concentration. Therefore, we can compare a series of dispersants and quantify the extent to which the dispersants can replace F127 on the SWNT surface. We firstly analyze a protein, leaving the case for low molecular weight dispersants for §3.2.2.

The protein Bovine Serum Albumin (BSA) is known to be a good dispersant of CNTs. Moreover, the use of BSA as dispersant is both important to 1) potentially enhance the CNT biocompatibility and 2) to use it as a model for CNT−biomolecules interactions. Understanding the binding competition between BSA and synthetic polymers is also important for drug formulations (were CNT acts as a drug carrier) or to mimic the mammalian body where albumins are present and would interact with CNTs.

In the light of this, we performed a study where BSA was added to a F127−SWNT dispersion (and conversely F127 to BSA-SWNT) to evaluate the relative binding strength and observe if one of the dispersants can replace the other (paper II). In order to assess and understand the effect of adding BSA to the F127-

SWNT dispersion, we started with a simpler scenario by adding a small aliquot of a F127 concentrated solution to the original SWNT dispersion. Figure 24a presents the diffusional decay of the oxyethylene signal after having increased by Δc_{F127} the concentration of F127 in the dispersion. Fitting the diffusional signal decay to a two-site model, it is possible to extract the fraction f_{F127} that is adsorbed to the nanotube surface. The obtained f_{F127} (Figure 24 b) shows that upon addition of F127 the relative population of F127 adsorbed to the nanotube decreases monotonically, indicating that the SWNT surface is saturated and the adding of F127 only increases the fraction of free F127.

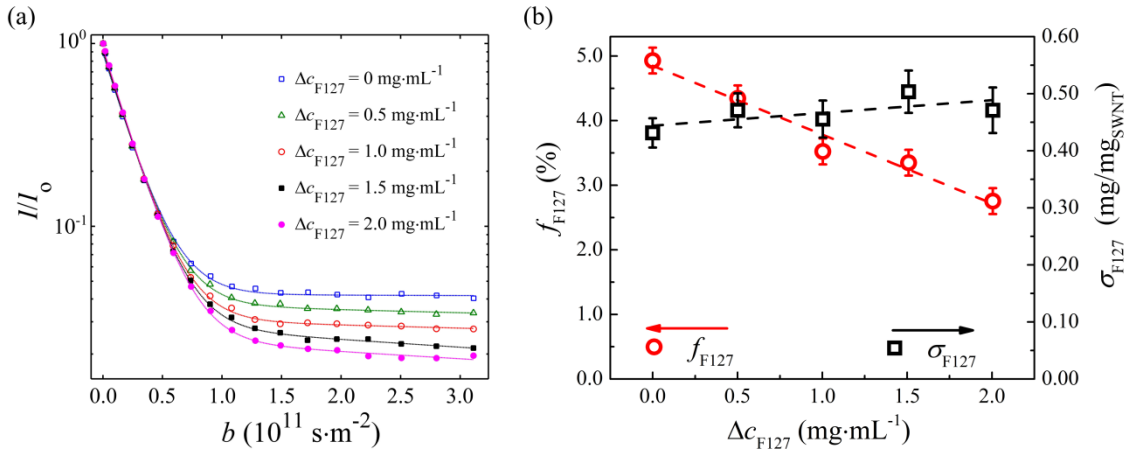

Figure 24. The diffusional decay of the 1H NMR signal from the F127 oxyethylene peak as function of Δc_{F127}, the amount of F127 added to an F127-SWNT dispersion. The lines are two-component exponential where the amplitudes of the two components provide the populations of the free aqueous (fast component) ad surface-adsorbed (slow component) F127 populations

Since we know both the total concentration of F127 (c_{F127}) and the total amount of SWNT (c_{SWNT}), the surface coverage of the nanotube (σ) is obtained by

$$\sigma_{F127} = (f_{127} \times c_{F127})/c_{SWNT} \qquad (3.1)$$

As figure 24 b shows, this apparent surface coverage remains constant (within the data uncertainty), or at best slightly increases, despite the fact that c_{F127} increased twofold.

Since we had previously established that the exchange time between these dispersants is below 1 s, a few minutes are expected to be enough to establish equilibrium between both dispersants and the nanotube surface. The dispersant with higher binding affinity should have a higher surface concentration. The effect of adding BSA to the F127-SWNT dispersion is shown in Figure 25. As is clear, adding BSA does not decrease significantly the apparent surface coverage of SWNTs by F127 (σ_{F127}). The most straightforward explanation for this behavior is that the binding strength of BSA to the SWNT surface is significantly lower than that of F127.

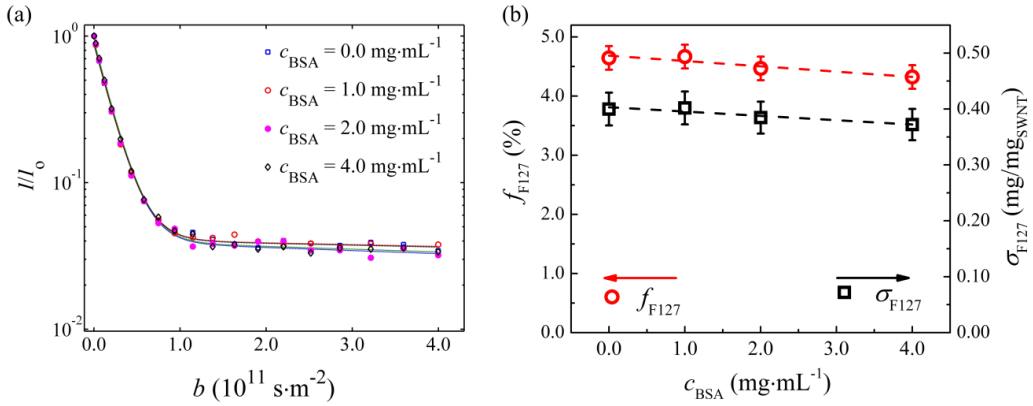

Figure 25. (a) The diffusional decay of the 1H NMR signal from the F127 oxyethylene peak as a function of BSA added to a F127-SWNT dispersion. The lines are two-component exponential fits; (b) The population fraction of F127 (f_{F127}) adsorbed on the SWNT surface and the corresponding apparent surface coverage σ_{F127} by F127 molecules. The dashed lines are linear fits.

The reverse effect (i.e. adding F127 to the BSA-SWNT dispersion) was also tested in order to confirm the stronger binding strength of F127 to SWNT surface. Figure 26 presents the diffusional NMR decays of F127 added to BSA-SWNT dispersion. It is observed that part of the F127 molecules added to the dispersion adsorb to the nanotube surface, as evidenced by the appearance of the slow diffusion component in the decay. Figure 26 shows that with the increasing of F127 concentration, the fraction of polymer adsorbed to SWNT surface decreases. However, the apparent surface coverage increases with the increase of F127 concentration.

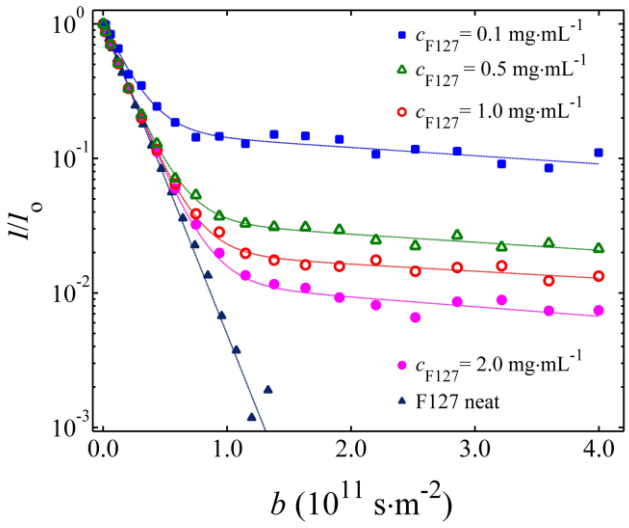

Figure 26. The diffusional decay of the 1H NMR signal from the F127 oxyethylene peak as a function of F127 added to a BSA-SWNT dispersion. The lines are two-component fits.

A comparison of Figure 25 and 26 can be most-easily interpreted as F127 binding to the CNT surface more strongly than BSA. Hence, in a system with dynamic equilibrium with continuously exchanging molecules, the CNT surface becomes preferentially covered by F127 even if it was originally covered by BSA. Conversely, an initial F127 coverage on the SWNT surface is kept, despite BSA having been added to the solution.

3.2. Dispersibility and binding dynamics: low molecular-weight dispersants

In this section a systematic study of the ability of low molecular-weight dispersants (herein, ionic surfactants) to disperse SWNTs and MWNTs is presented. The dispersed CNT concentration (c_{CNT}) in water was estimated using calibration curves (apparent extinction coefficient) obtained from thermogravimetric analysis combined with UV-vis spectroscopy. Two main types of surfactant, single- chained surfactants and gemini surfactants, were explored. For single-chained surfactants, the effects of 1) the presence of aromatic rings in the chemical structure, 2) alkyl chain length, 3) the head group charge and 4) morphology of CNTs (SWNT vs. MWNT) were assessed. The relative binding strength of some dispersants and the vortex mixing effect in the aggregation of nanotubes is also presented. Lastly, the dispersibility of CNTs using gemini surfactants, where the effect of the spacer and the hydrophobic chain length was evaluated, is presented.

3.2.1. Single-chained ionic surfactants: systematic studies and molecular insight

In Paper III the dispersion ability of several ionic surfactants (SDS, STS, SDBS, CPyCl, DTAB, TTAB and CTAB) to disperse CNTs was assessed. Both bath and tip sonication were employed to disperse CNTs and compared in terms of reproducibility of the obtained dispersions. Our main observations show that, even though the energy density transferred to the liquid is in the same order or magnitude, the tip is far more reproducible than the bath. Converting the energy density to shear stress both the sonication methods apply shear stress enough to exfoliate and fragment the CNTs. However, converting the power density to stress rate, the tip delivers much higher average stress rate. This stress rates can be related with the number of cavitation bubbles imploding *per* time, i.e. for tip sonication the implosions/s is much higher. Considering the kinetics effect of: 1) the rate of exposing a new CNT surface, 2) the rate of reattaching the exposed surface and 3) the rate of the surfactant to adsorb in the nanotube to avoid reaggregation; we can infer that the higher rates produced by the tip seem to be needed in order to assure a kind of “steady-state” to maintain the reproducibility of the data.

Figure 27 presents the dispersion curves, where the effect of varying c_s (surfactant concentration initially present in the dispersion, before sonication-centrifugation) on c_{CNT} dispersed is evaluated. All the dispersion curves show a sigmoidal profile. Several new metrics (presented for the first time) were extracted from dispersion curves after appropriate fittings to the data (Figure 27 d). The c_s required to effectively start dispersing CNTs is designated by us as the *critical dispersibility concentration* (*cdc*). After this point (i.e *cds*), c_{CNT} increases rapidly until a maximum value, $c_{CNT,max}$, is attained at the surfactant concentration denoted as $c_{s,max}$. In addition, two other metrics were introduced: the dispersion effectiveness, η, and the dispersion efficiency η^*. All these metrics were used to evaluate and compare the dispersion ability of the surfactants and rationalize it in the light of the chemical structure (presence of aromatic rings, alkyl chain length and polar head group).

The effect of nanotube morphology (MWNT vs. SWNT) on the nanotube dispersibility was evaluated Figure 27 (a and c). It is observed that the *cdc* and $c_{s,max}$ are always lower for MWNT than for SWNT. As concerning the dispersion effectiveness, η, and efficiency η^*, the studied surfactants are more effective dispersing MWNT (on a mass basis). However, we can analyze this result accounting the differences of the specific surface area (SSA) between SWNT and MWNT. We estimated that the SSA of SWNTs is ≈4 times that for MWNTs. Using that relation in the SSA, one can calculate the amount of surfactant $c_{s,max}$ at the $c_{cnt,max}$, which results in a surface concentration of 10 μmol·m^{-2}, that is ≈ 5 molecule·m^{-2} for both SWNT and MWNT. Thus, the surface concentration at saturation is similar for MWNT and SWNT pointing that adsorption of surfactant is not appreciably affected by the nanotube curvature.

The presence of the aromatic ring in the surfactant structure is assessed comparing the dispersibility of the pairs SDS vs. SDBS and CTAB vs. CPyCl. We observed that SDBS is the most efficient dispersant (both on mass and surface basis) for SWNT and MWNT. On the other hand, CPyCl that also possesses an aromatic pyridinium ring in the chemical structure does not present a significantly superior performance when compared with CTAB.

Analyzing the surfactant chain length effect, the dispersion effectiveness, η and efficiency η^* increases with the number of C atoms (nC) in the alkyl chain length. The zeta potential measurements also follow this trend. Since the zeta potential measurements were carried out at fixed c_s and c_{CNT} the increase in ζ is proportional to the increase of the surface charge, it seems reasonable to conclude that surfactants with higher nC adsorb more extensively, which is presumably related with a higher η and η^*.

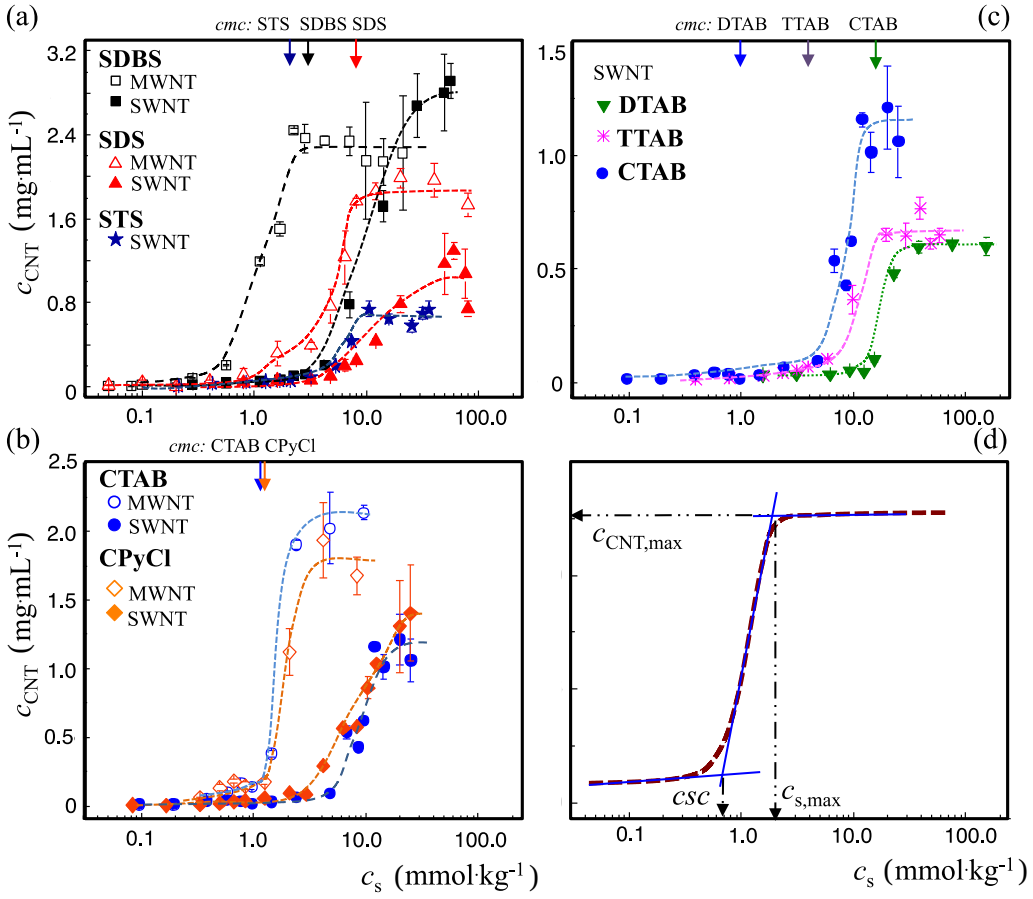

Figure 27. Concentration of dispersed MWNTs and SWNTs vs. surfactant concentration (log scale): (a) anionic surfactants SDBS, SDS and STS; (b) cationic surfactants CTAB and CPyCl; (c) homologous series DTAB, TTAB and CTAB; (d) representative curve with the graphical definition of the dispersion parameters. Lines are for visual guidance.

Due to the adsorption of surfactants onto CNTs surface, the presence of small bundles or individual nanotubes in a surfactant solution will shift the *cmc* to 10-50% higher values. However, before exfoliation, the nanotube powder is typically sedimented and we can assume that the fraction of the surfactant adsorbed on the powder has a minor effect on the *cmc*. Thus, it is valid use the *cmc* of neat surfactant to assess the role of micelles in the dispersibility of CNTs. During the exfoliation process two simple situations can happen: 1) micelles help as full aggregates in the exfoliation or 2) just act as a reservoir of unimer. In order to elucidate which of the situations are more favorable to the CNT exfoliation, we tried to find patterns in the dispersion curves correlating the *cdc* and the $c_{s,max}$ with the *cmc*. For the systems studied, no clear trends were observed in the metrics. Therefore, the presence of micelles does not seem to play any important role in the exfoliation process.

3.2.2. Surface coverage and competitive binding between polymer and surfactant

In paper IV the same methodology used to investigate the competing binding between the F127 and BSA was extended to ionic surfactants in order to assess the relative binding strength and correlate with other parameters such as dispersion efficiency and colloidal stability of nanotube dispersions.

For a given SWNT-F127 dispersion the surface coverage was calculate using equation 3.1. The addition of a second dispersant, the fraction of F127 adsorbed in the SWNT decreases. The replacement of F127 by DTAB, TTAB, CTAB, sodium cholate (SC), SDS, SDBS and CPyCl at different concentrations was evaluated. Figure 28 presents the relative capability of surfactants to displace the F127 from the SWNT surface. The results are correlated with the relative binding strength of each surfactant.

Clearly we can observe that DTAB has a limited capability to bind to the SWNT surface as compared to the other dispersants. On the other hand, SDBS is the surfactant with the highest relative adsorption strength. At lower concentration (0.5 mg mL^{-1}) CPyCl and S. cholate are the surfactants with higher affinity to the SWNT. As the concentration of surfactant is increased, SDS and SDBS are the surfactants with higher binding strength.

Within each class of (anionic and cationic) surfactants, those with aromatic rings present a higher relative binding strength to the SWNT surface. However, as concerning the charge of the polar head group, anionic surfactants present a relative higher binding strength.

Apparently the increase of the number of carbons in the chain length increases the binding affinity to the SWNT. Clearly DTAB has lower affinity to the surface than surfactants with higher number of carbons. However, comparing CTAB and TTAB the conclusions are not straightforward, and at higher concentration CTAB removes less F127 from the surface. However, we should have in mind that the measurements were carried out at 20 ºC (to avoid micellization of F127). Clearly this temperature is lower than the Krafft temperature of CTAB. The precipitation of CTAB was not detected by NMR, however, we cannot exclude the possibility that a small amount of CTAB is crystalized and thereby is not actively replacing the F127 on the SWNT surface.

In Figure 29 we tried to correlate the relative binding strength with the metric *cdc* obtained for the dispersants in paper III. The concentration unit was rescaled in units of *cdc*. We observe that all the data fall in a in a universal curve where at *cdc* all surfactants displace *ca* half of the F127 originally at the CNT surface. This finding provides us with a new hypothesis as concerning the origin of *cdc* – namely, dispersing by cleavage requires a particular threshold coverage that is characteristic for the nanotube.

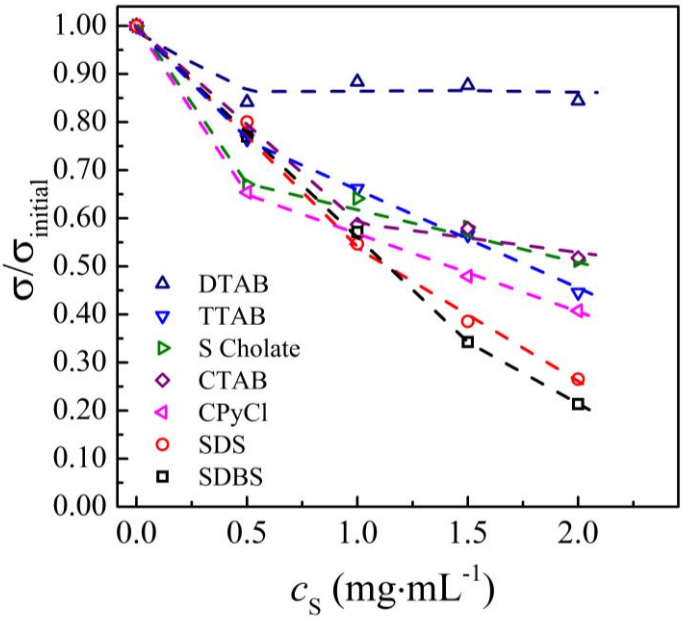

Figure 28. Normalized surface coverage as function of ionic surfactant addition. The lines are a visual guide.

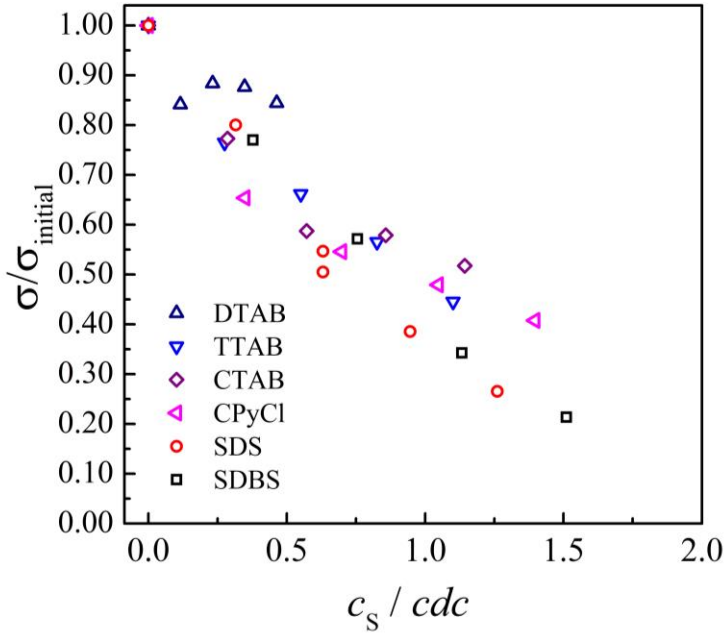

Figure 29. The change in surface coverage by F127 molecules (data as in Figure 28, except that for sodium cholate) with surfactants concentration normalized by the critical dispersion concentration, *cdc*. The *cdc* data was taken from paper III.

3.2.3. Aggregation of pre-dispersed CNTs induced by mechanical agitation

Vortex-shaking is typically used to fragment and disperse insoluble materials in a solvent. However, we observed an aggregation process of pre-dispersed CNTs that, contrary to expectation, is induced by vortexing. The vortex mixer produces a turbulent regime flow that enhances the collisions between the dispersed CNTs in water nanotubes, forming micron-sized loose structures.

In paper V the effect of the vortex mixing is evaluated for several SWNT−dispersants (cationic: DTAB, CTAB; anionic: SDS, SDBS; and nonionic: F127, F68 and TX-100). It was observed that the aggregates display an irregular morphology similar to a fractal. These aggregates are noncompact and are easily redispersed by bath sonication. Therefore, we designate them as loose aggregates.

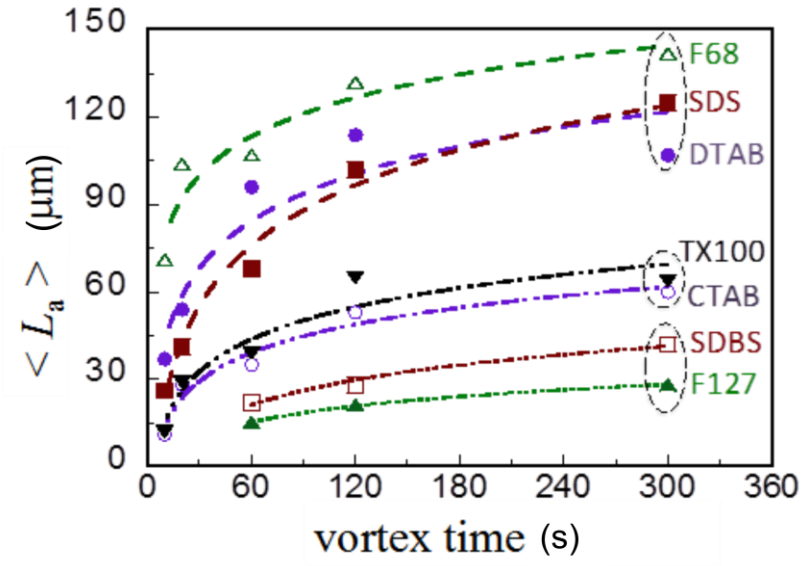

Figure 30. Dependence of average loose aggregate size with the vortex time for different surfactants. The c_{SWNT} was kept constant in all the studied systems.

The aggregates were visualized using video-enhanced light microscopy (VELM) and the size of the aggregate was characterized by the length (L_a) of the higher axis. In Figure 30, we present the average length $<L_a>$ of the loose aggregates as function of vortexing time for different the dispersant-SWNT systems. Clearly, some trends in the average size can be observed. Vortexing induces aggregation for all the surfactant–CNT systems, with $<L_a>$ increasing with vortexing time. However, there are significant differences in the average size $<L_a>$ for the different SWNT-surfactant systems. SDBS and F127 take longer time to form visible aggregates, experience a slower rate of growth and form the smallest ones ($<L_a>$ = 20–40 μm). On the other extreme, F68 and DTAB form the largest aggregates ($<L_a>$ = 40–140 μm) and undergo a sharper growth rate.

For the two block copolymers used (F127 and F68), we observed two extreme behaviors. On one hand for F127 $(PEO)_{97}$-$(PPO)_{69}$-$(PEO)_{97}$ the aggregates are quite

small, on other hand F68 $(PEO)_{76}$-$(PPO)_{29}$-$(PEO)_{76}$ display larger aggregates. Both the polymer and nanotube concentration are identical, thus we can argue that the main difference is due to the effective steric repulsion exerted by each polymer. Indeed, the longer hydrophobic block of F127 (≈69 PPO monomers), which provides a stronger anchoring to the nanotube, combined with a bigger PEO block (≈97 PEO monomers) is the cause for this difference between the two polymers. Not surprisingly, F127 shields more efficiently the CNT, which results in much smaller aggregates.

SDBS is a good dispersant of nanotubes (as shown in paper III), mainly due the π-π interactions established with the CNT surface. Therefore, it is expected that it will also be a good shielding surfactant, which will reflect on smaller aggregate size. Indeed, this is the case. Analyzing other surfactant with aromatic ring in the hydrophobic region, Tx-100, we observe that it is not as efficient as SDSB in shielding the nanotubes, hence producing bigger aggregates. This can be explained by the smaller (and branched) hydrophobic tail of Tx-100 (as compared with SDBS) which will perhaps result in a lower adsorption to the nanotube (less coating). In addition,TX-100 stabilizes the nanotubes by steric repulsion. The headgroup is a oxyethylene block $(PEO)_{10}$ composed by ≈ 10 monomers, but quite small when compared to the F127 or F68, and thus the steric repulsion is also weaker. The surfactant DTAB, which is not a very good dispersant as we pointed in paper III, not surprisingly also presents quite big aggregates suggesting that the shielding is weak. Conversely, CTAB, a surfactant with higher n_C and observed to be a good dispersant in paper III, also presents a quite good shielding effect. Analyzing the behavior of SDS aggregates, one observes an intermediate behavior - slightly better in shielding than DTAB at shorter vortexing times.

The effect of relative centrifugation force, g, was also assessed in the formation and growth of aggregates. The vortexing time effect was tested for a SDS-SWNT dispersion centrifuged at four different g-grades - [2, 4, 10, 30]×10^3 g. As presented in paper V, it was observed that for higher g values more vortexing time was necessary to induce the growth of the aggregates. At higher g, bigger bundles are sedimented in the precipitate. Thus, if bundles have a role similar to a nucleation process, i.e. the presence of bigger bundles are favorable to the formation and growth of aggregates, it is expected that for higher g forces more time will be necessary to grow the aggregates.

Different concentrations of SWNTs were also tested (at constant 4×10^3 g). The general observation was that as c_{SWNT} increases $\langle L_a \rangle$ also increases. This effect seems to be related with the higher amount of nanotubes which results in high frequency of collisions, originating a larger mesh structure.

Mechanism of aggregation

Molecular dynamics simulations have shown that the surfactant coating is more vulnerable for a pair of perpendicular tubes – i.e. shielding that prevents nanotube aggregation is less effective if nanotubes collide perpendicularly.[56, 151] Therefore, we can assume the same happens when nanotubes collide at more favorable angles. Additionally, if the nanotube is not totally coated and possess free areas, these areas can act as bridging points. Vortexing induces the collision of the nanotubes, creating bridging points that originate a network. In Figure 31, the microstructure of the aggregates can be observed at different scales. Clearly, an aggregate is observed using VELM. In the Cryo-SEM, an entangled structure of nanotubes is observed. By increasing the magnification (in the cryo-TEM), we can see several nanotubes linked forming a mesh-like network, which supports our molecular model (Figure 31 d).

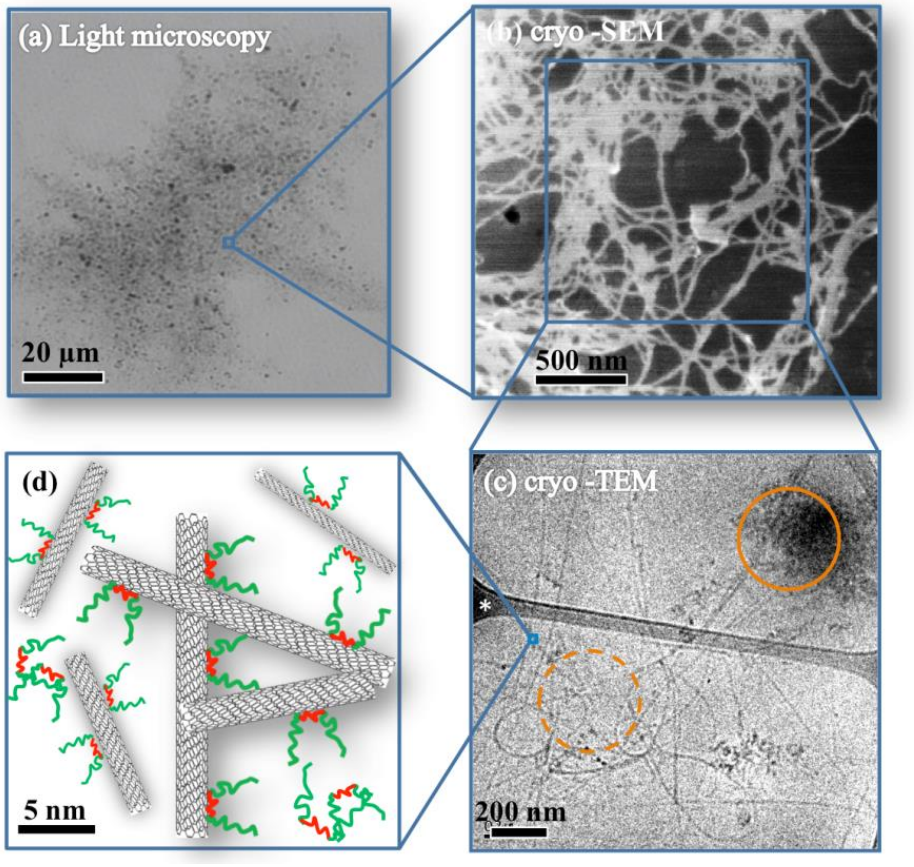

Figure 31. Imaging of the vortex-induced aggregates at different size scales: a) VELM shows the loose structure of the floc. It is also possible to discern dark particles (< 1 µm) inside the aggregate. b) Cryo-SEM magnification showing a network of entangled CNTs. c) Cryo-TEM showing individual CNTs, but also 200-300 nm dark regions d) Schematic view of the CNT cross-binding. Perpendicular junctions should be favored.

3.2.4. Gemini surfactant-assisted dispersions: spacer length and hydrophobicity effects

In paper VI, the dispersibility of multiwalled carbon nanotubes (MWNTs) using a set of bis-quat dicationic gemini surfactants of the n-s-n type was investigated. Both the lengths of the covalent spacer (s)—bridging the two cationic headgroups—and of the tail (n) were systematically varied. Hence, 12-s-12 gemini with s = 2, 6, and 12 were studied together with 16-s-16 (s = 2 and 12). In addition, the single-tailed homologues DTAB (n = 12) and CTAB (n = 16) were also used for direct comparison.

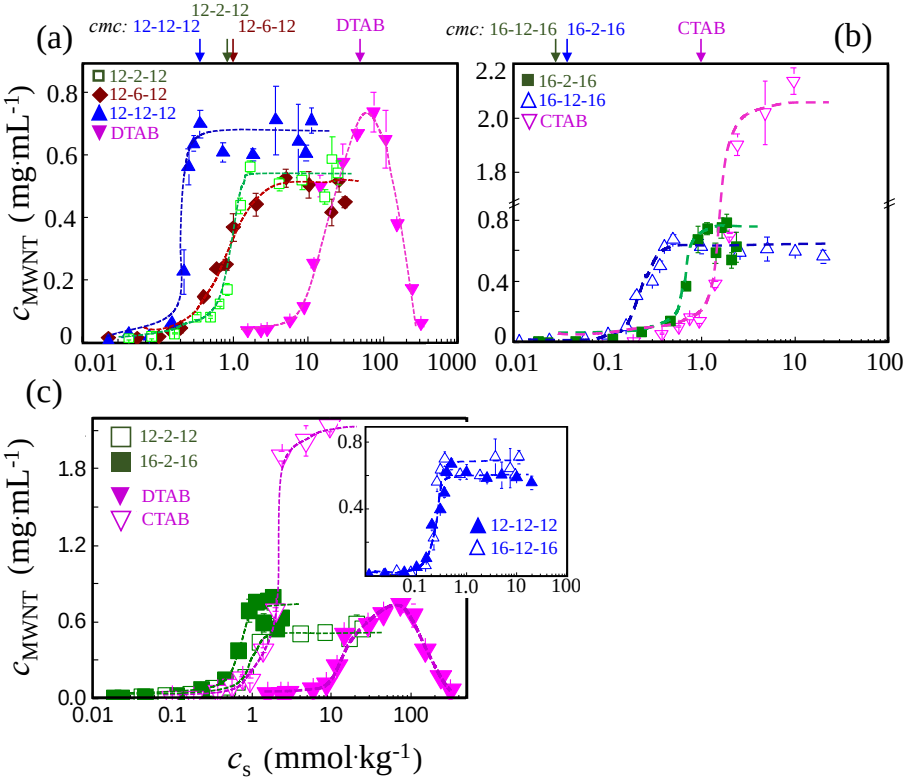

Figure 32. Concentration of dispersed MWNTs vs. surfactant concentration (log scale): (a) for the 12-s-12 gemini, including DTAB for comparison; (b) for the 16-s-16 gemini, including CTAB for comparison; (c) comparison of chain length effects for homologues 12-2-12/16-2-12, 12-12-12/16-12-16 (shown as an inset) and DTAB/CTAB.

Similar to the previous study for single chained ionic surfactants (paper III), high precision dispersion curves (Figure 32) were obtained through a well-controlled sonication/centrifugation procedure and accurate determination of MWNT concentration by a combined thermogravimetry/UV-vis spectroscopy method. This allowed us to extract some reliable metrics for each surfactant, for proper comparisons, namely the critical dispersibility concentration (*cdc*), the maximum dispersed CNT concentration ($c_{CNT,max}$) and respective surfactant concentration at that point ($c_{s,max}$), and the dispersion effectiveness (η) and efficiency (η^*).

All gemini surfactant showed a relatively modest capacity to disperse the nanotubes (about 20 %), comparable to that of DTAB, but strikingly inferior to that of CTAB. However, long spacer surfactants like 12-12-12 and 16-12-16 were found to be much more efficient that CTAB. Comparing only the gemini compounds, we found that spacer length has a more significant influence than tail length on the ability to disperse MWNTs. The effectiveness remains basically insensitive to both spacer and tail variation; however, the efficiency is clearly increased as the spacer length increases.

As one of the most important observations, we have noticed that $c_{s,max}$, the ratio $c_{s,max}/c_{CNT,max}$ and the surfactant amount per CNT area at $c_{s,max}$ all decrease linearly with spacer length. This suggests that the adsorption of gemini surfactants to the MWNT surface, even though governed principally by hydrophobicity, is rather different from the bulk micellization process, for which the *cmc* is well known to vary non-monotonically with spacer length. Moreover, our data also indicate that the presence of surfactant micelles in the exfoliation process does not seem to play any decisive role in the final dispersibility, in line with our observations for the common single-tailed surfactants (paper III). In conclusion, the broader picture that emerges from these observations is that of an adsorption mechanism that does not involve the formation of micelle-like aggregates on the MWNT surface, but rather a loose surfactant binding.

3.3. Carbon nanotube-liquid crystal interactions

3.3.1. Overview

The incorporation of CNTs in liquid crystals allows their orientation along the director axis of the liquid-crystalline phase, where the mesophase acts as a host.[152-154] The development of nanocomposites made by CNTs, where the thermotropic liquid crystal acts as the host has, however, been quite limited due to the poor dispersibility of CNTs directly in the liquid crystal.[155] Here, our goal was to circumvent this limitation by dispersing the nanotubes in gemini surfactant solutions, and by simple drying to obtain a nanocomposite film. In order to assess and rationalize the molecular interactions between CNTs and surfactants, it is important to know the phase behavior of neat surfactants. In the next section, we present the thermotropic phase behavior of gemini surfactants in the absence of nanotubes. Additionally, a very exploratory work of SWNT-thermotropic liquid crystals interactions, using gemini surfactants as dispersants, is presented.

3.3.2. Thermotropic liquid-crystalline behavior of gemini surfactants

Paper VII presents a systematic study on the thermotropic phase behavior of dimeric or gemini surfactant, based on differential scanning calorimetry, polarized light microscopy and X-ray diffraction. The compounds consist of a series of dimeric amphiphiles designated as 12-*s*-12, with covalent spacer lengths *s*=2, 3, 4, 5, 6, 8, 10 and 12. Such compounds display a structure-property versatility that may prove useful for the choice of liquid-crystalline matrices for the incorporation of CNTs.

The DSC thermograms for all the compounds show a strong effect on the thermal behavior produced by the increment of the spacer length, at constant tail length. All the compounds show several thermotropic phase transitions denoting a complex melting process. Inspection of the thermograms allows us to infer that the main peak corresponds to partial melting of the chains. Therefore, the phase formed on heating immediately after the strongest peak is considered as a (partially ordered) mesophase or a soft-crystalline phase, most likely with the headgroups positions fixed by the strong ionic interactions and with only partially molten alkyl chains.

The thermotropic behavior was characterized by combining the thermograms and direct PLM observations of birefringent defective structures. Below the main peak temperature, the 12-*s*-12 compounds exhibit a solid phase, which shows as birefringent crystallites. Although solid-solid transitions appear on the thermograms for some compounds, the PLM textures remain practically unchanged.

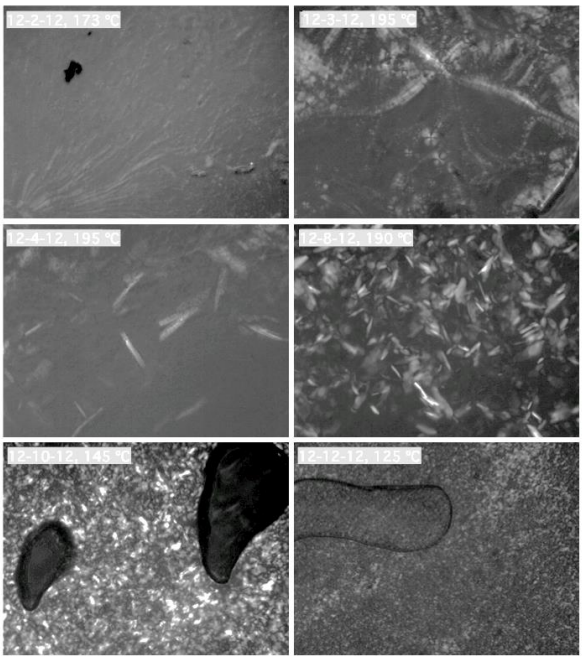

Figure 33. Different textures for the SmA liquid crystals of 12-s-12 amphiphile compounds: s = 2, oily streak; s = 3, oily streaks and focal conics; s = 4, narrow flake; s=8, feather-like flake; s = 10, mosaics; and s = 12, mosaics.

The mesophase textures depend on the spacer length of the gemini surfactant. Typical textures of mosaics and fan-shaped appear for the lower-temperature phases, while the upper-temperature more fluid mesophases appear as oily streaks and focal conics. Some of the textures only become better defined in the polarized light microscope upon several controlled heating-cooling cycles or the application of a small shearing force. Figure 33 shows some examples of textures: 12-2-12, oily streaks and fan-shaped textures; 12-3-12, oily streaks and focal conics; 12-4-12, narrow flakes; 12-8-12, feather-like flakes; 12-10-12, mosaic and fan-shapes; and 12-12-12, mosaics. Upon cooling the isotropic liquid of the four 12-*s*-12 surfactants with *s*=2, 8, 10, and 12, hysteresis effects are observed between the liquid and mesophases.

Gemini surfactants with spacer *s*=5 and 6 do not seem to show any fluid mesophases with oily streaks or focal conics below 200 °C but change instead into a brownish color. Thus, it is likely that they undergo decomposition before or concomitantly with isotropization. 12-3-12 and 12-4-12 exhibit fluid LCs but no isotropic liquid formation also because of decomposition.

Smectic structures are amongst the most frequently encountered liquid crystals when studying the thermotropic behavior of amphiphiles. Because of the structural asymmetry between hydrophilic headgroups and hydrophobic chains in the gemini compounds herein investigated, the smectic liquid crystal structure should possess a double layer with end-to-end or interdigitated chain arrangements. With respect to the relation between the director of the molecules and the bilayer plane, the long chains may be perpendicular to the plane (SmA phase) or tilted (SmC phase).

Combining the DSC and PLM studies, only briefly described here, it is possible to present a global thermal phase diagram (Figure 34), in which the effect of the spacer length on the thermotropic behavior of the gemini surfactants is apparent. The proposed assignment of the mesophases (soft crystals, ordered and disordered smectic liquid crystals) is shown in the phase diagram.

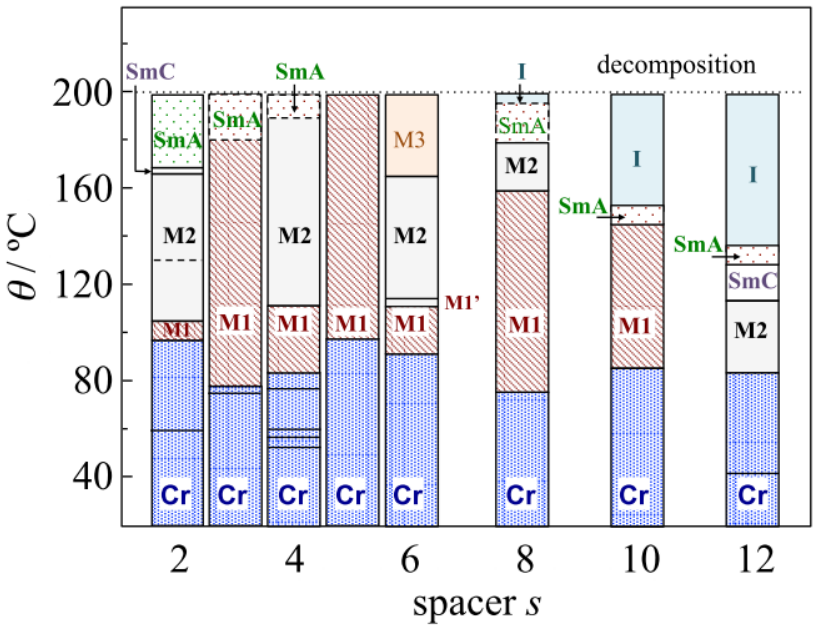

Figure 34. Thermal phase behavior of 12-s-12 gemini compounds. Notations are: Cr, crystalline solid phase region; M1, mesophase 1; M2, mesophase 2; M3, mesophase 3; SmA, smectic A liquid crystalline phase; SmB, smectic C liquid crystalline phase; I isotropic liquid phase.

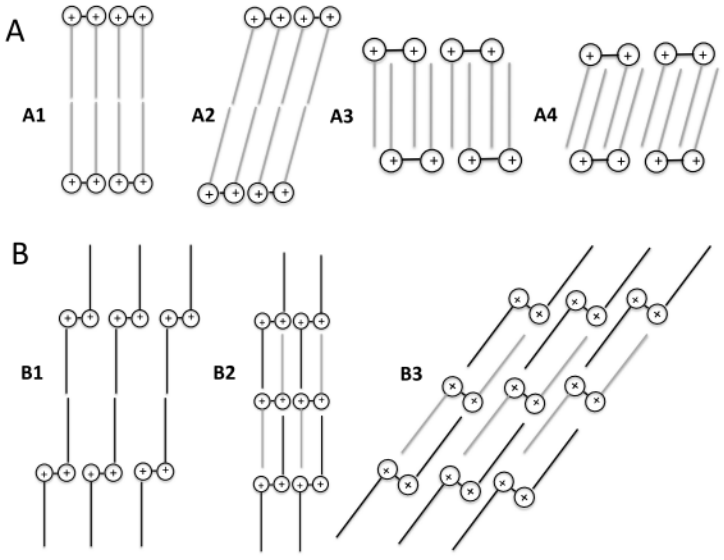

Figure 35. Possible packing configurations for the smectic layers in the 12-s-12 gemini, based on a cis (A) or trans (B) conformation for the tails. For A arrangements: A1, upright tails with no interdigitation (tail to tail); A2; tilted tails with no interdigitation; A3, upright tails with full interdigitation (tail to head); A4, tilted tails with full interdigitation. For B arrangements: B1, upright tails with no interdigitation (tail to tail); B2, upright tails full interdigitation (tail to head); B3, tilted tails with full interdigitation (tail to head).

Relating the information above with the d_{001} spacing obtained from X-ray diffraction, some possibilities for the molecular packing could be put forth. XRD

data for the solid phases agree qualitatively with the trends observed in thermal behavior. Essentially two different types of packing were proposed (Figure 35).

3.3.3. Exploratory investigations

Considering that the thermotropic behavior of gemini surfactants was previously assessed, some preliminary attempts were carried out in order to create a hybrid material – i.e. a nanocomposite. Chiral SWNT (6,5) were dispersed using a di-cationic gemini surfactant, with the tail length (n = 12), and spacer length (s = 12), i.e. gemini 12-12-12 (a good dispersant according to paper VI). After quantification of the SWNT dispersed, additional gemini surfactant was added to the dispersion in order to tune the proportion SWNT/surfactant. The solvent (water) is removed by vacuum-oven (40 ºC) drying and a SWNT-surfactant film was formed on the wall of the vial. During the drying process, the surfactant solid can undergo phase transitions to multiple liquid-crystalline phases until total remove of water. The crystal lattice of the surfactant can work as a template for SWNT alignment. However, the SWNT will also induce changes in the local organization of the surfactant lattice crystal. Our goal was to investigate the extent to which the inclusion of the SWNT in the crystal lattice changes the thermotropic behavior of the neat gemini surfactant.

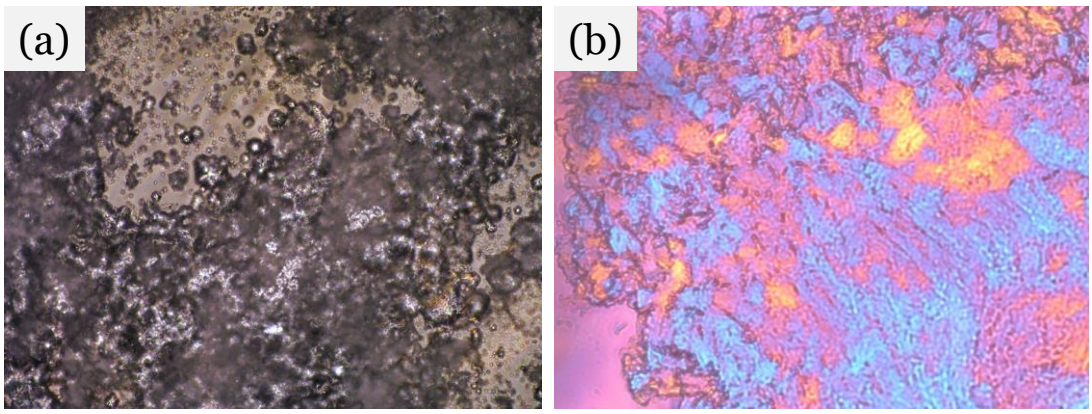

Figure 36. Polarized light microscopy images obtained at room temperature: (a) birefringent crystallites of the solid powder of gemini 12-12-12 surfactant; (b) texture of the 0.5 wt% SWNT–12-12-12 film nanocomposite - oily streaks domains seems to appear.

Several ratios of SWNT-surfactant were attempted, but samples with more than 0.5 wt% (in proportion to the surfactant mass) of nanotube resulted in a less uniform film. In Figure 36 we can observe textures, obtained under polarized light microscopy, for the gemini surfactant 12-12-12 powder and the nanocomposite SWNT–12-12-12. Birefringent crystallites are observed for the neat surfactant, whereas oily streaks textures seem to appear for nanocomposite. Additional observations are needed to full characterize the obtained nanocomposite.

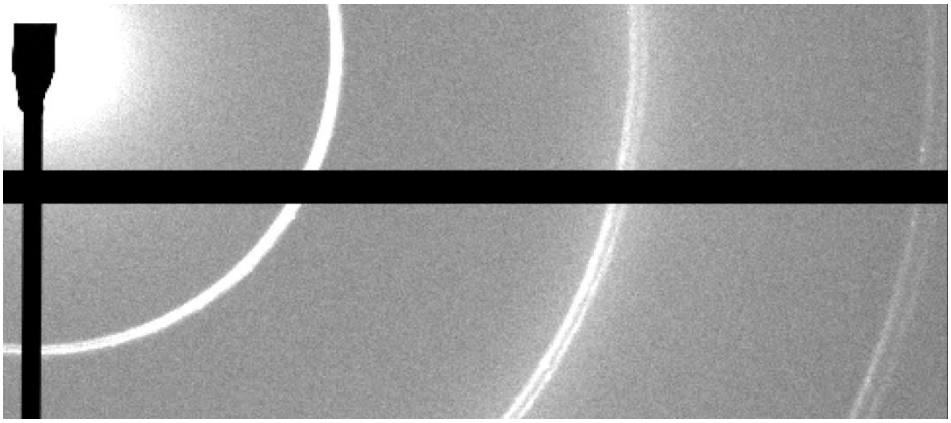

Figure 37. SAXS pattern of the sample 0.5 wt% SWNT—12-12-12, shows very clear split peaks.

In addition, X-ray analysis was performed on the film, and two *d*-spacing domains could be observed in the pattern (Figure 37). In summary, some attempts were made to produce a SWNT-gemini composite. Tuning the relative proportion of SWNT to surfactant resulted in different morphology of the film deposited. Further work, such as thermal behavior, can be performed in order to characterize and explore this type of nanocomposites.

4. Concluding remarks

In this work, aqueous dispersions of carbon nanotubes were studied by resorting to several characterization methods, namely NMR diffusometry, light and electron microscopy, UV-vis spectroscopy and TGA. The results allowed us to obtain molecular-level information on the dispersant-nanotube interactions, and rationalize them in light of the chemical structure of the dispersants. Additionally, it was shown that NMR diffusometry can be a versatile, non-invasive and valuable technique to assess the dynamics of the dispersant adsorbed onto the CNTs.

The exchange time between free and bound F127, a polymeric dispersant, onto the SWNT surface was found to be in the time scale of NMR diffusometry (1−103 ms), which in turn allowed estimating the residence time of F127 on the CNT surface, the fraction adsorbed, and the lateral displacement of this dispersant on the NT surface−observations in line with a non-wrapping model. Moreover, the amount of F127 adsorbed onto CNT detected by diffusion NMR permitted to carry out surface coverage and competitive adsorption studies of several types of dispersants (F127, BSA and ionic surfactants) onto SWNTs. It was shown that BSA is not able to replace F127 on the nanotube surface. However, the addition of ionic surfactants was found to cause displacement of F127 from the nanotube surface, which allowed gauging the relative binding strength of ionic surfactants to SWNTs.

Dispersibility studies of CNTs in water as a function of the concentration of dispersant (namely ionic surfactants) were carried out. The effect of the molecular properties of the surfactants were assessed and rationalized according to objective metrics obtained from the sigmoidal profile of the dispersibility curves. Among the most relevant results, we found that a minimum dispersant concentration, designated as critical dispersibility concentration (cdc), is needed to start dispersing CNTs. Additionally, the concentration of surfactant required to attain maximal dispersibility depends linearly on alkyl chain length for a series of homologue surfactants, which indicates that the CNT-surfactant association, although hydrophobic in nature, is rather different from a micellization process.

An interesting and somewhat counterintuitive result obtained was the effect of mechanical agitation, through vortex shaking, on SWNT dispersions, namely the formation of weakly bound micron-sized aggregates, which can be easily redispersed by mild sonication. The effect of vortexing time on the size of the aggregates was investigated and significant differences were found between different dispersants. The results were rationalized in terms of vortex-driven tube-tube contacts and the shielding effect of dispersants, which in turn were related to factors such as surface coverage and binding strength of the dispersants.

For dicationic gemini surfactants of the n-s-n type, with alkyl spacer length s and alkyl tail length n, it was observed that the spacer length has a more significant influence than tail length on the dispersibility of MWNTs. The overall data pointed

further to an adsorption mechanism that does not involve the formation of aggregates on the MWNT surface, and suggested that the hydrocarbon tails (in contrast to the spacer) do not take active part in the binding process. In addition, the data also indicated that the presence of surfactant micelles does not play any decisive role in the exfoliation process and in the final dispersibility, in line with a pattern observed for the single-tailed surfactants previously explored.

With the prospective goal of incorporating nanotubes in liquid crystalline (LC) phases to prepare nanocomposites, the effect of the spacer length on the thermotropic behavior of the gemini 12-s-12 surfactant was explored. The spacer length (s) on the 12-s-12 gemini was found to present a sharp and non-monotonous effect on the thermotropic behavior of these compounds. This was related to differences in packing in the solid state caused by variations in spacer length, and some packing models were presented on the basis of XRD data. Some exploratory work was attempted concerning the imbedding of SWNTs on the surfactant solids and birefringent films were obtained. This work opened the possibility of future investigations, exploring the structure and thermal behavior of the nanocomposites formed.

List of abbreviations

BSA	Bovine Serum Albumin
cdc	critical dispersibility concentration
cmc	critical micelle concentration
CoMoCAT	Cobalt-Molybdenium Catalysis process
CPyCl	Cetylpyridinium Chloride
Cryo-SEM	Cryo-Scanning Electron Microscopy
Cryo-TEM	Cryo-Transmission Electron Microscopy
CTAB	Cetyltrimethylammonium Bromide
CVD	Chemical Vapor Deposition
DCS	Differential Scanning Calorimetry
DIC	Differential Interference Contrast
DMF	Dimethylformamide
DTAB	Dodecyltrimethylammonium Bromide
FID	Free Induction Decay
HiPCO	High-Pressure Carbon Monoxide Process
LC	Liquid Crystalline
MWNT	Multiwalled Carbon Nanotubes
NMP	*N*-methyl-2-pyrrolidone
NMR	Nuclear Magnetic Resonance
PEO	Poly(ethylene oxide)
PGSE	Pulsed Gradient Spin-Echo
PGSTE	Pulsed Gradient Stimulated-Echo
PPO	Poly(propylene oxide)
RF	Radio Frequency
SANS	Small-Angle Neutron Scattering
SDBS	Sodium Dodecyl Benzene Sulfonate
SDS	Sodium Dodecyl Sulfate
SSA	Specific Surface Area
STS	Sodium Tetradecyl Sulfate
SWNT	Single-Walled Carbon Nanotube
TGA	Thermogravimetric Analysis
TTAB	Tetradecyltrimethylammonium Bromide
Tx-100	Triton X-100
UV-vis	Ultraviolet-visible Spectroscopy
VELM	Video-Enhanced Light Microscopy
XRD	X-ray Diffraction

Acknowledgements

Like almost all the works, nothing would be possible without the help and collaboration of many people. The work presented in this thesis is no exception. Therefore I address my deeply thanks to:

My supervisors **Prof. Eduardo Marques** and **Prof. István Furó** for accepting me as a PhD student. Both of you (complementarily) made this work very interesting and enjoyable.

Prof. Eduardo Marques, my curiosity about gravity and surface tension lead me to you. I dropped the gravity, and started studying the surface tension of surfactant solutions. Thanks for everything that you taught me through the last years, the introduction in the colloidal science and in the Ph.D. hard work. Thanks for always encouraging me to make things better, for your open mind, for your advices and the opportunity to work with you.

Prof. István Furó, you introduced me to the NMR, which made this journey challenging and extremely interesting. Thank you since day one; you made me feel at home when I arrived at Sweden. Thanks for sharing your knowledge, ideas, pragmatic advises, your vision of how to make science and for inspiring me to never give up.

Prof. Oren Regev, this work was only possible due to your commitment and valuable help. Thanks for opening the doors of your lab and introduce me to the interesting nano-world of carbon materials. The time that I stayed at Israel was very enriching. Thank you for being an extremely nice host, for sharing many things with me and for the great times at your place.

To all my coauthors, **Matat Buzaglo**, **Michael Shtein**, **Dr. Ilan Pri-Bar**, **Bárbara Claro**, **Bárbara Abreu**, **Jessica Rocha**, **Jing Dai**, **Dr. Yuji Wang**, **Prof. Pedro Tavares, Dr. Sandra C.C. Nunes** and **Prof. Alberto A.C.C. Pais**. Thanks for the shared experiences and fruitful collaborations.

Prof. Sergey Dvinskikh for sharing your NMR knowledge and for always being ready to answer to my questions. **Prof. Peter Stilbs** for being such a nice host at our lab and make the Physical Chemistry division a scientific and inspiring place to work. **Dr. Pavel Yushmanov** for all your support building everything that we could imagine, for your nice suggestions and improvements in the design of any device used during this work. I also thank you for the nice times that we shared in our office and your invitations after work.

Prof. Eric Tyrode for reviewing this thesis and making valuable comments.

All the seniors at Physical Chemistry group at Porto University, **Prof. Margarida Bastos**, **Prof. M.ª João Sottomayor**, **Prof. M.ª Dores Ribeiro da Silva**, **Prof. Ana Reis**, **Prof. Agostinha Matos** and **Prof. João Monte** −thanks for the knowledge that you transmitted me during my graduation. **Prof. Jorge Gonçalves** and **Prof. Luís Belchior** thanks for your valuable advices and nice

chats (both scientific and nonscientific). **Dr. Ana Paula Carvalho** thanks for always helping me with the lab logistics.

All the administrative staff from U.Porto and KTH who made the international co-supervision agreement possible. **Lena Skowron**, **Vera Jovanovic** and **Dr. Ulla Jacobsson** are kindly acknowledged for the all the administrative matters at KTH. At Porto University I acknowledge the administrative help of **M.ª João Cabral** and **Paula Marques**; and the technical help from **Aurora Leal**, **M.ª José Vasconcelos**, **M.ª Arminda Silva** and **Moisés Xavier**.

Swedish Research Council (VR) and Portuguese Science Foundation (FCT-Portugal) are gratefully acknowledged for the financial support.

My colleagues at Physical chemistry at Porto university, **Bruno**, **Rodrigo**, **Sandra**, **Isabel**, **Vanessa**, **Wang**, **Carlos**, **Marisa**, **Ana Rodrigues**, **José Carlos**, **Ana Lobo** and **Lia**. I also address kind words to my colleagues working at molecular energetics. Thanks for everything that we shared and for your friendship. A special thanks to **Bruno** for the suggestions in this thesis.

My colleagues at Division of Applied Physical Chemistry KTH, **Erik**, **Boris**, **Marianne, Camilla T.**, **Yuan**, **Fredrik**, **Jing**, **Michal**, **Evgeny**, **Christofer**, **Joakim**, **Björn**, **Camilla G.**, **Kristina** and **Mika**. Thanks for the pleasant time in the labs, and for the nice after-works. Thank you also **Dr. Robert Corkery** for the help with the SAXS measurements, PLM observations and for our nice discussions about science, liquid crystals, van der Waals interactions, global warming, etc.

The members at Department of Chemical Engineering at Ben Gurion University for the warm welcome and for make feel integrated. Thanks to **Ilan**, **Matat**, **Roey**, **Abigail**, **Sivan**, **Cheli** and **Yoav** for sharing with me nice times in the department (and outside). **Michael** thanks a lot for your valuable help both inside and outside the lab and your kind invitations after work. **Dima**, **Shenhav** and **Mohammed** thanks for the time that we spent together.

Tack **Fredrik**, **Joakim**, **Victor**, **Erik** och **Marco** för den tid som vi tillbringade tillsammans, delade erfarenheter, vänskap och stöd.

Agradeço a todos os meus amigos em Portugal. Felizmente sois muitos para vos enumerar aqui, mas vós sabeis quem sois. Agradeço também aos meus antigos colegas da ASJTrute pela compreensão da minha ausência e por terem continuado o projeto.

Agradeço a toda a minha família, em particular aos meus pais, **Gabriel** e **Clara** e ao meu irmão **Cristiano** por todo o apoio incondicional. Este trabalho só foi possível graças a vós. **Patrick**, **Christiane**, **Vitalina** e **Avó**, obrigado!

Thanks are due to FCT (Fundação para a Ciência e Tecnologia, Portugal) for the Ph.D. grant SFRH/BD/72612/2010. We also acknowledge financial support from FCT and FEDER/Compete, and Centro de Investigação em Química da Universidade do Porto (CIQ-UP), through grants PTDC/QUI-QUI/114212/2009, PEst-C/QUI/UI0081/2011, PEst-C/QUI/UI0081/2013 and NORTE-07-0124-FEDER-000065.

References

1. Schaefer, H.-E., *Nanoscience*. 1st ed.; Springer-Verlag: Berlin-Heidelberg, **2010**.

2. Iijima, S., Helical Microtubules of Graphitic Carbon. *Nature* **1991**, 354, 56-58.

3. Britz, D. A.; Khlobystov, A. N., Noncovalent interactions of molecules with single walled carbon nanotubes. *Chem Soc Rev* **2006**, 35, 637-659.

4. Atkins, P.; De Paula, J., *Physical Chemistry*. 8th ed.; Oxford University Press: Oxford, **2006**.

5. Vaisman, L.; Wagner, H.; Marom, G., The role of surfactants in dispersion of carbon nanotubes. *Adv Colloid Interfac* **2006**, 128, 37-46.

6. Grady, B., *Carbon Nanotube Polymer Composites: Manufacture, Properties and Applications*. 1st ed.; John Wiley & Sons, Inc.: Hoboken, **2011**.

7. Backes, C., *Noncovalent Functionalization of Carbon Nanotubes: Fundamental Aspects of Dispersion and Separation in Water*. 1st ed.; Springer-Verlag: Berlin-Heidelberg, **2012**.

8. Reich, S.; Thomsen, C.; Maultzsch, J., Structure and Symmetry. In *Carbon Nanotubes: Basic Concepts and Physical Properties*, 1st ed.; Wiley-VCH Verlag GmbH: Weinheim, Germany, **2004**.

9. Hönlein, W.; Kreupl, F., Kohlenstoff-Nanoröhrchen für die mikroelektronik. *Physik Journal* **2004**, 3, 39-44.

10. Delhaès, P.; Issi, J. P.; Bonnamy, S.; Launois, P., Polymorphism and Structure of Carbons. In *Understanding Carbon Nanotubes*, Springer-Verlag: Berlin Heidelberg, Germany, **2006**.

11. Wang, X.; Li, Q.; Xie, J.; Jin, Z.; Wang, J.; Li, Y.; Jiang, K.; Fan, S., Fabrication of Ultralong and Electrically Uniform Single-Walled Carbon Nanotubes on Clean Substrates. *Nano Lett* **2009**, 9, 3137-3141.

12. Harris, P. J. F., *Carbon Nanotube Science : Synthesis, Properties and Applications*. 1st ed.; Cambridge University Press: Cambridge, **2009**.

13. Lu, J. P., Elastic Properties of Carbon Nanotubes and Nanoropes. *Phys Rev Lett* **1997**, 79, 1297-1300.

14. Hernández, E.; Goze, C.; Bernier, P.; Rubio, A., Elastic properties of C and $B_xC_yN_z$ composite nanotubes. *Phys Rev Lett* **1998**, 80, 4502-4505.

15. Ruoff, R. S.; Tersoff, J.; Lorents, D. C.; Subramoney, S.; Chan, B., Radial deformation of carbon nanotubes by van der Waals forces. *Nature* **1993**, 364, 514-516.

16. Yu, M.-F.; Kowalewski, T.; Ruoff, R. S., Investigation of the Radial Deformability of Individual Carbon Nanotubes under Controlled Indentation Force. *Phys Rev Lett* **2000**, 85, 1456-1459.

17. Palaci, I.; Fedrigo, S.; Brune, H.; Klinke, C.; Chen, M.; Riedo, E., Radial Elasticity of Multiwalled Carbon Nanotubes. *Phys Rev Lett* **2005**, 94, 175502-175504.

18. Berber, S.; Kwon, Y.-K.; Tománek, D., Unusually High Thermal Conductivity of Carbon Nanotubes. *Phys Rev Lett* **2000**, 84, 4613-4616.

19. Sinha, S.; Barjami, S.; Iannacchione, G.; Schwab, A.; Muench, G., Off-axis Thermal Properties of Carbon Nanotube Films. *J Nanopart Res* **2005**, 7, 651-657.

20. Nikolaev, P.; Bronikowski, M. J.; Bradley, R. K.; Rohmund, F.; Colbert, D. T.; Smith, K. A.; Smalley, R. E., Gas-phase catalytic growth of single-walled carbon nanotubes from carbon monoxide. *Chem Phys Lett* **1999**, 313, 91-97.

21. Resasco, D. E.; Alvarez, W. E.; Pompeo, F.; Balzano, L.; Herrera, J. E.; Kitiyanan, B.; Borgna, A., A Scalable Process for Production of Single-walled Carbon Nanotubes (SWNTs) by Catalytic Disproportionation of CO on a Solid Catalyst. *J Nanopart Res* **2002**, 4, 131-136.

22. Backes, C.; Hirsch, A., Noncovalent Functionalization of Carbon Nanotubes. In *Chemistry of Nanocarbons*, John Wiley & Sons, Ltd: Chichester, UK, **2010**.

23. Shih, C.-J.; Lin, S.; Strano, M. S.; Blankschtein, D., Understanding the Stabilization of Single-Walled Carbon Nanotubes and Graphene in Ionic Surfactant Aqueous Solutions: Large-Scale Coarse-Grained Molecular Dynamics Simulation-Assisted DLVO Theory. *J Phys Chem C* **2015**, 119, 1047-1060.

24. Thess, A.; Lee, R.; Nikolaev, P.; Dai, H.; Petit, P.; Robert, J.; Xu, C.; Lee, Y. H.; Kim, S. G.; Rinzler, A. G.; Colbert, D. T.; Scuseria, G. E.; Tománek, D.; Fischer, J. E.; Smalley, R. E., Crystalline Ropes of Metallic Carbon Nanotubes. *Science* **1996**, 273, 483-487.

25. Ma, P.-C.; Siddiqui, N. A.; Marom, G.; Kim, J.-K., Dispersion and functionalization of carbon nanotubes for polymer-based nanocomposites: A review. *Composites Part A* **2010**, 41, 1345-1367.

26. Premkumar, T.; Mezzenga, R.; Geckeler, K. E., Carbon Nanotubes in the Liquid Phase: Addressing the Issue of Dispersion. *Small* **2012**, 8, 1299-1313.

27. Ham, H. T.; Choi, Y. S.; Chung, I. J., An explanation of dispersion states of single-walled carbon nanotubes in solvents and aqueous surfactant solutions using solubility parameters. *J Colloid Interface Sci* **2005**, 286, 216-223.

28. Kim, K. K.; Yoon, S. M.; Choi, J. Y.; Lee, J.; Kim, B. K.; Kim, J. M.; Lee, J. H.; Paik, U.; Park, M. H.; Yang, C. W.; An, K. H.; Chung, Y.; Lee, Y. H., Design of Dispersants for the Dispersion of Carbon Nanotubes in an Organic Solvent. *Adv Funct Mater* **2007**, 17, 1775-1783.

29. Bergin, S.; Nicolosi, V.; Streich, P.; Giordani, S.; Sun, Z.; Windle, A.; Ryan, P.; Niraj, N.; Wang, Z.-T.; Carpenter, L.; Blau, W.; Boland, J.; Hamilton, J.; Coleman, J., Towards solutions of single-walled carbon nanotubes in common solvents. *Adv Mater* **2008**, 20, 1876-1881.

30. Bergin, S. D.; Sun, Z.; Rickard, D.; Streich, P. V.; Hamilton, J. P.; Coleman, J. N., Multicomponent solubility parameters for single-walled carbon nanotube- solvent mixtures. *Acs Nano* **2009**, 3, 2340-2350.

31. Bergin, S.; Sun, Z.; Streich, P.; Hamilton, J.; Coleman, J., New Solvents for Nanotubes: Approaching the Dispersibility of Surfactants. *J Phys Chem C* **2010**, 114, 231-237.

32. Hughes, J.; Aherne, D.; Bergin, S.; O'Neill, A.; Streich, P.; Hamilton, J.; Coleman, J., Using solution thermodynamics to describe the dispersion of rod-like solutes: application to dispersions of carbon nanotubes in organic solvents. *Nanotechnology* **2012**, 23, 265604-265612.

33. Hughes, J. M.; Aherne, D.; Coleman, J. N., Generalizing solubility parameter theory to apply to one- and two-dimensional solutes and to incorporate dipolar interactions. *J Appl Polym Sci* **2013**, 127, 4483-4491.

34. Kharissova, O. V.; Kharisov, B. I.; de Casas Ortiz, E. G., Dispersion of carbon nanotubes in water and non-aqueous solvents. *RSC Advances* **2013**, 3, 24812-24852.

35. Lustig, S. R.; Jagota, A.; Khripin, C.; Zheng, M., Theory of Structure-Based Carbon Nanotube Separations by Ion-Exchange Chromatography of DNA/CNT Hybrids. *J Phys Chem B* **2005**, 109, 2559-2566.

36. Krupke, R.; Hennrich, F.; Löhneysen, H. v.; Kappes, M. M., Separation of Metallic from Semiconducting Single-Walled Carbon Nanotubes. *Science* **2003**, 301, 344-347.

37. Ghosh, S.; Bachilo, S. M.; Weisman, R. B., Advanced sorting of single-walled carbon nanotubes by nonlinear density-gradient ultracentrifugation. *Nat Nano* **2010**, 5, 443-450.

38. Flavel, B. S.; Kappes, M. M.; Krupke, R.; Hennrich, F., Separation of Single-Walled Carbon Nanotubes by 1-Dodecanol-Mediated Size-Exclusion Chromatography. *Acs Nano* **2013**, 7, 3557-3564.

39. Strano, M. S.; Moore, V. C.; Miller, M. K.; Allen, M. J.; Haroz, E. H.; Kittrell, C.; Hauge, R. H.; Smalley, R. E., The Role of Surfactant Adsorption during Ultrasonication in the Dispersion of Single-Walled Carbon Nanotubes. *J Nanosci Nanotech* **2003**, 3, 81-86.

40. Israelachvili, J., *Intermolecular and surface forces*. 2nd ed.; Academic Press: San Diego, **1991**.

41. Islam, M. F.; Rojas, E.; Bergey, D. M.; Johnson, A. T.; Yodh, A. G., High Weight Fraction Surfactant Solubilization of Single-Wall Carbon Nanotubes in Water. *Nano Lett* **2003**, 3, 269-273.

42. Moore, V. C.; Strano, M. S.; Haroz, E. H.; Hauge, R. H.; Smalley, R. E.; Schmidt, J.; Talmon, Y., Individually Suspended Single-Walled Carbon Nanotubes in Various Surfactants. *Nano Lett* **2003**, 3, 1379-1382.

43. Marchesan, S.; Prato, M., Under the lens: carbon nanotube and protein interaction at the nanoscale. *Chem Comm* **2015**, 51, 4347-4359.

44. Nativ-Roth, E.; Shvartzman-Cohen, R.; Bounioux, C.; Florent, M.; Zhang, D.; Szleifer, I.; Yerushalmi-Rozen, R., Physical Adsorption of Block Copolymers to SWNT and MWNT: A Nonwrapping Mechanism. *Macromolecules* **2007**, 40, 3676-3685.

45. Frise, A. E.; Edri, E.; Furo, I.; Regev, O., Protein Dispersant Binding on Nanotubes Studied by NMR Self-Diffusion and Cryo-TEM Techniques. *J Phys Chem Lett* **2010**, 1, 1414-1419.

46. Hunter, C. A.; Sanders, J. K. M., The nature of π-π interactions. *J Am Chem Soc* **1990**, 112, 5525-5534.

47. Backes, C.; Schmidt, C. D.; Hauke, F.; Bottcher, C.; Hirsch, A., High population of individualized SWCNTs through the adsorption of water-soluble perylenes. *J Am Chem Soc* **2009**, 131, 2172-2184.

48. Napper, D. H., Steric stabilization. *J Colloid Interf Sci* **1977**, 58, 390-407.

49. Evans, D. F.; Wennerström, H., *The Colloidal Domain*. 1st ed.; VCH: New York, **1994**.

50. Tadros, T., Steric Stabilization. In *Encyclopedia of Colloid and Interface Science*, Tadros, T., Ed. Springer Berlin Heidelberg: **2013**; pp 1048-1049.

51. Pashley, R. M.; Karaman, M. E., Van der Waals Forces and Colloid Stability. In *Applied Colloid and Surface Chemistry*, John Wiley & Sons, Ltd: Chichester, UK, **2005**.

52. Sun, Z.; Nicolosi, V.; Rickard, D.; Bergin, S. D.; Aherne, D.; Coleman, J. N., Quantitative evaluation of surfactant-stabilized single-walled carbon nanotubes: Dispersion quality and its correlation with zeta potential. *J Phys Chem C* **2008**, 112, 10692-10699.

53. Zhang, R.; Somasundaran, P., Advances in adsorption of surfactants and their mixtures at solid/solution interfaces. *Adv Colloid Interface Sci* **2006**, 123-126, 213-229.

54. Wenseleers, W.; Vlasov, I. I.; Goovaerts, E.; Obraztsova, E. D.; Lobach, A. S.; Bouwen, A., Efficient isolation and solubilization of pristine single-walled nanotubes in bile salt micelles. *Adv Funct Mater* **2004**, 14, 1105-1112.

55. Wang, H., Dispersing carbon nanotubes using surfactants. *Curr Opin Colloid Interface Sci* **2009**, 14, 364-371.

56. Angelikopoulos, P.; Bock, H., The science of dispersing carbon nanotubes with surfactants. *Phys Chem Chem Phys* **2012**, 14, 9546-9557.

57. Oh, H.; Sim, J.; Ju, S. Y., Binding Affinities and Thermodynamics of Noncovalent Functionalization of Carbon Nanotubes with Surfactants. *Langmuir* **2013**, 29, 11154-11162.

58. Tummala, N. R.; Morrow, B. H.; Resasco, D. E.; Striolo, A., Stabilization of Aqueous Carbon Nanotube Dispersions Using Surfactants: Insights from Molecular Dynamics Simulations. *Acs Nano* **2010**, 4, 7193-7204.

59. Clark, M. D.; Subramanian, S.; Krishnamoorti, R., Understanding surfactant aided aqueous dispersion of multi-walled carbon nanotubes. *J Colloid Interface Sci* **2011**, 354, 144-151.

60. Ernst, F.; Heek, T.; Setaro, A.; Haag, R.; Reich, S., Functional Surfactants for Carbon Nanotubes: Effects of Design. *J Phys Chem C* **2013**, 117, 1157-1162.

61. Yurekli, K.; Mitchell, C. A.; Krishnamoorti, R., Small-angle neutron scattering from surfactant-assisted aqueous dispersions of carbon nanotubes. *J Am Chem Soc* **2004**, 126, 9902-9903.

62. Gubitosi, M.; Trillo, J. V.; Alfaro Vargas, A.; Pavel, N. V.; Gazzoli, D.; Sennato, S.; Jover, A.; Meijide, F.; Galantini, L., Characterization of Carbon Nanotube Dispersions in Solutions of Bile Salts and Derivatives Containing Aromatic Substituents. *J Phys Chem B* **2014**, 118, 1012-1021.

63. Blanch, A. J.; Lenehan, C. E.; Quinton, J. S., Optimizing Surfactant Concentrations for Dispersion of Single-Walled Carbon Nanotubes in Aqueous Solution. *J Phys Chem B* **2010**, 114, 9805-9811.

64. Bandyopadhyaya, R.; Nativ-Roth, E.; Regev, O.; Yerushalmi-Rozen, R., Stabilization of Individual Carbon Nanotubes in Aqueous Solutions. *Nano Lett* **2002**, 2, 25-28.

65. Backes, C.; Mundloch, U.; Schmidt, C. D.; Coleman, J. N.; Wohlleben, W.; Hauke, F.; Hirsch, A., Enhanced adsorption affinity of anionic perylene-based surfactants towards smaller-diameter SWCNTs. *Chemistry* **2010**, 16, 13185-13192.

66. Haggenmueller, R.; Rahatekar, S. S.; Fagan, J. A.; Chun, J.; Becker, M. L.; Naik, R. R.; Krauss, T.; Carlson, L.; Kadla, J. F.; Trulove, P. C.; Fox, D. F.; DeLong, H. C.; Fang, Z.; Kelley, S. O.; Gilman, J. W., Comparison of the Quality of Aqueous Dispersions of Single Wall Carbon Nanotubes Using Surfactants and Biomolecules. *Langmuir* **2008**, 24, 5070-5078.

67. Nativ-Roth, E.; Nap, R. J.; Szleifer, I.; Yerushalmi-Rozen, R., Order-disorder transition induced by surfactant micelles in single-walled carbon nanotubes dispersions. *Soft Matter* **2010**, 6, 5289-5292.

68. Nativ-Roth, E.; Regev, O.; Yerushalmi-Rozen, R., Shear-induced ordering of micellar arrays in the presence of single-walled carbon nanotubes. *Chem Comm* **2008**, 17, 2037-2039.

69. Angelikopoulos, P.; Bock, H., Directed self-assembly of surfactants in carbon nanotube materials. *J Phys Chem B* **2008**, 112, 13793-13801.

70. Bai, Y.; Lin, D.; Wu, F.; Wang, Z.; Xing, B., Adsorption of Triton X-series surfactants and its role in stabilizing multi-walled carbon nanotube suspensions. *Chemosphere* **2010**, 79, 362-367.

71. Wang, H.; Zhou, W.; Ho, D. L.; Winey, K. I.; Fischer, J. E.; Glinka, C. J.; Hobbie, E. K., Dispersing single-walled carbon nanotubes with surfactants: A small angle neutron scattering study. *Nano Lett* **2004**, 4, 1789-1793.

72. Shin, J. Y.; Premkumar, T.; Geckeler, K. E., Dispersion of single-walled carbon nanotubes by using surfactants: are the type and concentration important? *Chemistry* **2008**, 14, 6044-6048.

73. Tardani, F.; La Mesa, C., Attempts to control depletion in the surfactant-assisted stabilization of single-walled carbon nanotubes. *Colloid Surface A* **2014**, 443, 123-128.

74. Angelikopoulos, P.; Gromov, A.; Leen, A.; Nerushev, O.; Bock, H.; Campbell, E. E. B., Dispersing Individual Single-Wall Carbon Nanotubes in Aqueous Surfactant Solutions below the cmc. *J Phys Chem C* **2010**, 114, 2-9.

75. Shastry, T. A.; Morris-Cohen, A. J.; Weiss, E. A.; Hersam, M. C., Probing Carbon Nanotube–Surfactant Interactions with Two-Dimensional DOSY NMR. *J Am Chem Soc* **2013**, 135, 6750-6753.

76. O'Connell, M. J.; Boul, P.; Ericson, L. M.; Huffman, C.; Wang, Y. H.; Haroz, E.; Kuper, C.; Tour, J.; Ausman, K. D.; Smalley, R. E., Reversible water-solubilization of single-walled carbon nanotubes by polymer wrapping. *Chem Phys Lett* **2001**, 342, 265-271.

77. Frise, A. E.; Pages, G.; Shtein, M.; Pri Bar, I.; Regev, O.; Furo, I., Polymer binding to carbon nanotubes in aqueous dispersions: residence time on the nanotube surface as obtained by NMR diffusometry. *J Phys Chem B* **2012**, 116, 2635-2642.

78. Granite, M.; Radulescu, A.; Cohen, Y., Small-Angle Neutron Scattering from Aqueous Dispersions of Single-Walled Carbon Nanotubes with Pluronic F127 and Poly(vinylpyrrolidone). *Langmuir* **2012**, 28, 11025-11031.

79. Granite, M.; Radulescu, A.; Pyckhout-Hintzen, W.; Cohen, Y., Interactions between Block Copolymers and Single-Walled Carbon Nanotubes in Aqueous Solutions: A Small-Angle Neutron Scattering Study. *Langmuir* **2011**, 27, 751-759.

80. Xin, X.; Xu, G.; Zhao, T.; Zhu, Y.; Shi, X.; Gong, H.; Zhang, Z., Dispersing Carbon Nanotubes in Aqueous Solutions by a Starlike Block Copolymer. *J Phys Chem C* **2008**, 112, 16377-16384.

81. Wang, B.; Han, Y.; Song, K.; Zhang, T., The Use of Anionic Gum Arabic as a Dispersant for Multi-Walled Carbon Nanotubes in an Aqueous Solution. *J Nanosci Nanotech* **2012**, 12, 4664-4669.

82. Liu, M.; Jia, Z.; Zhou, C., Dispersion of Single-Walled Carbon Nanotubes in Water by a Conjugated Surfactant. *Adv Mater Res* **2012**, 415, 562-565.

83. Edri, E.; Regev, O., pH effects on BSA-dispersed carbon nanotubes studied by spectroscopy-enhanced composition evaluation techniques. *Anal Chem* **2008**, 80, 4049-4054.

84. Hirano, A.; Maeda, Y.; Yuan, X.; Ueki, R.; Miyazawa, Y.; Fujita, J.; Akasaka, T.; Shiraki, K., Controlled dispersion and purification of protein-carbon nanotube conjugates using guanidine hydrochloride. *Chemistry* **2010**, 16, 12221-12228.

85. Bomboi, F.; Bonincontro, A.; La Mesa, C.; Tardani, F., Interactions between single-walled carbon nanotubes and lysozyme. *J Colloid Interf Sci* **2011**, 355, 342-347.

86. Valenti, L. E.; Fiorito, P. A.; Garcia, C. D.; Giacomelli, C. E., The adsorption-desorption process of bovine serum albumin on carbon nanotubes. *J Colloid Interf Sci* **2007**, 307, 349-356.

87. Edri, E.; Regev, O., "Shaken, Not Stable": Dispersion Mechanism and Dynamics of Protein-Dispersed Nanotubes Studied via Spectroscopy. *Langmuir* **2009**, 25, 10459-10465.

88. Nepal, D.; Geckeler, K. E., Proteins and carbon nanotubes: Close encounter in water. *Small* **2007**, 3, 1259-1265.

89. Edri, E.; Regev, O., Cryo-staining techniques in cryo-TEM studies of dispersed nanotubes. *Ultramicroscopy* **2010**, 110, 754-760.

90. Sanz, V.; Borowiak, E.; Lukanov, P.; Galibert, A. M.; Flahaut, E.; Coley, H. M.; Silva, S. R. P.; McFadden, J., Optimising DNA binding to carbon nanotubes by non-covalent methods. *Carbon* **2011**, 49, 1775-1781.

91. Ostojic, G. N.; Ireland, J. R.; Hersam, M. C., Noncovalent functionalization of DNA-wrapped single-walled carbon nanotubes with platinum-based DNA cross-linkers. *Langmuir* **2008**, 24, 9784-9789.

92. Tardani, F.; La Mesa, C.; Poulin, P.; Maugey, M., Phase Behavior of DNA-Based Dispersions containing Carbon Nanotubes: Effects of Added Polymers and Ionic Strength on Excluded Volume. *J Phys Chem C* **2012**, 116, 9888-9894.

93. Dror, Y.; Pyckhout-Hintzen, W.; Cohen, Y., Conformation of Polymers Dispersing Single-Walled Carbon Nanotubes in Water: A Small-Angle Neutron Scattering Study. *Macromolecules* **2005**, 38, 7828-7836.

94. Plisko, T.; Bildyukevich, A., Debundling of multiwalled carbon nanotubes in N, N-dimethylacetamide by polymers. *Colloid Polym Sci* **2014**, 292, 2571-2580.

95. Gao, J.; Loi, M. A.; de Carvalho, E. J. F.; dos Santos, M. C., Selective Wrapping and Supramolecular Structures of Polyfluorene–Carbon Nanotube Hybrids. *Acs Nano* **2011**, 5, 3993-3999.

96. Rahmat, M.; Hubert, P., Carbon nanotube-polymer interactions in nanocomposites: A review. *Compos Sci Technol* **2011**, 72, 72-84.

97. Samanta, S. K.; Fritsch, M.; Scherf, U.; Gomulya, W.; Bisri, S. Z.; Loi, M. A., Conjugated polymer-assisted dispersion of single-wall carbon nanotubes: the power of polymer wrapping. *Acc Chem Res* **2014**, 47, 2446-2456.

98. Tallury, S. S.; Pasquinelli, M. A., Molecular dynamics simulations of flexible polymer chains wrapping single-walled carbon nanotubes. *J Phys Chem B* **2010**, 114, 4122-4129.

99. Kusner, I.; Srebnik, S., Conformational behavior of semi-flexible polymers confined to a cylindrical surface. *Chem Phys Lett* **2006**, 430, 84-88.

100. Tallury, S. S.; Pasquinelli, M. A., Molecular dynamics simulations of polymers with stiff backbones interacting with single-walled carbon nanotubes. *J Phys Chem B* **2010**, 114, 9349-9355.

101. Zheng, M.; Jagota, A.; Semke, E. D.; Diner, B. A.; McLean, R. S.; Lustig, S. R.; Richardson, R. E.; Tassi, N. G., DNA-assisted dispersion and separation of carbon nanotubes. *Nat Mater* **2003**, 2, 338-342.

102. Zheng, M.; Jagota, A.; Strano, M. S.; Santos, A. P.; Barone, P.; Chou, S. G.; Diner, B. A.; Dresselhaus, M. S.; Mclean, R. S.; Onoa, G. B.; Samsonidze, G. G.; Semke, E. D.; Usrey, M.; Walls, D. J., Structure-Based Carbon Nanotube Sorting by Sequence-Dependent DNA Assembly. *Science* **2003**, 302, 1545-1548.

103. Tu, X.; Manohar, S.; Jagota, A.; Zheng, M., DNA sequence motifs for structure-specific recognition and separation of carbon nanotubes. *Nature* **2009**, 460, 250-253.

104. Maji, B.; Samanta, S. K.; Bhattacharya, S., Role of pH controlled DNA secondary structures in the reversible dispersion/precipitation and separation of metallic and semiconducting single-walled carbon nanotubes. *Nanoscale* **2014**, 6, 3721-3730.

105. Kastrisianaki-Guyton, E. S.; Chen, L.; Rogers, S. E.; Cosgrove, T.; van Duijneveldt, J. S., Adsorption of F127 onto Single-Walled Carbon Nanotubes Characterized Using Small-Angle Neutron Scattering. *Langmuir* **2015**, 31, 3262-3268.

106. Han, Y.; Ahn, S. K.; Zhang, Z.; Smith, G. S.; Do, C., Tunable Encapsulation Structure of Block Copolymer Coated Single-Walled Carbon Nanotubes in Aqueous Solution. *Macromolecules* **2015**, 48, 3475-3480.

107. Calvaresi, M.; Zerbetto, F., The devil and holy water: protein and carbon nanotube hybrids. *Acc Chem Res* **2013**, 46, 2454-2463.

108. Du, P.; Zhao, J.; Mashayekhi, H.; Xing, B., Adsorption of Bovine Serum Albumin and Lysozyme on Functionalized Carbon Nanotubes. *J Phys Chem C* **2014**, 118, 22249-22257.

109. Doi, M., *Soft Matter Physics*. 1st ed.; Oxford University Press: Oxford, **2013**.

110. Hirst, L. S., *Fundamentals of Soft Matter Science*. 1st ed.; CRC Tailor & Francis: Boca Raton, **2012**.

111. Hamley, I. W., *Introduction to Soft Matter: Synthetic and Biological Self-Assembling Materials* Rev. ed.; John Wiley & Sons, Ltd: Chichester, **2007**.

112. Liu, Z. F.; Fang, S.; Moura, F. A.; Ding, J. N.; Jiang, N.; Di, J.; Zhang, M.; Lepró, X.; Galvão, D. S.; Haines, C. S.; Yuan, N. Y.; Yin, S. G.; Lee, D. W.; Wang, R.; Wang, H. Y.; Lv, W.; Dong, C.; Zhang, R. C.; Chen, M. J.; Yin, Q.; Chong, Y. T.; Zhang, R.; Wang, X.; Lima, M. D.; Ovalle-Robles, R.; Qian, D.; Lu, H.; Baughman, R. H., Hierarchically buckled sheath-core fibers for superelastic electronics, sensors, and muscles. *Science* **2015**, 349, 400-404.

113. Marques, E.; Silva, B. B., Surfactants, Phase Behavior. In *Encyclopedia of Colloid and Interface Science*, Tadros, T., Ed. Springer: Berlin Heidelberg, **2013**.

114. Marques, E.; Silva, B. B., Surfactant Self-Assembly. In *Encyclopedia of Colloid and Interface Science*, Tadros, T., Ed. Springer: Berlin Heidelberg, **2013**.

115. Holmberg, K.; Jönsson, B.; kronberg, B.; Lindman, B., *Surfactants and Polymers in Aqueous Solution*. 2nd ed.; John Wiley and Sons, Ltd: Chichester, **2006**.

116. Fried, J., *Polymer science and technology*. 3rd ed.; Prentice Hall: New York, **2014**.

117. Alexandridis, P.; Holzwarth, J. F.; Hatton, T. A., Micellization of Poly(Ethylene Oxide)-Poly(Propylene Oxide)-Poly(Ethylene Oxide) Triblock Copolymers in Aqueous-Solutions - Thermodynamics of Copolymer Association. *Macromolecules* **1994**, 27, 2414-2425.

118. Tschierske, C., Non-conventional liquid crystals-the importance of micro-segregation for self-organisation. *J Mater Chem* **1998**, 8, 1485-1508.

119. Tschierske, C., Micro-segregation, molecular shape and molecular topology - partners for the design of liquid crystalline materials with complex mesophase morphologies. *J Mater Chem* **2001**, 11, 2647-2671.

120. Dierking, I., *Textures of liquid crystals*. Wyley-VCH verlag GmbH Weinheim, **2003**.

121. Collings, P. J.; Hird, M., *Introduction to liquid cristals*. Taylor&Francis: London, **1997**.

122. Xu, H.; Zeiger, B. W.; Suslick, K. S., Sonochemical synthesis of nanomaterials. *Chem Soc Rev* **2013**, 42, 2555-2567.

123. Matarredona, O.; Rhoads, H.; Li, Z.; Harwell, J. H.; Balzano, L.; Resasco, D. E., Dispersion of Single-Walled Carbon Nanotubes in Aqueous Solutions of the Anionic Surfactant NaDDBS. *J Phys Chem B* **2003**, 107, 13357-13367.

124. Grossiord, N.; Regev, O.; Loos, J.; Meuldijk, J.; Koning, C. E., Time-dependent study of the exfoliation process of carbon nanotubes in aqueous dispersions by using UV-visible spectroscopy. *Anal Chem* **2005**, 77, 5135-5139.

125. Hennrich, F.; Krupke, R.; Arnold, K.; Rojas Stütz, J. A.; Lebedkin, S.; Koch, T.; Schimmel, T.; Kappes, M. M., The Mechanism of Cavitation-Induced Scission of Single-Walled Carbon Nanotubes. *J Phys Chem B* **2007**, 111, 1932-1937.

126. Lucas, A.; Zakri, C.; Maugey, M.; Pasquali, M.; Schoot, P. v. d.; Poulin, P., Kinetics of Nanotube and Microfiber Scission under Sonication. *J Phys Chem C* **2009**, 113, 20599-20605.

127. Pagani, G.; Green, M. J.; Poulin, P.; Pasquali, M., Competing mechanisms and scaling laws for carbon nanotube scission by ultrasonication. *Proc Natl Acad Sci USA* **2012**, 109, 11599-11604.

128. Dassios, K. G.; Alafogianni, P.; Antiohos, S. K.; Leptokaridis, C.; Barkoula, N.-M.; Matikas, T. E., Optimization of Sonication Parameters for Homogeneous Surfactant-Assisted Dispersion of Multiwalled Carbon Nanotubes in Aqueous Solutions. *J Phys Chem C* **2015**, 119, 7506-7516.

129. Fagan, J. A.; Becker, M. L.; Chun, J.; Hobbie, E. K., Length Fractionation of Carbon Nanotubes Using Centrifugation. *Adv Mater* **2008**, 20, 1609-1613.

130. Blanch, A. J.; Lenehan, C. E.; Quinton, J. S., Parametric analysis of sonication and centrifugation variables for dispersion of single walled carbon nanotubes in aqueous solutions of sodium dodecylbenzene sulfonate. *Carbon* **2011**, 49, 5213-5228.

131. Shtein, M.; Pri-bar, I.; Regev, O., A simple solution for the determination of pristine carbon nanotube concentration. *Analyst* **2013**, 138, 1490-1496.

132. Levitt, M., *Spin dynamics: basics of nuclear magnetic resonance*. John Wiley and Sons, Ltd: Chichester, **2008**.

133. Keeler, J., *Understanding NMR spectroscopy*. John Wiley and Sons, Ltd: Chichester, **2010**.

134. Hahn, E. L., Spin Echoes. *Phys Rev* **1950**, 80, 580-594.

135. Stilbs, P., Fourier transform pulsed-gradient spin-echo studies of molecular diffusion. *Prog Nucl Mag Res Sp* **1987**, 19, 1-45.

136. Price, W., *NMR studies of translational motion*. Cambridge University Press: Cambridge, **2009**.

137. Stejskal, E. O.; Tanner, J. E., Spin Diffusion Measurements: Spin Echoes in the Presence of a Time-Dependent Field Gradient. *J Chem Phys* **1965**, 42, 288-292.

138. Price, W. S., Pulsed-field gradient nuclear magnetic resonance as a tool for studying translational diffusion: Part 1. Basic theory. *Concepts Magn Reson* **1997**, 9, 299-336.

139. Abramowitz, M., *Microscope: Basics and Beyond*. Olympus America: Melvine, **2003**.

140. Goodhew, P. J.; Humphreys, J.; Beanland, R., *Electron Microscopy and Analysis*. Taylor & Francis: London, **2001**.

141. Suryanarayana, C.; Norton, M. G., *X-Rays and Diffraction*. Springer US: New York, **1998**.

142. Als-Nielsen, J.; McMorrow, D., *Elements of Modern X-Ray Physics*. 1st ed.; Wiley: Chichester, **2001**.

143. Seeck, O. H., Overview of X-Ray Scattering and Diffraction Theory and Techniques. In *X-Ray Diffraction*, Seeck, O. H.; Murphy, B., Eds. CRC Press Taylor & Francis, LLC: Boca Raton, **2015**.

144. Höhne, G. W. H.; Hemminger, W. F.; Flammersheim, H. J., Theoretical Fundamentals of Differential Scanning Calorimeters. In *Differential Scanning Calorimetry*, Springer-Verlag: Berlin-Heidelberg, **2003**.

145. Gabbott, P., A Practical Introduction to Differential Scanning Calorimetry. In *Principles and Applications of Thermal Analysis*, 1st ed.; Blackwell Publishing Ltd: Oxford, **2008**.

146. Bottom, R., Thermogravimetric Analysis. In *Principles and Applications of Thermal Analysis*, Blackwell Publishing Ltd: Oxford, **2008**.

147. Kärger, J., Der Einfluß der Zweibereichdiffusion auf die Spinechodämpfung unter Berücksichtigung der Relaxation bei Messungen mit der Methode der gepulsten Feldgradienten. *Annalen der Physik* **1971**, 482, 107-109.

148. Schönhoff, M.; Söderman, O., PFG-NMR Diffusion as a Method To Investigate the Equilibrium Adsorption Dynamics of Surfactants at the Solid/Liquid Interface. *J Phys Chem B* **1997**, 101, 8237-8242.

149. Callaghan, P. T.; Soderman, O., Examination of the Lamellar Phase of Aerosol Ot-Water Using Pulsed Field Gradient Nuclear Magnetic-Resonance. *J Phys Chem* **1983**, 87, 1737-1744.

150. Florent, M.; Shvartzman-Cohen, R.; Goldfarb, D.; Yerushalmi-Rozen, R., Self-assembly of pluronic block copolymers in aqueous dispersions of single-wall carbon nanotubes as observed by spin probe EPR. *Langmuir* **2008**, 24, 3773-3779.

151. Angelikopoulos, P.; Schou, K.; Bock, H., Surfactant-Induced Forces between Carbon Nanotubes. *Langmuir* **2010**, 26, 18874-18883.

152. Weiss, V.; Thiruvengadathan, R.; Regev, O., Preparation and Characterization of a Carbon Nanotube–Lyotropic Liquid Crystal Composite. *Langmuir* **2006**, 22, 854-856.

153. Puech, N.; Blanc, C.; Grelet, E.; Zamora-Ledezma, C.; Maugey, M.; Zakri, C.; Anglaret, E.; Poulin, P., Highly Ordered Carbon Nanotube Nematic Liquid Crystals. *J Phys Chem C* **2011**, 115, 3272-3278.

154. Puech, N.; Dennison, M.; Blanc, C.; van der Schoot, P.; Dijkstra, M.; van Roij, R.; Poulin, P.; Grelet, E., Orientational Order of Carbon Nanotube Guests in a Nematic Host Suspension of Colloidal Viral Rods. *Phys Rev Lett* **2012**, 108.

155. Ji, Y.; Huang, Y. Y.; Terentjev, E. M., Dissolving and Aligning Carbon Nanotubes in Thermotropic Liquid Crystals. *Langmuir* **2011**, 27, 13254-13260.

I

Lateral diffusion of dispersing molecules on nanotubes as probed by NMR

Ricardo M.F. Fernandes, Matat Buzaglo, Michael Shtein, Ilan Pri Bar, Oren Regev, Eduardo F. Marques and István Furó

J Phys Chem C, **2014**, 118, 582–589

THE JOURNAL OF PHYSICAL CHEMISTRY C

Article

pubs.acs.org/JPCC

Lateral Diffusion of Dispersing Molecules on Nanotubes As Probed by NMR

Ricardo M. F. Fernandes,[†,‡] Matat Buzaglo,[§] Michael Shtein,[§] Ilan Pri Bar,[§] Oren Regev,*[,§] Eduardo F. Marques,*[,†] and István Furó*[,‡]

[†]Centro de Investigação em Química, Department of Chemistry and Biochemistry, Faculty of Science, University of Porto, Rua do Campo Alegre, s/n P-4169-007 Porto, Portugal

[‡]Division of Applied Physical Chemistry, Department of Chemistry, KTH Royal Institute of Technology, SE-10044 Stockholm, Sweden

[§]Department of Chemical Engineering and the Ilse Katz Institute for Nanotechnology, Ben-Gurion University of the Negev, 84105 Beer-Sheva, Israel

Supporting Information

ABSTRACT: Noncovalent dispersion of carbon nanotubes is essential to most applications but still poorly understood at the molecular level. The interaction of the dispersing molecule with the nanotube, wrapping or nonwrapping, still awaits consensus. Herein, we have studied by ^{1}H NMR diffusometry some features of molecular dynamics in the system of carbon nanotubes dispersed by triblock copolymer Pluronics F127 in water. The diffusional decays obtained at different diffusion times, Δ, are not single-exponential and have a complex Δ-dependent profile, ultimately implying that the polymer is observed in two states: free (in unimeric form) and nanotube-bound. Fitting a two-site exchange model to the data indicates that at any instant, only a small fraction of polymers are adsorbed on the nanotubes, with polydisperse residence times in the range of 100−400 ms. Most significantly, we further provide an estimate of $D = (3-8) \times 10^{-12}$ m^2 s^{-1} for the coefficient of lateral diffusion of the polymer along the nanotube surface, which is an order of magnitude slower than the corresponding self-diffusion coefficient in water. The emerging picture is that of a nonwrapping mode for the polymer−nanotube interaction.

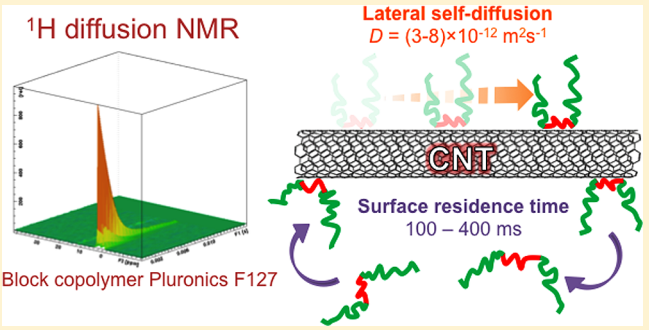

1. INTRODUCTION

Carbon nanotubes (CNTs) are interesting materials that present many promises, many questions, and many challenges. A lot of potential applications, such as drug delivery, require them to be dispersed, but individual nanotubes attract each other by strong van der Waals interactions and are not easily separated in neat liquids, with few recently reported exceptions, such as *N*-methyl-2-pyrrolidone.[1] In particular, CNTs, hydrophobic in nature, do not disperse well in water, where they require either surface modification or dispersing agents such as surfactants, proteins, or polymers, which are assumed to adsorb onto the CNT outer surface and exert steric or electrostatic repulsion among the individual CNTs.

Not only is the physical state of the surface-adsorbed dispersants interesting from the point of view of the nature of the dispersion process, but it also forms part of the broader question of the state of molecules on CNT surfaces. The variety in behavior is large. For example, polymers with aromatic repeating units or proteins bind strongly to CNTs and, in one model with some experimental support, were hypothesized to wrap themselves around the thin CNT cylinder.[2−4] The same model has been assumed by others to be valid for other species,[5,6] too. Meanwhile, weaker association without substantial conformational changes has also been envisaged,[7,8] particularly for dispersants in aqueous solutions. The assumed wrapping−unwrapping process, and adsorbed species in general, have been subject to extensive simulation studies.[9−17] Both the strength and the mode of association have, of course, profound consequences as concerning (i) the adsorption isotherm and thereby the amount of molecules adsorbed to CNTs and (ii) the residence time of the molecules on the CNT surface. These issues are also extremely relevant for drug delivery applications. Unfortunately, the experimental data are sparse on any of these issues.

The present study focuses on the behavior of one specific class of polymers, namely, Pluronics, on CNT surfaces. These block copolymers are, depending on their size and the ratio of their hydrophobic polypropylene oxide (PPO) and hydrophilic polyethylene oxide (PEO) blocks, a good dispersant for CNTs in water.[18,19] Plausibly, the hydrophobic PPO blocks are

Received: November 20, 2013
Revised: December 13, 2013
Published: December 13, 2013

attached to the CNT surface while the PEO blocks' expanding into the surrounding water provides steric repulsion that facilitates dispersion. Indeed, this general arrangement is found to be consistent with small-angle neutron scattering data[7,8] with no indication for strong conformational changes or wrapping of the polymer. On the other hand, we have shown by NMR diffusometry[20] that the fraction of polymers attached to the surface is low and the residence time on the surface is rather short, on the order of 10−100 ms. An even shorter residence time (below experimental time scale) was indicated by NMR diffusometry for some ionic surfactants,[21] and protein bovine serum albumin,[22] which was also found to displace Pluronics from dispersed SWNTs within <700 ms.[6,23]

Although the milliseconds time scale may be perceived as short in some context, it is still long as concerning conformational dynamics of the polymer. In particular, PEO and PPO chains are known to possess high flexibility and fast internal dynamics.[24] This internal dynamics should permit the polymer to change its conformation also in relation to CNT, thus providing a mechanism for molecular displacement on the CNT surface. In contrast, tight wrapping has been indicated by simulations to lead to slow surface diffusion. Here, we investigate this question by NMR diffusion measurements.

2. MATERIALS AND METHODS

2.1. Sample Preparation. CNTs (with nominal product name "SWCNT, HDPlas") with an outer diameter in the range of 1−4 nm and length in the range of 3−30 μm, produced by the CCVD method and plasma purified, were obtained from CheapTubes (Brattleboro, VT). This material contains a very low fraction of paramagnetic impurities, which would otherwise complicate the NMR experiments.[22] On the other hand, our own transmission electron microscopy studies (see below) have shown that multiwalled carbon nanotubes were also present in the material obtained. Pluronic F-127 $(PEO)_x$−$(PPO)_y$−$(PEO)_x$ block copolymer, with an approximate molecular weight of 12 500 and with x = 97 and y = 69, was purchased from Sigma-Aldrich. Heavy water (99.9 atom % D) was purchased from Isotec, Inc. (Miamisburg, OH). All materials were used as received.

The SWNT dispersions were prepared from a stock solution of F127 0.3 wt % with D_2O, where the initial concentration of SWNT was 0.3 wt %. The procedure has been described in detail previously.[20] The sonication was performed by a calibrated Qsonica Q-500 (Qsonica, Newtown, CT) tip sonicator equipped with a 3 mm microtip; care was taken that the tip surface, while used, was kept smoothly polished. The sonication time was 10 min, and the power delivered by the tip to the 3 mL total sample volume was 3.2 W, which sets the total sonication energy to an estimated 640 J/mL. The temperature during sonication was kept at 18 °C using an external water bath. When exploring the effect of sonication on the sample components, the same sonication power was used, but for different periods. The NMR experiments were done on the decanted supernatants within a few hours after sample preparation. Immediately before each NMR experiment (that is, a series of diffusion measurements lasting on the order of a day), the CNT dispersions were resonicated under mild conditions (bath sonicator Elma Sonic S10H, Elma Hans Schmidbauer GmbH, Singen, Germany) for 5 min to redisperse any CNT that could be rebundled. This step was taken as a precaution; visually, we have observed no precipitates in the used supernatants for months.

To test the reproducibility of the samples and their composition, we have repeated preparations with identical initial CNT and polymer concentrations. The final concentrations of those two components were obtained either from UV/vis absorbance (for CNT, calibrated accurately to mass concentration[25]) or from the ^{1}H NMR intensity of the CH_2 signal (integral intensity, proportional to F127 concentration[20]). As shown by Table 1, the samples were reproducible, as concerning their composition. One should note that some of the CNT remain bundled and precipitate, taking with them a fraction of the polymer. We use the decanted supernatant in our experiments, and there, the concentrations of CNT and F127 (see Table 1) are less than the initial ones. This has been studied in detail previously.[20]

Table 1. The Composition of Samples in Repeated Preparations, As Obtained by UV/Vis (CNT) or ^{1}H NMR (F127) Experiments

sample	init F127 concn, mg/mL	init CNT concn, mg/mL	final CNT concn[a] mg/mL	final F127 concn[a] (rel to sample 5)
1	3.0	3.0	0.46	0.94
2	3.0	3.0	0.54	1.08
3	3.0	3.0	0.54	1.11
4	3.0	3.0	0.51	1.05
5	3.0	3.0	0.51	1.00

[a]Final concentration refers to the concentration in the supernatant.

2.2. NMR Diffusion Experiments. The NMR experiments were performed on a Bruker 300 Avance III spectrometer (7.0 T, 300 MHz ^{1}H frequency), equipped with a DIFF25 Bruker diffusion probe. The probe has the capacity for generating magnetic field gradient pulses with a maximum gradient value of 9.7 T/m. The gradient strength, g, was calibrated by measuring the diffusion of ^{1}HDO in D_2O (1.63×10^{-9} m^2 s^{-1} at 20 °C, interpolated from literature data[26]). The diffusion experiments were performed using stimulated echo. The 90° pulse length was ∼20 μs; the gradient pulse length was set to δ = 2 ms; the gradient stabilization delay, to 2 ms; and the diffusion time, Δ, was set in separate experiments to values between 10 and 500 ms. The gradient strength, g, was increased stepwise in 16−40 steps to a maximum gradient of typically 7.5 T/m. The longitudinal relaxation time, T_1, was obtained at ∼500 ms for all Pluronic peaks, and the recycle delay was set to 3 s (∼5T_1). Other experimental details were typically as provided previously.[20]

To provide a homogeneous gradient, the samples were contained in 10 mm Shigemi tubes. Since they are prone to convection, the temperature (measured intermittently in situ by an external thermocouple) was set by the circulating cooling water for the gradient coil that provided negligible temperature distribution within the sample. The set temperature (20 ± 1 °C) was well below the known onset temperature for micellization.[28,29] Thus, diffusion experiments in neat F127 solutions (see Figure 1) provided single-exponential diffusional attenuations that, moreover, were independent of the diffusion time, Δ, set in separate experiments.[30] The self-diffusion coefficient of the free F127 molecules was obtained at 5.0×10^{-11} m^2 s^{-1}. This indicates that the polymer in solution is in unimeric form (the diffusion coefficient of the F127 aggregates was estimated[30] to be 1×10^{-11} m^2 s^{-1}). One should note that the size polydispersity of F127[30] is typically characterized by a

dx.doi.org/10.1021/jp4114046 | J. Phys. Chem. C 2014, 118, 582−589

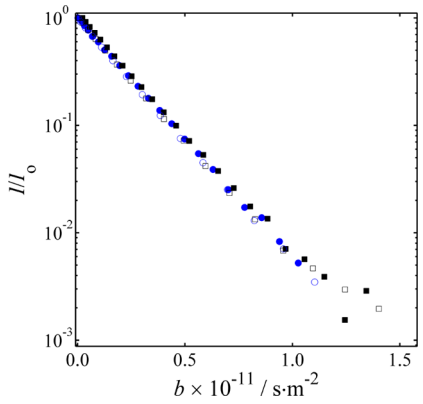

Figure 1. Diffusional decay of the ^{1}H NMR signal of the methylene protons of Pluronics F127 in 0.3 wt % aqueous solution, recorded with different diffusion times, Δ = 20 ms (circles) and Δ = 250 ms (squares); open and closed symbols correspond to repeated experiments. Symbol b is the conventional Stejskal–Tanner[27] factor, $(\gamma g \delta)^2(\Delta - \delta/3)$.

rather large PDI (= 1.2); however, our own data in Figure 1 is consistent with a polydispersity significantly smaller than that value.

2.3. Sonication Effects Investigated by Electron Microscopy and by NMR Diffusometry. The preparation of the CNT-F127 dispersion involves tip sonication. There have been diverse indications that sonication breaks CNTs. Since CNT (and polymer) size and, thereby, the diffusion coefficient have a significant bearing on our conclusions below, this effect had to be investigated in detail.

TEM micrographs were obtained by FEI Tecnai 12 G2 TWIN TEM (FEI, Hillsboro, OR). Dry samples were prepared on holey-carbon-coated copper grids (300 mesh, lacey carbon, Ted Pella) by placing a drop of dispersion on a grid and allowing it to dry at ambient conditions before storage. The microscope was operated at 120 kV in low electron dose mode (to reduce radiation damage) and with a few micrometers underfocus to increase phase contrast. Images were recorded on a Gatan 794 CCD camera and analyzed by Digital Micrograph 3.6 software.

The obtained size distributions are presented in Figure 2. From the number of nanotubes, $N(L)$, within a given length range centered on average length, L, we derive and display the $L \times N(L)$ distribution. Under the assumption that length and diameter are not correlated and, therefore, both surface and mass associated with a given nanotube are proportional to L, the $L \times N(L)$ distribution represents the length distribution of the CNT surface. As is clearly shown in Figure 2, sonication has an effect on the CNT length. Nevertheless, if we assume that CNT breakage is linearly proportional to the sonication time, from the difference between the 10 and 60 min distributions, we can conclude that at our sonication time (10 min and estimated 640 J/mL total delivered power), the size distribution is affected only slightly. Importantly, the distribution recorded after 10 min of sonication provides $L_{av} \approx 2.5$ μm as the average of the $L \times N(L)$ distribution. Considering that the amount of polymer adsorbed to a CNT is proportional to the nanotube surface, L_{av} is interpreted as the average length of CNTs to which a polymer molecule is adsorbed.

Whether sonication affects the F127 polymer itself was also investigated by performing NMR diffusion experiments in neat F127 solutions sonicated for different periods of time. The

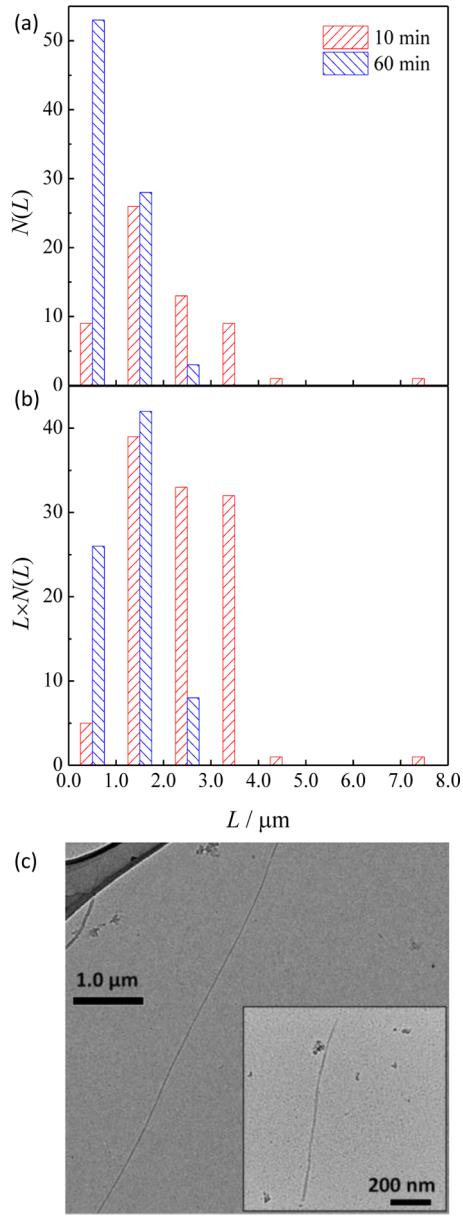

Figure 2. (a) The length distribution $N(L)$ of the CNTs in the dispersions prepared by 10 and 60 min tip sonication and as obtained by TEM analysis. (b) The distribution of accessible surface calculated as $L \times N(L)$ as derived from the data in part a. (c) Typical TEM micrographs with CNT images shown in samples with 10 min sonication (typical length > 2 μm) and 60 min sonication (see inset, typical length below 1 μm).

results without sonication and with a 10 min tip sonication did not differ (a small increase in the polymer diffusion coefficient was found first after a 60 min tip sonication, indicating decreasing polymer size). Hence, sonication did not affect the polymer component in our prepared samples.

3. RESULTS AND DISCUSSION

In this study, we recorded the diffusional decay of the ^{1}H NMR methylene signal. As has been previously established,[20] this decay is not single-exponential, but has a more complex shape that, together with its variation with the diffusion time, Δ, set to different values in different experiments, is consistent with having the F127 unimers in exchange between a slowly

dx.doi.org/10.1021/jp4114046 | J. Phys. Chem. C 2014, 118, 582–589

diffusing and a quickly diffusing molecular pool. The former pool was identified as the F127 molecules adsorbed on the CNT surface, and the latter pool, as free F127 unimers in the aqueous phase. As it has also been found, the residence time, τ_{bound}, of the polymer on the CNT surface was in the range of the NMR diffusion times, Δ, experimentally accessible in this system (∼10−500 ms).

3.1. The Reproducibility of the Amount of Adsorbed Polymer. In a two-site exchanging system having a free (with high concentration) and a bound (with low concentration) state and at diffusion times, Δ, shorter than the residence time, τ_{bound}, the diffusional decay is essentially double-exponential where the amplitudes of the two signal attenuation components are proportional to the population of molecules at the two involved sites. As shown in Figure 3, the F127 ^{1}H diffusional decay is, indeed, consistent with a two-exponential behavior. However, we observe a significant (by a factor of ∼1.2 between the extremes) variation among samples prepared in identical manner with respect to the amplitude (but not the decay slope) of the slow component identified previously as belonging to the surface-adsorbed state. As is shown in Table 1, both the amount of nanotubes and the amount of dispersed polymer is essentially (within ±10%) constant in the prepared samples. The most plausible explanation for this behavior is that the amount of exposed CNT surface varies from sample to sample and, with the dispersed CNT mass roughly constant, this might be a consequence of a varying degree of debundling in the various prepared samples (one to few SWNTs per dispersed bundle).[31] The analysis below concerns data from one of the samples (sample 5 in Figure 3) from a group of identically (within experimental error) behaving group of samples (samples 3−5). With respect to the analysis below, data from the other two samples (samples 1−2) indicate up to a factor of 2 less CNT-bound polymers.

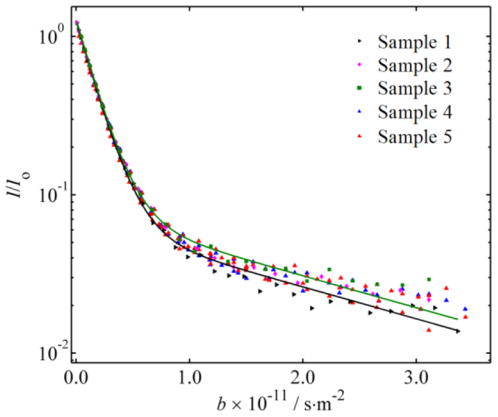

Figure 3. Diffusional decays of the ^{1}H NMR signal of the methylene protons of Pluronics F127 recorded in aqueous SWNT dispersions (see text), recorded with diffusion time Δ = 20 ms. The different symbols represent data recorded in samples numbered as in Table 1. Factor b is defined as in Figure 1. Fits to data from two samples (samples 1 and 3, colors identical to that of the corresponding symbols) are also shown.

3.2. The Lateral Surface Diffusion and the Residence Time and Its Distribution. Having previously obtained (see data in Figure 1) the self-diffusion coefficient of the free F127 molecules to 5.0 × 10^{-11} m^2 s^{-1}, we use this parameter as a fixed value (for D_{free}; see below) when attempting to fit the well-known Kärger model[32−34] (see the Supporting Information for details) to the diffusional decay obtained at different diffusion times. In our previous study,[20] performed with another CNT sample, the data obtained were well described by this model and with single values of its fitted model parameters: the fraction of surface-adsorbed F127 molecules, p_{bound}; the fraction of F127 molecules in solution, p_{free} (with p_{bound} + p_{free} = 1); and the residence time, τ_{bound}, on the nanotube surface. In that study,[20] the values of the self-diffusion coefficients in the two states, D_{bound} and D_{free}, were fixed, D_{free} to the value measured in a neat F127 solution, and D_{bound} to zero. The reason for this latter assumption was 2-fold: First, we did not consider that lateral diffusion played a role and, therefore, identified D_{bound} as the (plausibly) very slow diffusion of the CNTs. Second, in our previous studies,[20,22] the maximum value of the explored Stejskal−Tanner factor, $b = (\gamma g \delta)^2(\Delta - \delta/3)$, that scales the diffusional displacement and thereby detectable diffusion coefficient, was almost 1 order of magnitude smaller than the maximum value here. Hence, there, we were less sensitive to slow diffusion, and data had to be analyzed under some simplifying assumption, such as immobile bound F127 (D_{bound} = 0, fixed in the fits). In contrast to our previous study, the data obtained here are far more sensitive to both slow diffusion and exchange and, therefore, were fitted with all molecular properties as free parameters. Under these conditions, we found that decays that recorded different values of diffusion time could not be fitted jointly and with single values of the involved molecular parameters, as is illustrated in Figure 4a.

To explain this behavior, we investigated whether a distribution of residence times on the nanotube surface can explain the observed behavior. If that were the case, the longer the diffusion times we explore, the longer the residence times we should obtain. Hence, the diffusional decays were fitted as pairs, consisting on one hand of the data with the shortest available diffusion times (Δ = 10 and 20 ms) and on the other hand of data with one of the longer diffusion times (Δ = 100, 250, and 500 ms). As shown by Figure 4b−d and Table 2, the fitted residence times are, indeed, getting longer with increasing diffusion times.

There are two important arguments that support the validity of this model. First, the evaluation procedure is valid if the obtained residence time is longer than the shortest explored diffusion times. As is clear from Table 2, this condition is met. Under such conditions, the data at the shortest diffusion times are close to slow exchange, in which case a simple two-exponential fit (that is, independent diffusion processes in the surface-bound and free states) should provide the characteristic diffusion coefficient and the population fractions. If the model is correct, D_{bound} and p_{bound} obtained in this manner should be close to the corresponding values given in Table 2. As shown in Figure 5, this is, indeed, the case. Second, although the fits in Figure 4b−d provide a more than 3-fold variation in τ_{bound}, the variation in the other parameters obtained is merely 30%. A distribution of residence times on CNTs was also indicated in other systems and experiments.[35]

In our analysis, we have so far assumed that the diffusion of all components is three-dimensional; under that assumption, the data can be evaluated within the Kärger model; however, the diffusion on the nanotube surface is essentially one-dimensional, along the nanotube axis. Although currently, there exist no models that encompass both low dimensionality and exchange, we can evaluate the data at the shortest diffusion times, where the exchange is slow. Hence, we assume two static

dx.doi.org/10.1021/jp4114046 | J. Phys. Chem. C 2014, 118, 582−589

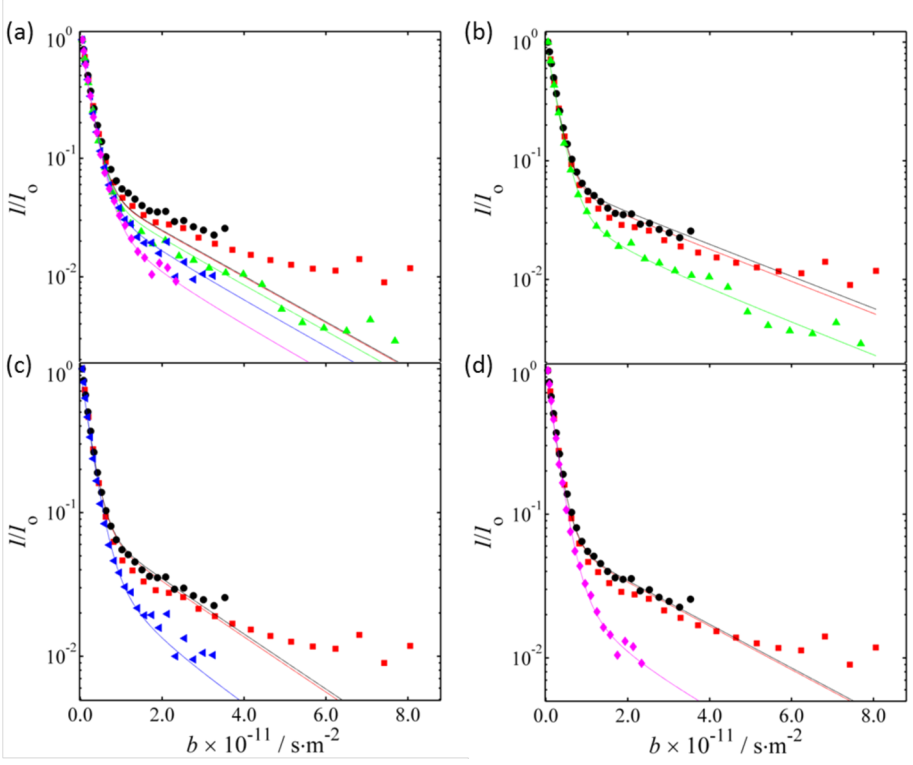

Figure 4. (a) Fitting the Kärger model[32−34] (see text) simultaneously to all diffusion data collected with diffusion times ranging from 10 to 500 ms. In b−d, the fits are to the data collected on one hand at the shortest diffusion times (Δ = 10 ms, black symbols; Δ = 20 ms, red symbols) and on the other hand to data collected at one of the longer diffusion times: (b) Δ = 100 ms, green; (c) Δ = 250 ms, blue; and (d) Δ = 500 ms, magenta.

Table 2. Values of Surface Diffusion Coefficient, Polymer Residence Time on the CNT Surface, And Fraction of Bound Polymer As Obtained from Least-Square Fitting (using the Levenberg−Marquardt algorithm) of the Kärger Model[32−34] to the Data As Illustrated in Figure 4[a]

fitting	$D_{bound}/10^{-12}$ m^2 s^{-1}	τ_{bound}/ms	p_{bound}/%
b	3.1 ± 0.1	96 ± 4	7.5
c	4.4 ± 0.1	190 ± 12	8.6
d	3.5 ± 0.1	325 ± 9	7.0

[a]See also the text. Fitting indexed as b−c−d were performed on data sets as shown in Figure 4.

pools: one with three-dimensional self-diffusion of the free F127 molecules (D = 5.0 × 10^{-11} m^2 s^{-1}) and another with unknown one-dimensional diffusion of the polymer molecules on the CNT surface, with the CNT orientations distributed isotropically in space. The latter case leads to a decay[36−38] that differs significantly form the well-known Stejskal−Tanner expression for the three-dimensional case. A full fit of this model to all data leads to large covariance among the involved parameters. Hence, the fit presented in Figure 5 was done to that range of data points where the b values provide complete decay (<10^{-3}) of the signal from the free F127 polymers. The one-dimensional lateral diffusion coefficient is obtained to $D_{1Dbound}$ = 8.0 × 10^{-12} m^2 s^{-1}. One probable complication (and a possible explanation for the systematic deviation of the fit from the data) that we do not attempt to account for at this time is preferential orientation of nanotubes along the magnetic field,[39−41] which challenges a basic assumption (isotropic distribution of the nanotube orientation) behind the model used. Such an orientational effect would render $D_{1Dbound}$ = 8.0 × 10^{-12} m^2 s^{-1} an overestimate of the real diffusion value that,

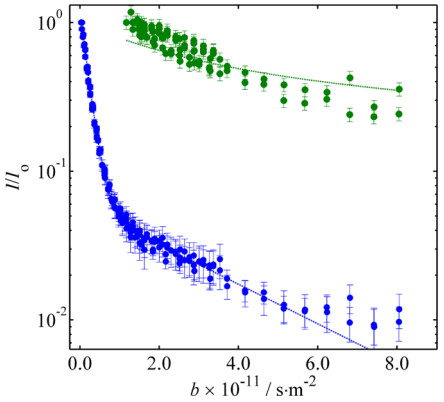

Figure 5. Fitting (blue) a simple two-component Stejskal−Tanner expression,[27] representing one quickly and one slowly diffusing pool with no exchange, to all data obtained with the shortest diffusion times Δ = 10 and 20 ms. The results of this fit (D_{bound} = 3.1 × 10^{-12} m^2 s^{-1} and p_{bound} = 5.9%) are consistent with the results in Table 2. The data collected in the b > 1.5 × 10^{11} m^{-2} s range, where freely diffusing polymers do not significantly contribute to the signal, were fitted (green, data normalized to first retained point) by a model[36−38] with explicit one-dimensional diffusion along the nanotube. This yields $D_{1Dbound}$ = 8.0 × 10^{-12} m^2 s^{-1}.

nevertheless, should be above D_{bound} obtained without having low dimensionality taken into account. Hence, to summarize, our data set was D_{bound} consistently in the range of (3−8) × 10^{-12} m^2 s^{-1}.

3.3. Lateral Diffusion vs Nanotube Diffusion. We also need to rule out the possibility that the observed diffusion coefficient characterizes the diffusion of the nanotubes themselves with the polymers tightly attached to them. The

dx.doi.org/10.1021/jp4114046 | J. Phys. Chem. C 2014, 118, 582−589

most usual formalism describing the translational diffusion of rodlike objects (at infinite dilution) is the Kirkwood model.[42,43] Evaluating the slowest of our D_{bound} values, 3.1×10^{-12} m^2 s^{-1}, within this model provides the upper bound for length of diffusing CNTs that could provide our observed diffusion coefficients. As is clear from Table 3, these upper bounds are much below the average CNT size as presented in Figure 2a. In addition, rodlike objects with concentrations as here provide significant obstruction to each other. Although theories[44−51] describing this effect are slightly discordant, both they and experiments[50,52−54] in similar systems as well as in nanotubes[55] provide that rodlike objects on the order of 2.5 μm length and 1−2 nm width should diffuse 10−20% more slowly than the infinite dilution value provided by the Kirkwood model. In other words, the expected diffusion coefficient of such an object should be clearly below 1×10^{-12} m^2 s^{-1}. Hence, we can safely identify our $D_{bound} = (3-8) \times 10^{-12}$ m^2 s^{-1} range as characteristic of the lateral diffusion of F127 on the surface of the nanotubes and not to diffusing CNTs.

Table 3. The Calculated Length of CNT Fragments of Different Assumed Tube Diameters That, within the Kirkwood Model,[42,43] Provide Our Lowest Self-Diffusion Coefficient Value of 3.1×10^{-12} m^2 s^{-1}

	assumed tube diameter/nm			
	1	2	4	6
calcd tube length/μm	0.89	0.78	0.66	0.59

3.4. Overview of Surface Dynamics in Related Systems. To our knowledge, this is the first experimental characterization of diffusion on a nanotube surface. There are very few comparisons available. NMR and quasi-elastic neutron scattering experiments have revealed a strong variation in behavior of simple adsorbed molecules on graphite. Hence, ammonia has shown a surface diffusion coefficient that was much larger than that in bulk, which was explained by the lack of H bonds for ammonia on the graphite surface.[56] Molecules such as *n*-hexane, benzene, neopentane, and butane have shown surface diffusion coefficients close (within 1 order of magnitude) to that in bulk.[57−60] On the other hand, the surface diffusion of anthracene on graphite was slowed down by 4−5 orders of magnitude, which was attributed to its strong interaction with the graphite surface.[61] Although there are scores of simulations of polymer diffusion on graphite and graphite-like (such as graphene) surfaces, experimental data seem to be lacking. As concerning simulations of polymer diffusion on the surface of nanotubes, one should exercise caution when comparing their outcomes to our experimental data; both the chemical nature of the simulated monomeric units and the solvent environment may differ, and the explored time scale is generally much shorter. Still, our data seem to contradict the results of that simulation in which the diffusion of a polyethylene chain on a CNT was obtained up to more than 2 orders of magnitude faster[17] than that found here. Other simulations[10] yielded a significant slowing of diffusion nearby CNTs in melt. As a related experimental finding, the local segmental dynamics of poly(ethylene) chains was shown by NMR relaxation experiments to slow down adjacent to fullerene surfaces.[62]

4. CONCLUSIONS

In this paper, we have investigated by NMR diffusion measurements the behavior of Pluronic F127 block copolymer molecules in aqueous dispersions of single/double-walled carbon nanotubes. This block copolymer is assumed to adsorb to the nanotubes' surfaces,[7,8] where it provides steric repulsion that leads to debundling of the original nanotube aggregates. In line with our previous studies,[20,22] we found that the polymer is exchanging on the time scale of the NMR diffusion experiment between its surface-bound and free states and, further, that it is only a small fraction of polymer that is at any given time bound to the nanotube surface. In contrast to what we established previously,[20] we also find that the polymer residence time on the nanotube surface seems to exhibit a rather broad distribution, from a few tens of milliseconds up to a few hundred milliseconds. Whether this feature is generic or is characteristic to the present dispersant-nanotube system remains to be investigated.

Our most important finding is that the $(3-8) \times 10^{-12}$ m^2 s^{-1} diffusion coefficient that is associated with the nanotube-bound polymer characterizes the lateral diffusion of the polymer on the nanotube surface. To our knowledge, this is a novel result. Ideally, one would wish to provide more accurate data instead of the range obtained. On one hand, this may require improvements in sample and material control, such as reducing nanotube polydispersity by density gradient ultracentrifugation that was shown to be advantageous in other NMR studies.[21] Moreover, we need improved models that simultaneously include low-dimensional diffusion and exchange among different sites. Despite these limitations, we find that the surface diffusion coefficient is ∼1 order of magnitude slower than the bulk diffusion of the same polymer in aqueous solution. Even if slowed down by interaction with the nanotube surface, the polymer exhibits significant mobility that is not easily consistent with tight-wrapping models of its association to CNTs.

■ ASSOCIATED CONTENT

Ⓢ Supporting Information

Calculations and additional details. This material is available free of charge via the Internet at http://pubs.acs.org.

■ AUTHOR INFORMATION

Notes

The authors declare no competing financial interest.

■ ACKNOWLEDGMENTS

Support from Fundação para a Ciência e Tecnologia (FCT, Lisbon) through projects PTDC/QUI-QUI/115212/2009, Pest/C-QUI/UI0081/2011 (CIQ-UP) and a Ph.D. grant SFRH/BD/72612/2010, and from the Swedish Research Council (VR) is gratefully acknowledged.

■ REFERENCES

(1) Bergin, S. D.; Nicolosi, V.; Streich, P. V.; Giordani, S.; Sun, Z.; Windle, A. H.; Ryan, P.; Niraj, N. P. P.; Wang, Z.-T. T.; Carpenter, L.; et al. Towards Solutions of Single-Walled Carbon Nanotubes in Common Solvents. *Adv. Mater.* **2008**, *20*, 1876−1881.

(2) O'Connell, M. J.; Boul, P.; Ericson, L. M.; Huffman, C.; Wang, Y. H.; Haroz, E.; Kuper, C.; Tour, J.; Ausman, K. D.; Smalley, R. E. Reversible Water-Solubilization of Single-Walled Carbon Nanotubes by Polymer Wrapping. *Chem. Phys. Lett.* **2001**, *342*, 265−271.

(3) Moore, V. C.; Strano, M. S.; Haroz, E. H.; Hauge, R. H.; Smalley, R. E.; Schmidt, J.; Talmon, Y. Individually Suspended Single-Walled

Carbon Nanotubes in Various Surfactants. *Nano Lett.* **2003**, *3*, 1379−1382.
(4) Strano, M. S.; Dyke, C. A.; Usrey, M. L.; Barone, P. W.; Allen, M. J.; Shan, H.; Kittrell, C.; Hauge, R. H.; Tour, J. M.; Smalley, R. E. Electronic Structure Control of Single-Walled Carbon Nanotube Functionalization. *Science* **2003**, *301*, 1519−1522.
(5) Numata, M.; Shinkai, S. 'Supramolecular Wrapping Chemistry' by Helix-Forming Polysaccharides: A Powerful Strategy for Generating Diverse Polymeric Nano-Architectures. *Chem. Commun.* **2011**, *47*, 1961−1975.
(6) Cherukuri, P.; Gannon, C. J.; Leeuw, T. K.; Schmidt, H. K.; Smalley, R. E.; Curley, S. A.; Weisman, R. B. Mammalian Pharmacokinetics of Carbon Nanotubes Using Intrinsic Near-Infrared Fluorescence. *P. Natl. Acad. Sci. USA* **2006**, *103*, 18882−18886.
(7) Granite, M.; Radulescu, A.; Cohen, Y. Small-Angle Neutron Scattering from Aqueous Dispersions of Single-Walled Carbon Nanotubes with Pluronic F127 and Poly(vinylpyrrolidone). *Langmuir* **2012**, *28*, 11025−11031.
(8) Granite, M.; Radulescu, A.; Pyckhout-Hintzen, W.; Cohen, Y. Interactions between Block Copolymers and Single-Walled Carbon Nanotubes in Aqueous Solutions: A Small-Angle Neutron Scattering Study. *Langmuir* **2011**, *27*, 751−759.
(9) Gurevitch, I.; Srebnik, S. Monte Carlo Simulation of Polymer Wrapping of Nanotubes. *Chem. Phys. Lett.* **2007**, *444*, 96−100.
(10) Karatrantos, A.; Composto, R. J.; Winey, K. I.; Kröger, M.; Clarke, N. Entanglements and Dynamics of Polymer Melts Near a SWCNT. *Macromolecules* **2012**, *45*, 7274−7281.
(11) Pang, J. Y.; Xu, G. Y. Molecular Dynamics Simulations of the Interactions between SWNT and Surfactants. *Comput. Mater. Sci.* **2012**, *65*, 324−330.
(12) Tallury, S. S.; Pasquinelli, M. A. Molecular Dynamics Simulations of Flexible Polymer Chains Wrapping Single-Walled Carbon Nanotubes. *J. Phys. Chem. B* **2010**, *114*, 4122−4129.
(13) Xin, X.; Xu, G. Y.; Zhao, T. T.; Zhu, Y. Y.; Shi, X. F.; Gong, H. J.; Zhang, Z. Q. Dispersing Carbon Nanotubes in Aqueous Solutions by a Starlike Block Copolymer. *J. Phys. Chem. C* **2008**, *112*, 16377−16384.
(14) Yang, M. J.; Koutsos, V.; Zaiser, M. Interactions between Polymers and Carbon Nanotubes: A Molecular Dynamics Study. *J. Phys. Chem. B* **2005**, *109*, 10009−10014.
(15) Zaminpayma, E.; Mirabbaszadeh, K. Interaction between Single-Walled Carbon Nanotubes and Polymers: A Molecular Dynamics Simulation Study with Reactive Force Field. *Comput. Mater. Sci.* **2012**, *58*, 7−11.
(16) Zheng, Q. B.; Xue, Q. Z.; Yan, K. O.; Hao, L. Z.; Li, Q.; Gao, X. L. Investigation of Molecular Interactions between SWNT and Polyethylene/Polypropylene/Polystyrene/Polyaniline Molecules. *J. Phys. Chem. C* **2007**, *111*, 4628−4635.
(17) Liu, J.; Wang, X. L.; Zhao, L.; Zhang, G.; Lu, Z. Y.; Li, Z. S. The Adsorption and Diffusion of Polyethylene Chains on the Carbon Nanotube: A Molecular Dynamics Study. *J. Polym. Sci., Polym. Phys.* **2008**, *46*, 272−280.
(18) Nativ-Roth, E.; Shvartzman-Cohen, R.; Bounioux, C.; Florent, M.; Zhang, D.; Szleifer, I.; Yerushalmi-Rozen, R. Physical Adsorption of Block Copolymers to SWNT and MWNT: A Nonwrapping Mechanism. *Macromolecules* **2007**, *40*, 3676−3685.
(19) Shvartzman-Cohen, R.; Florent, M.; Goldfarb, D.; Szleifer, I.; Yerushalmi-Rozen, R. Aggregation and Self-Assembly of Amphiphilic Block Copolymers in Aqueous Dispersions of Carbon Nanotubes. *Langmuir* **2008**, *24*, 4625−4632.
(20) Frise, A. E.; Pagès, G.; Shtein, M.; Bar, I. P.; Regev, O.; Furó, I. Polymer Binding to Carbon Nanotubes in Aqueous Dispersions: Residence Time on the Nanotube Surface as Obtained by NMR Diffusometry. *J. Phys. Chem. B* **2012**, *116*, 2635−2642.
(21) Shastry, T. A.; Morris-Cohen, A. J.; Weiss, E. A.; Hersam, M. C. Probing Carbon Nanotube-Surfactant Interactions with Two-Dimensional DOSY NMR. *J. Am. Chem. Soc.* **2013**, *135*, 6750−6753.
(22) Frise, A. E.; Edri, E.; Furó, I.; Regev, O. Protein Dispersant Binding on Nanotubes Studied by NMR Self-Diffusion and Cryo-TEM Techniques. *J. Phys. Chem. Lett.* **2010**, *1*, 1414−1419.
(23) Tsyboulski, D. A.; Bakota, E. L.; Witus, L. S.; Rocha, J.-D. R.; Hartgerink, J. D.; Weisman, R. B. Self-Assembling Peptide Coatings Designed for Highly Luminescent Suspension of Single-Walled Carbon Nanotubes. *J. Am. Chem. Soc.* **2008**, *130*, 17134−17140.
(24) Cau, F.; Lacalle, S. ^{1}H NMR Relaxation Studies of the Micellization of a Poly(ethylene oxide) Poly(propylene oxide) Poly(ethylene oxide) Triblock Copolymer in Aqueous Solution. *Macromolecules* **1996**, *29*, 170−178.
(25) Shtein, M.; Pri-Bar, I.; Regev, O. A Simple Solution for the Determination of Pristine Carbon Nanotube Concentration. *Analyst* **2013**, *138*, 1490−1496.
(26) Mills, R. Self-Diffusion in Normal and Heavy Water in Range of 1−45 Degrees. *J. Phys. Chem. B* **1973**, *77*, 685−688.
(27) Stejskal, E. O.; Tanner, J. E. Spin Diffusion Measurements: Spin Echoes in the Presence of a Time-Dependent Field Gradient. *J. Chem. Phys.* **1965**, *42*, 288−292.
(28) Alexandridis, P.; Holzwarth, J. F.; Hatton, T. A. Micellization of Poly(ethylene oxide)-Poly(propylene oxide)-Poly(ethylene oxide) Triblock Copolymers in Aqueous Solutions. Thermodynamics of Copolymer Association. *Macromolecules* **1994**, *27*, 2414−2425.
(29) Svensson, B.; Olsson, U.; Alexandridis, P. Self-Assembly of Block Copolymers in Selective Solvents: Influence of Relative Block Size on Phase Behavior. *Langmuir* **2000**, *16*, 6839−6846.
(30) Nilsson, M.; Håkansson, B.; Söderman, O.; Topgaard, D. Influence of Polydispersity on the Micellization of Triblock Copolymers Investigated by Pulsed Field Gradient Nuclear Magnetic Resonance. *Macromolecules* **2007**, *40*, 8250−8258.
(31) Dror, Y.; Pyckhout-Hintzen, W.; Cohen, Y. Conformation of Polymers Dispersing Single-Walled Carbon Nanotubes in Water: A Small-Angle Neutron Scattering Study. *Macromolecules* **2005**, *38*, 7828−7836.
(32) Kärger, J. Zur Bestimmung der Diffusion in einem Zweibereichsystem mit Hilfe von gepulsten Feldgradienten. *Ann. Phys.* **1969**, *479*, 1−4.
(33) Kärger, J. Der Einfluss der Zweibereichdiffusion auf die Spinechodämpfung unter Berücksichtigung der Relaxation bei Messungen mit der Methode der gepulsten Feldgradienten. *Ann. Phys.* **1971**, *482*, 107−109.
(34) Andrasko, J. Water Diffusion Permeability of Human Erythrocytes Studied by a Pulsed Gradient NMR Technique. *Biochim. Biophys. Acta* **1976**, *428*, 304−311.
(35) Roxbury, D.; Tu, X.; Zheng, M.; Jagota, A. Recognition Ability of DNA for Carbon Nanotubes Correlates with their Binding Affinity. *Langmuir* **2011**, *27*, 8282−8293.
(36) Callaghan, P. T.; Söderman, O. Examination of the Lamellar Phase of Aerosol OT/Water Using Pulsed Field Gradient Nuclear Magnetic Resonance. *J. Phys. Chem.* **1983**, *87*, 1737−1744.
(37) Callaghan, P. T.; Jolley, K. W.; Lelievre, J. Diffusion of Water in the Endosperm Tissue of Wheat Grains as Studied by Pulsed Field Gradient Nuclear Magnetic Resonance. *Biophys. J.* **1979**, *28*, 133−141.
(38) Price, W. S. *NMR Studies of Translational Motion: Principles and Applications*; Cambridge University Press: Cambridge, 2009.
(39) Fischer, J. E.; Zhou, W.; Vavro, J.; Llaguno, M. C.; Guthy, C.; Haggenmueller, R.; Casavant, M. J.; Walters, D. E.; Smalley, R. E. Magnetically Aligned Single Wall Carbon Nanotube Films: Preferred Orientation and Anisotropic Transport Properties. *J. Appl. Phys.* **2003**, *93*, 2157−2163.
(40) Fujiwara, M.; Oki, E.; Hamada, M.; Tanimoto, Y.; Mukouda, I.; Shimomura, Y. Magnetic Orientation and Magnetic Properties of a Single Carbon Nanotube. *J. Phys. Chem. A* **2001**, *105*, 4383−4386.
(41) Hone, J.; Llaguno, M. C.; Nemes, N. M.; Johnson, A. T.; Fischer, J. E.; Walters, D. A.; Casavant, M. J.; Schmidt, J.; Smalley, R. E. Electrical and Thermal Transport Properties of Magnetically Aligned Single Wall Carbon Nanotube Films. *Appl. Phys. Lett.* **2000**, *77*, 666−668.

(42) Kirkwood, J. D.; Auer, P. L. The Visco-Elastic Properties of Solutions of Rod-like Macromolecules. *J. Chem. Phys.* **1951**, *19*, 281−283.
(43) Teraoka, I. *Polymer Solutions*; Wiley: New York, 2002.
(44) Doi, M.; Edwards, S. F. Dynamics of Rod-like Macromolecules in Concentrated Solution 1. *J. Chem. Soc., Faraday Trans. II* **1978**, *74*, 560−570.
(45) Doi, M.; Edwards, S. F. Dynamics of Rod-like Macromolecules in Concentrated Solution 2. *J. Chem. Soc., Faraday Trans. II* **1978**, *74*, 918−932.
(46) Doi, M.; Yamamoto, I.; Kano, F. Monte-Carlo Simulations of the Dynamics of Thin Rodlike Polymers in Concentrated Solution. *J. Phys. Soc. Jpn.* **1984**, *53*, 3000−3003.
(47) Fixman, M. Simulation of Polymer Dynamics 2. Relaxation Rates and Dynamic Viscosity. *J. Chem. Phys.* **1978**, *69*, 1538−1545.
(48) Fixman, M. Entanglements of Semidilute Polymer Rods. *Phys. Rev. Lett.* **1985**, *54*, 337−339.
(49) Löwen, H. Brownian Dynamics of Hard Spherocylinders. *Phys. Rev. E* **1994**, *50*, 1232−1242.
(50) Phillies, G. D. J. The Hydrodynamic Scaling Model for Polymer Self-Diffusion. *J. Phys. Chem.* **1989**, *93*, 5029−5039.
(51) Sato, T.; Teramoto, A. Dynamics of Stiff-Chain Polymers in Isotropic Solution. Zero-Shear Viscosity of Rodlike Polymers. *Macromolecules* **1991**, *24*, 193−196.
(52) Bitsanis, I.; Davis, H. T.; Tirrell, M. Brownian Dynamics of Nondilute Solutions of Rodlike Polymers 2. High Concentrations. *Macromolecules* **1990**, *23*, 1157−1165.
(53) Cush, R. C.; Russo, P. S. Self-Diffusion of a Rodlike Virus in the Isotropic Phase. *Macromolecules* **2002**, *35*, 8659−8662.
(54) Russo, P. S.; Karasz, F. E.; Langley, K. H. Dynamic Light-Scattering Study of Semidilute Solutions of a Stiff-Chain Polymer. *J. Chem. Phys.* **1984**, *80*, 5312−5325.
(55) Tsyboulski, D. A.; Bachilo, S. M.; Kolomeisky, A. B.; Weisman, R. B. Translational and Rotational Dynamics of Individual Single-Walled Carbon Nanotubes in Aqueous Suspension. *ACS Nano* **2008**, *2*, 1770−1776.
(56) Tabony, J.; Cosgrove, T. Diffusion Coefficients of Small Molecules at the Gas-Solid Interface As Measured by the Nuclear Magnetic Resonance Pulsed Field Gradient Method. *Chem. Phys. Lett.* **1979**, *67*, 103−106.
(57) Tabony, J. Nuclear Magnetic Resonance Studies of Molecules Physisorbed on Homogeneous Surfaces. *Prog. Nucl. Magn. Reson. Spectrosc.* **1980**, *14*, 1−26.
(58) Boddenberg, B.; Grundke, V.; Auer, G. Dynamics and Orientation of Molecules Adsorbed on Graphite Studied by Deuteron NMR Spectroscopy. *Ber. Bunsenges. Phys. Chem.* **1990**, *94*, 348−353.
(59) Boddenberg, B.; Neue, G. An NMR Study of an *n*-Butane Film on Graphite 1. ^{2}H Relaxation of the 2D Fluid State. *Mol. Phys.* **1989**, *67*, 385−398.
(60) Grundke, V.; Boddenberg, B. One- and Two-Component Adsorption Layers of *n*-Hexane and Benzene on Graphite Studied by ^{2}H NMR Spectroscopy. *Mol. Phys.* **1993**, *79*, 1215−1226.
(61) Neue, G. Anthracene Adsorbed at the Solid/Liquid Interface. A ^{2}H-NMR Study of the Dynamics and Structure. *Z. Naturforsch.* **1987**, *43a*, 30−34.
(62) Li, M. J.; Chen, Q. Interactions between Fullerene(C-60) and Poly(ethylene oxide) in their Complexes as Revealed by High-Resolution Solid-State ^{13}C NMR Spectroscopy. *Polymer* **2003**, *44*, 2793−2798.

Supporting information

Lateral diffusion of dispersing molecules on nanotubes as probed by NMR

Ricardo M. F. Fernandes[1,2], Matat Buzaglo[3], Michael Shtein[3], Ilan Pri Bar[3], Oren Regev[3]*, Eduardo F. Marques[1]*, and István Furó[2]*

[1]*Centro de Investigação em Química, Department of Chemistry and Biochemistry, Faculty of Science, University of Porto, Rua do Campo Alegre, s/n, P-4169-007 Porto, Portugal.*

[2]*Division of Applied Physical Chemistry, Department of Chemistry, KTH Royal Institute of Technology, SE-10044 Stockholm, Sweden.*

[3]*Department of Chemical Engineering and the Ilse Katz Institute for Nanotechnology, Ben-Gurion University of the Negev, 84105 Beer-Sheva, Israel.*

In the case of free diffusion in three dimensional media, pulsed-field-gradient spin-echo-type NMR experiments[1, 2] provide an attenuation of the signal S that is described by the well-known Stejskal-Tanner expression[3]

$$S = S_0 \, \mathrm{e}^{-bD} \tag{1a}$$

where S_0 the signal intensity in the absence of gradients, D the self-diffusion coefficient, and the b factor is given as

$$b = \gamma^2 \delta^2 g^2 (\Delta - \delta / 3) \tag{1b}$$

where γ is the magnetogyric ratio of the nucleus, δ the length of the gradient pulse of magnitude g, and Δ is the diffusion time.

The Kärger model

If the nuclear magnetization is allowed to exchange (either by cross-relaxation or by atomic/molecular exchange) between different states that are characterized by their own distinct diffusion coefficients, the signal decay takes a more complex form. Below, we re-capitulate the well-known model suggested originally by Kärger.[4-6] Specifically, we consider that case of stimulated echo, where the longitudinal evolution period (τ_2, the delay between the second and third 90º pulse in the conventional experiment) is much longer than the encoding-decoding periods (τ_1, the delay between the first and second 90º pulse). Hence, we assume $\Delta \approx \tau_2$.

The two-site exchange model is introduced in Fig. S1; $k_{f/b}$, $R_{f/b}$ and $D_{f/b}$ represent the exchange rates, longitudinal relaxation rates and translational self-diffusion coefficients, respectively for "free" (*f*) and "bound" (*b*) states.

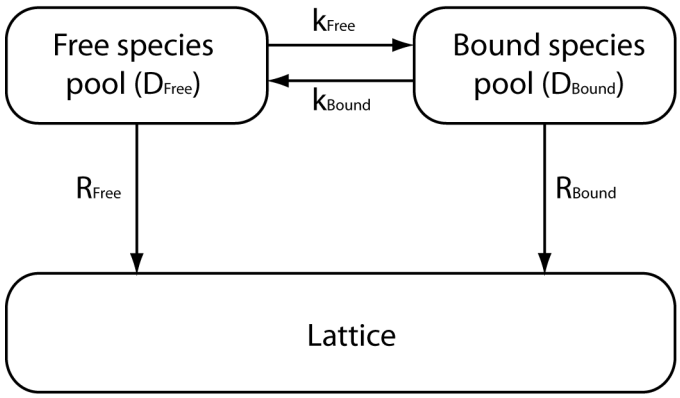

Figure S1*: Schematic representation of the two-site exchange model used to evaluate the results of stimulated-echo-type diffusion experiments performed in systems with exchanging pools of nuclear magnetization. k and R denote exchange and spin relaxation rates, respectively.*

This model yields the following coupled differential equations for the (arbitrarily scaled) nuclear magnetization *M* detected for the two components:

$$\frac{dM_f(t)}{dt} = -((2\pi q)^2 D_f + k_f + R_f)M_f(t) + k_b M_b(t) \qquad (2a)$$

and

$$\frac{dM_b(t)}{dt} = -((2\pi q)^2 D_b + k_b + R_b)M_b(t) + k_f M_f(t) \qquad (2b)$$

with $q = \frac{\gamma g \delta}{2\pi}$. With initial conditions

$$M_f(0) = P_f = 1 - P_b \qquad (3a)$$

and

$$M_b(0) = P_b \qquad (3b)$$

where P_f and P_b are the relative spin populations, one obtains that the attenuation of the total signal intensity is

$$S(q,\Delta) \propto (1-P_2)e^{-(2\pi q)^2 D_1 \Delta} + P_2 e^{-(2\pi q)^2 D_2 \Delta} \qquad (4a)$$

with

$$D_{1,2} = \frac{1}{2}\left[D_f + D_b + \frac{k_f + k_b + R_f + R_b}{(2\pi q)^2} \mp \left\{ \left(D_f - D_b + \frac{k_f - k_b + R_f - R_b}{(2\pi q)^2} \right)^2 + \frac{4k_f k_b}{(2\pi q)^4} \right\}^{\frac{1}{2}} \right] \qquad (4b)$$

and

$$P_2 = \frac{P_f\left(D_f + \frac{R_f}{(2\pi q)^2} \right) + P_b\left(D_b + \frac{R_b}{(2\pi q)^2} \right) - D_1}{D_2 - D_1} \qquad (4c)$$

In equilibrium, detailed balance sets the populations as

$$P_{f/b} = \frac{k_{b/f}}{k_f + k_b} \qquad (5)$$

First-order corrections apply in experimental situations where τ_1 is not of negligible length. The results are valid for the case where the transverse relaxation is sufficiently long ($T_2 >> \tau_1$). If that assumption is not valid, one obtains a modified expression, with the same apparent decay constants $D_{1,2}$ but with different intensities. In the analysis in our accompanying paper, we assumed the same longitudinal relaxation rates for the free and bound pools.

One-dimensional diffusion with isotropic distribution of orientation

Since the nanotube width is negligible with respect to the displacements that can contribute to signal decay in NMR diffusion experiments, it is only the displacement parallel to the nanotube axis, $D_{||}$ (denoted as $D_{1Dbound}$ in the accompanying paper), that is relevant. In effect, the diffusion propagator is then characterized by an axially symmetric diffusion tensor with two of its elements describing diffusion perpendicular to the nanotube axis set to zero, $D_{\perp} = 0$. The resulting decay[1, 2] is

$$S = \frac{S_0}{2}\left(\frac{\pi}{bD_{||}}\right) erf(\sqrt{bD_{||}}) \qquad (6)$$

where *erf* denotes the error function.

1. Callaghan, P. T., *Translational Dynamics and Magnetic Resonance: Principles of Pulsed Gradient Spin Echo NMR*. Oxford University Press: 2011.
2. Price, W. S., *NMR Studies of Translational Motion: Principles and Applications*. Cambridge University Press: 2009.
3. Stejskal, E. O.; Tanner, J. E. Spin diffusion measurements: Spin echoes in the presence of a time-dependent field gradient. *J. Chem. Phys.* **1965,** *42*, 288-292.
4. Andrasko, J. Water diffusion permeability of human erythrocytes studied by a pulsed gradient NMR technique. *Biochim. Biophys. Acta* **1976,** *428*, 304-311.

5. Kärger, J. Zur Bestimmung der Diffusion in einem Zweibereichsystem mit Hilfe von gepulsten Feldgradienten. *Ann. Phys.* **1969,** *479*, 1-4.
6. Kärger, J. Der Einfluss der Zweibereichdiffusion auf die Spinechodämpfung unter Berücksichtigung der Relaxation bei Messungen mit der Methode der gepulsten Feldgradienten. *Ann. Phys.* **1971,** *482*, 107-109.

II

Surface coverage and competitive adsorption on carbon nanotubes

Ricardo M.F. Fernandes, Matat Buzaglo, Oren Regev, Eduardo F. Marques and István Furó

J Phys Chem C, **2015**, 119, 22190–22197

THE JOURNAL OF PHYSICAL CHEMISTRY C

Article

pubs.acs.org/JPCC

Surface Coverage and Competitive Adsorption on Carbon Nanotubes

Ricardo M. F. Fernandes,[†,§] Matat Buzaglo,[‡] Oren Regev,[‡] Eduardo F. Marques,[§] and István Furó*[,†]

[†]Division of Applied Physical Chemistry, Department of Chemistry, KTH Royal Institute of Technology, SE-10044 Stockholm, Sweden

[‡]Department of Chemical Engineering and the Ilse Katz Institute for Nanotechnology, Ben-Gurion University of the Negev, 84105 Beer-Sheva, Israel

[§]Centro de Investigação em Química, Department of Chemistry and Biochemistry, Faculty of Science, University of Porto, Rua do Campo Alegre, s/n, P-4169-007 Porto, Portugal

Supporting Information

ABSTRACT: The binding strength of dispersants to the surface of carbon nanotubes is of crucial importance for the efficiency of the dispersion process and for potential applications, yet data are scarce on this subject. Here we present the results of diffusion NMR experiments in dispersions of single-walled carbon nanotubes (SWNTs) prepared by either the polymer Pluronics F127 or the protein bovine serum albumin (BSA). The experiments detect the amount of F127 molecules adsorbed onto the SWNT surface. This quantity is recorded (i) in F127-SWNT dispersions to which BSA molecules are added and (ii) in BSA-SWNT dispersions to which F127 molecules are added. The data clearly show that F127 replaces BSA adsorbed at the SWNT surface, while BSA leaves the adsorbed F127 coverage intact. Consequently, F127 binds to the nanotube surface more strongly than BSA. Hence, we provide a way to categorize dispersants by adsorption strength. We also provide evidence showing that the nanotubes dispersed by BSA form loose aggregates where a large part of the surface is not in direct contact with the surrounding liquid. The results are discussed in relation to previous findings in the literature.

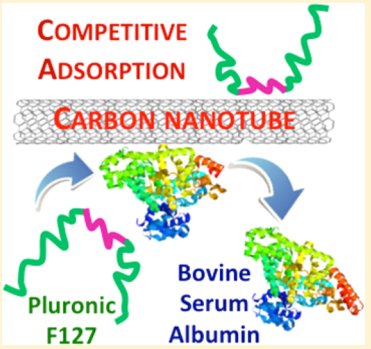

INTRODUCTION

Carbon nanotubes (CNTs) are a challenging nanomaterial to work with because their most promising applications—from molecular electronics and energy storage to composite reinforcement—require them to be separated and individually dispersed; however, individual nanotubes are attracted to each other by van der Waals forces preventing stable dispersion in most liquids. In particular, pristine CNTs, that are hydrophobic in nature, do not disperse at all in water and require either covalent surface modification or the addition of dispersing agents.[1−4] These latter molecules are assumed to adsorb on the CNT outer surface and exert steric or electrostatic repulsion between the individual CNTs. Examples for CNT dispersants are bovine serum albumin (BSA) protein[5−10] and the Pluronics[8,11−16] polymers. The physical state of the dispersants could be either surface-absorbed or free in the host liquid.[17−19] In this respect, the dispersants are characterized by their binding affinity to the CNTs and the kinetics of their adsorption. Conversely, separating different sorts of nanotubes (such as metallic or semiconducting) from each other is permitted by different binding affinity of dispersants to those different nanotube sorts.[20]

To date, the rational design of CNT dispersions is to maximize the coating affinity of the dispersant to the CNT surface to enhance its dispersibility in aqueous media. Assorted molecular properties such as aromatic content, hydrophobicity, and charge have a joint influence.[4,21,22] In addition, the process of dispersing CNTs is seemingly rather complex. Starting from large and dense bundles, it is typically sonication that is used to open up clefts and the first crucial role of the dispersant is assumed to be to quickly adsorb on the previously unexposed CNT surfaces within the cleft and thereby prevent it to reclose.[23] The performance of a particular dispersant during this step must depend on binding strength, local dispersant concentration, and adsorption kinetics. The second and different role of the dispersant is to prevent the reaggregation of already dispersed CNTs, either individual or in the form of small bundles.[24] The fact that these two particular roles are distinct and are governed by distinct properties of the dispersant is strikingly demonstrated by the previous observation by diffusion NMR experiments,[5,11,12] namely, that only a minor fraction (a few percent) of all dispersant molecules is actually adsorbed on the CNT surface. It is this fraction that seems to be required to keep a given amount of CNT dispersed. Contrariwise, a solution with total dispersant concentration equal to that minor amount of dispersant cannot, by itself, yield dispersions with any comparable CNT concentration.

Received: July 12, 2015
Revised: September 3, 2015
Published: September 4, 2015

DOI: 10.1021/acs.jpcc.5b06685
J. Phys. Chem. C 2015, 119, 22190−22197

Because dispersing CNTs is a complex process, it is not surprising that a series of dispersing agents such as various ionic surfactants produce a series of corresponding dispersions in a manner that is not always easy to rationalize[1,25] even if stringent experimental protocols are used. This highlights the need to assess individual properties that play a role in the dispersion process. In particular, the binding strength of the dispersant to the CNT surface is of interest. In aqueous medium, dispersant binding has been scarcely assessed. One method to use is intrinsic near-IR fluorescence that is sensitive only to individual SWCNTs[13] and varies with the nature of its surrounding medium.[13,26,27] In this manner, one observed dispersant replacement on SWNTs when blood serum proteins were added to Pluronics-coated SWNT dispersions.[13] Raman spectroscopy could also detect the fluorescence of individual SWNTs (~2300 cm^{-1}) providing insight into the dispersion efficiency, which was related to the dispersant affinity to the SWNT surface.[7] AFM has also been used as a method to visualize the amount of various proteins associated with SWNTs.[28] Previously, a diffusion NMR approach has been suggested by us[5,11,12] and others[29,30] to study the binding of dispersants in aqueous dispersions to SWNTs. In particular, we found that the dispersant is exchanging between its surface-bound and free states, an exchange that—for Pluronic F127—proceeded with a short (on the order of 100 ms) residence time on the surface.[11,12] Furthermore, we have shown that the CNT-bound F127 molecules diffuse laterally on the nanotube surface with a diffusion coefficient that is significantly smaller than that for bulk diffusion of the same polymer in aqueous solution.[12]

In this work, we return to diffusion NMR to characterize another aspect of dispersant binding to SWNT, namely, the binding strength. What we exploit here is the ability of diffusion NMR to detect the extent of the surface-adsorbed fraction of F127 molecules, and we investigate how that fraction changes upon adding another dispersant. In this way, we intend to gauge the relative binding strength under the rather straightforward assumption that more strongly bound dispersants replace weakly bound ones on the nanotube surface. As presented later, we find that Pluronic F127 binds more strongly to the SWNT surface than BSA does. One should note that dispersions, particularly those with high SWNT content, contain a dominant fraction of SWNT in the form of small bundles.[15] Individual dispersed nanotubes can be investigated by removing bundles by ultracentifugation;[20,31] indeed, this is a necessary step for those spectroscopic techniques where the detection of dispersant replacement requires individual nanotubes.[13] The NMR method explored here does not distinguish between bundles and individual nanotubes and works for both.

EXPERIMENTAL SECTION

Materials and Sample Preparation. CoMoCat single-walled carbon nanotubes of nominal (6,5) chirality and median diameter of 0.78 nm (SG65i, SouthWest NanoTechnologies) were investigated as provided by the manufacturer. The pristine material was described as dominantly semiconducting (95%), with its largest (41%) single fraction consisting of (6,5) nanotubes (with major residual fractions of (8,4), (7,5), and (9,2) nanotubes and, in addition, 28% of nanotubes with unknown chirality) and is assumedly also a mixture of different enantiomers. Pluronic F127 (~12.5 kDa), BSA (~66.5 kDa, assay ≥98%), and heavy water (99.9 atom % D) were purchased from Sigma-Aldrich. All materials were used as received.

The SWNT powder was weighted (3.0 mg) to a vial with a spherical bottom to which 3 mL of the selected dispersant solution (either with F127, initial concentration of 2.0 or 3.0 mg/mL for samples in Figures 1 and 2, or with BSA, initial concentration of 2.0 mg/mL) was subsequently added. The sample was sonicated using a Qsonica Q-500 tip sonicator equipped with a 3 mm microtip. It is known that the geometry of the vial used affects the sonication result, and it is particularly important to avoid the so-called dead zones without cavitation.[32] In our case, the microtip was always carefully inserted 1 cm below the liquid surface and at the center of a vial with a spherical bottom, 1.4 cm inner diameter and 3.8 cm length; such an arrangement was indicated to minimize the dead zones.[32] The sonication time was set to 10 min during which 750 $J \cdot mL^{-1}$ (1.25 $W \cdot mL^{-1}$) was transferred to the liquid

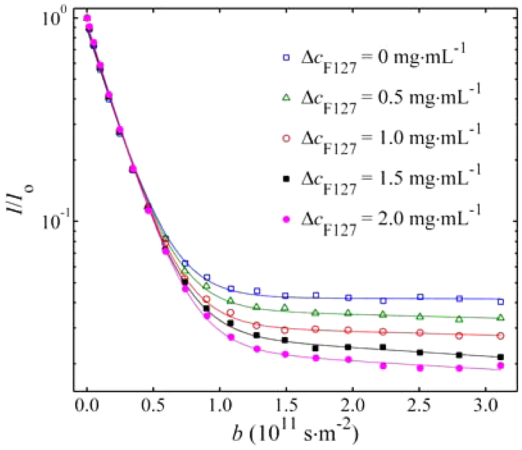

Figure 1. Diffusional decay of the ^1H NMR signal from the F127 oxyethylene peak as a function of Δc_{F127}, the amount of F127 added to an F127-SWNT dispersion. The initial concentrations in the dispersion were $c_{F127\text{-}NMR}$ = 2.1 mg·mL^{-1} and c_{SWNT} = 0.24 mg·mL^{-1}. The lines are two-component exponential fits (see eqs S1−S3 in Supporting Information) where the amplitudes of the two components provide the populations of the free aqueous (fast component) and surface-adsorbed (slow component) F127 populations. The individual exponential components are described by the conventional Stejskal−Tanner expression[34] for diffusional decay.

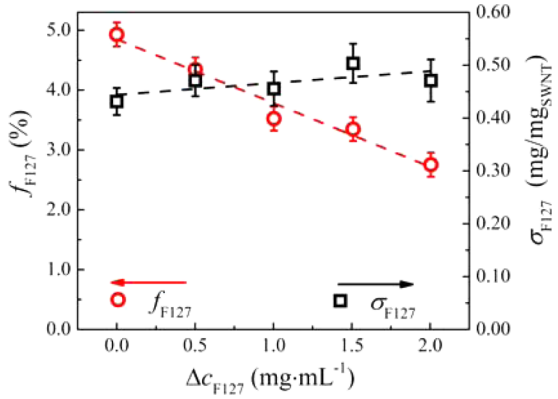

Figure 2. Fraction f_{F127} of F127 adsorbed on the SWNT surface and the corresponding apparent surface coverage σ_{F127} by F127 molecules (see eq 2) as a function of F127 added to a dispersed system with start concentrations $c_{F127\text{-}NMR}$ = 2.1 mg·mL^{-1} and c_{SWNT} = 0.24 mg·mL^{-1}. The dashed lines are linear fits. Errors are as calculated in the Supporting Information.

DOI: 10.1021/acs.jpcc.5b06685
J. Phys. Chem. C 2015, 119, 22190−22197

medium (estimated by calorimetry). The sample temperature during sonication was kept at 18 °C using a circulated water bath. After the sonication step, the sample was transferred to a narrower (9 mm inner diameter) tube and then centrifuged at 4 × $10^3 g$ during 30 min. The supernatant (ca. half the total volume, corresponding to the liquid more than 15 mm above the precipitate line) was carefully collected by a pipet for performing the various experiments detailed later.

SWNT and Dispersant Quantification in the Supernatant. The SWNT concentration in the supernatant was determined using the methodology published elsewhere.[33] The TGA analysis of the dried supernatant and the neat dispersant were carried out with a Mettler Toledo TGA/DSC 1 Star system (alumina crucible 70 μL) with an N_2 flow rate of 50 mL·min^{-1}. The thermal analysis was set with an initial isotherm at 25 °C during 10 min, followed by a ramp of 25−500 °C (at the rate 10 °C/min) and an isotherm at 500 °C during 15 min. Because SWNTs do not decompose under the previously described conditions, the mass loss observed has been assigned to the dispersant fraction in the dried supernatant.

A known volume (V_s) of the supernatant was vacuum-oven-dried (T = 40 °C) during 24 h. Thermogravimetric analysis yielded the TGA mass loss fraction obtained in the dry supernatant ϕ_s and the TGA mass loss fraction in neat dry surfactant ϕ_d. Assuming mass balance allows one to obtain the SWNT concentration in the supernatant c_{SWNT}

$$c_{SWNT} = \left[\frac{m_s}{V_s} \times \left(1 - \frac{\phi_s}{\phi_d}\right)\right] \quad (1)$$

where the ϕ_s/ϕ_d ratio accounts for incomplete surfactant decomposition and m_s is the dried supernatant mass (mg). Table S1 (Supporting Information) presents the actual data.

A double-beam spectrophotometer (Varian Cary 300 Bio) was used to record the optical density. All measurements were carried out in the range 600−800 nm (see Supporting Information, SI) using a cuvette with an optical path of 0.4 cm, without dilution; water was used as reference. The optical density measured at 660 nm was used to quantify the SWNT dispersed.[33] By combining the optical density measurements and c_{SWNT} obtained by TGA, one can estimate the apparent extinction coefficient as ε_{660} = 41.2 mL·mg^{-1}·cm^{-1}. Subsequently, this value was used to estimate the SWNT concentrations of the dispersions prepared by simple optical density measurement at 660 nm.

NMR Diffusion Experiments. The ^{1}H NMR experiments were carried out in Bruker Avance III spectrometer equipped with a standard-bore magnet providing a 500 MHz resonance for ^{1}H Bruker and a z-gradient probe DIFF30. The gradient pulses were provided by a Bruker GREAT 60 gradient. The diffusion experiments were performed using the stimulated echo sequence.[34,35] The 90° pulse length was ∼7 μs, the gradient pulse length was set to δ = 2 ms, the gradient stabilization delay to 1 ms, and the diffusion time to Δ = 20 ms. All the measurements were carried out at 20.0 °C and the gradient strength was calibrated by measuring the diffusion of ^{1}HDO in D_2O (1.63 × 10^{-9} m^2·s^{-1} at 20 °C, reference value from literature[36]). The longitudinal relaxation time, T_1, obtained for Pluronic and BSA peaks is ∼500 ms, and the recycle delay was set to 3 s (∼5T_1). To use low sample volumes (∼100 μL) and provide a homogeneous gradient, the samples were placed in 5 mm Shigemi tubes. Additional parameters used were as previously provided.[5,11,12]

RESULTS AND DISCUSSION

State of Dispersants Adsorbed on SWNTs As Seen by Diffusion NMR. The behavior of the block copolymer dispersant F127 has been previously investigated.[11,12] With diffusion NMR experiments like the ones performed here we detected double-exponential diffusional decays and from those and their variation with the set diffusion time we obtained some important insights.

First, we have clearly identified two distinct populations of dispersant molecules, one with fast and one with much slower self-diffusion coefficients. Because the experiments were performed under conditions where F127 molecules do not self-assemble, those two populations were identified as (i) free F127 molecules in bulk aqueous solution that exhibited fast diffusion and (ii) F127 molecules that were adsorbed on the surface of the dispersed SWNTs and exhibited slow diffusion. Here, a word of caution. While we identified those two populations, we could not directly exclude the possibility that some additional small adsorbed F127 populations existed yet remained undetected in NMR experiments.[37] To quantify the maximum extent of such a hypothetical population, we can compare the concentration data of F127 in a dispersion, on the one hand, from ^{1}H NMR (that yields the total concentration of suitably mobile and thereby detectable F127 molecules, i.e., $c_{F127\text{-}NMR}$) and, on the other hand, from TGA (that provides the total concentration of F127, i.e., $c_{F127\text{-}TGA}$) The small difference $\delta c = (c_{F127\text{-}TGA} - c_{F127\text{-}NMR})$ = 0.19 mg·mL^{-1} signifies that, if anything, such a hypothetical population is small (<8%, from the data in Table S1 in the Supporting Information.)

Second, we could also show with good accuracy that the minor fraction adsorbed on the SWNT surface had the extent of a few % of the total F127 content. Hence, while dispersing the SWNTs required a rather large F127 concentration, having to keep the dispersed nanotubes or nanotube bundles apart and hinder them from reaggregation (at least, on the time scale of days) requires much less adsorbed dispersant. Indirectly, this has pointed to the potentially important role of the kinetics, in particular, the dispersant diffusion to and dispersant adsorption on the NT surface as governing factors during the cleavage of large NT bundles into smaller components.

Third, this last issue of kinetics was further elaborated by having detected a dynamic equilibrium established by exchange of the F127 molecules between their two reservoirs, free and NT-adsorbed. From the results of NMR diffusion experiments performed with different diffusion times in the 10 to 500 ms range, we could clearly demonstrate that the residence time of F127 on the NT surface is on the order of 10^2 ms.[38]

Because BSA disperses SWNTs, one must assume it adsorbs to some extent to the SWNT surface. Our previous results obtained in systems dispersed by BSA[5] indicated that, similarly to F127, it was only a minor fraction of all BSA, initially required for dispersing the NT, that was adsorbed at the NT surface in the (quasi-) equilibrium state of dispersion. The NMR diffusion experiments performed on the BSA signal were much less permissive as concerning choosing experimental parameters. In particular, the transverse relaxation rate for the BSA spectral peaks was much higher than that for the F127 oxyethylene peak. Hence, the signal-to-noise ratio was far lower for BSA; however, the signal collected in sufficiently long experiments (see Figure S4 in Supporting Information) reveals a diffusional decay that is essentially monoexponential. This finding provides indication for not having a significant (>1%)

DOI: 10.1021/acs.jpcc.5b06685
J. Phys. Chem. C 2015, 119, 22190−22197

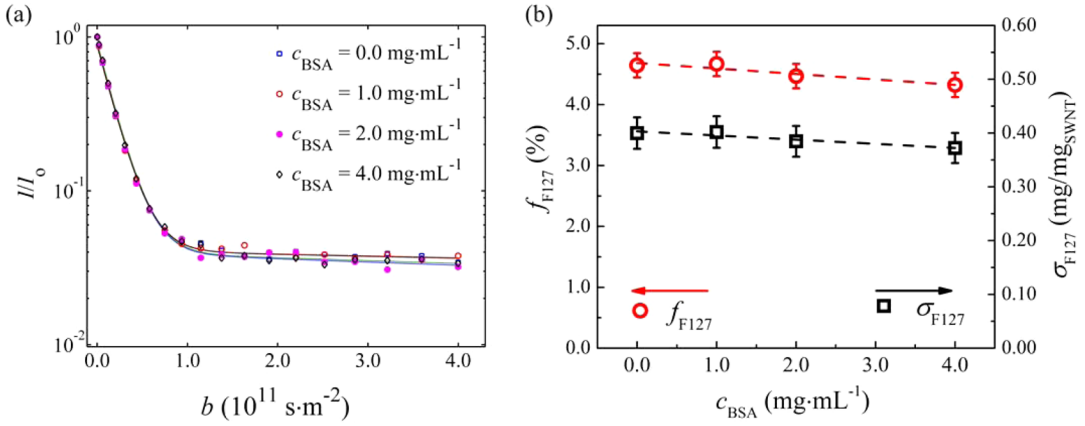

Figure 3. (a) Diffusional decay of the ^{1}H NMR signal from the F127 oxyethylene peak as a function of BSA added to a F127-SWNT dispersion with an initial concentration of $c_{F127\text{-}NMR}$ = 1.0 mg·mL^{-1} and c_{SWNT} = 0.12 mg·mL^{-1}. The lines are two-component exponential fits; see Figure 1. (b) Fraction f_{F127} of F127 adsorbed on the SWNT surface and the corresponding apparent surface coverage σ_{F127} by F127 molecules, with increasing amount of added BSA. The dashed lines are linear fits.

population of BSA with long (that is, comparable to the set diffusion time Δ = 20 ms) residence time on the NT surface. As an important methodological point, because we could not detect any slowly exchanging BSA population, the fraction of BSA residing on the NT surface was estimated from the slower *average* diffusion coefficient.[5] Because the estimate of the adsorbed fraction has been derived from the difference between two rather close diffusion coefficient values (denoted[5] as D_{obs} and D_{free}), it is consequently laden by an experimental error that was much larger than that for the same quantity for adsorbed F127. A short (<20 ms) residence time for BSA may, under the assumption of having a first-order process for the desorption step,[39] be considered as a sign of binding to the SWNT surface that is weaker for BSA than that for F127. In case of a more complex kinetics or interactions between the adsorbed species, the connection between residence time and binding strength is less straightforward, yet a monotonic relation between residence time and binding strength is often observed in, for example, drug binding.[40] It is the relative strength of binding that will be further addressed by some of the results later.

Dynamic Equilibrium and Surface Coverage of a Single Dispersant: F127 on SWNT. As previously discussed, NMR diffusion experiments indicated that there exists a dynamic equilibrium between the different F127 reservoirs.[11,12] It is this point we investigate further by studying in more detail the nature of that dynamic equilibrium. The results obtained here also constitute the baseline against which we develop below our results on competitive absorption between F127 and BSA. The experimental procedure was: (i) to record the variation of the ^{1}H NMR diffusional decay of the oxyethylene signal after having increased by Δc_{F127} the concentration of F127 in the dispersion (see Figure 1) by adding a small amount of highly concentrated F127 solution to the original dispersion and (ii) to extract the fraction of the NT-adsorbed population by least-squares fitting the recorded NMR diffusional decays to a simple two-site model (see details in the Supporting Information).

As is clear in Figure 1, the *relative* population of NT-adsorbed F127 molecules decreases (see data in Table S2 in Supporting Information) upon the addition of more and more F127, which shows that the added F127 contributes more to the free aqueous population than to the NT-adsorbed population. For a more quantitative evaluation, one should recall that there is much more F127 in the bulk aqueous phase than in surface-adsorbed form. Hence, the bulk phase can be well approximated as an infinite reservoir, and we can rationalize the adsorption behavior in terms of adsorption isotherms.

In Figure 2, we display first the relative population of F127 in the NT-adsorbed state, f_{F127} identified as the relative population of the slowly diffusing F127 molecules. (See eq S4 in the Supporting Information.) Second, because we know both the total F127 ($c_{F127} = c_{F127\text{-}NMR} + \Delta c_{F127}$) and the total SWNT ($c_{SWNT}$) concentrations of the explored samples, a measure of surface coverage (although on a mass basis) can be simply obtained as

$$\sigma_{F127} = (f_{F127} \times c_{F127})/c_{SWNT} \quad (2)$$

As is clear in Figure 2, this apparent surface coverage is, within experimental error, constant or increases very weakly. (The value suggested by the fit in Figure 2 is 6% upon a 2-fold increase in the total F127 concentration; the initial $c_{F127\text{-}NMR}$ is approximately the maximum value of Δc_{F127}.) Even though it is not well established which particular adsorption isotherm, and for what reasons, various macromolecules exhibit on SWNT surfaces, a constant surface coverage in a sufficiently wide range of concentration is usually taken as an indication for surface saturation.[41,42] Hence, we can conclude that in the prepared dispersions the SWNT surface is rather close to saturation by F127.

The apparent surface coverage σ_{F127} can be used, together with the theoretical specific outer surface area SSA = 1315 m^2·g^{-1} of SWNTs[43] and the approximate σ_{PPO} = 300 m^2·g^{-1} specific area of adsorption of the PPO block[44] of the F127 molecule, to estimate that ca. 10% of the total (that is, assuming complete debundling) available SWNT surface is covered by the PPO blocks. If we assume that saturation by F127 is equivalent to saturation surface coverage by PPO and posit that only the outer surface of bundles is available for F127 adsorption,[43] we obtain a conservative upper limit of ca. 10^2 nanotubes for the average size of the bundles in the current dispersions.

Lack of Displacement of Adsorbed F127 by BSA. As has been previously discussed, both F127 and BSA molecules exchange between their respective surface-adsorbed and bulk

DOI: 10.1021/acs.jpcc.5b06685
J. Phys. Chem. C 2015, 119, 22190−22197

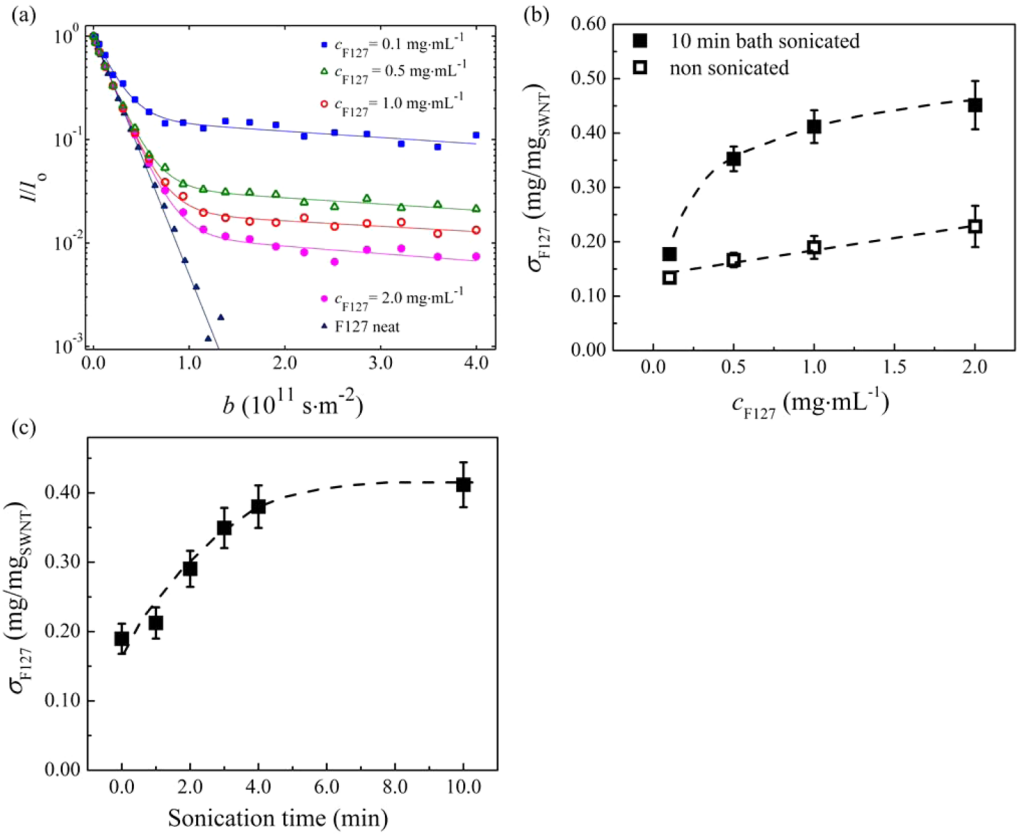

Figure 4. (a) Diffusional decay of the ^{1}H NMR signal from the F127 oxyethylene peak as a function of F127 added to a BSA-SWNT dispersion with an initial concentration of c_{BSA} = 1.4 mg·mL^{-1} and c_{SWNT} = 0.11 mg·mL^{-1}. The lines are two-component fits (see Figure 1); the fitted amplitudes provide the "non-sonicated" data in panel b. (b) The apparent surface coverage σ_{F127} by F127 molecules on initially-BSA-suspended SWNTs, without and with bath sonication with increasing amount of added F127. (c) The effect of bath-sonication time on the apparent surface coverage at c_{F127} = 1.0 mg·mL^{-1}. Dashed lines in panels b and c are guides for the eye.

aqueous states.[5,11,12] Hence, one can plausibly assume that the addition of one of these dispersants, to dispersions prepared with the other dispersant, provides a new equilibrium, permitted by molecular exchange, that can be participated in by both dispersants. Given enough time (>1 s, much longer than any of the involved residence times), the relative concentrations of these dispersants on the SWNT surface will be governed by the relative interaction strength of those dispersants with the nanotube surface: Dispersants that bind more strongly shall gain a higher surface concentration.

In Figure 3, we present the diffusion NMR decays of F127 molecules in SWNT dispersions originally prepared using F127 as dispersant, to which BSA was added at set concentrations.[45] As is clear, the apparent surface coverage of SWNTs by F127 (σ_{F127}) does not decrease significantly (that is, by <10% upon a 4-fold increase of dispersant mass concentration, as suggested by the slope in Figure 3b) upon adding BSA. The most straightforward explanation for this behavior is that the binding strength (that is, the Gibbs energy of binding) of BSA to the SWNT surface is significantly lower than that of F127. The results presented later strengthen this explanation.

Displacement of Adsorbed BSA by F127. The last step is to study the diffusion NMR decays of F127 molecules (Figure 4) added at set concentrations to SWNT dispersions initially prepared using BSA as dispersant, that is, a sequence of events opposite to that in Figure 3. As is clear from Figure 4a, some of the added F127 molecules adsorb to the surface, as signified by the appearance of the slow-diffusion tail of the decay. While in Figure 4a the *fraction* of F127 molecules that is adsorbed to the NT surface *decreases* with increasing amount of added F127, the apparent surface coverage supplied by F127 increases continually (Figure 4b, as provided by the $f_{F127} \times c_{F127}$ product eq 2, and yet remains below the coverage (Figure 3b) achieved with F127 as initial dispersant.

A comparison of Figure 3a,b to Figure 4a,b can be most-easily interpreted as F127 binding to the NT surface more strongly than BSA. Hence, in a system with dynamic equilibrium with continuously exchanging molecules, the NT surface becomes preferentially covered by F127, even if it was originally covered by BSA. Conversely, an initial F127 coverage on the SWNT surface is kept, despite BSA having been added to the solution.

In addition to the simple mixing of the molecular components in solution, we also explored if any effect of resonication could be detected. The working hypothesis was that dispersant-covered nanotubes may loosely aggregate to some extent, and, if such aggregates are present, some NT surface may not be accessible to accommodate added extra dispersant. Hence, dispersions were bath-sonicated after the addition of F127. One should recall that all starting dispersions were prepared with much more intensive tip sonication. As is shown in Figure 4b, mild sonication has, indeed, led to an increase in the apparent surface coverage by F127 to the extent that was roughly the same as the previously established saturation value (Figure 3b). Hence, under the conditions explored, F127 replaces all BSA.

DOI: 10.1021/acs.jpcc.5b06685
J. Phys. Chem. C 2015, 119, 22190−22197

Starting from pristine SWNT and F127, bath sonication for 4 to 5 min leads to negligible SWNT dispersion. On the contrary, as shown by Figure 4c, 4 to 5 min bath sonication was sufficient to double the apparent surface coverage by F127. Hence, mild sonication creates no new surface by additional exfoliation of bundles, but it rather re-exposes area that may have vanished by weak aggregation of BSA-dispersed SWNTs. Here we also add that the same bath sonication procedure of the dispersions in Figure 3 has *not* led to any change of the observed diffusional decays. Hence, even if there is weak aggregation in F127-prepared SWNT dispersions, making more surface reaccessible does not lead to any replacement of F127 by BSA. Hence, our previous conclusions regarding the relative strength of F127 and BSA binding to SWNT stand.

Comparison to Previous Experiments. Displacement of one dispersant by another in SWNT dispersions has been approached previously on a number of different ways. In some studies, this phenomenon was in the actual focus, while in some other investigations it was a more marginal issue. One example for the former is a comparative study of the binding of peptides where binding strength was qualitatively assessed by detecting concentration changes of peptide indicators upon sequential increase in a nonionic surfactant in the dispersion.[46] As an example for the latter, the bile salt sodium cholate, considered a strong binder to SWNT, was removed by dialysis and replaced stepwise (over the course of days) by a phospholipid−PEO dispersant.[47]

As concerning quantitative or semiquantitative results, we relate to a few studies. We note first that quantitative results such as full adsorption isotherms for surfactants on SWNTs have been obtained previously by rare and careful depletion-type measurements.[48,49] In addition, protein (including BSA) adsorption isotherms have also been recorded but for functionalized CNTs that can be dispersed in water without any dispersant.[50] Regarding replacement, the behavior of different particular blood proteins (including BSA) has been investigated semiquantitatively by measuring the concentration of those various proteins in the supernatant by SDS-PAGE (polyacrylamide gel electrophoresis).[28] Protein adsorption was detected as a decrease in SDS-PAGE bands, while displacement of one protein sort by another was detected as opposite changes in the respective band intensities. While the time resolution of the method is a bit unclear, band intensity changes were relatively fast (<5 min).

Our results have a close relation to the study[13] by Cherukuri et al. where SWNT dispersions prepared by a Pluronic (F108) were treated by mixing into them solutions of blood serum proteins and, specifically, a solution of rabbit serum albumin RSA. Before and after mixing the near-infrared emission spectra were detected and authors relied on the well-established sensitivity of those spectra of individual SWNTs upon the nature of the adsorbed molecules.[27] In accordance with what would be expected from the residence time established by us previously,[11,12] most of the spectral changes associated by the replacement of the Pluronic took place quickly (within the experimental time resolution of 0.7 s). Importantly, Cherukuri et al. obtained a complete displacement of Pluronics by RSA;[13] however, there are two important differences between the present study and that by Cherukuri et al.[13] First, RSA (used by Cherukuri et al.[13]) and BSA (used here) differ a lot in terms of their solvent-accessible aromatic groups.[51] Second, the BSA/Pluronic mass ratio in their solution was higher than that here. Because they worked with dispersions of strictly individual nanotubes, their apparent surface coverage calculated on mass basis must have been significantly higher than ours; however, even if we set that Figure 10 times higher than ours (that is, corresponding to complete surface coverage by PPO of completely debundled SWNTs, see Results and Discussion), the BSA/Pluronic mass ratio in solution explored by Cherukuri et al. becomes ca. 600. In our case, the same mass ratio is <4. A large excess of BSA may be a factor in shifting the equilibrium on the surface toward BSA.

CONCLUSIONS

The results previously presented clearly and quantitatively demonstrate several interesting surface phenomena in SWNT dispersions. We emphasize that the dispersions prepared by us exhibited rather high (that is, in comparison with most other studies we refer to) SWNT concentrations, at which most SWNTs resided in the solution in the form of bundles or loose aggregates. Nevertheless, this complication has no influence on the NMR diffusion behavior.

We confirm that, in accordance with previous findings, the dispersants are in dynamic equilibrium between their surface-adsorbed and free states and that it is the surface-adsorbed state that is constituted by a minor fraction of molecules.[11,12] For F127, the NT surface seems to be close to being saturated in the explored dispersions in the sense that adding more dispersant molecules did not lead to significantly higher surface coverage on the SWNT.

Previously, we have established that the residence time of F127 on the nanotube surface is longer than that for BSA molecules. Here we report that F127 molecules displace BSA at the nanotube surface, while, at comparable F127 and BSA concentrations, there is no displacement in the reverse direction. This clearly shows that F127 binds stronger to the nanotube surface stronger than does BSA. The method developed here permits us to compare the strength of binding of other dispersants, too, to the strength of binding of F127 molecules. Further work is in progress in that direction.

In general, the preference of one dispersant over another could assist in a handful of nanotube applications such as composite materials and sensing, where high nanotube concentration or selectivity are required. This approach could also be extended to dispersions of other colloids such as graphene, clay, or spherical nanoparticles.

ASSOCIATED CONTENT

Supporting Information

The Supporting Information is available free of charge on the ACS Publications website at DOI: 10.1021/acs.jpcc.5b06685.

TGA thermograms, UV−vis and ^{1}H NMR spectra, ^{1}H NMR diffusional decay of BSA in a BSA/SWNT dispersion, details of data evaluation, and results of the fits of the F127 diffusional decays. (PDF)

AUTHOR INFORMATION

Corresponding Author

*E-mail: furo@kth.se.

Notes

The authors declare no competing financial interest.

ACKNOWLEDGMENTS

Support from Fundação para a Ciência e Tecnologia (FCT, Portugal) through projects PEst-C/QUI/UI0081/2013 (CIQ-

UP) and the Ph.D. grant SFRH/BD/72612/2010, from FEDER and FCT/MES through FCUP-NORTE-07-0124-FEDER-000065 and from the Swedish Research Council VR is gratefully acknowledged.

REFERENCES

(1) Angelikopoulos, P.; Bock, H. The Science of Dispersing Carbon Nanotubes with Surfactants. *Phys. Chem. Chem. Phys.* **2012**, *14*, 9546−9557.
(2) Britz, D. A.; Khlobystov, A. N. Noncovalent Interactions of Molecules with Single Walled Carbon Nanotubes. *Chem. Soc. Rev.* **2006**, *35*, 637−659.
(3) Kharissova, O. V.; Kharisov, B. I.; de Casas Ortiz, E. G. Dispersion of Carbon Nanotubes in Water and Non-Aqueous Solvents. *RSC Adv.* **2013**, *3*, 24812−24852.
(4) Calvaresi, M.; Zerbetto, F. The Devil and Holy Water: Protein and Carbon Nanotube Hybrids. *Acc. Chem. Res.* **2013**, *46*, 2454−2463.
(5) Frise, A. E.; Edri, E.; Furó, I.; Regev, O. Protein Dispersant Binding on Nanotubes Studied by NMR Self-Diffusion and Cryo-TEM Techniques. *J. Phys. Chem. Lett.* **2010**, *1*, 1414−1419.
(6) Bertulli, C.; Beeson, H. J.; Hasan, T.; Huang, Y. Y. S. Spectroscopic Characterization of Protein-Wrapped Single-Wall Carbon Nanotubes and Quantification of their Cellular Uptake in Multiple Cell Generations. *Nanotechnology* **2013**, *24*, 265102.
(7) Holt, B. D.; McCorry, M. C.; Boyer, P. D.; Dahl, K. N.; Islam, M. F. Not All Protein-Mediated Single-Wall Carbon Nanotube Dispersions are Equally Bioactive. *Nanoscale* **2012**, *4*, 7425−7434.
(8) Boyer, P. D.; Holt, B. D.; Islam, M. F.; Dahl, K. N. Decoding Membrane- versus Receptor-Mediated Delivery of Single-Walled Carbon Nanotubes into Macrophages using Modifications of Nanotube Surface Coatings and Cell Activity. *Soft Matter* **2013**, *9*, 758−764.
(9) Holt, B. D.; Dahl, K. N.; Islam, M. F. Quantification of Uptake and Localization of Bovine Serum Albumin-Stabilized Single-Wall Carbon Nanotubes in Different Human Cell Types. *Small* **2011**, *7*, 2348−2355.
(10) Wang, X.; Xia, T. A.; Ntim, S. A.; Ji, Z. X.; George, S.; Meng, H. A.; Zhang, H. Y.; Castranova, V.; Mitra, S.; Nel, A. E. Quantitative Techniques for Assessing and Controlling the Dispersion and Biological Effects of Multiwalled Carbon Nanotubes in Mammalian Tissue Culture Cells. *ACS Nano* **2010**, *4*, 7241−7252.
(11) Frise, A. E.; Pagès, G.; Shtein, M.; Pri Bar, I.; Regev, O.; Furó, I. Polymer Binding to Carbon Nanotubes in Aqueous Dispersions: Residence Time on the Nanotube Surface as Obtained by NMR Diffusometry. *J. Phys. Chem. B* **2012**, *116*, 2635−2642.
(12) Fernandes, R. M. F.; Buzaglo, M.; Shtein, M.; Pri Bar, I.; Regev, O.; Marques, E. F.; Furó, I. Lateral Diffusion of Dispersing Molecules on Nanotubes as Probed by NMR. *J. Phys. Chem. C* **2014**, *118*, 582−589.
(13) Cherukuri, P.; Gannon, C. J.; Leeuw, T. K.; Schmidt, H. K.; Smalley, R. E.; Curley, S. A.; Weisman, R. B. Mammalian Pharmacokinetics of Carbon Nanotubes using Intrinsic Near-Infrared Fluorescence. *Proc. Natl. Acad. Sci. U. S. A.* **2006**, *103*, 18882−18886.
(14) Yaron, P. N.; Holt, B. D.; Short, P. A.; Losche, M.; Islam, M. F.; Dahl, K. N. Single Wall Carbon Nanotubes Enter Cells by Endocytosis and Not Membrane Penetration. *J. Nanobiotechnol.* **2011**, *9*, 45.
(15) Granite, M.; Radulescu, A.; Pyckhout-Hintzen, W.; Cohen, Y. Interactions between Block Copolymers and Single-Walled Carbon Nanotubes in Aqueous Solutions: A Small-Angle Neutron Scattering Study. *Langmuir* **2011**, *27*, 751−759.
(16) Anson-Casaos, A.; Gonzalez-Dominguez, J. M.; Martinez, M. T. Separation of Single-Walled Carbon Nanotubes from Graphite by Centrifugation in a Surfactant or in Polymer Solutions. *Carbon* **2010**, *48*, 2917−2924.
(17) O'Connell, M. J.; Boul, P.; Ericson, L. M.; Huffman, C.; Wang, Y. H.; Haroz, E.; Kuper, C.; Tour, J.; Ausman, K. D.; Smalley, R. E. Reversible Water-Solubilization of Single-Walled Carbon Nanotubes by Polymer Wrapping. *Chem. Phys. Lett.* **2001**, *342*, 265−271.
(18) Moore, V. C.; Strano, M. S.; Haroz, E. H.; Hauge, R. H.; Smalley, R. E.; Schmidt, J.; Talmon, Y. Individually Suspended Single-Walled Carbon Nanotubes in Various Surfactants. *Nano Lett.* **2003**, *3*, 1379−1382.
(19) Strano, M. S.; Dyke, C. A.; Usrey, M. L.; Barone, P. W.; Allen, M. J.; Shan, H.; Kittrell, C.; Hauge, R. H.; Tour, J. M.; Smalley, R. E. Electronic Structure Control of Single-Walled Carbon Nanotube Functionalization. *Science* **2003**, *301*, 1519−1522.
(20) Arnold, M. S.; Green, A. A.; Hulvat, J. F.; Stupp, S. I.; Hersam, M. C. Sorting Carbon Nanotubes by Electronic Structure using Density Differentiation. *Nat. Nanotechnol.* **2006**, *1*, 60−65.
(21) Zorbas, V.; Smith, A. L.; Xie, H.; Ortiz-Acevedo, A.; Dalton, A. B.; Dieckmann, G. R.; Draper, R. K.; Baughman, R. H.; Musselman, I. H. Importance of Aromatic Content for Peptide/Single-Walled Carbon Nanotube Interactions. *J. Am. Chem. Soc.* **2005**, *127*, 12323−12328.
(22) Zuo, G. H.; Kang, S. G.; Xiu, P.; Zhao, Y. L.; Zhou, R. H. Interactions between Proteins and Carbon-Based Nanoparticles: Exploring the Origin of Nanotoxicity at the Molecular Level. *Small* **2013**, *9*, 1546−1556.
(23) Strano, M. S.; Moore, V. C.; Miller, M. K.; Allen, M. J.; Haroz, E. H.; Kittrell, C.; Hauge, R. H.; Smalley, R. E. The Role of Surfactant Adsorption during Ultrasonication in the Dispersion of Single-Walled Carbon Nanotubes. *J. Nanosci. Nanotechnol.* **2003**, *3*, 81−86.
(24) Dror, Y.; Pyckhout-Hintzen, W.; Cohen, Y. Conformation of Polymers Dispersing Single-Walled Carbon Nanotubes in Water: A Small-Angle Neutron Scattering Study. *Macromolecules* **2005**, *38*, 7828−7836.
(25) Wang, H. Dispersing Carbon Nanotubes using Surfactants. *Curr. Opin. Colloid Interface Sci.* **2009**, *14*, 364−371.
(26) Shi Kam, N. W.; O'Connell, M.; Wisdom, J. A.; Dai, H. Carbon Nanotubes as Multifunctional Biological Transporters and Near-Infrared Agents for Selective Cancer Cell Destruction. *Proc. Natl. Acad. Sci. U. S. A.* **2005**, *102*, 11600−11605.
(27) Tsyboulski, D. A.; Bakota, E. L.; Witus, L. S.; Rocha, J. D. R.; Hartgerink, J. D.; Weisman, R. B. Self-Assembling Peptide Coatings Designed for Highly Luminescent Suspension of Single-Walled Carbon Nanotubes. *J. Am. Chem. Soc.* **2008**, *130*, 17134−17140.
(28) Ge, C. C.; Du, J. F.; Zhao, L. N.; Wang, L. M.; Liu, Y.; Li, D. H.; Yang, Y. L.; Zhou, R. H.; Zhao, Y. L.; Chai, Z. F.; et al. Binding of Blood Proteins to Carbon Nanotubes Reduces Cytotoxicity. *Proc. Natl. Acad. Sci. U. S. A.* **2011**, *108*, 16968−16973.
(29) Kato, H.; Mizuno, K.; Shimada, M.; Nakamura, A.; Takahashi, K.; Hata, K.; Kinugasa, S. Observations of Bound Tween80 Surfactant Molecules on Single-Walled Carbon Nanotubes in an Aqueous Solution. *Carbon* **2009**, *47*, 3434−3440.
(30) Kato, H.; Nakamura, A.; Horie, M. Behavior of Surfactants in Aqueous Dispersions of Single-Walled Carbon Nanotubes. *RSC Adv.* **2014**, *4*, 2129−2136.
(31) Ghosh, S.; Bachilo, S. M.; Weisman, R. B. Advanced Sorting of Single-Walled Carbon Nanotubes by Nonlinear Density-Gradient Ultracentrifugation. *Nat. Nanotechnol.* **2010**, *5*, 443−450.
(32) Capelo, J. L.; Galesio, M. M.; Felisberto, G. M.; Vaz, C.; Pessoa, J. C. Micro-Focused Ultrasonic Solid-Liquid Extraction (mu FUSLE) Combined with HPLC and Fluorescence Detection for PAHs Determination in Sediments: Optimization and Linking with the Analytical Minimalism Concept. *Talanta* **2005**, *66*, 1272−1280.
(33) Shtein, M.; Pri Bar, I.; Regev, O. A Simple Solution for the Determination of Pristine Carbon Nanotube Concentration. *Analyst* **2013**, *138*, 1490−1496.
(34) Stejskal, E. O.; Tanner, J. E. Spin Diffusion Measurements: Spin Echoes in the Presence of a Time-Dependent Field Gradient. *J. Chem. Phys.* **1965**, *42*, 288−292.
(35) Price, W. S. *NMR Studies of Translational Motion: Principles and Applications*; Cambridge University Press: Cambridge, U.K., 2009.
(36) Mills, R. Self-Diffusion in Normal and Heavy Water in the Range 1−45°. *J. Phys. Chem.* **1973**, *77*, 685−688.
(37) In particular, the recorded NMR spectra were subject to the limitation of reasonably fast intramolecular dynamics (segmental

DOI: 10.1021/acs.jpcc.5b06685
J. Phys. Chem. C 2015, 119, 22190−22197

motions) of the ethyleneoxide chains within the PEO blocks of F127, which made their ^{1}H NMR line width suitably small. Conversely, if there existed a population of F127 molecules that were adsorbed to the SWNT in a manner that strongly limited their intramolecular dynamics, the NMR spectrum of ethyleneoxide chains in those molecules could possibly suffer a large spectral broadening and consequent loss of their contribution to the detected spectra.

(38) Interestingly, recent experiments of similar type—data not presented—have clearly shown that the residence time and the surface diffusion coefficient depend not only on the commercial source of the SWNTs but also on the batch number of otherwise nominally identical NT products.

(39) Douglas, J. F.; Johnson, H. E.; Granick, S. A Simple Kinetic Model of Polymer Adsorption and Desorption. *Science* **1993**, *262*, 2010−2012.

(40) Copeland, R. A.; Pompliano, D. L.; Meek, T. D. Drug−Target Residence Time and its Implications for Lead Optimization. *Nat. Rev. Drug Discovery* **2006**, *5*, 730−739.

(41) Rouquerol, F.; Rouquerol, J.; Sing, K. *Adsorption by Powders and Porous Solids*; Academic Press: San Diego, 1999.

(42) Tóth, J. *Adsorption*; Marcel Dekker: New York, 2002.

(43) Peigney, A.; Laurent, C.; Flahaut, E.; Bacsa, R. R.; Rousset, A. Specific Surface Area of Carbon Nanotubes and Bundles of Carbon Nanotubes. *Carbon* **2001**, *39*, 507−514.

(44) Lin, Y. N.; Alexandridis, P. Temperature-Dependent Adsorption of Pluronic F127 Block Copolymers onto Carbon Black Particles Dispersed in Aqueous Media. *J. Phys. Chem. B* **2002**, *106*, 10834−10844.

(45) The initial SWNT and F127 concentrations are slightly lower than those respective ones in Figure 1. This is because we want to compare these solutions with dispersions initially prepared by BSA, and with BSA one can achieve lower SWNT concentrations than that with F127.

(46) Wang, S. Q.; Humphreys, E. S.; Chung, S. Y.; Delduco, D. F.; Lustig, S. R.; Wang, H.; Parker, K. N.; Rizzo, N. W.; Subramoney, S.; Chiang, Y. M.; et al. Peptides with Selective Affinity for Carbon Nanotubes. *Nat. Mater.* **2003**, *2*, 196−200.

(47) Welsher, K.; Liu, Z.; Sherlock, S. P.; Robinson, J. T.; Chen, Z.; Daranciang, D.; Dai, H. J. A Route to Brightly Fluorescent Carbon Nanotubes for Near-Infrared Imaging in Mice. *Nat. Nanotechnol.* **2009**, *4*, 773−780.

(48) Sa, V.; Kornev, K. G. Analysis of Stability of Nanotube Dispersions using Surface Tension Isotherms. *Langmuir* **2011**, *27*, 13451−13460.

(49) Zhong, W. H.; Claverie, J. P. Probing the Carbon Nanotube-Surfactant Interaction for the Preparation of Composites. *Carbon* **2013**, *51*, 72−84.

(50) Du, P.; Zhao, J.; Mashayekhi, H.; Xing, B. S. Adsorption of Bovine Serum Albumin and Lysozyme on Functionalized Carbon Nanotubes. *J. Phys. Chem. C* **2014**, *118*, 22249−22257.

(51) Majorek, K. A.; Porebski, P. J.; Dayal, A.; Zimmerman, M. D.; Jablonska, K.; Stewart, A. J.; Chruszcz, M.; Minor, W. Structural and Immunologic Characterization of Bovine, Horse, and Rabbit Serum Albumins. *Mol. Immunol.* **2012**, *52*, 174−182.

DOI: 10.1021/acs.jpcc.5b06685
J. Phys. Chem. C 2015, 119, 22190−22197

Supporting Information

for

Surface coverage and competitive adsorption on carbon nanotubes

Ricardo M.F. Fernandes,[1,3] Matat Buzaglo,[2] Oren Regev,[2] Eduardo F. Marques,[3] and István Furó[1] *

Supernatant characterization: SWNT and F127 quantification

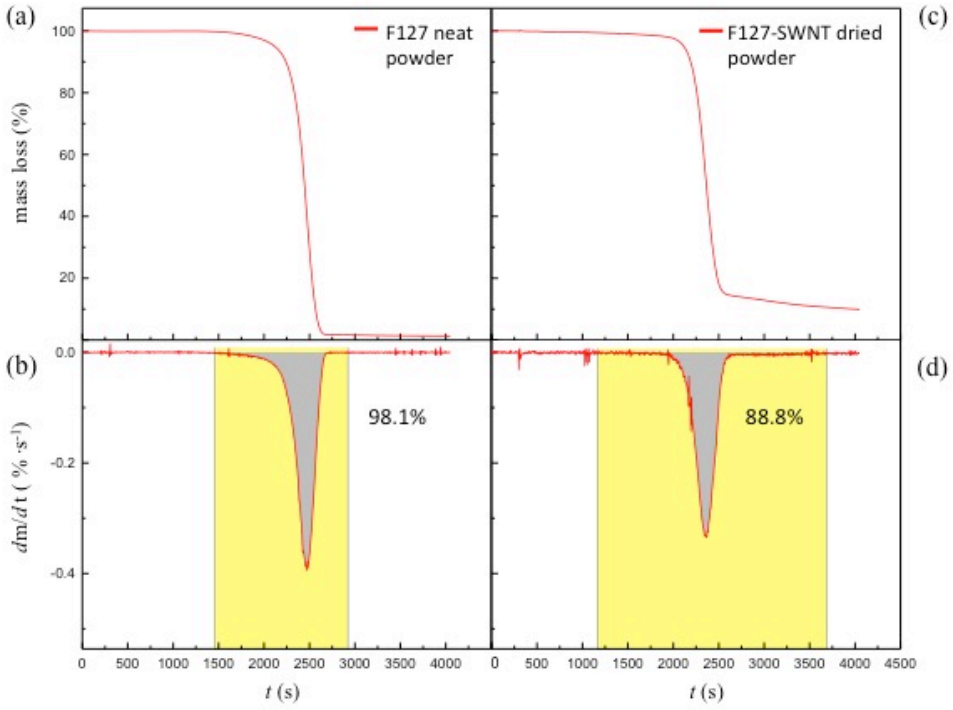

Figure S1. *TGA thermograms for: the F127 powder, (a) and (b) sample mass loss and integration of first derivate (mass variation), respectively; and F127-SWNT dispersion, (c) and (d), idem.*

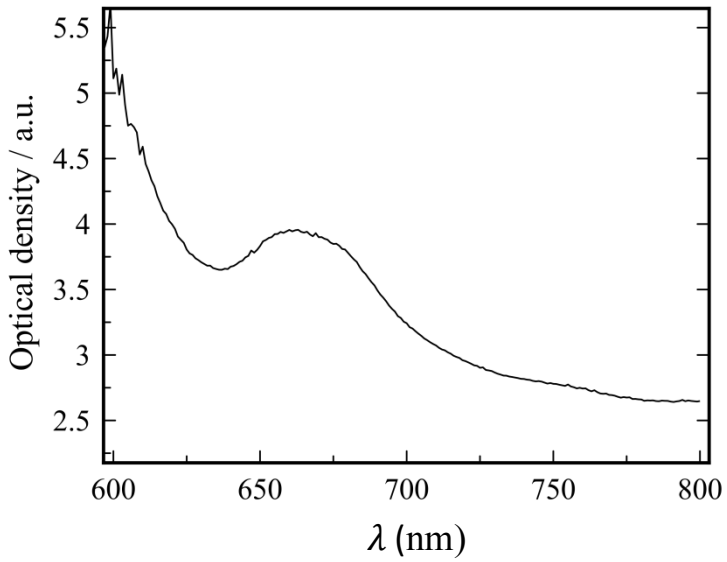

Figure S2. *UV-Vis spectrum of a non-diluted F127-SWNT dispersion. Optical path = 0.4 cm. The optical density at 660 nm was used to determine the apparent extinction coefficient.*

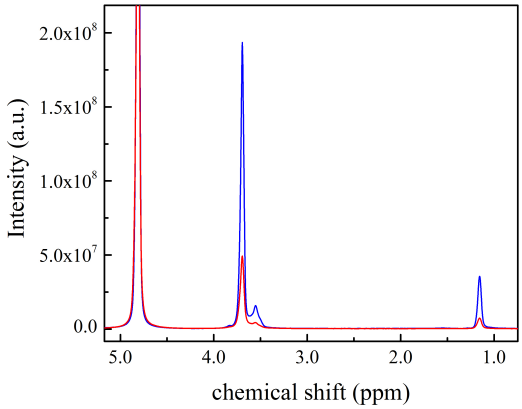

Figure S3. *^{1}H NMR spectrum of neat F127 solution c=3.0 mg·mL^{-1} (blue) and F127-SWNT dispersion (red). The integration of the region between 3.1 and 4.2 ppm was used to estimate the F127 concentration (2.1 mg·mL^{-1}) in the SWNT dispersion. The integration of the methyl peak gives a lower concentration (1.7 mg·mL^{-1}) plausibly because some part of the signal is lost (line broadening) due of the stronger adsorption of the PPO block (that is, as compared to that of the PEO block) onto the SWNT.*

Table S1. *Parameters for supernatant characterization: V_s, m_s, ϕ_s, ϕ_d, c_{SWNT}, concentration of F127 in the supernatant (determined by NMR and TGA, referred to as $c_{F127\text{-}NMR}$ and $c_{F127\text{-}TGA}$ in the main text, respectively), the optical density and the apparent extinction coefficient.*

m_s/ mg	V_s / mL	ϕ_s	ϕ_d	c_{SWNT} / mg.mL^{-1}	Final conc. of F127 (TGA) / mg.mL^{-1}	Final conc. of F127 (NMR) / mg.mL^{-1}	Apparent absorbance 660 nm	ε_{660}/ mL·mg^{-1}·cm^{-1}
3.81	1.50	0.888	0.981	0.24	2.29	2.1	3.96	41.2

BSA-SWNT signal decay

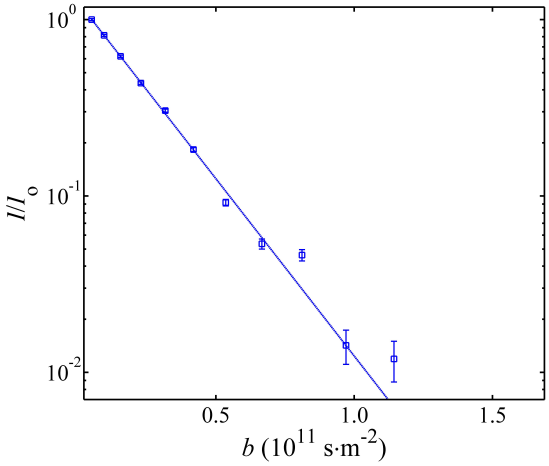

Figure S4. *Normalized diffusional decay of the ^{1}H NMR signal of BSA in a stimulated echo experiment performed in a BSA-SWNT dispersion with c_{SWNT} = 0.11 mg/mL and c_{BSA}=1.8 mg/mL. The data were obtained at T = 20 C in a fresh sample with 512 scans, gradient pulse length δ = 1 ms and diffusion time Δ = 20 ms.*

Two-site model of diffusion

The diffusional decay of the NMR peak intensity I is described by the Stejskal-Tanner equation[1]

$$I / I_o = e^{-bD} \qquad \text{(S1)}$$

where, I_o is the signal intensity in the absence of gradients, D the self-diffusion coefficient, and b the factor given by:

$$b = (g\delta\gamma)^2 (\Delta - \delta/3) \qquad \text{(S2)}$$

where, where γ is the magnetogyric ratio of the nucleus, δ the length of the gradient pulse of magnitude g, and Δ is the diffusion time. It is the gradient strength g that is stepped when the diffusion decay is recorded.

In the presence of two different populations of molecules characterized by their own diffusion coefficients, the diffusional decay depends on the rate of exchange (set by the residence time in the minor fraction) of molecules between the two populations.[2, 3] In case of having a residence time that is longer than the diffusion time set in the experiment, the exchange regime is called slow and the decay is characterized as the weighted sum of diffusional decays for each population

$$I / I_o = p_1 e^{-bD_1} + p_2 e^{-bD_2} \qquad \text{(S3)}$$

where p_1 and p_2 are the population fractions and D_1 and D_2 the corresponding diffusion coefficients. Below, p_1 and D_1 are associated with the fraction of F127 molecules in the solvent and p_2 and D_2 with the surface adsorbed F127 molecules. The diffusional decay is in addition made more complex by the fact that the diffusion of the F127 molecules on elongated objects like single nanotubes or bundles is described exactly by the Stejskal-Tanner equation that is valid only for isotropic three-dimensional diffusion. This complication[2] is neglected here.

The results presented in the tables below were obtained by Levenberg-Marquardt least-square fits of Eq.(3) to the obtained raw data. The diffusion coefficient of in the bulk solution was fixed to the value $D_1 = 5.3\times10^{-11}$ m^2 s^{-1}, obtained in a separate experiment. Because of the arbitrary normalization factor for the raw data (for methodological reasons, the data with $b = 0$ were not recorded), the relative population f_{F127} of surface-adsorbed F127 molecules was calculated as

$$f_{F127} = \frac{p_2}{p_1 + p_2} \ . \qquad \text{(S4)}$$

The estimated absolute error of f_{F127} varies a bit among the samples investigated but its compounded value is estimated to be ±(0.2) %. This error has two main contributions, one is the scatter as established from repeated experiments and the other from the variation of p_2 with having D_1 fixed in the fit to slightly (±5% relative error, a very conservative way of accounting for experimental error in the separate determination of D_1) different values. In addition, there is an additional source of error in the apparent surface coverage σ_{F127}, that arises from the error in the obtained concentrations c_{F127} and c_{SWNT}. Note that the main effect of those errors is an even shift of the obtained points σ_{F127} – in other words, the absolute values of σ_{F127} are influenced but the observed trends with added dispersants are rather robust. For that reason, the error bars provided for the σ_{F127} values in Figs. 2, 3, and 4 are strong overestimates as concerning the relative variation with Δc_{F127}.

Table S2. The results of the fits to data in Fig. 1 in the main text.

Δc_{F127} / mg.mL^{-1}	D_2 / 10^{-12} m^2.s^{-1}	f_{F127} / %	σ_{F127} / (mg/mg$_{SWNT}$)
0.0	0.4± 0.1	4.9	0.43
0.5	0.7± 0.1	4.3	0.47
1.0	0.8± 0.1	3.5	0.46
1.5	1.4± 0.1	3.3	0.50
2.0	1.4± 0.1	2.8	0.47

Table S3 The results of the fits to data in Fig. 3b in the main text.

c_{BSA} / mg.mL^{-1}	D_2 / 10^{-12} m^2.s^{-1}	f_{F127} / %	σ_{F127} / (mg/mg$_{SWNT}$)
0.0	0.3 ± 0.1	4.6	0.40
1.0	0.3 ± 0.1	4.7	0.41
2.0	0.5 ± 0.1	4.5	0.38
4.0	0.4 ± 0.1	4.3	0.37

Table S4. The results of the fits to non-sonicated data in Fig. 4b in the main text.

c_{F127} / mg.mL^{-1}	D_2 / 10^{-12} m^2.s^{-1}	f_{F127} / %	σ_{F127} / (mg/mg$_{SWNT}$)
0.10	1.4±0.1	15.1	0.13
0.50	1.4± 0.1	3.8	0.17
1.0	1.2±0.1	2.1	0.19
2.0	1.6±0.1	1.3	0.23

Table S5 The results of the fits to sonicated data in Fig. 4b in the main text.

c_{F127} / mg.mL^{-1}	D_2 / 10^{-12} m^2.s^{-1}	f_{F127} / %	σ_{F127} / (mg/mg$_{SWNT}$)
0.10	1.6±0.1	19.9	0.18
0.50	2.2 ± 0.1	8.0	0.35
1.0	2.7±0.1	4.7	0.41
2.0	2.6±0.1	2.5	0.45

Table S6. The results of the fits to data in Fig. 4c in the main text.

t / min	D_2 / 10^{-12} $m^2.s^{-1}$	f_{F127} / %	σ_{F127} / (mg/mg_{SWNT})
0.0	1.2±0.1	2.1	0.19
1.0	1.1±0.1	2.4	0.21
2.0	1.7±0.1	3.3	0.29
3.0	2.3±0.1	3.9	0.35
4.0	2.6±0.1	4.3	0.38
10.0	2.7±0.1	4.7	0.41

1. Stejskal, E. O.; Tanner, J. E. Spin diffusion measurements: Spin echoes in the presence of a time-dependent field gradient. *J. Chem. Phys.* **1965,** *42*, 288-292.
2. Fernandes, R. M. F.; Buzaglo, M.; Shtein, M.; Pri Bar, I.; Regev, O.; Marques, E. F.; Furó, I. Lateral diffusion of dispersing molecules on nanotubes as probed by NMR. *J. Phys. Chem. C* **2014,** *118*, 582-589.
3. Frise, A. E.; Pagès, G.; Shtein, M.; Bar, I. P.; Regev, O.; Furó, I. Polymer binding to carbon nanotubes in aqueous dispersions: Residence time on the nanotube surface as obtained by NMR diffusometry. *J. Phys. Chem. B* **2012,** *116*.

III

Dispersing carbon nanotubes with ionic surfactants under controlled conditions: comparisons and insight

Ricardo M.F. Fernandes, Bárbara Abreu, Bárbara Claro, Matat Buzaglo, Oren Regev, István Furó and Eduardo F. Marques

Langmuir, **2015**, 31, 10955-10965

Langmuir

Article

pubs.acs.org/Langmuir

Dispersing Carbon Nanotubes with Ionic Surfactants under Controlled Conditions: Comparisons and Insight

Ricardo M. F. Fernandes,[†,‡] Bárbara Abreu,[†] Bárbara Claro,[†] Matat Buzaglo,[§] Oren Regev,[§,∥] István Furó,[‡] and Eduardo F. Marques*[,†]

[†]Centro de Investigação em Química, Department of Chemistry and Biochemistry, Faculty of Science, University of Porto, Rua do Campo Alegre, s/n, P-4169-007 Porto, Portugal

[‡]Division of Applied Physical Chemistry, Department of Chemistry, KTH Royal Institute of Technology, SE-10044 Stockholm, Sweden

[§]Department of Chemical Engineering and [∥]Ilse Katz Institute for Nanotechnology, Ben-Gurion University of the Negev, 84105 Beer-Sheva, Israel

Supporting Information

ABSTRACT: A fundamental understanding of the mechanisms involved in the surfactant-assisted exfoliation and dispersion of carbon nanotubes (CNTs) in water calls for well-controlled experimental methodologies and reliable comparative metrics. We have assessed the ability of several ionic surfactants to disperse single and multiwalled carbon nanotubes, resorting to a stringently controlled sonication-centrifugation method for the preparation of the dispersions. The CNT concentration was accurately measured for a wide range of surfactant concentration, using combined thermogravimetric analysis and UV−vis spectroscopy. The obtained dispersibility curves yield several quantitative parameters, which in turn allow for the effects of nanotube morphology and surfactant properties (aromatic rings, chain length, headgroup charge, and *cmc*) to be assessed and rationalized, both in terms of dispersed nanotube mass and surface area. The data also indicate that the CNT-surfactant association follows patterns that are markedly different from other equilibrium processes governed by hydrophobicity (such as micellization); in particular, the surfactant concentration needed for maximum dispersibility, $c_{s,max}$, and the number of surfactant molecules per unit CNT area at $c_{s,max}$ are shown to depend linearly on chain length. The results further suggest that the presence of micelles in the exfoliation process is not a key factor either for starting CNT dispersibility or attaining its saturation value.

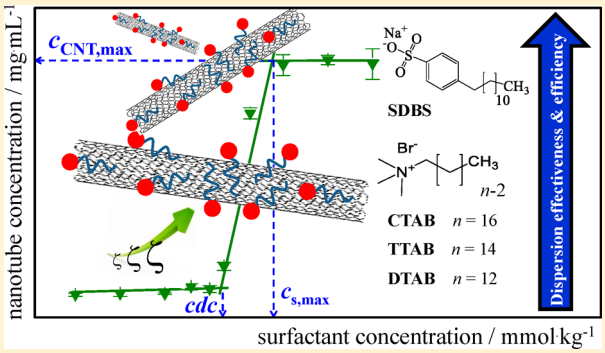

1. INTRODUCTION

Carbon nanotubes (CNTs) possess a combined set of unique mechanical, thermal, and electrical properties and have thus emerged as promising materials for many applications (e.g., polymer nanocomposites and nanoelectronic devices).[1,2] The high aspect ratio and strong van der Waals (vdW) cohesive forces[3,4] of CNTs, however, cause detrimental entanglement and bundling.[5−7] This is a major drawback, as many applications require well-dispersed tubes in order to make full use of their remarkable properties. Three main approaches can be pursued to disperse CNTs: (i) use of organic solvents; (ii) covalent attachment of hydrophilic groups to the nanotube surface; and (iii) physical adsorption of amphiphilic molecules (surfactants or polymers).[6,7] While organic solvents may suffice in some applications, they are of no help if aqueous dispersions are required. Chemical functionalization changes the nanotube surface and its properties. Hence, physical adsorption, where the dispersant weakly binds to the nanotube surface, is often preferred because it better preserves the unique properties of CNTs. Thus far, several types of dispersants in water have been successfully used, namely, synthetic polymers,[8−12] proteins[13−17] and surfactants.[4,18−26] Physical dispersion also involves strong mechanical shear forces and ensuing exfoliation or debundling, typically by bath or tip sonication, or both. The duration and intensity of ultrasound processing vary widely in the literature.[20,25,27,28] A consecutive centrifugation step is usually employed to sediment larger bundles, microscale particles, larger carbonaceous/non-nanotube material and metal catalyst particles.[22,25] Similarly to sonication, reported centrifugation procedures vary broadly in acceleration grade ("g-force") and time employed.[25,29] The quality of the final dispersion, usually defined in terms of the fraction of isolated tubes present, is key to most applications and, ideally, it should be maximized.

Received: June 4, 2015
Revised: September 8, 2015
Published: September 21, 2015

DOI: 10.1021/acs.langmuir.5b02050
Langmuir 2015, 31, 10955−10965

Surfactants with diverse chemical structure have been explored as CNT dispersants.[21−31] At the microscopic level, if no surfactant is present, presonicated aqueous dispersions are unstable, and nanotube rebundling quickly occurs through vdW forces. If surfactant is present, when an individual nanotube detaches from a bundle or a bundle is cleaved by sonication-induced shear forces, the surfactant is thought to adsorb along the tube length in an unzipping mechanism until full separation occurs.[32] The obtained systems are not true solutions but kinetically stabilized colloidal dispersions,[7] where stability stems from the electrostatic repulsions between surfactant-coated CNTs for ionic surfactants, or steric repulsions for nonionic ones. The adsorption strength of the surfactant, primarily driven by hydrophobic interactions with the tube wall, is critically important. Amphiphiles with aromatic rings are particularly good dispersants, owing to the $\pi-\pi$ interactions between the ring and the CNT surface.[19,30]

Despite active research, there is still no definitive understanding of the dispersion mechanisms and the microscopic configuration of surfactants around the nanotubes. The fact that, for identical surfactant concentrations, the literature has often reported rather disparate CNT dispersibilities at saturation (e.g., for sodium dodecyl sulfate (SDS), differing by as much as a 40-fold factor[33])—and even the variety of CNT lots cannot account for such discrepancies—seems to obscure fundamental analyses of the dispersion process, highlighting the need for more systematic and carefully controlled studies.[4,23,33]

A dynamic equilibrium between adsorbed and nonadsorbed surfactant is found to occur in the dispersions, sensitive to surfactant concentration.[12,34,35] The critical micelle concentration of the surfactant in the CNT dispersion, cmc_d, is expected to be higher than that of the neat surfactant *cmc*, because a fraction of the surfactant is adsorbed on the CNT surface; for SDS, e.g., cmc_d was estimated as 10−50% bigger than *cmc* depending on nanotube loading.[36] Bearing this in mind, methodical studies evaluating the dispersion ability of surfactants over a wide range of concentrations (below and above *cmc*) are scarce and either cover limited ranges or suffer from the mentioned scattering in CNT dispersibility.[24,37] Hence, the effect of the relation between c_s, the surfactant concentration initially present in the dispersion (i.e., prior to the sonication/centrifugation steps), and *cmc* on the dispersibility of the nanotubes—in other words, the role of *neat* surfactant micelles in the initial step of the exfoliation/debundling process—has not been clarified. On the other hand, it is known that at high enough surfactant concentration (typically $c_s > 10 \times cmc$), depletion-driven aggregation takes place, owing to the presence of free micelles in the dispersion, which results in a dramatic decrease in CNT dispersibility.[23,25,38]

Regarding the configurational state of the adsorbed surfactant, direct experimental evidence is also relatively meager.[4,23] Cryogenic transmission electron microscopy (cryo-TEM) imaging has seemingly shown discrete micellar aggregates adsorbed on single-walled nanotubes (SWNTs),[39,40] but otherwise further direct evidence of surface self-aggregation is lacking. Molecular dynamics simulations indicate that weakly hydrophobic surfactants form only random monolayers while more hydrophobic surfactants self-aggregate on the tube surface, yielding hemimicelles, spherical micelles, or dense cylindrical micelles engulfing the CNT.[4,41] In this respect, the picture for macromolecular dispersants is not consensual either, with some invoking a wrapping[9] and others a nonwrapping[42] polymer configuration. Recent NMR self-diffusion studies have shown significant lateral mobility of a polymer along the tube surface, consistent with a nonwrapping picture.[34]

In this work, our main goals have been, first, to evaluate in a systematic way the ability of some common ionic surfactants to disperse SWNTs and multiwalled nanotubes (MWNTs) using a stringently controlled methodology (hence attempting to fill the above-mentioned gaps in the literature),[4,23,33] and, second, to compare and rationalize the effects of the surfactant properties on the dispersibility, on the basis of carefully obtained quantitative metrics. The chemical structure of the surfactants is shown in Figure 1, with their abbreviations. The

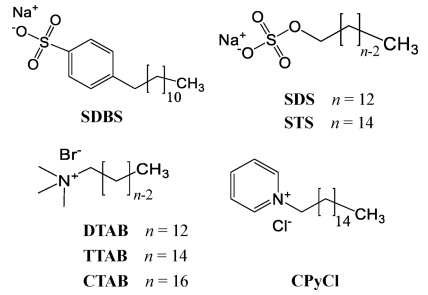

Figure 1. Chemical structure of the surfactants herein used. The abbreviations are SDBS, sodium dodecylbenzenesulfonate; SDS, sodium dodecyl sulfate; STS, sodium tetradecyl sulfate; DTAB, dodecyltrimethylammonium bromide; TTAB, tetradecyltrimethylammonium bromide; CTAB, cetyltrimethylammonium bromide; and CPyCl, cetylpyridinium chloride.

effects to be assessed dictated the choice of the surfactants: presence of aromatic rings (sodium dodecylbenzenesulfonate (SDBS)/cetylpyridinium chloride (CPyCl) vs all others), alkyl chain length variation (dodecyl-/tetradecyl-/cetyl-trimethylammonium bromide (DTAB/TTAB/CTAB)) and headgroup charge (e.g., SDS vs DTAB). Two other effects were investigated: the CNT morphology, by using SWNTs and MWNTs, and the surfactant *cmc*, by varying in all cases c_s over a wide range (typically $0.1-10 \times cmc$). Several studies have reported that the choice of sonication and centrifugation parameters has a considerable influence on the concentration of dispersed CNT, and on the bundle length and width distributions.[3,20,25,27] Therefore, in our study, to obtain reliable comparisons between surfactants and hence molecular insight, a stringent experimental protocol had to be implemented. Reproducibility could be attained by a strict control of the processing parameters, sample repetition, and statistical sampling. For accurate CNT quantification, combined TGA and UV−vis absorption spectroscopy were used to determine calibration curves (hence, apparent extinction coefficients) for each surfactant−CNT system. The quality of the dispersion curves obtained allowed us to define and extract several comparative metrics, viz., the critical surfactant concentration for dispersibility, the maximum dispersed CNT concentration and respective surfactant concentration at that point, the dispersion effectiveness, and dispersion efficiency. The results are rationalized and critically compared, also in the light of available data from the literature.

2. EXPERIMENTAL SECTION

2.1. Materials. Carbon nanotubes under the product name SWCNT/HDPlas were used as received from CheapTubes, being

DOI: 10.1021/acs.langmuir.5b02050
Langmuir 2015, 31, 10955−10965

specified as a mixture of single-walled and double-walled nanotubes (outer diameter d = 1−4 nm and length L = 3−30 μm) produced by catalytic chemical vapor deposition. MWNTs (d = 8−15 nm and L = 10−50 μm) were also used as received from CheapTubes. Figure 2

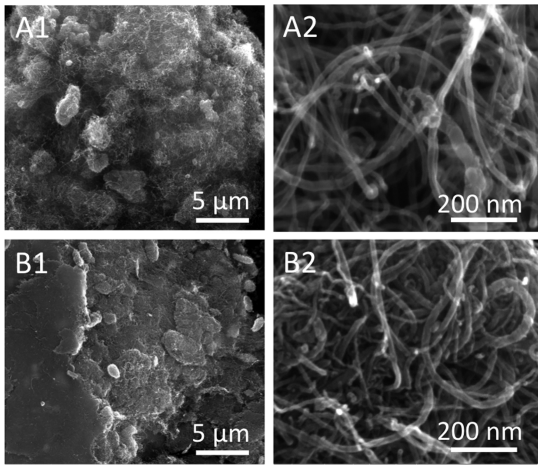

Figure 2. SEM imaging of the dry powders of MWNTs (A1 and A2) and SWNTs (B1 and B2).

shows SEM micrographs of the starting dry powders of MWNTs and SWNTs, obtained with a JEOL JSM 6301F high resolution scanning electron microscope, following the dry method described elsewhere.[29] The powders contain micrometer-sized agglomerates (Figure 2, A1 and B1) that under higher resolution appear as entangled, polydisperse bundles and ropes (Figure 2, A2 and B2). Previous NMR studies with this SWNT type have shown that metallic (paramagnetic) impurities are absent in any meaningful amount.[34] All the surfactants (Figure 1) were acquired from Sigma-Aldrich (purities ≥99%) and used as received. Conductivity measurements yielded *cmc* values similar to those usually reported (cf. also Figure S1 in the Supporting Information (SI)).[43]

2.2. Preparation of CNT Dispersions. The starting CNT−surfactant mixtures processed by tip sonication (the standard method, as described below) were prepared by weighing the carbon material, 9 mg, followed by addition of the desired surfactant solution, 3 mL, resulting in a 0.3 wt % CNT mixture. For the bath sonication, mixtures of 30 mg CNT in 10 mL surfactant solution (also 0.3 wt % CNT) were prepared. All stock surfactant solutions were prepared in ultrapure water above their respective Krafft temperatures to ensure full dissolution.

Sonication. Since both tip and bath sonication are commonly employed in the preparation of CNT dispersions, these methods were initially compared for the choice of the most suitable one for routine use. For tip sonication, a Bandelin Sonoplus Vb 2070 probe with a freshly polished 3 mm micro tip was used, with a vibration amplitude set to 30% and a sonication time of 8.5 min. In order to ensure identical sample treatment, a rigorous procedure was followed: (1) the energy density transferred to the sample was kept constant and estimated as 5.3 × 10^2 J·mL^{-1} from calorimetric measurements (cf. Note 1 and Tables S1−S2, SI), resulting in an average power density of 1.0 W·mL^{-1} (energy density/sonication time); 2) the tip was always placed in the same position inside the vial (1 cm from the bottom); (3) temperature was controlled with an external thermostated bath, set to a constant value above the surfactant Krafft temperature. For bath sonication, an Elma Sonic (model S10; 30W 37 kHz) sonicator was employed, for a processing time of 3 h and an estimated transferred energy density of 3.5 × 10^2 J·mL^{-1}, resulting in an average power density of 3.2 × 10^{-2} W·mL^{-1}. Bath and tip sonication were then compared in terms of reproducibility of the obtained dispersions. To illustrate the large qualitative difference between those two sonication methods, we present data from MWNT/SDS and MWNT/SDBS dispersions that were prepared over a wide range of surfactant concentrations (0.1−10 × *cmc*). In Figure 3, each point represents the scatter of the final CNT concentration Δc_{CNT} obtained in three to five

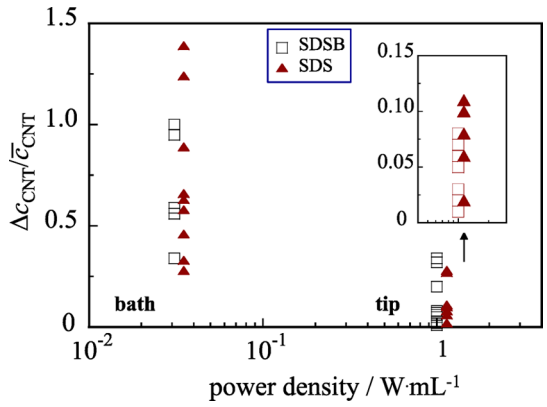

Figure 3. Scatter of relative uncertainties of MWNT concentration in SDBS- and SDS-assisted dispersions prepared with bath sonication (left data points) or tip sonication (right data points), versus the estimated power density delivered to the samples.

independent preparations at the same initial concentrations and normalized by the average CNT concentration $\bar{c}_{CNT}$ (note: the determination of c_{CNT} will be detailed in section 2.3). In this representation, having $\Delta c_{CNT}/\bar{c}_{CNT}$ on the order of 1 indicates statistically meaningless results.

Our data show that bath sonication typically fails to deliver significant data on CNT dispersion. A qualitatively similar (even if explored less on a systematic manner) behavior was observed for SWNTs. These results deserve a few comments. Since the cavitation/implosion events induced by ultrasonic waves result in strong shear forces on the CNT surfaces, it is relevant to convert energy density to shear stress, and power density to stress rates. The shear stress applied can be compared with the van der Waals cohesive pressure (∼0.1 MPa) and scission pressure (∼0.5 MPa) of the type of MWNTs (L/d ∼ 1000) used here, obtained from theoretical estimates.[3] While bath and tip sonication involve similar total delivered stress, 5.3 × 10^2 and 3.5 × 10^2 MPa, respectively (in principle, high enough to debundle and even fragment the MWNTs),[27] the tip method produces significantly higher average stress rates than the bath one, 1 MPa·s^{-1} compared to 3 × 10^{-2} MPa·s^{-1} (cf. Tables S1−S2, SI). These results seem thus to imply that kinetic parameters are important in producing the dispersions, and may reflect the interplay of the rate of local stress in exposing individual surfaces and the rate of binding of surfactant. Previous works on MWNT dispersions produced by bath sonication also showed significant uncertainty in nanotube concentrations.[24] All dispersions in this work were henceforth prepared by tip sonication.

Centrifugation. After sonication, the samples were centrifuged (Breda Scientific centrifuge) during 20 min at 4000*g*. After centrifugation, the top 2 mL of the supernatant were separated from the precipitate by decantation for the measurement of CNT concentration.

2.3. Quantification of CNT Concentration. Absolute carbon nanotube concentration in the supernatant was determined using a recently published method.[44] An accurately measured aliquot of each dispersion was lyophilized during 24−48 h. In order to quantify the mass fraction of surfactant present on the solid, thermogravimetric analysis (TGA) was performed using a Mettler Toledo Star System under N_2 atmosphere (flow rate of 50 mL·min^{-1}). Simple mass balance allows the quantification of CNT concentration in the supernatant, according to the equation

$$c_{CNT} = \left\{ m_s \times \left(1 - \frac{\phi_s}{\phi_d} \right) \right\} \frac{1}{V_s} \quad (1)$$

DOI: 10.1021/acs.langmuir.5b02050
Langmuir 2015, 31, 10955−10965

where c_{CNT} is the CNT concentration in the supernatant (in mg·mL^{-1}), m_s is the dried supernatant mass (in mg), ϕ_s is the TGA mass loss fraction obtained in the dry supernatant, ϕ_d is TGA mass loss fraction in neat dry surfactant, and V_s is the supernatant volume (in mL); the ϕ_s/ϕ_d ratio accounts for incomplete surfactant decomposition. Calibration curves were then obtained for each surfactant, by measuring absorbance versus c_{CNT} at λ = 660 nm (ensuring null absorption from surfactant), using dilutions from a stock dispersion with known CNT mass concentration. On the basis of Beer–Lambert law and the linear regimes observed, the apparent extinction coefficients, ε_{660}, were determined. The CNT concentrations were then determined from their apparent absorbance and the ε_{660} values. A double-beam Spectrophotometer U-2001 was used, with a plastic cuvette with an optical path of 1 cm. For each dispersion composition, three to five independent preparations were made and three sampling spectrophotometric measurements done.

2.4. Zeta Potential. The zeta potential, ζ, of the dispersions was measured at 25 °C using a zeta sizer Nano ZS, ZN 3500, with a 4 mW He–Ne laser (633 nm) and DTS 1060C disposable zeta cells. The electrophoretic mobility, μ, was measured using a combination of electrophoresis and laser Doppler velocimetry techniques, and ζ was calculated from μ using the known Henry equation.[22,45] A dielectric constant of 78.5, a medium viscosity of 0.89 cP, and a $f(\kappa a)$ function value of 1.5 (Smoluchowsky approximation) were used, following previously reported assumptions.[22,45] All ζ values are average values based on at least two independent dispersions and five quality criteria reports per dispersion.

3. RESULTS AND DISCUSSION

3.1. Methodological Aspects. *3.1.1. Sonication–Centrifugation Parameters and Final Dispersion State.* In the surfactant-assisted process of debundling and exfoliation of CNTs from as-received powders, sonication is a critical first step.[20,27] Increasing power density and sonication time is expected to induce higher concentrations of CNTs with reduced bundle size and likely higher fraction of individual tubes.[25,27,46,47] However, tube scission may reduce the length and quality of dispersed CNTs and hence a compromise has to be sought. The shear stress used here with tip (~5 × 10^2 MPa) lies well above both the vdW cohesive and scission pressures of the MWNTs (~0.1 and ~0.5 MPa, respectively);[3] moreover, with an average stress rate of 1 MPa s^{-1} one can reasonably assume that extensive exfoliation and debundling occurs (cf. also Tables S1–S2, SI), also in line with recent observations.[27] For SWNTs, the imposed stress is of the same order of magnitude as their cohesive pressure (~500 MPa) and also sizably higher than the scission pressure (similar to that of MWNTs); judging from the low data scatter in the SWNT dispersion curves (Figure 6), one can presume that exfoliation and debundling also takes place to a significant extent in the respective dispersions. Higher tip power density was ruled out as previous works indicated a significant increase in tube fragmentation.[20,25,27]

The next step, centrifugation, is also of fundamental importance.[25,47] The choice of centrifugal acceleration grade ("g-force") and centrifugation time affects not only the concentration of suspended CNTs, but also the average size of the aggregates present.[25] Under the sonication conditions of this work, the initially produced dispersions are expected to be somewhat polydisperse. All these dispersions were then subject to the same centrifugation step of 20 min and 4 × 10^3 g. With these parameters, the supernatants are not expected to contain spheroidal micron-sized particles,[22,25] some of which are visible in the initial dry powders (Figure 2). For rod-like particles, the sedimentation time depends on the aspect ratio L/d and density ρ.[48] Given the polydispersity of L and d for the used SWNTs and MWNTs and the corresponding uncertainty of their ρ,[48,49] estimations of the size of the remaining particles become more complex and are merely qualitative. Non-sedimented rods would be consistent with species ranging from individual CNTs to bundles of a few tens of tubes.[22,25] While in the literature various experimental methods have been employed to assess the CNT species distribution[9,22,25,50] (some qualitatively, others quantitatively with different advantages and limitations[50]), this type of study was outside the scope of this paper. However, it has been shown—e.g. on the basis of cryo-TEM,[15,51] SANS,[51] AFM,[22,25] and Raman/UV–vis-NIR/photoluminescence[25] spectroscopies—that surfactant-assisted CNT dispersions, prepared with sonication that preserves sufficient tube length, possess both individual tubes and a distribution of thin bundles. As concerning dispersions with high CNT mass content, bundles dominate as they do also here at the conditions set (see section 2.2). In order to further qualitatively assess the species distributions in the final centrifuged dispersions, we investigated the effects of centrifugation force and time on c_{CNT}. Figure 4. shows the

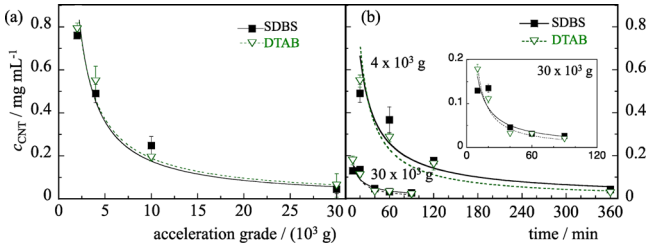

Figure 4. Concentration of MWNTs in SDBS- and DTAB-assisted dispersions versus (a) acceleration grade, for constant centrifugation time of 20 min, and (b) centrifugation time, for constant acceleration grade of 4 × 10^3 g and 30 × 10^3 g.

results obtained for MWNTs dispersions with SDBS (a highly effective dispersant[23]) and DTAB (a weakly effective dispersant[41]), using similar initial concentration of nanotubes in the two stock dispersions for proper comparisons (n.b.: the surfactant concentrations differ, though, owing to the different dispersing ability of SDBS and DTAB).

When the time is kept constant, 20 min, and acceleration varied between (2–30) × 10^3 g, c_{CNT} in the supernatant of both surfactants decreases, asymptotically approaching a constant value of ~0.05–0.06 mg·mL^{-1} (ca. 2% of the initial mass). The same trend is seen when centrifugation time is varied for constant acceleration grade (4 × 10^3 and 30 × 10^3 g), with an asymptote of $c_{CNT} \approx$ 0.03–0.04 mg·mL^{-1} (ca. 1% of initial mass). These curves qualitatively confirm, using two surfactants with rather different dispersive power, that the obtained dispersions are a distribution of individually separated tubes and different bundle sizes, in both d and L. Power-law fits ($y = ax^b$ with $b \approx -1.0$) can be loosely adjusted to the data in Figure 4 and, consistently with similar reported observations,[25] they suggest a log-normal size distribution of bundle sizes.

3.1.2. Quantification of Dispersed CNT Concentration. Figure 5 depicts the calibration curves obtained from combined TGA and UV–vis spectroscopy measurements. The apparent absorbance accounts for both true absorption and light scattering (colloidal dispersions of large objects are present),[52] but since both processes rely on transmittive interference of dispersed particles, they both linearly scale with concen-

DOI: 10.1021/acs.langmuir.5b02050
Langmuir 2015, 31, 10955–10965

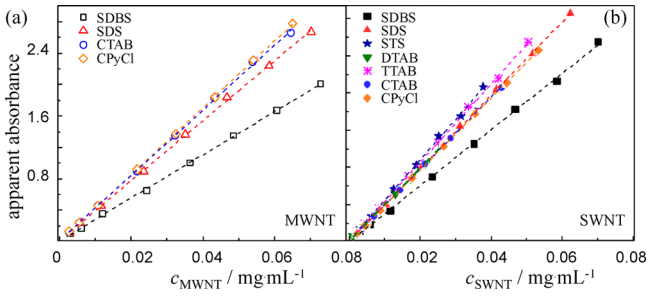

Figure 5. Apparent absorbance (λ = 660 nm) versus nanotube concentration for (a) MWNT/surfactant dispersions, and (b) SWNT/surfactant dispersions.

tration.[24] The linearity observed for a wide absorbance range (from 0 to 2−3) in all studied dispersions shows that, whatever the extracted state of CNTs, dilution with water does not seem to have any detectable effect on that state, and, furthermore, on the kinetic stability of the dispersion. In fact, typically, no meaningful change of the apparent absorbance occurs for these diluted samples over a period of a few days.

Three further observations are noteworthy. First, for any given surfactant, the obtained apparent extinction coefficients at 660 nm, ε_{660}, are very close for the SWNT and MWNT dispersions, clustering around 41 ± 2 mL·mg^{1}·cm^{-1} (cf. Table S3, SI). Second, all surfactants except SDBS (i.e., six different surfactants, covering a rather large range of properties) present very similar ε_{660}. Finally, dispersions prepared by SDBS (ε_{660} ∼ 29 mL·mg^{-1}·cm^{-1}) are significantly different from all others. These results can be compared with the literature data. Extinction coefficients vary with CNT character (metallic or semiconducting) and likely with aggregated state (individuals or bundles), and therefore they have also a wavelength dependence.[25] For MWNT dispersions in various surfactants, a ε_{500} = 46 ± 1.4 mL·mg^{-1}·cm^{-1} was reported,[24] while other studies present ε_{500} = 22.3 mL·mg^{-1}·cm^{-1} for SWNTs dispersed with SDBS, CTAB and a few polymers.[53] For SWNTs prepared by different processes, it was shown that ε has no correlation with nanotube diameter and length, falling in the range of 44.8 (λ = 206.1 nm) to 54.5 (λ = 251.2 nm) mL·mg^{-1}·cm^{-1}.[54] More significantly, for SWNT/SDBS dispersions, different authors[25] obtained ε_{660} values of 30.8, 32.6, and 33.9 mL·mg^{-1}·cm^{-1}, essentially in line with our values. First, we investigate the origin of the observed apparent absorbance. Scattered intensity roughly scales by the square of the radius of gyration, R_g, and hence depends on the size but also on the shape of the scattering particles. In our system, the centrifugation data above and ensuing considerations suggest that the dispersed bundles are rodlike. For rods, R_g scales with the length, L, and the scattered intensity with L.[2] In the other limit, scattering scales as R^6 for globular particles with radius R. Here, we observe very similar (within 5%) apparent ε values for six different surfactant/SWNT dispersions for SWNT and MWNT dispersions. It is very unlikely that average particle sizes in all these dispersions coincided within a range of ±5%. Further, recent studies could not confirm that SWNT absorbance is length dependent.[46] Thus, the results indicate that the contribution of scattering to apparent absorption is minor. As for the lower apparent ε_{660} (by about 30%) of SDBS, aromatic adsorbents are long known to affect the NT electronic structure[55,56] and therefore also their optical absorbance.[57] That could be an indication that in our dispersions the aromatic headgroup of SDBS interacts closely with the nanotube surface.[19,30]

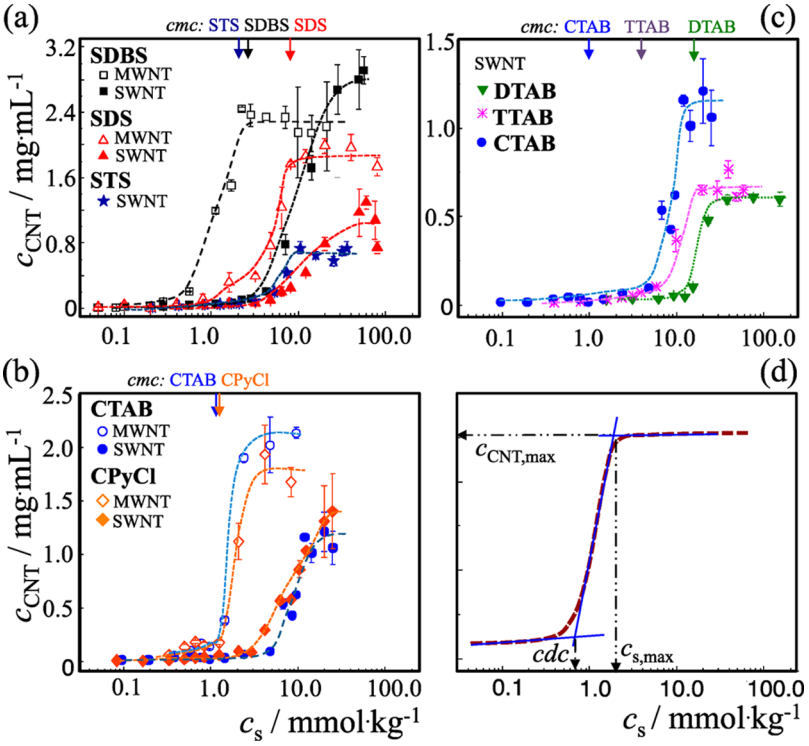

Figure 6. Concentration of dispersed MWNTs and SWNTs versus surfactant concentration (log scale): (a) anionic surfactants SDBS, SDS and STS; (b) cationic surfactants CTAB and CPyCl; (c) homologous series DTAB, TTAB, and CTAB; (d) representative curve with the graphical definition of the dispersion parameters. Lines are for visual guidance.

DOI: 10.1021/acs.langmuir.5b02050
Langmuir 2015, 31, 10955−10965

3.2. Surfactant-Assisted Dispersion of CNTs. The effect of varying surfactant concentration, c_s, on the dispersed CNT concentration, c_{CNT}, was monitored, and the obtained curves for MWNTs and SWNTs are shown in Figure 6a–c, where c_s is in log scale (in order to enhance features at low c_s). Prior to analysis of the data, a few points should be noted. First, the initial undispersed CNT mass is constant for all systems, 3 mg·mL^{-1}. Second, and as mentioned before, c_s is the surfactant concentration in the initial (untreated) sample, not the final one in the collected supernatant; it is expressed here in molality (amount of surfactant per kg of solvent; for conversion to other units cf. Tables S4–S5, SI). Third, the *cmc* of each neat surfactant, indicated by an arrow at the top of the graph, is slightly lower than cmc_d (the surfactant concentration above which free micelles exist in the dispersion), due to the uptake of surfactant unimers by the dispersed tubes.[36] Finally, we note that we chose to represent in the dispersion curves of Figure 6 a maximum surfactant concentrations that is below the concentration where the CNT dispersibility drops dramatically (an effect that we could typically reproduce at $c_s > 10 \times cmc$).[23]

All the dispersion curves in Figure 6 clearly show a sigmoidal profile. Beyond a given surfactant concentration, dispersibility rises more or less steeply, similar to cooperative binding isotherms of surfactants on various surfaces,[43] and then tends to a plateau value. From this general profile, some characteristic parameters can be extracted using appropriate linear regression statistics, as represented schematically in Figure 6d (cf. also Tables S4–S5, SI). The surfactant concentration required to effectively start dispersing the CNT ("takeoff" concentration) is designated as the critical dispersibility concentration, *cdc*. Beyond the *cdc*, c_{CNT} has a more or less sharp increase, depending on surfactant, until a maximum value, $c_{CNT,max}$, is attained at the surfactant concentration denoted as $c_{s,max}$. Two other metrics were used here for comparative purposes: the dispersion effectiveness, η, and the dispersion efficiency, η^*. The effectiveness is defined as

$$\eta = \frac{c_{CNT,max}}{c_{CNT,in}} \times 100 \quad (2)$$

where $c_{CNT,in}$ is the initial powder CNT mass per volume of added solution (herein, 3 mg·mL^{-1}). η is a measure of the capability of a surfactant to disperse a given bulk mass of CNT (the desired intent). We also introduce the dispersion efficiency, η^*, defined as

$$\eta^* = \frac{\eta}{c_{s,max}} \quad (3)$$

and expressed in units of %·kg·mmol^{-1}. For an ideal dispersant, maximal dispersibility (high η) should be attained at the lowest possible $c_{s,max}$. An effective surfactant may not be very efficient, yet an efficient surfactant must necessarily be somewhat effective (for high dispersibility is inconceivable with very low surfactant concentration). The efficiency η^* not only has a clear practical relevance (less surfactant amount implies lower cost) but also carries a molecular meaning. Hence, comparatively higher η^* could imply either (i) a higher binding fraction of surfactant (reflecting higher binding strength), (ii) a more advantageous configuration of the surfactant on the CNT surface, (iii) stronger intertube repulsive forces, or a combination of these factors acting synergistically.[4,23]

3.2.1. General Comparison between MWNTs and SWNTs. The results in Figure 6a,b, and Figure 7 allow us to compare

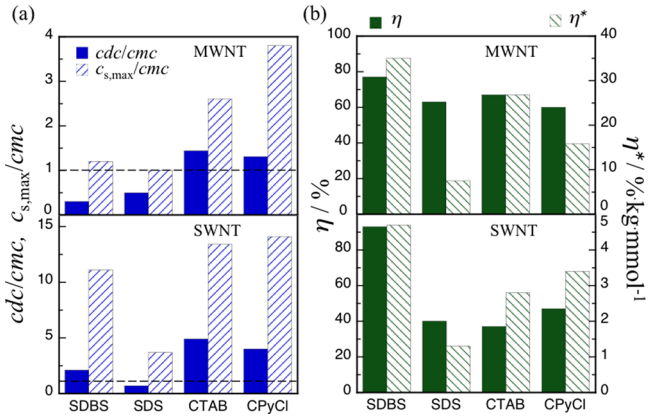

Figure 7. Comparisons between MWNT and SWNT dispersions for surfactants SDBS, SDS, CTAB, and CPyCl: (a) *cdc* and $c_{s,max}$ relative to *cmc*; the dashed horizontal lines mark the unity value; (b) dispersion effectiveness, η, and dispersion efficiency, η^*.

MWNT vs SWNT dispersions for the surfactants SDBS, SDS, CTAB, and CPyCl. The *cdc* and $c_{s,max}$ points for MWNTs are always lower than for SWNTs for any given surfactant and also when we compare any MWNT/surfactant system with a SWNT/surfactant one (Figure 7). Because the *cmc* is an important property of each surfactant, highlighting the role of the surfactant state (unimer vs micelle) in the dispersibility, the ratios cdc/cmc and $c_{s,max}/cmc$ are used in Figure 7a.

A relevant result is that for MWNT dispersions assisted by SDBS and SDS, dispersibility takes off below *cmc* ($cdc/cmc < 1$) and maximal dispersibility occurs just about *cmc* ($cdc/cmc \sim 1$). In comparison, for all other surfactants (either with MWNTs or SWNTs), the ratios are above 1, implying that a significant percentage of micellized surfactant is initially present either at takeoff or at maximal dispersibility (typically >30% in both cases; cf. also Table S6, SI). Moreover, the effectiveness is higher for MWNTs ($\eta \geq 60\%$) than for SWNTs ($\eta \leq 47\%$), with the exception of the SWNT/SDBS dispersion, which has a remarkable $\eta = 93\%$. Comparing the efficiency η^*, all the values are usually 1 order of magnitude higher for MWNTs than for SWNTs (including SDBS). While these comparisons rest on the dispersibility of CNTs on a mass basis, further insight comes if we consider surface area. Individual MWNTs and SWNTs differ significantly not only in curvature but also in specific surface area, SSA. SSA of individual tubes of various shapes has previously been estimated on the basis of simple geometric considerations.[17,58] For the current NTs, supplier data are SSA $\sim 4 \times 10^2$ m^2 g^{-1} for SWNTs and $\sim 2 \times 10^2$ m^2 g^{-1} for MWNTs. For individual SWNTs, given that the calculated SSA is 13×10^2 m^2 g^{-1} (irrespective of d),[58] the sizably lower value of the undispersed powder indicates, as expected, a large fraction of inaccessible area and thereby tight CNT aggregates. In aqueous dispersions, SSA is not well accessible both because of the lack of suitable experimental methods and because it depends not only on bundle size distribution but also on the tightness of those bundles. Nevertheless, assuming full debundling into individual tubes, and using d = 2–4 nm for SWNTs and d_{outer} = 8–15 nm for MWNTs, we can roughly estimate the SSA of SWNTs to be about 3–4 times that for MWNTs.[58] This nominal relation has some bearing on the results. First, we note that the ratio $c_{s,max}/c_{CNT,max}$ yields the surfactant amount needed to maximize dispersibility per mass of CNT (units: μmol·mg^{-1}). Correcting

DOI: 10.1021/acs.langmuir.5b02050
Langmuir 2015, 31, 10955–10965

that ratio for SWNTs by a factor of 1/4 (to account for the SSA difference), shows that $c_{s,max}/c_{CNT,max}$ for the two types of tubes become similar (cf. Table S7, SI). By choosing SSA = 13×10^2 $m^2 \cdot g^{-1}$ for the dispersed SWNTs (full debundling) and 3×10^2 $m^2 \cdot g^{-1}$ for the MWNTs (a somewhat arbitrary but reasonable value),[58] we can estimate the surfactant amount per surface area. That measure becomes similar—in the order of 10 μmol·m^{-2}, that is ~5 molecule·nm^{-2} (cf. Table S8, SI)—for both types of tubes. Interestingly, this result is not far from a saturated surface coverage of 3 molecule·nm^{-2} reported by several authors for SDS[59] and SDBS[60] on single-walled and for SDBS[35] on multiwalled tubes. Second, we can also correct the effectiveness, η, and efficiency, η^*, shown in Figure 7, by multiplying the values for SWNTs by a factor of 2, since the SSA of this powder is ~2 times that of the MWNT (cf. note 5, SI).

A few comments are in order here. Our centrifugation data in Figure 4 point to a relatively significant presence of small bundles in the SWNT dispersions that should reduce the exposed surface area for the SWNTs. On the other hand, the sonication stress rates permit complete MWNT debundling. This would somewhat mitigate the apparent differences between the mass- and the surface-based evaluations. Thus, and in summary, our data show that the investigated surfactants are, in general, much more effective and efficient in dispersing multiwalled than single-walled tubes on a mass basis, in line with previous works,[35] whereas in terms of dispersed surface area the surfactants seem to perform only slightly better for MWNTs. The data also suggests that surface coverage at saturation is rather similar for MWNTs and SWNTs (SI, Table S8).

3.2.2. Effect of Aromatic Ring in Surfactant Structure. This effect can be analyzed by comparing SDBS versus SDS (both with C12 alkyl chains), and CPyCl versus CTAB (C16 alkyl chains). SDBS is clearly the most effective and efficient dispersant for MWNTs and SWNTs, not only compared to SDS but also with the two C16 surfactants. This superior dispersing ability of SDBS has been recognized before[4,22] and is clearly confirmed here, both on unit mass and unit surface basis. The separated aromatic ring of SBDS is part of the hydrophobic region, and this is expected to increase the effective hydrophobicity of the molecule and promote $\pi-\pi$ interactions with the CNT surface, hence contributing to a stronger binding for this surfactant.[55−57] The surfactant CPyCl also possesses an aromatic pyridinium ring in its structure, yet in contrast with SDBS, the ring is part of the polar headgroup containing the cationic charge, and this does not seem to particularly favor its performance. In fact, while CPyCl has the second best η and η^* for SWNTs after SDBS on a mass basis, this advantage is practically vanished on a surface basis. Comparison with CTAB, a surfactant of equal chain length but devoid of ring, also shows that in terms of molecule/nm^2 at saturation the two surfactants behave essentially the same for both single- and double-walled tubes (SI, Table S8).

3.2.3. Effect of Surfactant Chain Length. The increase of alkyl chain length enhances the hydrophobic character of a surfactant and, consequently, its tendency to adsorb onto hydrophobic surfaces, such as the CNT wall. This is expected to enhance both dispersion effectiveness and efficiency. In fact, this trend is generally apparent in Figure 8a, where η and η^*, are plotted versus the number of C atoms in the alkyl chain length for the SWNT dispersions (SDSB is excluded from the apparent linear fits due to the outlying ring effect). Another

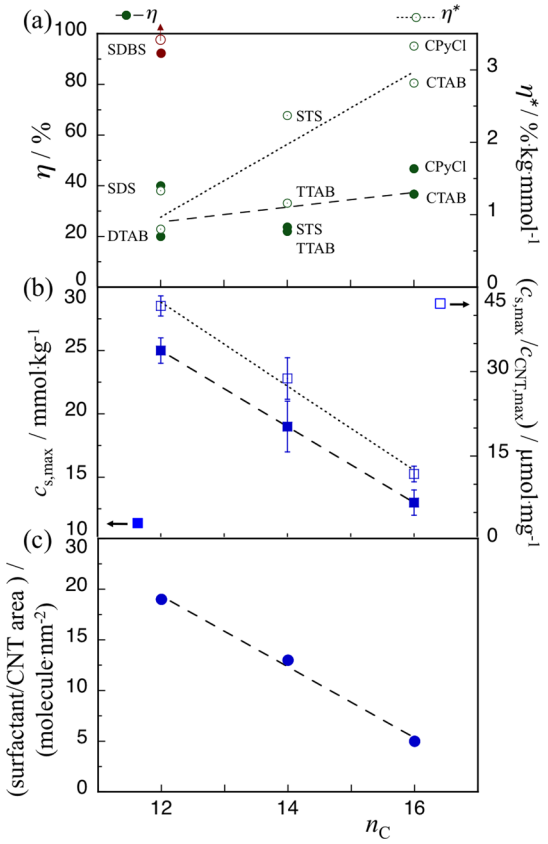

Figure 8. Results for SWNT dispersions: (a) η and η^* versus n_C (number of C atoms in alkyl chain) for all surfactants (values for SDSB not considered for the fits, with η^* beyond the *y*-axis limit as denoted by the arrow); (b) $c_{s,max}$, ratio $c_{s,max}/c_{CNT,max}$ and (c) surfactant molecules per unit nanotube area at $c_{s,max}$ versus n_C for alkyltrimethylammonium bromides. Lines are linear regression fits.

significant observation is that η^* increases by a larger factor within the n_C range than η, indicating that more hydrophobic surfactants not only disperse more nanotube mass (and surface area), but do it more efficiently.

The chain length effect can be more sharply analyzed in the SWNT dispersions produced by the homologous series of alkyltrimethylammonium bromides, Figures 6c and 8b. Increasing chain length brings about a decrease of surfactant concentration at saturation, $c_{s,max}$, and also an increase in the dispersed CNT, $c_{CNT,max}$. Interestingly, linear dependencies are apparent if we plot $c_{s,max}$ and the ratio $c_{s,max}/c_{CNT,max}$ versus n_C, as shown in Figure 8b. Conversely, a linear decrease with n_C is also found for the number of surfactant molecules per unit area at saturation (obtained from the surface analysis), as can be seen in Figure 8c. The linear trends in $c_{s,max}/c_{CNT,max}$ or in surfactant molecule per unit area suggest that the dispersing ability of the surfactant is rising drastically with n_C. Two mechanisms can be envisaged. In one, if we assume that identical surface coverage is needed at saturation for the three surfactants (say, 3 molecule/nm^2), then a more hydrophobic surfactant like CTAB would achieve this value at lower concentration because the fraction of adsorbed surfactant is expected to rise with hydrophobicity. Conversely, for a less hydrophobic surfactant like DTAB, depletion effects take over and undermine dispersibility. In another mechanism, we could assume that it is the degree of surface coverage that increases with chain length. A supporting argument for this last

DOI: 10.1021/acs.langmuir.5b02050
Langmuir 2015, 31, 10955−10965

hypothesis comes from the zeta potential measurements shown below in section 3.2.5, Figure 10a: the ζ values of SWNT dispersions (measured at fixed c_s and c_{CNT}) increase with n_C for this series of surfactants, and the simplest interpretation is that more densely charged species are present. Molecular simulations for the interaction of DTAB and CTAB with SWNTs have shown that upon increasing concentration, CTAB adsorbs more extensively,[41] and that is consistent with our observations. Finally, we note that the linear correlations in Figure 8b also bear a wider implication. While it is known that *cmc* decays exponentially with n_C for homologous surfactants,[43] we find here that $c_{s,max}$ decays linearly with n_C. Thus, surfactant-CNT association seems to display rather different equilibrium (or quasi-equilibrium) features compared to other phenomena that are also driven by hydrophobic interactions, such as micellization.

3.2.4. Effect of Surfactant Concentration and cmc. The diversity of surfactants and conditions used in experimental studies[23] and the picture from molecular simulations[4] do not yet convey a consensual picture on the role of surfactant concentration on dispersing ability, and in particular the role of micelles in the dispersion process. Micelles could help in the initial exfoliating process as full aggregates or they could just act as reservoirs for surfactant molecules. Let us first consider our results for MWNTs in Figure 7a,b (upper plots). For SDS and SDBS, both *cdc* and $c_{s,max}$ are below or just about *cmc* (no micelles or few micelles present), whereas they lie above *cmc* for CTAB and CPyCl (significant fraction of surfactant in micellar form, cf. Table S6, SI). Still, η is similar for all surfactants (namely SDS, CTAB, and CPyCl), while η^* is scattered with no trend. Hence, as far as MWNTs are concerned, the initial state of the surfactant (unimer or micelle) does not seem to play any decisive role in dispersed CNT amount and efficiency. As concerning SWNT dispersions, the larger number of surfactants studied allows further conclusions. In Figure 9a, it can be seen that even though the *cdc*/*cmc* ratio increases (roughly linearly) between 1 and 5, *cdc* is essentially independent of n_C.

This indicates that a minimum surfactant concentration in solution is required to induce meaningful dispersibility, but that value does not seem to vary with molecular properties. When maximal dispersibility is attained, the fraction of surfactant initially in micellar form is now considerable in all cases, typically higher than 73% (Table S6, SI). In addition, Figure 9b, shows that $c_{s,max}$ decreases roughly linearly with increasing n_C by a factor of 2, while the ratio $c_{s,max}/cmc$ rises (similarly to *cdc*/*cmc*) but by a factor ~8. In combination, these observations also support the view that for SWNTs, micelle concentration is not decisive for the attainment of maximal dispersibility. In fact, the increase in the ratios *cdc*/*cmc* and $c_{s,max}/cmc$ with n_C could just be coupled to the trivial fact that *cmc* decreases with n_C, but bear no further significance than that. Hence, our data support the view that micelles act essentially as labile reservoirs supplying surfactant molecules for the binding onto the CNT surface.

3.2.5. Zeta Potential Studies. In order to gain further molecular insight, we probed the effect of surfactant concentration on the zeta potential of the dispersions. The validity of the approximations used in the Henry equation has previously been discussed.[22,45] We use similar approximations, and since comparisons under identical conditions are made, the approximations are not critical. It is expected that individual tubes or bundles coated by anionic or cationic surfactants will

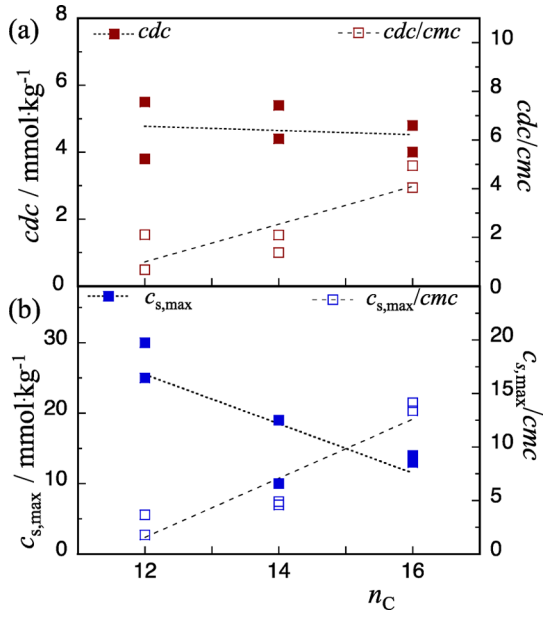

Figure 9. Effect of surfactant *cmc* on SWNT dispersions: (a) *cdc* and *cdc*/*cmc* vs number of C atoms in alkyl chain, for all surfactants; (b) similarly, $c_{s,max}$ and $c_{s,max}/cmc$ versus n_C. The lines are linear regression fits.

have, respectively, negative and positive ζ. Larger $|\zeta|$ reflects in principle higher surface charge density, and hence $|\zeta|$ can be seen as an indicator of surfactant binding strength. Moreover, coated species with $|\zeta| > 30$ mV will be kinetically stable for long periods of time. Figure 10a shows the results for SWNT dispersions using the anionic surfactants SDS and SDBS, and the cationic homologues DTAB, TTAB, and CTAB.

For meaningful comparisons, all these dispersions have the same concentration of SWNTs, 0.1 mg·mL^{-1}, and surfactant, 15 mmol·kg^{-1} (cf. also Note 6, SI). Also shown in Figure 10a is a horizontal line marking ζ for a dispersion prepared with a nonionic surfactant (Pluronics F127, a triblock copolymer), which yielded a negative value, −6 mV (neat solutions of F127 were used as controls). This dispersion was prepared in order to check whether the CNT surface had some effective (nonzero) surface charge, considering that negative ζ has been reported in pristine SWNT/nonionic surfactant dispersions.[45] We could indeed qualitatively confirm these results. In the experiments, the scattered light is detected. For any reasonable size consideration, scattering from CNT bundles dominates over scattering from free surfactant micelles. Hence, what one measures is the zeta potential of surfactant coated-CNT species. As further support, at c_s = 15 mmol·kg^{-1}, very few (if any) free micelles can be present for surfactant DTAB, and the results for the other surfactants are in line with those for DTAB. The first observation from Figure 10a is that all dispersions yield $|\zeta| > 30$ mV, indicating a high kinetic stability. For the alkytrimethylammonium bromides, ζ increases with chain length. This is not only consistent with a stronger adsorption as hydrophobicity increases, but further suggests that there is increasing charge density associated, in line with the trend discussed for $c_{s,max}/c_{CNT,max}$ in Figure 8b.

One can also tentatively analyze the effect of charge, comparing equal chain lengths. For DTAB, SDS, and SDBS (all n_C = 12), both effectiveness and efficiency are higher for the anionic surfactants (Figure 8a), in particular with respect to η^*. SDBS and SDS exhibit a higher relative change of ζ than

DOI: 10.1021/acs.langmuir.5b02050
Langmuir 2015, 31, 10955−10965

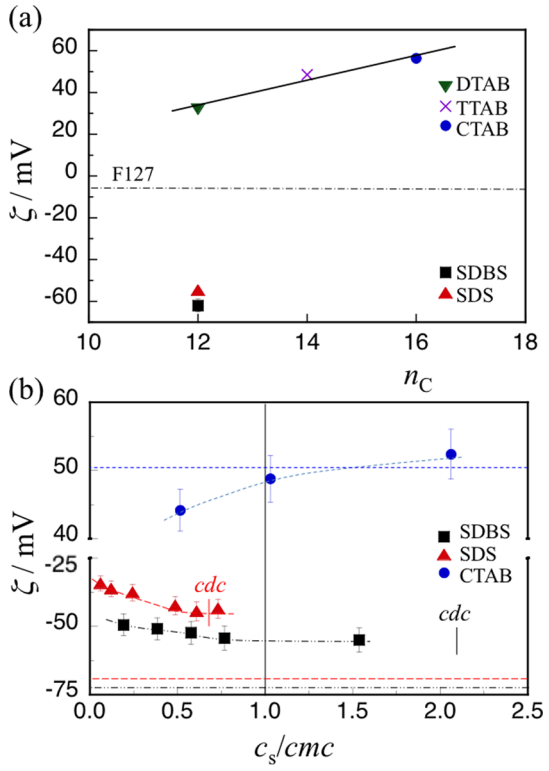

Figure 10. Zeta potential for SWNT dispersions: (a) versus n_C, for alkyltrimethylammonium bromides (DTAB, TTAB, and CTAB) and anionic surfactants SDBS and SDS, all with c_{CNT} = 0.1 mg·mL^{-1} and c_s = 15 mmol·kg^{-1}; the dash-point line marks the negative ζ-potential of a F127/SWNT dispersion; (b) versus surfactant concentration/*cmc* for SDBS, SDS and CTAB; dashed lines mark ζ for the neat micelles of each surfactant; also marked are the *cdc* of SDS and SDBS, while that of CTAB is beyond the *x*-axis limit (4.9).

DTAB. While for SDBS the aromatic ring complicates comparison, the bigger change for SDS hints at a more favored binding for anionic than cationic surfactants. Anionic surfactants have been known to be more efficient than cationic ones in processes that involve adsorption at negatively charged surfaces (e.g., fibers, metals and minerals).[43] The common view is that the electrostatic attraction of the surface with the cationic headgroups favors a "head-on" binding, while for the anionic one a "tail-on" binding is preferred. The latter is more effective in that the charges are water-exposed and the tails hydrophobicaly bound to the surface. Similar effects could be at play in the interaction of ionic surfactants with CNT surfaces.

Figure 10b shows ζ versus surfactant concentration for SDS, SDBS, and CTAB. Two points are noteworthy. First, despite that all concentrations lie below *cdc* and hence c_{CNT} is relatively small, the ζ values are physically realistic and trends emerge from the data. Second, surfactant concentrations are also below neat *cmc* and hence ζ can only originate from CNT/surfactant particles. The dashed horizontal lines represent ζ for the neat surfactant micelles, for proper comparison. SDBS yields more negative ζ than SDS consistent with its higher binding strength; further, as c_s increases, ζ becomes increasingly negative and seems to attain a plateau near *cdc*. For CTAB, only three points could be measured, but the trend is similar. These observations suggest that it is only when the CNT surface attains a sufficient degree of surface coverage and hence of $|\zeta|$ (of the order of 50 mV) that the dispersed particles will remain stable against aggregation. This could well signal the point where dispersibility starts taking off massively, which does not seem to differ much from surfactant to surfactant—in line with Figure 8a and previous suggestion.[23]

4. CONCLUSIONS

By resorting to a carefully controlled experimental procedure and to statistical sampling, we have shown that high-precision dispersibility curves of MWNTs and SWNTs in water, as assisted by various types of surfactants, could be obtained. This allowed us to extract some reliable metrics for each surfactant, for proper comparisons, viz., the critical dispersibility concentration (*cdc*), the maximum dispersed CNT concentration ($c_{CNT,max}$) and respective surfactant concentration at that point ($c_{s,max}$), and the dispersion effectiveness (η) and efficiency (η^*). On a nanotube mass basis, MWNTs not only require, in general, less surfactant than SWNTs for maximal dispersibility (saturation), but also more mass is dispersed, hence higher η and η^* are achieved. However, conversion of dispersed nanotube mass to surface area shows that the better surfactant performance for MWNTs is significantly lessened and likely only marginal. Similar values of surfactant amount per nanotube surface area obtained at the ($c_{s,max}$, $c_{CNT,max}$) point, comparing MWNTs and SWNTs, suggest that nanotube curvature does not appreciably affect surface coverage at saturation. Both η and η^* increase notably with surfactant chain length and the presence of an aromatic ring (in the surfactant tail but not in the headgroup), and are slightly higher for anionic than cationic surfactants. Efficiency, more than effectiveness, is especially enhanced upon proper choice of surfactant properties. From the seven surfactants studied, covering a wide range of properties, SDBS is clearly the best dispersant (both on mass or surface basis) for both types of tubes. The following order of performance was observed: SDBS > CTAB ≈ CPyCl > STS > TTAB ≈ SDS > DTAB. Significantly, we have found that $c_{s,max}$ and the surfactant amount per SWNT area at $c_{s,max}$ both decrease linearly with surfactant chain length. This implies that the equilibrium (or quasi-equilibrium) features of CNT-surfactant association are fundamentally distinct from those of other surfactant hydrophobicity-mediated phenomena, such as micellization (where *cmc* is well-known to decrease exponentially with chain length). Markedly, the presence of surfactant micelles in the exfoliation process does not seem to play any decisive role in the final dispersibility, implying that it is surfactant binding affinity to the CNT surface and surfactant availability that ultimately dictate the effectiveness and efficiency of the process. Finally, the high $|\zeta|$ of the coated nanotubes (even at low surfactant concentrations) clearly indicate that electrostatic repulsions are responsible for the kinetic stability of these dispersions.

■ ASSOCIATED CONTENT

Supporting Information

The Supporting Information is available free of charge on the ACS Publications website at DOI: 10.1021/acs.langmuir.5b02050.

Note 1: Determination of the energy and power densities used in the sonication step; Tables S1 and S2. Note 2: Apparent extinction coefficients of CNT-surfactant dispersions; Table S3. Note 3: Parameters obtained from the CNT dispersion curves; Tables S4−6. Note 4: Conductometric curves for the determination of the *cmc* of the surfactants. (Figure S2). Note 5: Comparisons of

DOI: 10.1021/acs.langmuir.5b02050
Langmuir 2015, 31, 10955−10965

SWNT and MWNT dispersibility on a surface area basis; Tables S7−8; Figure S1. Note 6: Zeta potential measurements (Table S9). (PDF)

AUTHOR INFORMATION

Corresponding Author

*E-mail: efmarque@fc.up.pt.

Notes

The authors declare no competing financial interest.

ACKNOWLEDGMENTS

We kindly acknowledge support from Fundação para a Ciência e Tecnologia (FCT, Portugal) through PEst-C/QUI/UI0081/2013 (CIQ-UP) and the Ph.D. Grant SFRH/BD/72612/2010. Thanks are also due to FEDER and FCT/MES through NORTE-07-0124-FEDER-000065. The Swedish Research Council VR is also gratefully acknowledged.

REFERENCES

(1) Hecht, D. S.; Hu, L.; Irvin, G. Emerging Transparent Electrodes Based on Thin Films of Carbon Nanotubes, Graphene, and Metallic Nanostructures. *Adv. Mater.* **2011**, *23*, 1482−1513.

(2) Breuer, O.; Sundararaj, U. Big returns from small fibers: A review of polymer/carbon nanotube composites. *Polym. Compos.* **2004**, *25*, 630−645.

(3) Huang, Y. Y.; Terentjev, E. M. Dispersion of Carbon Nanotubes: Mixing, Sonication, Stabilization, and Composite Properties. *Polymers* **2012**, *4*, 275−295.

(4) Angelikopoulos, P.; Bock, H. The science of dispersing carbon nanotubes with surfactants. *Phys. Chem. Chem. Phys.* **2012**, *14*, 9546−9557.

(5) Britz, D. A.; Khlobystov, A. N. Noncovalent interactions of molecules with single walled carbon nanotubes. *Chem. Soc. Rev.* **2006**, *35*, 637−659.

(6) Kharissova, O. V.; Kharisov, B. I.; de Casas Ortiz, E. G. Dispersion of carbon nanotubes in water and non-aqueous solvents. *RSC Adv.* **2013**, *3*, 24812−24852.

(7) Premkumar, T.; Mezzenga, R.; Geckeler, K. E. Carbon Nanotubes in the Liquid Phase: Addressing the Issue of Dispersion. *Small* **2012**, *8*, 1299−1313.

(8) Grossiord, N.; Loos, J.; Regev, O.; Koning, C. E. Toolbox for dispersing carbon nanotubes into polymers to get conductive nanocomposites. *Chem. Mater.* **2006**, *18*, 1089−1099.

(9) Haggenmueller, R.; Rahatekar, S. S.; Fagan, J. A.; Chun, J.; Becker, M. L.; Naik, R. R.; Krauss, T.; Carlson, L.; Kadla, J. F.; Trulove, P. C.; Fox, D. F.; DeLong, H. C.; Fang, Z.; Kelley, S. O.; Gilman, J. W. Comparison of the quality of aqueous dispersions of single wall carbon nanotubes using surfactants and biomolecules. *Langmuir* **2008**, *24*, 5070−5078.

(10) Shvartzman-Cohen, R.; Florent, M.; Goldfarb, D.; Szleifer, I.; Yerushalmi-Rozen, R. Aggregation and self-assembly of amphiphilic block copolymers in aqueous dispersions of carbon nanotubes. *Langmuir* **2008**, *24*, 4625−4632.

(11) Saint-Aubin, K.; Poulin, P.; Jaillet, C.; Maugey, M.; Zakri, C. Changes of morphology and properties of block copolymers induced by carbon nanotubes. *Polymer* **2013**, *54*, 2285−2291.

(12) Frise, A. E.; Pages, G.; Shtein, M.; Pri Bar, I.; Regev, O.; Furó, I. Polymer binding to carbon nanotubes in aqueous dispersions: Residence time on the nanotube surface As Obtained by NMR diffusometry. *J. Phys. Chem. B* **2012**, *116*, 2635−2642.

(13) Karajanagi, S. S.; Yang, H. C.; Asuri, P.; Sellitto, E.; Dordick, J. S.; Kane, R. S. Protein-assisted solubilization of single-walled carbon nanotubes. *Langmuir* **2006**, *22*, 1392−1395.

(14) Edri, E.; Regev, O. "Shaken, Not Stable": Dispersion Mechanism and Dynamics of Protein-Dispersed Nanotubes Studied via Spectroscopy. *Langmuir* **2009**, *25*, 10459−10465.

(15) Frise, A. E.; Edri, E.; Furo, I.; Regev, O. Protein Dispersant Binding on Nanotubes Studied by NMR Self-Diffusion and Cryo-TEM Techniques. *J. Phys. Chem. Lett.* **2010**, *1*, 1414−1419.

(16) Horn, D. W.; Tracy, K.; Easley, C. J.; Davis, V. A. Lysozyme Dispersed Single-Walled Carbon Nanotubes: Interaction and Activity. *J. Phys. Chem. C* **2012**, *116*, 10341−10348.

(17) Karchemsky, F.; Drug, E.; Mashiach-Farkash, E.; Fadeev, L.; Wolfson, H. J.; Gozin, M.; Regev, O. Diameter-selective dispersion of carbon nanotubes by beta-lactoglobulin whey protein. *Colloids Surf., B* **2013**, *112*, 16−22.

(18) Moore, V. C.; Strano, M. S.; Haroz, E. H.; Hauge, R. H.; Smalley, R. E.; Schmidt, J.; Talmon, Y. Individually suspended single-walled carbon nanotubes in various surfactants. *Nano Lett.* **2003**, *3*, 1379−1382.

(19) Islam, M. F.; Rojas, E.; Bergey, D. M.; Johnson, A. T.; Yodh, A. G. High weight fraction surfactant solubilization of single-wall carbon nanotubes in water. *Nano Lett.* **2003**, *3*, 269−273.

(20) Badaire, S.; Poulin, P.; Maugey, M.; Zakri, C. In situ measurements of nanotube dimensions in suspensions by depolarized dynamic light scattering. *Langmuir* **2004**, *20*, 10367−10370.

(21) Vaisman, L.; Wagner, H. D.; Marom, G. The role of surfactants in dispersion of carbon nanotubes. *Adv. Colloid Interface Sci.* **2006**, *128-130*, 37−46.

(22) Sun, Z.; Nicolosi, V.; Rickard, D.; Bergin, S. D.; Aherne, D.; Coleman, J. N. Quantitative evaluation of surfactant-stabilized single-walled carbon nanotubes: Dispersion quality and its correlation with zeta potential. *J. Phys. Chem. C* **2008**, *112*, 10692−10699.

(23) Wang, H. Dispersing carbon nanotubes using surfactants. *Curr. Opin. Colloid Interface Sci.* **2009**, *14*, 364−371.

(24) Clark, M. D.; Subramanian, S.; Krishnamoorti, R. Understanding surfactant aided aqueous dispersion of multi-walled carbon nanotubes. *J. Colloid Interface Sci.* **2011**, *354*, 144−151.

(25) Blanch, A. J.; Lenehan, C. E.; Quinton, J. S. Parametric analysis of sonication and centrifugation variables for dispersion of single walled carbon nanotubes in aqueous solutions of sodium dodecylbenzene sulfonate. *Carbon* **2011**, *49*, 5213−5228.

(26) Oh, H.; Sim, J.; Ju, S. Y. Binding Affinities and Thermodynamics of Noncovalent Functionalization of Carbon Nanotubes with Surfactants. *Langmuir* **2013**, *29*, 11154−11162.

(27) Dassios, K. G.; Alafogianni, P.; Antiohos, S. K.; Leptokaridis, C.; Barkoula, N.-M.; Matikas, T. E. Optimization of Sonication Parameters for Homogeneous Surfactant-Assisted Dispersion of Multiwalled Carbon Nanotubes in Aqueous Solutions. *J. Phys. Chem. C* **2015**, *119*, 7506−7516.

(28) Grossiord, N.; Regev, O.; Loos, J.; Meuldijk, J.; Koning, C. E. Time-dependent study of the exfoliation process of carbon nanotubes in aqueous dispersions by using UV-visible spectroscopy. *Anal. Chem.* **2005**, *77*, 5135−5139.

(29) Decker, J. E.; Hight Walker, A. R.; Bosnick, K.; Clifford, C. A.; Dai, L.; Fagan, J.; Hooker, S.; Jakubek, Z. J.; Kingston, C.; Makar, J.; Mansfield, E.; Postek, M. T.; Simard, B.; Sturgeon, R.; Wise, S.; Vladar, A. E.; Yang, L.; Zeisler, R. Sample preparation protocols for realization of reproducible characterization of single-wall carbon nanotubes. *Metrologia* **2009**, *46*, 682−692.

(30) Ernst, F.; Heek, T.; Setaro, A.; Haag, R.; Reich, S. Functional Surfactants for Carbon Nanotubes: Effects of Design. *J. Phys. Chem. C* **2013**, *117*, 1157−1162.

(31) Di Crescenzo, A.; Cambre, S.; Germani, R.; Di Profio, P.; Fontana, A. Dispersion of SWCNTs with Imidazolium-Rich Surfactants. *Langmuir* **2014**, *30*, 3979−3987.

(32) Strano, M. S.; Moore, V. C.; Miller, M. K.; Allen, M. J.; Haroz, E. H.; Kittrell, C.; Hauge, R. H.; Smalley, R. E. The role of surfactant adsorption during ultrasonication in the dispersion of single-walled carbon nanotubes. *J. Nanosci. Nanotechnol.* **2003**, *3*, 81−86.

(33) Duan, W. H.; Wang, Q.; Collins, F. Dispersion of carbon nanotubes with SDS surfactants: a study from a binding energy perspective. *Chem. Sci.* **2011**, *2*, 1407−1413.

(34) Fernandes, R. M. F.; Buzaglo, M.; Shtein, M.; Pri Bar, I.; Regev, O.; Marques, E. F.; Furó, I. Lateral Diffusion of Dispersing Molecules

DOI: 10.1021/acs.langmuir.5b02050
Langmuir 2015, 31, 10955−10965

on Nanotubes As Probed by NMR. *J. Phys. Chem. C* **2014**, *118*, 582−589.
(35) Zhong, W.; Claverie, J. P. Probing the carbon nanotube-surfactant interaction for the preparation of composites. *Carbon* **2013**, *51*, 72−84.
(36) Sa, V.; Kornev, K. G. Analysis of Stability of Nanotube Dispersions Using Surface Tension Isotherms. *Langmuir* **2011**, *27*, 13451−13460.
(37) Angelikopoulos, P.; Gromov, A.; Leen, A.; Nerushev, O.; Bock, H.; Campbell, E. E. B. Dispersing Individual Single-Wall Carbon Nanotubes in Aqueous Surfactant Solutions below the cmc. *J. Phys. Chem. C* **2010**, *114*, 2−9.
(38) Tardani, F.; La Mesa, C. Attempts to control depletion in the surfactant-assisted stabilization of single-walled carbon nanotubes. *Colloids Surf., A* **2014**, *443*, 123−128.
(39) Richard, C.; Balavoine, F.; Schultz, P.; Ebbesen, T. W.; Mioskowski, C. Supramolecular self-assembly of lipid derivatives on carbon nanotubes. *Science* **2003**, *300*, 775−778.
(40) Nativ-Roth, E.; Nap, R. J.; Szleifer, I.; Yerushalmi-Rozen, R. Order-disorder transition induced by surfactant micelles in single-walled carbon nanotubes dispersions. *Soft Matter* **2010**, *6*, 5289−5292.
(41) Poorgholami-Bejarpasi, N.; Sohrabi, B. Self-assembly of cationic surfactants on the carbon nanotube surface: insights from molecular dynamics simulations. *J. Mol. Model.* **2013**, *19*, 4319−4335.
(42) Nativ-Roth, E.; Shvartzman-Cohen, R.; Bounioux, C.; Florent, M.; Zhang, D.; Szleifer, I.; Yerushalmi-Rozen, R. Physical adsorption of block copolymers to SWNT and MWNT: A nonwrapping mechanism. *Macromolecules* **2007**, *40*, 3676−3685.
(43) Holmberg, K.; Jönsson, B.; Kronberg, B.; Lindman, B. *Surfactant and Polymers in Aqueous Solution*; John Wiley & Sons: Chichester, U.K., 2002.
(44) Shtein, M.; Pri-bar, I.; Regev, O. A simple solution for the determination of pristine carbon nanotube concentration. *Analyst* **2013**, *138*, 1490−1496.
(45) White, B.; Banerjee, S.; O'Brien, S.; Turro, N. J.; Herman, I. P. Zeta-potential measurements of surfactant-wrapped individual single-walled carbon nanotubes. *J. Phys. Chem. C* **2007**, *111*, 13684−13690.
(46) Naumov, A. V.; Tsyboulski, D. A.; Bachilo, S. M.; Weisman, R. B. Length-dependent optical properties of single-walled carbon nanotube samples. *Chem. Phys.* **2013**, *422*, 255−263.
(47) Krause, B.; Mende, M.; Poetschke, P.; Petzold, G. Dispersability and particle size distribution of CNTs in an aqueous surfactant dispersion as a function of ultrasonic treatment time. *Carbon* **2010**, *48*, 2746−2754.
(48) Nair, N.; Kim, W.-J.; Braatz, R. D.; Strano, M. S. Dynamics of surfactant-suspended single-walled carbon nanotubes in a centrifugal field. *Langmuir* **2008**, *24*, 1790−1795.
(49) Laurent, C.; Flahaut, E.; Peigney, A. The weight and density of carbon nanotubes versus the number of walls and diameter. *Carbon* **2010**, *48*, 2994−2996.
(50) Green, M. J. Analysis and measurement of carbon nanotube dispersions: nanodispersion versus macrodispersion. *Polym. Int.* **2010**, *59*, 1319−1322.
(51) Dror, Y.; Pyckhout-Hintzen, W.; Cohen, Y. Conformation of polymers dispersing single-walled carbon nanotubes in water: A small-angle neutron scattering study. *Macromolecules* **2005**, *38*, 7828−7836.
(52) Priya, B. R.; Byrne, H. J. Investigation of Sodium Dodecyl Benzene Sulfonate Assisted Dispersion and Debundling of Single-Wall Carbon Nanotubes. *J. Phys. Chem. C* **2008**, *112*, 332−337.
(53) Anson-Casaos, A.; Gonzalez-Dominguez, J. M.; Lafragueta, I.; Carrodeguas, J. A.; Martinez, M. T. Optical absorption response of chemically modified single-walled carbon nanotubes upon ultra-centrifugation in various dispersants. *Carbon* **2014**, *66*, 105−118.
(54) Rance, G. A.; Marsh, D. H.; Nicholas, R. J.; Khlobystov, A. N. UV-vis absorption spectroscopy of carbon nanotubes: Relationship between the pi-electron plasmon and nanotube diameter. *Chem. Phys. Lett.* **2010**, *493*, 19−23.
(55) Zhao, J. J.; Lu, J. P.; Han, J.; Yang, C. K. Noncovalent functionalization of carbon nanotubes by aromatic organic molecules. *Appl. Phys. Lett.* **2003**, *82*, 3746−3748.
(56) Wang, F.; Sfeir, M. Y.; Huang, L. M.; Huang, X. M. H.; Wu, Y.; Kim, J. H.; Hone, J.; O'Brien, S.; Brus, L. E.; Heinz, T. F. Interactions between individual carbon nanotubes studied by Rayleigh scattering spectroscopy. *Phys. Rev. Lett.* **2006**, *96*, 167401.
(57) Tabakman, S. M.; Welsher, K.; Hong, G. S.; Dai, H. J. Optical Properties of Single-Walled Carbon Nanotubes Separated in a Density Gradient: Length, Bundling, and Aromatic Stacking Effects. *J. Phys. Chem. C* **2010**, *114*, 19569−19575.
(58) Peigney, A.; Laurent, C.; Flahaut, E.; Bacsa, R. R.; Rousset, A. Specific surface area of carbon nanotubes and bundles of carbon nanotubes. *Carbon* **2001**, *39*, 507−514.
(59) Grossiord, N.; van der Schoot, P.; Meuldijk, J.; Koning, C. E. Determination of the surface coverage of exfoliated carbon nanotubes by surfactant molecules in aqueous solution. *Langmuir* **2007**, *23*, 3646−3653.
(60) Suttipong, M.; Tummala, N. R.; Kitiyanan, B.; Striolo, A. Role of Surfactant Molecular Structure on Self-Assembly: Aqueous SDBS on Carbon Nanotubes. *J. Phys. Chem. C* **2011**, *115*, 17286−17296.

DOI: 10.1021/acs.langmuir.5b02050
Langmuir 2015, 31, 10955−10965

Supporting Information

Note 1. Estimation of energy and power density delivered by sonication

A procedure to estimate the delivered ultrasound energy during the sonication process using bath and probe was established. Briefly, the temperature increase was recorded over time in a certain mass of water in a properly insulated vial that was irradiated with ultrasounds, at a given output power setting of the sonicator. The average energy and power delivered were calculated, respectively, according to expressions:

$$\langle E \rangle = m c_p \langle \Delta T \rangle \quad \text{(S1)}$$

$$\langle P \rangle = \langle E \rangle / \Delta t \quad \text{(S2)}$$

where E and P are the delivered energy and power, respectively, T is the temperature, ΔT is the sample temperature variation (averaged over different essays), Δt is the sonication time, m is the mass of liquid and c_p is the specific heat capacity of the liquid. Average energy density and average power density are then calculated as $\langle E \rangle / V$ and $\langle P \rangle / V$, where V is the sample volume (different volumes and sample vials geometries were tested). The final results are shown in Table S1.

Table S1. Sonication parameters in this work

sonication method	**total energy density**[a] **/ J mL^{-1} (= shear stress / MPa)**	**processing time / min**	**average power density**[b] **/ W mL^{-1} (= shear rate / MPa s^{-1})**
tip	5.3 x 10^2	8.5	1.0
bath	3.5 x 10^2	180	0.032

[a] $E / V = F \times L / (L \times A) = F / A = p$.

[b] $P / V = E / (V \times \Delta t) = p / \Delta t$.

Table S2. Estimated ranges of cohesive (vdW) and scission pressure of SWNTs and MWNTs with an aspect ratio $L / d \sim 1000$ according to ref.[1]

tube ($L/d \sim 1000$)	**cohesive pressure / MPa**	**scission pressure / MPa**
SWNT	~ (50 - 500)	~ (0.05 - 0.5)
MWNT	~ (0.01 - 0.1)	

[1] Huang, Y. Y.; Terentjev, E. M. Dispersion of Carbon Nanotubes: Mixing, Sonication, Stabilization, and Composite Properties. *Polymers* **2012,** *4*, 275-295.

Note 2. Apparent extinction coefficients for CNT-surfactant dispersions

Table S3. Apparent extinction coefficients of SWNT and MWNT for the different surfactants derived from the linear dependence of the apparent absorbance on NT concentration.

Surfactant	ε_{660} / mL·mg^{-1}·cm^{-1}	
	MWNT	SWNT
SDBS	27.5 ± 0.1	30.1 ± 0.2
SDS	38.4 ± 0.2	39.4 ± 0.1
STS	-	43.9 ± 0.3
DTAB	-	39.7 ± 0.3
TTAB	-	42.5 ± 0.2
CTAB	41.8 ± 0.2	38.9 ± 0.1
CPyCl	42.5 ± 0.1	38.6 ± 0.1

Note 3. Parameters obtained from the dispersion curves

Table S4. Parameters obtained from the MWNT/surfactant curves

Surf.	***cmc*** [a,c]	***cdc*** [a]	$c_{s,max}$ [a]	$c_{CNT,max}$ [b]	η / %	η^* / % kg·mmol^{-1}
SDBS	1.8 0.63 0.063	0.52 ± 0.04 0.18 0.018	2.2 ± 0.4 0.77 0.077	2.3 ± 0.1 0.23	77	35
SDS	8.2 2.4 0.24	2.5 ± 0.2 0.72 0.072	8.4 ± 0.4 2.4 0.24	1.9 ± 0.1 0.19	63	7.5
CTAB	0.97 0.35 0.035	1.4 ± 0.1 0.51 0.051	2.5 ± 0.6 0.91 0.091	2.0 ± 0.1 0.20	67	27
CPyCl	0.99 0.34 0.034	1.3 ± 0.7 0.051 0.044	3.8 ± 1.1 1.3 0.13	1.8 ± 0.2 0.18	60	16

[a]Values in units of mmol·kg^{-1}, mg·mL^{-1} and wt%, respectively (useful for comparative purposes with literature data). The uncertainties in mmol·kg^{-1} were obtained from the statistical treatment of data fittings.

[b]Values in mg·mL^{-1} and wt%, respectively.

[c]Values obtained from conductivity measurements (cf. Fig. S1 below).

Table S5. Parameters obtained from the SWNT/surfactant curves

Surf.	cmc[a,c]	cdc[a]	$c_{s,max}$[a]	$c_{CNT,max}$[b]	η / %	η^* / %kg·mmol^{-1}
SDBS	1.8 0.63 0.063	3.8 ± 2.2 1.3 0.13	20 ± 2 7.0 0.70	2.8 ± 0.1 0.28	93	4.7
SDS	8.2 2.4 0.24	5.5 ± 1.0 1.6 0.16	30 ± 1 8.7 0.87	1.2 ± 0.1 0.12	40	1.3
STS	2.1[d] 0.66 0.066	4.4 ± 0.2 1.39 0.139	10 ± 1 3.2 0.32	0.71 ± 0.04 0.071	24	2.4
DTAB	14.0 4.32 0.432	14 ± 1 4.32 0.432	25 ± 1 7.7 0.77	0.60 ± 0.01 0.060	20	0.80
TTAB	3.9 1.31 0.131	5.4 ± 0.2 1.82 0.182	19 ± 2 6.4 0.64	0.66 ± 0.05 0.066	22	1.2
CTAB	0.97 0.35 0.035	4.8 ± 1.8 1.75 0.175	13 ± 1 4.7 0.47	1.1 ± 0.1 0.11	37	2.8
CPyCl	0.99 0.34 0.034	4.0 ± 0.6 1.36 0.136	14 ± 1 4.8 0.48	1.4 ± 0.1 0.14	47	3.3

[a]Values in mmol·kg^{-1}, mg·mL^{-1} and wt%, respectively, (useful for comparative purposes with literature data). Uncertainties in mmol·kg^{-1} obtained by statistical treatment from data fittings.
[b]Values in mg·mL^{-1} and wt%, respectively.
[c]Values obtained from conductivity measurements (cf. Fig. S1 below).
[d]Data from: Holmberg, K.; Jõnsson, B.; Kronberg, B.; Lindman, B. *Surfactant and Polymers in Aqueous Solution*; John Wiley & Sons: Chichester, 2002.

Table S6. Critical concentrations with respect to *cmc* and corresponding fraction of micellized surfactant

Surf.	cdc/cmc		f_{mic}[a]		$c_{s,max}/cmc$		$f_{mic,\,max}$[a]	
	MWNT	SWNT	MWNT	SWNT	MWNT	SWNT	MWNT	SWNT
SDBS	0.30	2.1	0	0.53	1.2	11.1	0.18	0.91
SDS	0.50	0.7	0	0	1.0	3.7	0.02	0.73
STDS	---	2.1	---	0.52		4.8		0.79
DTAB	---	1.0	---	0		1.8		0.44
TTAB	---	1.4	---	0.28		4.9		0.79
CTAB	1.44	4.9	0.31	0.80	2.6	13.4	0.61	0.93
CPyCl	1.31	4.0	0.24	0.75	3.8	14.1	0.74	0.93

[a]Calculated as $f = (c_s - cmc) / c_s$, where c_s is the specified surfactant concentration.

Note 4. Conductimetric curves for the determination of the *cmc* of the surfactants.

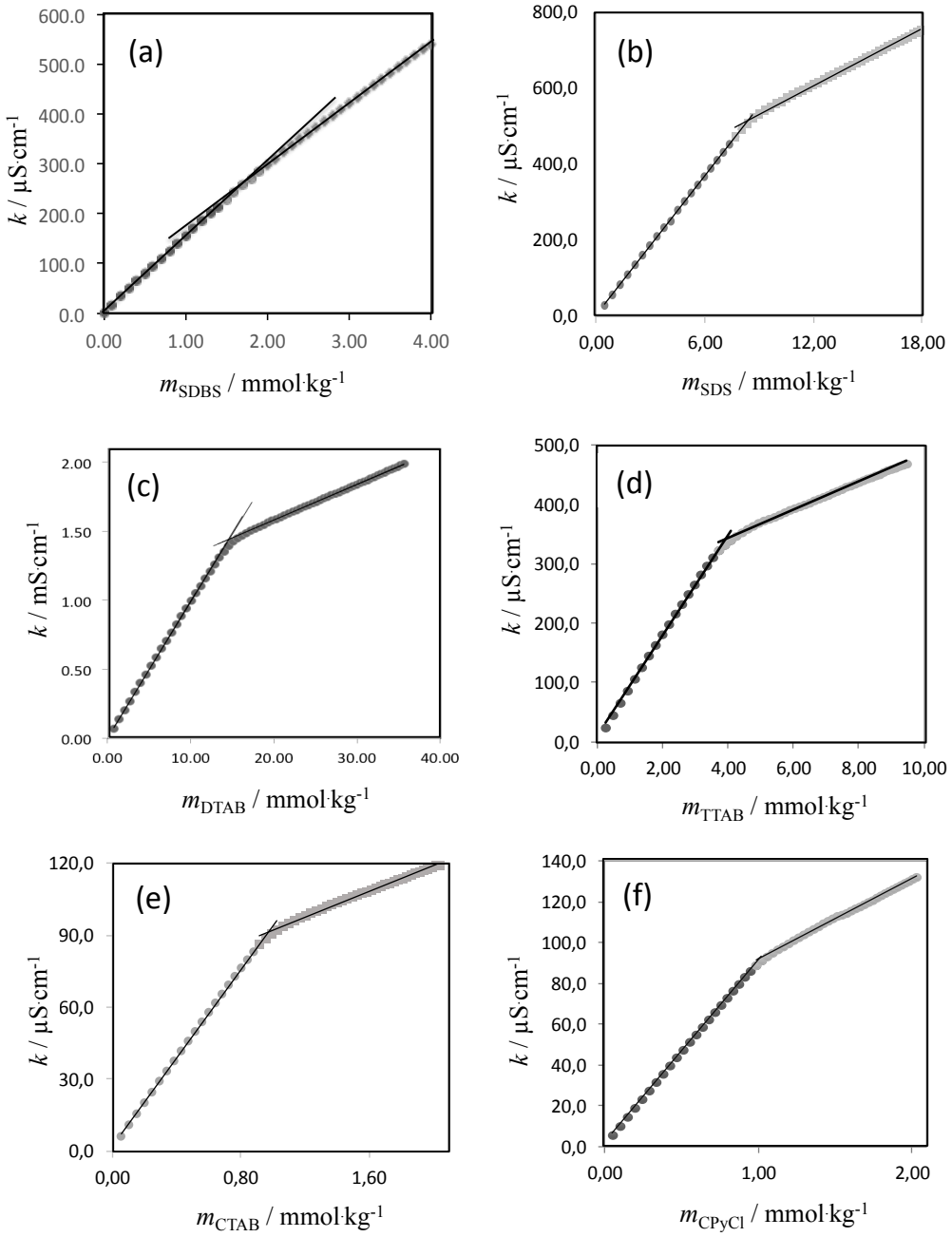

Figure S1 – Conductivity plots for *cmc* measurements: (a) SDBS; (b) SDS; (c) DTAB; (d) TTAB; (e) CTAB; (f) CPyCl. Cmc values are in Table S4 and S5. Uncertainties < 4 %.

Note 5. Comparisons of SWNT and MWNT dispersability on a surface area basis

i) The ratio $c_{s,max}/c_{CNT,max}$ indicates the surfactant amount per unit mass of CNT when the maximum dispersability is achieved. If we assume that in the aqueous dispersions SSA (SWNTs) ~ 4 x SSA (MWNTs), then the $c_{s,max}/c_{CNT,max}$ values for SWNTs should be divided by 4 for comparison on a surface area basis.

ii) For the conversion of the effectiveness on a mass basis:

$$\eta = \frac{c_{CNT,max}}{c_{CNT,in}}$$

to that on a surface area basis, the expression is:

$$\eta_{surface} = \frac{c_{CNT,max} \times \text{SSA(dispersion)}}{c_{CNT,in} \times \text{SSA(powder)}} = \eta \times \frac{\text{SSA(dispersion)}}{\text{SSA(powder)}}$$

Since for the dipersions we assume SSA (SWNTs) ~ 4 x SSA (MWNTs) and for the powders it is known that SSA (SWNTs) ~ 2 x SSA (MWNTs), it follows that:

$$\frac{\eta_{surface}(\text{SWNTS})}{\eta_{surface}(\text{MWNTS})} \approx 2$$

Hence the values of η and $\eta*$ for SWNTs were doubled for comparison with those of MWNTs on a surface area basis.

Table S7. Comparison of dispersability parameters of MWNTs and SWNTs (values in bold) using a 4-factor difference in the SSA of dispersed SWNTs

Surf.	$c_{s,max}/c_{CNT,max}$ /(μmol·mg^{-1})			η / %			η^* / %·kg·mmol^{-1}		
	MWNT	SWNT	**SWNT[a)]**	**MWNT**	SWNT	**SWNT[b)]**	**MWNT**	SWNT	SWNT[b)]
SDBS	**0.96**	7.1	**1.8**	**77**	93	**100**	**35**	4.7	**9.4**
SDS	**4.4**	25	**6.3**	**63**	40	**80**	**7.5**	1.3	**2.6**
CTAB	**1.3**	12	**3.0**	**67**	37	**74**	**27**	2.8	**5.6**
CPyCl	**2.1**	10	**2.5**	**60**	47	**94**	**16**	3.3	**6.6**

[a)] Original value / 4.
[b)] Original value x 2.

Calculation in Table S8 assume that in the dispersions:

- SSA = 1.3 x 10^2 $m^2 \cdot g^{-1}$ for SWNTs (i.e. full debundling);

- SSA = 300 $m^2 \cdot g^{-1}$ for MWNTs.

Table S8. Surfactant amount per CNT area at saturation ($c_{s,max}$, $c_{CNT,max}$)

Surf.	$c_{s,max}$ /(μmol·mL^{-1})		$c_{CNT,max}$ /(mg·mL^{-1})		surfactant amount per CNT area / (μmol·m^{-2})		surfactant molecules per CNT area / (molecule·nm^{-2})	
	MWNT	SWNT	MWNT	SWNT	MWNT	SWNT	MWNT	SWNT
SDBS	2.2	20	2.3	2.8	3.2	5.5	2	3
SDS	8.4	30	1.9	1.2	15	19	9	12
CTAB	2.5	13	2.0	1.1	4.2	9.1	3	5
TTAB	-	19	-	0.66	-	22	-	13
DTAB	-	25	-	0.60	-	32	-	19
CPyCl	3.8	14	1.8	1.4	7.0	7.7	4	5

Note 6. Zeta potential measurements

Table S9. ζ for neat surfactant micelles, and for surfactant-assisted CNT dispersions with c_{CNT} = 0.1 mg·mL^{-1} CNT and c_s = 15 mmol·kg^{-1} for SDS and CTAB[a]

surfactant	ζ / mV		
	neat micelles	MWNT-surfactant dispersion	SWNT-surfactant dispersion
F127	--	– 11.0[b]	– 6.1[b]
SDBS	– 69.5	– 64.5	– 62.0
SDS	– 72.7	– 56.6	– 54.7
CTAB	+ 51.5	+ 57.8	+ 56.4

[a]Observed distributions are unimodal and meet quality criteria. Typical uncertainties in ζ-potential are ± 5 % (5 runs on average).

[b]c_{F127} = 3 mg·mL^{-1}.

For these measurements, because the curves in Fig. 6 show that the dispersed c_{CNT} varies differently with c_s for different surfactants, a careful procedure was followed. All dispersions were prepared in the usual manner using c_s = 15 mmol·kg^{-1}, which yielded different c_{CNT} values between surfactants, but all well above 0.1 mg·mL^{-1} (Fig. 6). Then, the dispersions were diluted with its respective neat surfactant aqueous solution (c_s = 15 mmol·kg^{-1}) to the final desired c_{SWNT} (0.1 mg·mL^{-1}), which was chosen for its suitability for the ζ measurement.

IV

Assessing surfactant binding to carbon nanotubes via competitive adsorption: binding strength and critical coverage

Ricardo M.F. Fernandes, Jing Dai, Oren Regev, Eduardo F. Marques and István Furó

Manuscript

Assessing Surfactant Binding to Carbon Nanotubes via Competitive Adsorption: Binding strength and critical coverage

Ricardo M.F. Fernandes,[1,3] Jing Dai,[1] Oren Regev,[2] Eduardo F. Marques,[3] and István Furó[1 *]

[1]*Division of Applied Physical Chemistry, Department of Chemistry, KTH Royal Institute of Technology, SE-10044 Stockholm, Sweden.*

[2]*Department of Chemical Engineering and the Ilse Katz Institute for Nanotechnology, Ben-Gurion University of the Negev, 84105 Beer-Sheva, Israel.*

[3]*Centro de Investigação em Química, Department of Chemistry and Biochemistry, Faculty of Science, University of Porto, Rua do Campo Alegre, P-4169-007 Porto, Portugal.*

*email: furo@kth.se

Abstract

The displacement of a nonionic polymeric dispersant, Pluronic F127, adsorbed at the surface of single-walled carbon nanotubes, by low molecular-weight ionic dispersants (surfactants) is studied in aqueous dispersion. The method applied is diffusion NMR spectroscopy that can accurately measure the fraction of F127 molecules adsorbed at the tube surface because of the slow exchange (over the experimental time scale) of F127 between bulk and surface. In a series of surfactants with varying chain length and headgroups, we find that anionic surfactants replace in general more nonionic F127 than do cationic surfactants. The data collected show a strong correlation with the *critical dispersibility concentration* of the different surfactants, a parameter that signifies the concentration at which one obtains significant dispersed nanotube concentration by ultrasonication. We posit that this finding indicates the existence of a threshold surface coverage for dispersants that constitutes a necessary condition for de-bundling by ultrasonication. The results are discussed in relation to previous findings in the literature.

1. Introduction

Dispersing carbon nanotubes (NT), in particular single-walled ones (SWNT), in aqueous environment has been motivating hundreds of studies during the recent years.[1-4] Yet, despite this large volume of information available, crucial questions remain seemingly unresolved. This apparent contradiction has several reasons. First and particularly at early times, pristine SWNT materials were often impure and irreproducible. Even though this may still be an issue, nowadays one can commercially access rather reproducible and pure (that is, free of catalysts and amorphous carbon) SWNT batches. It is harder though to obtain chiral and enantiomeric purity. Secondly, a majority of the studies, and particularly so the comparative ones, about dispersing nanotubes seem to have been performed with multiwalled carbon nanotubes (MWNTs) and not on SWNTs. Thirdly, it still remains a question what constitutes a dispersion (that is, individual nanotubes or thin bundles of them or both) and, if that can be assessed, how should one then classify different dispersions.[5] Fourthly, conditions for preparing nanotube dispersions remain diverse. In particular, the effects of ultrasonication are extremely dependent on issues that may seem unimportant, yet are not,[6] such as the geometric constraints. This might be part of the explanation for the huge discrepancy among experimental data such as when metrics assessing the molecular composition of dispersions – such as the number of dispersant molecules per tube unit area at saturation – scatter by two orders of magnitude when it comes to the popular system of SWNT dispersed in aqueous solution of sodium dodecyl sulfate (SDS).[7] Finally and most importantly, dispersing nanotubes is a complex process. In particular, the popular unzipping model[8] for dispersing nanotubes by ultrasonication stipulates that exfoliation proceeds by having clefts forced open by stresses created by ultrasonic cavitation. Subsequently, the newly exposed pristine NT surfaces within those clefts adsorb surfactants or polymers, which prevents the clefts to re-close. Clearly, this must depend not only on the binding strength of dispersants on NTs but also on kinetic factors such as the rate by which dispersants adsorb. This complicates the interpretation of comparative studies in molecular terms.

Here, we wish to progress towards a clearer picture by investigating one factor, the binding strength and binding mode of dispersants to NTs, free of influences from kinetics. The method for doing so is based on studying the replacement of one sort of dispersant – the amphiphilic and nonionic block copolymer Pluronic F127 – by another one from a range of

several ionic low molecular-weight dispersants – surfactants. The data we present are quantitative and rather accurate. The reason for that is that, in contrast to most other related experiments that try to detect how concentrations of dispersant vary in the bulk solvent of dispersions, we measure directly, with the help of diffusion NMR, the amount of F127 adsorbed on the CNT surface. Since the adsorbed fraction of dispersants is much smaller than the bulk fraction,[9-12] our method is inherently more sensitive. Previously we have analyzed on the same manner the surface coverage of NTs by F127 and the binding strength of F127 relative to that of the protein bovine serum albumin (BSA).[9]

A classical way toward understanding of the nature of interactions between adsorbed dispersant molecules and CNTs and both the equilibrium and kinetic factors involved in the adsorption process[13-16] is to rely on adsorption isotherms. However, even though there are numerous works where the concentration of the dispersed CNT was quantified, the surfactant concentration, let alone the partitioning between adsorbed and free surfactant has been often left unquantified or has been quantified with insufficient accuracy. Hence, is it clear that those types of results (in form of CNT dispersion curves) are in themselves helpful but certainly not comprehensive. Special, and experimentally rather demanding methodologies have been adopted to construct binding isotherms proper.[17, 18] Such examples are, however, rare.

One should note that dispersant-to-nanotube binding strength is also an important factor in sorting carbon nanotubes by chiral and diameter through selective binding of dispersants.[16, 19-21] Although we do not directly investigate this issue here, the method developed can be easily extended in that direction. Moreover, competitive replacement of dispersants is also a strategy explored for either drug release[22] or improved dispersibility.

2. Experimental Section

2.1 Materials and sample preparation

CoMoCat single-walled carbon nanotubes of nominal (6,5) chirality and median diameter of 0.78 nm (SG65i, SouthWest NanoTechnologies Inc.) were investigated as provided by the manufacturer. The pristine material is dominantly semiconducting (95 %) with its largest (41 %)

single fraction consisting of (6,5) nanotubes (with major residual fractions of (8,4), (7,5) and (9,2) nanotubes and, in addition, 28% of nanotubes with unknown chirality) and is assumedly also a mixture of different enantiomers. Pluronic F127 (~ 12.5 kD, $HO(C_2H_4O)_x(C_3H_6O)_y(C_2H_4O)_xH$, a (PEO)−(PPO)−(PEO) block copolymer, with x = 97 and y = 69), DTAB, TTAB, CTAB, dodecyl, tetradecyl and hexadecyl trimethylammonium bromide, respectively; CPyCl, hexadecylpyridinium chloride; SDBS, sodium dodecyl benzenesulfonate; SDS, sodium dodecyl sulfate; SC sodium cholate and heavy water (99.9 atom % D) were purchased from Sigma-Aldrich. All materials were used as received.

The samples were prepared by a procedure carefully tested and used previously.[6, 9] The SWNT powder was weighted (3.0 mg) to a vial with a spherical bottom to which 3 mL of F127 solution, with initial concentration of 3.0 mg/mL, was subsequently added. The sample was sonicated using a Qsonica Q-500 tip sonicator equipped with a 3 mm microtip that was inserted 1 cm below the liquid surface and at the center of a vial with a spherical bottom (1.4 cm inner diameter and 3.8 cm length). Such an arrangement was indicated to minimize the sonication dead zones.[23] The sonication time was set to 10 min during which 750 $J \cdot mL^{-1}$ (1.25 $W \cdot mL^{-1}$) was transferred to the liquid medium. The sample temperature during sonication was kept at 18 ºC using a circulated water bath. After sonication, the sample was centrifuged at 4×10^3 *g* during 30 min. The supernatant (*ca* half the total volume) was collected by a pipette for performing the various experiments detailed below. The SWNT concentration in the supernatant (see Supporting Information) was determined using a combined TGA/UV-Vis methodology published elsewhere.[24] In short, UV-Vis experiments are used to characterize the relative amount of SWNT in the prepared dispersions via the optical density (or, apparent absorbance) and TGA experiments provide the calibration by which optical density is translated into mass concentration. Therefore, we know accurately the dispersant and the SWNT concentration in the studied dispersion. As has been discussed previously, the SWNTs present in the obtained dispersions are in the form of individual tubes or small bundles.[6, 25]

To given volumes of dispersion prepared on the manner described above, set small (a few microliters) volumes of concentrated solutions of individual surfactants were added. Those new dispersion samples were homogenized by careful mixing. All prepared dispersions were stable (lacking any significant sign of aggregation or precipitation) for at least a day; after that time

there were occasional observations of aggregation. Hence, to keep a safe margin the NMR experiments described below were performed within <12 hours after having had prepared the initial F127 dispersion (see details in Supporting Information). Within that time frame, we could not perform all experiments using a single batch of freshly prepared F127 dispersion. Hence, we performed the experiments with one particular surfactant type starting with an F127 dispersion freshly prepared under identical conditions.[6] Hence, we experienced a small scatter in the initial conditions because both F127 (*ca* ± 5 %) and SWNT (*ca* ± 6 %) concentrations scattered slightly for those starting dispersions (see also Supporting Information).

2.2 *NMR diffusion experiments*

The ^{1}H NMR experiments were carried out in Bruker Avance III spectrometer equipped with a standard-bore magnet providing a 500 MHz resonance for ^{1}H Bruker and a z-gradient probe DIFF30. The gradient pulses were provided by a Bruker GREAT 60 gradient. The diffusion experiments were performed using the stimulated echo sequence.[26] The 90º pulse length was ~ 7 μs, the gradient pulse length was set to δ = 2 ms, the gradient stabilization delay to 1 ms, and the diffusion time to Δ = 20 ms. All the measurements were carried out at 20.0 ºC and the gradient strength was calibrated by measuring the diffusion of ^{1}HDO in D_2O (1.63×10^{-9} $m^2 \cdot s^{-1}$ at 20 ºC, reference value from literature[27]). The longitudinal relaxation time, T_1, obtained for Pluronic peaks is ~ 500 ms, and the recycle delay was set to 3 s (~5T_1). In order to use low sample volumes (~100 μL) and provide a homogeneous gradient, the samples were placed in 5 mm Shigemi tubes. Additional parameters used were as provided previously.[9-12]

3. Results and Discussion

3.1 The state of dispersants adsorbed on SWNTs as seen by diffusion NMR

The experiments performed provide information about surfactant binding indirectly, by detecting the fraction of F127 molecules that is NT-adsorbed. This is made possible by having the residence time of the F127 molecules on the NT surface (τ_{res}, the average time between the adsorption and desorption events of a particular molecule) longer than the experimental time scale in the NMR diffusion experiment. In such experiments, we detect a signal decay

characterized by a decay constant that is proportional to the self-diffusion coefficient D of the species. If the species is exchanging between two different environments, the obtained experimental decays depend on the diffusion time Δ (see above) that can be set within limits, typically 10-20 ms at the short end and the longitudinal relaxation time T_1 (here *ca* 500 ms, see above) at the long end. The $\tau_{res}>>\Delta$ regime is termed slow exchange and there the diffusional decays are sums of the decays for the species in the two separate environments obtained. For F127 molecules that are, with Δ = 20 m, in the slow exchange regime,[6, 9] the molecules free in solution exhibit a large diffusion coefficient and a diffusional decay that is rapid while the molecules attached to large nanotubes exhibit a small diffusion coefficient and a diffusional decay that is slow. Hence, the diffusional decay of the F127 signal in a SWNT dispersion is two-component with its components easily separable; their relative intensity provides the fraction, a few %, of the F127 molecules adsorbed at the NT surface.

The $\tau_{res}<<\Delta$ regime is termed fast exchange and there the diffusional decay is single-component with a decay constant that is characterized by the population-weighted average of the involved diffusion coefficients. In contrast to F127, the protein BSA exhibits this case, that is, a short residence time on the NT surface.[11] We obtained the same behavior (a single-component diffusional decay, data not shown) for the NMR signals of all surfactants investigated here, which indicates that they are also in the fast-exchange regime. To extract the fraction of surface-bound molecules from such single-component decays is laden by a much larger experimental error[11] than that for the two-component decays obtained for F127.

While the residence time of F127 on the SWNT surface is in the order of 100 ms and thereby is long as compared to the diffusion time (Δ) set here, it is sufficiently short so that equilibrium between the NT-surface-bound and free-in-solution species can be established quickly, within seconds. Hence, changing the concentration of F127 molecules in solution leads to changes in the amount of NT-adsorbed molecules unless the NT surface is saturated. Indeed, we have detected a behavior close to that at F127 concentrations equal to the one here.[9] Ideally, this method may provide a way to record the adsorption isotherm.

If we add other molecules, M, to the NT dispersion prepared by F127 and those molecules have the capacity to adsorb to the nanotube surface, a fraction of the F127 molecules is gradually replaced by the molecules M. The degree of replacement depends on (i) how strong

binding to NT the M molecules exhibit (that is, how high is their Gibbs energy of binding ΔG_M compared to that of the F127 molecules), and (ii) on their concentration in solution, c_M. We expect that the amount of F127 displaced from the NT surface increases both by ΔG_M and c_M. In addition, one should note that ΔG_M may not be constant upon changing concentration of dispersants on the NT surface because of, for example, the formation of surface aggregates.

3.2 *The results of F127 displacement experiments*

In Fig. 1, we present the NMR diffusional decays obtained for the F127 molecules in the prepared dispersions. As discussed above, the slowly decaying component is identified as belonging to NT-adsorbed F127. Upon addition of SDS, that component decreases (Fig. 1a) to an extent that is increasing with added SDS concentration, which is interpreted as SDS replacing F127 molecules on the NT surface. On a distinctly different manner, the addition of DTAB has almost no effect on the slow component, which is a qualitative sign of DTAB binding to the NT surface less strongly than SDS. A DTAB with weak binding is not capable to displace F127.

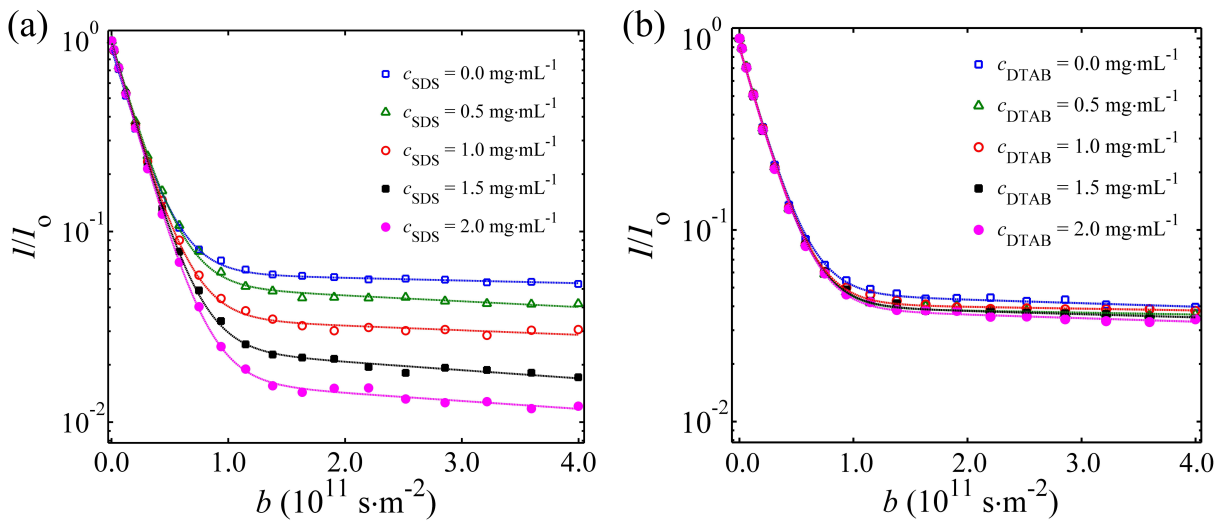

Figure 1. *The diffusional decay of the normalized ^{1}H NMR signal from the F127 oxyethylene peak as a function of concentration of SDS (a) and DTAB (a) added to an F127-SWNT dispersion. The lines are fits of two-component decays described with the customary Stejskal-Tanner equation with $b = \gamma^2\delta^2g^2D(\Delta-\delta/3)$. The fraction of the surface-adsorbed F127 is calculated from that relative intensity of the slowly decaying component, see details in Supporting Information.*

A more quantitative analysis can be made on the basis of the obtained relative populations of F127 in the NT-adsorbed state, f_{F127} (see details of the performed fits in Supporting Information). Since we know both the total F127 concentration, c_{F127}, and the total SWNT concentration, c_{SWNT}, in the explored samples, a measure of the apparent surface coverage (i.e. coverage on a mass basis) by F127, σ_{F127}, can be simply obtained as

$$\sigma_{F127} = (f_{F127} \times c_{F127})/c_{SWNT}. \quad (1)$$

Figure 2 shows that this surface coverage decreases strongly with having added SDS (Fig 2a) while upon addition of DTAB the coverage seems to decrease very little (the value suggested by the fit in Fig. 2b is *ca* 6 % roughly at the same mass concentration as c_{F127}).

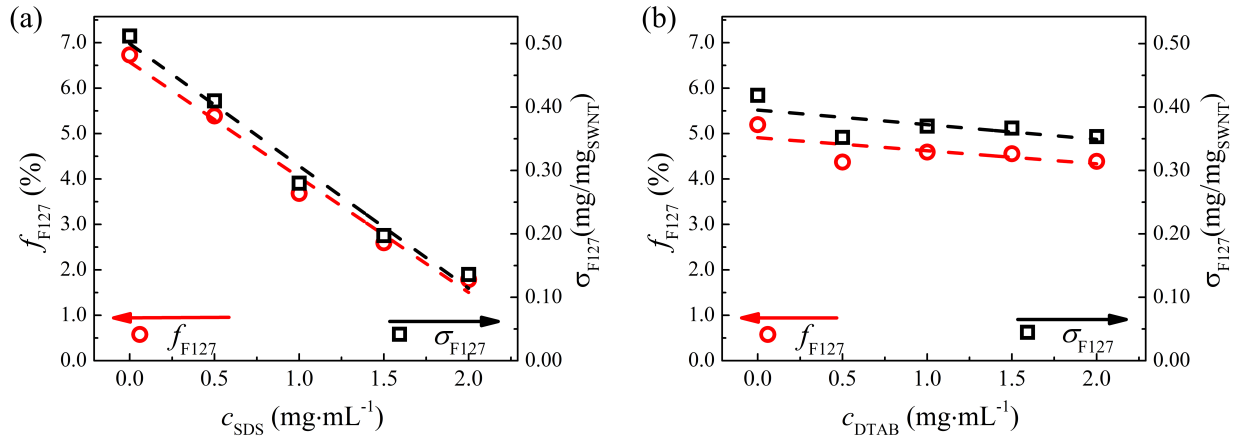

Figure 2. *Fraction f_{F127} of F127 molecules adsorbed on the SWNT surface and the corresponding apparent surface coverage σ_{F127} by F127 molecules as a function of the concentration of SDS (a) and DTAB (b) added to system originally dispersed by F127. The dashed lines are linear fits.*

Below, we consider the situation where two distinct adsorbates, denoted by A and B, are present in a system and compete for the same adsorption sites. The following assumptions can be

made: (i) all unit areas on the NT surface available for adsorption are equivalent, (ii) each surface area unit can be covered either by A or B but not by both, and (iii) there are no lateral interactions between any two different adsorbates (A-A, B-B or A-B) and thereby there is no aggregation (lateral or multilayer) of any sort. Assuming this Langmuir-type behavior, one can derive[28] that the ratio of surface coverage is given as

$$\frac{\sigma_A}{\sigma_B} = \frac{K_A c_A}{K_B c_B} \qquad (2)$$

where K_x and c_x are the binding constant and concentration of the respective adsorbates.

Clearly, the NT surface area covered by a F127 molecule on one hand and a surfactant molecule (like SDS or CTAB) on the other hand are different. Previous results also indicated that, in the starting dispersions, the surface coverage of the dispersed SWNT species (individual nanotubes and thin bundles thereof) by F127 was close to saturation for similar c_{SWNT} and c_{F127} concentrations.[9] In F127, it is plausibly the PPO segment of the polymer that is attached to the nanotube surface; this notion has support from neutron scattering[29] and molecular dynamics simulation[30] studies. Similarly, the primary NT-interfacing groups in surfactants like the ones here (viz. SDS and CTAB) are the hydrophobic methyl and methylene moieties.[31] In what follows, we assume that the adsorbing unit is the individual methylene/methyl group, either 12 ones in the alkyl chain of SDS or the 69 ones in the PPO block of F127 (specifically, we also assume that the polar ether oxygens in the flexible PPO block avoid the NT surface; without this assumption the argument below still holds, but with slight re-scaling). The results we obtain below concern then the binding of that unit, identified as A in SDS molecules and B in the PPO units, to the NT surface. Eq.(2) yields that the difference between the Gibbs energies of binding can be obtained as

$$\Delta(\Delta G) = RT \ln \frac{c_B \sigma_A}{c_A \sigma_B}, \qquad (3)$$

except for a negligibly small term due to differences in the relevant partition functions. Under the assumption that all NT surface freed from F127 methylene/methyl groups is covered by SDS methylene/methyl groups (that is, a fraction of its alkyl chain), Fig. 2a indicates (see black

dashed line) that the system exhibits $\sigma_{\mathrm{mSDS}} \approx \sigma_{\mathrm{mPPO}}$ at c_{SDS} = 1.2 mg/mL, where indices mSDS and mPPO refer to coverage by methylene/methyl groups in the respective molecule/block. At this point

$$\Delta(\Delta G)_{\mathrm{mSDS\text{-}mPPO}} = RT \ln \frac{c_{\mathrm{mSDS}}}{c_{\mathrm{mPPO}}} \qquad (4)$$

and c_{mSDS} = 0.7 mg/mL and c_{mPPO} = 0.75 mg/mL (from the initial concentration c_{F127} = 2.3 mg/mL and by considering both CH_2 and CH_3 groups in the PPO unit). This yields an estimate of c, that is, a small difference in Gibbs energy by which the binding of a SDS methylene/methyl moiety is favored. Note that this Gibbs energy difference, though calculated on the basis of the methylene-methyl groups providing surface coverage, represents the difference between the molecules as a whole, hence including contributions from the PEO blocks (in F127) or the headgroups (in all ionic surfactants).

At this point, one should recall that the residence times of F127 (~100 ms) and SDS (<<20 ms, as established above) clearly differ despite the fairly similar Gibbs energies of binding per binding group. This is a simple consequence of having a block of PPO units in individual F127 molecules that is much larger than the alkyl chains in individual SDS molecules, a situation reminiscent of that experienced (i) in a homologous series of surfactants where residence time increases with increasing alkyl chain length[32] or (ii) in hydrophobically modified polymers[33] where individual sidechains exhibit fast exchange between different environments even though whole polymer chains containing a large number of sidechains exhibit slow exchange. In other words, the Gibbs energy of binding *per molecule* is much larger for F127.

3.3 Comparison of the binding of different surfactants

The relative binding strength of different surfactants to SWNTs is illustrated well by comparing directly the amount of F127 coverage they displace upon addition to the initial dispersions. The results presented above were obtained for a series of ionic surfactants (SDBS, SDS, CPyCl, CTAB, TTAB, DTAB) for which we have recent data[6] regarding their dispersion behavior. In addition, we also investigated the behavior of sodium cholate, a surfactant often described as a particularly good dispersant for carbon nanotubes.[34]

The dispersion behavior of larger series of surfactants has seldom (e.g., relative to pairwise comparisons) been studied and the results are rather scattered. Here, we try to relate to one particular metric, the critical dispersibility concentration, *cdc*.[6] The *cdc* of a particular surfactant is assigned to the concentration where the slope of the sigmoidal-like curve that relates the amount of dispersed NT to the amount of dissolved surfactant steeply takes off. There are also different metrics available such as the dispersion efficiency, which relates the maximum amount of dispersed SWNT to the surfactant concentration needed to achieve this maximum; this particular metric shows a rather strong scatter,[7] presumably also because different preparation procedures achieve different dispersions as concerning composition by individual tubes and small bundles. The *cdc* should be less sensitive to such effects (although, it may certainly be sensitive to other differences between procedures such as sonication power). The study[6] we relate to revealed some regularities among different ionic surfactants, such as a dependence of *cdc* on the alkyl chain length that was much weaker than the dependence of the critical micelle concentration, *cmc*, on the same parameter.

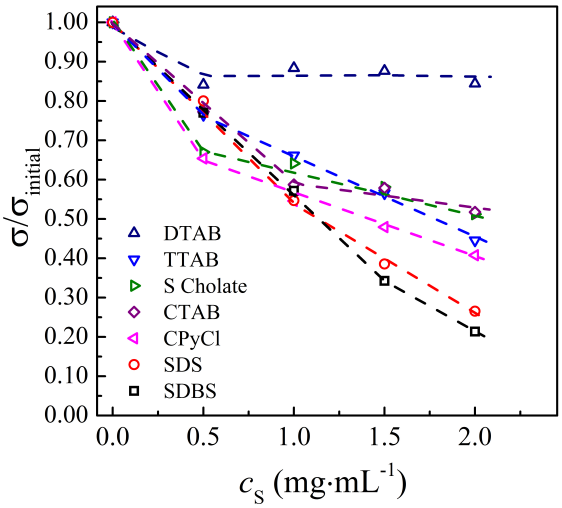

Figure 3. *The change in surface coverage by F127 molecules as a result of addition of different surfactant sorts to the initial F127-SWNT dispersion. The dashed lines are guides for the eye.*

At first glance, Fig. 3 demonstrates few clear trends. Having the concentration displayed in molar instead of mass terms accentuates the difference among surfactants (see Supporting Information). Generally speaking, anionic surfactants like SDS and SDBS exhibit the strongest effect in replacing F127 and thereby, by conjecture, the strongest binding to SWNTs. The difference between them and DTAB that has an alkyl chain of the same length is strikingly big. The alkyl chain length in itself seems to have a more moderate effect as revealed by the rough equivalence of TTAB and CTAB. Finally, sodium cholate in particular shows a very strong displacement effect at low concentrations which then levels off at higher concentrations – a difference that must reflect its very different hydrophobic tail structure with aromatic groups that presumably exhibit strong π–π interactions with the SWNT surface.

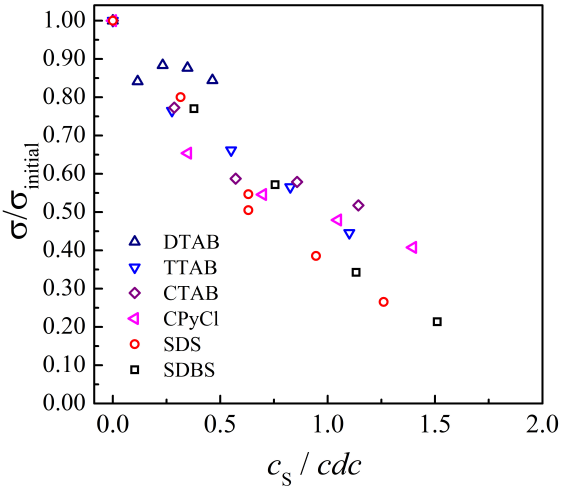

Figure 4. *The change in surface coverage by F127 molecules (data as in Fig. 3, except that for sodium cholate) with surfactants concentration given as multiples of the critical dispersibility concentration, cdc. The cdc data are taken from a previous investigation[6] with a strictly controlled experimental procedure.*

While we have no comprehensive explanation for all features observed, we present in Fig. 4 the data with the concentration of the added dispersant, c_s, normalized by *cdc* of the particular dispersant as obtained previously;[6] in this representation, the data from the different surfactants seem to fall on a universal master curve where at *cdc* all surfactants displace *ca.* half of the F127 originally at the NT surface. This finding indicates that at *cdc,* the different

surfactants provide the same surface coverage. This yields a new physical insight as concerning the origin of *cdc* – namely, dispersing by cleavage/exfoliation requires a particular threshold coverage that is characteristic for the nanotube. In other words, we state that dispersing SWNTs becomes significant at the point where the surface coverage by a particular surfactant reaches this universal threshold.

It is interesting to put our findings in relation to the findings of Zhong and Claverie[17] and Sa and Kornev,[18] the two careful studies where the adsorption isotherm on SWNT of one surfactant common to the ones we used, SDS, was investigated. Regarding both works, two significant differences are that (i) here we do not measure the amount of SDS adsorbed but the amount of F127 that SDS replaces while (ii) the other works[17, 18] are depletion-type experiments that do not try to measure the amount of SDS adsorbed on the surface but the amount that is left in solution. At our current conditions, the amount of surface-bound surfactants is low (currently, we do not have sufficiently accurate data but the surfactant diffusion coefficients with or without nanotubes are within a few % to each other, which would indicate that the amount of surface-adsorbed ionic surfactant is also in the order of a few %). Hence, depletion-type experiments that try to establish the amount of adsorbed surfactant from a slight decrease in bulk concentration are expected to provide large errors and quantitative data from them may be prone to artifacts.

An additional significant difference is that in both the works of Zhong and Claverie[17] and Sa and Kornev[18], the SWNT was added at a set concentration and there was no attempt to separate out SWNT material that was not exfoliated and thereby dispersed (that is, remained in form of large bundles) at the end of the sonication procedure. In our case, we removed those by centrifugation. It is very clear that those different sample portions (sedimented after centrifugation and not sedimented and, in our case, forming the investigated dispersion) may have rather different adsorption characteristics. For F127 here, NMR intensities and TGA analysis provide that *ca* 20-25 % of the all the initially added F127 (3 mg/mL) went to the sediment, plausibly in the form of molecules adsorbed upon large aggregates/bundles (see also Supporting Information). Those large aggregates made up of *ca* 70 % the initial SWNT mass (1 mg/mL). Hence, the surface coverage in the sediment is, using the same metrics as that in Fig. 2, in the order of $\sigma_{\mathrm{F127}}^{\mathrm{sediment}} \approx 1$ mg/mg$_{\mathrm{SWNT}}$, that is in the same order than that for the small bundles/individual tubes in our dispersion. Hence, on one hand, it is not surprising that Zhong

and Claverie[17] find that, at conditions comparable to ours, the amount of surface-adsorbed SDS is rather high, in the order of 10-20 % of the initial SDS. In both sets of experiments,[17, 18] one finds that the dispersion behavior is correlated by the degree of surface coverage; yet, since the dispersions studied are clearly fundamentally different it is difficult to relate our findings above (see Fig. 4) to those of Zhong and Claverie[17] and Sa and Kornev.[18] On the other hand, it also remains a most interesting question *why* we obtain similar coverages by F127 in the sediment and in the dispersion while one would expect the nanotubes to be in rather different states in those media.

Considering specifically displacement of one dispersant by another on SWNTs, there exist some previous studies. The effective replacement of FMN (flavin mononucleotide)-bound SWNTs by surfactant was found to occur in the order SDBS, sodium cholate (SC) and SDS. The resulting average Gibbs energy changes $\Delta(\Delta G)$ from FMN to SDBS-, SC-, and SDS-wrapped SWNTs were −2.4, −0.4, and +2.1 kJ/mol at 25°C, respectively.[15] $\Delta G > 0$ for SDS was associated with re-bundling after exchange of surfactant. It should be noted also that replacement occurred only once a given surfactant concentration was attained, which is qualitatively different from what we observe here.

For other dispersants that exhibit tighter "wrapping" on the nanotube, the displacement phenomena may become more complex. Hence, Roxbury et al. showed that CNTs assumed to be wrapped with ssDNA shows distinctive two-step replacement by SDBS (mediated by two different surfactant organizations), namely a rapid first stage lasting less than a few seconds, followed by progressive removal lasting tens of minutes.[14] In a related work, Kato et al. reported on the thermodynamic analysis of an exchange process between SC and single-stranded oligo DNAs (ssDNAs) with various lengths on SWNTs using absorption spectroscopy.[34]

4. Conclusions

In this study, we investigate the displacement of the block copolymer F127 on the surface of dispersed nanotubes by a group of ionic surfactants. The F127 molecules were used to prepare the initial aqueous dispersions from pristine nanotubes and we observe by diffusion NMR

experiments that the surface coverage provided by F127 molecules is decreasing upon increasing surfactant concentration. From previous investigations we know that the residence time of both the polymers and the surfactants is rather short (< 1 s) on the nanotube surface, and therefore foreign dispersant molecules can easily participate in the dynamic equilibrium and establish a new distribution on the nanotube surface once their concentration in the bulk has been changed. Hence, the decrease of F127 coverage is interpreted as a consequence of building up corresponding surface coverage by the added surfactants. Under the assumption of identical coverage by methylene/methyl moieties and within the framework of simple models of adsorption, we derive that the difference of Gibbs energy of binding per methylene/methyl moiety between selected ionic surfactants and F127 is rather small, in the order of $\Delta(\Delta G)_{mSDS-mPPO} \approx$ - 0.2 kJ/mol, as concerning SDS and the hydrophobic block of F127.

Different surfactants display somewhat different trends upon increasing surfactant concentration – this might be a consequence of specific interactions. Yet, a universal master curve seems to appear if the surfactant concentration is normalized with respect to the critical dispersibility concentration, *cdc*. This quantity signifies the surfactant concentration where the nanotubes start to disperse in water. Based on this finding, we propose that *cdc* is the point where surfactant coverage crosses a particular threshold value. Some inferences here are based on the assumption that the amount of surfactant bound on the NT surface can be estimated as that providing the same coverage as the displaced F127 molecules. This may not be the case. Hence, future studies – such as very accurate NMR diffusion measurements of the self-diffusion of coefficient of surfactants from which the amount of NT-bound surfactant could be accurately estimated – would be very useful to complement our findings here.

Supporting Information

- Details of sample compositions, details of data evaluation, results of the fits of the F127 diffusional decays, and presentation of the data in Fig. 3 on alternative concentration scales.

Acknowledgments

Support from Fundação para a Ciência e Tecnologia (FCT, Portugal) through projects PEst-C/QUI/ UI0081/2013 (CIQ-UP) and the Ph.D. grant SFRH/BD/72612/2010, from FEDER and FCT/MES through FCUP-NORTE-07-0124-FEDER-000065, and from the Swedish Research Council VR is gratefully acknowledged.

References

1. Angelikopoulos, P.; Bock, H. The Science of Dispersing Carbon Nanotubes with Surfactants. *Phys. Chem. Chem. Phys.* **2012,** *14*, 9546-9557.
2. Wang, H. Dispersing Carbon Nanotubes using Surfactants. *Curr. Opin. Colloid Interface Sci.* **2009,** *14*, 364-371.
3. Britz, D. A.; Khlobystov, A. N. Noncovalent Interactions of Molecules with Single Walled Carbon Nanotubes. *Chem. Soc. Rev.* **2006,** *35*, 637-659.
4. Kharissova, O. V.; Kharisov, B. I.; de Casas Ortiz, E. G. Dispersion of Carbon Nanotubes in Water and Non-Aqueous Solvents. *RSC Adv.* **2013,** *3*, 24812-24852.
5. Green, M. J. Analysis and measurement of carbon nanotube dispersions: nanodispersion versus macrodispersion. *Polym Int* **2010,** *59*, 1319-1322.
6. Fernandes, R. M. F.; Abreu, B.; Claro, B.; Buzaglo, M.; Regev, O.; Furó, I.; Marques, E. F. Dispersing Carbon Nanotubes with Ionic Surfactants under Controlled Conditions: Comparisons and Insight. *Langmuir* **2015,** *31*, 10955−10965.
7. Duan, W. H.; Wang, Q.; Collins, F. Dispersion of Carbon Nanotubes with SDS Surfactants: A Study from a Binding Energy Perspective. *Chem. Sci.* **2011,** *2*, 1407-1413.
8. Strano, M. S.; Moore, V. C.; Miller, M. K.; Allen, M. J.; Haroz, E. H.; Kittrell, C.; Hauge, R. H.; Smalley, R. E. The Role of Surfactant Adsorption during Ultrasonication in the Dispersion of Single-Walled Carbon Nanotubes. *J Nanosci Nanotechno* **2003,** *3*, 81-86.
9. Fernandes, R. M. F.; Buzaglo, M.; Regev, O.; Marques, E. F.; Furó, I. Surface coverage and competitive adsorption on carbon nanotubes. *J. Phys. Chem. C* **2015,** *119*, 22190–22197.
10. Fernandes, R. M. F.; Buzaglo, M.; Shtein, M.; Pri Bar, I.; Regev, O.; Marques, E. F.; Furó, I. Lateral Diffusion of Dispersing Molecules on Nanotubes As Probed by NMR. *J. Phys. Chem. C* **2014,** *118*, 582-589.
11. Frise, A. E.; Edri, E.; Furó, I.; Regev, O. Protein Dispersant Binding on Nanotubes Studied by NMR Self-Diffusion and Cryo-TEM Techniques. *J. Phys. Chem. Lett.* **2010,** *1*, 1414-1419.
12. Frise, A. E.; Pagès, G.; Shtein, M.; Pri Bar, I.; Regev, O.; Furó, I. Polymer Binding to Carbon Nanotubes in Aqueous Dispersions: Residence Time on the Nanotube Surface as Obtained by NMR Diffusometry. *J. Phys. Chem. B* **2012,** *116*, 2635-2642
13. Kato, Y.; Niidome, Y.; Nakashima, N. Thermodynamics of the Exchange of Solubilizers on Single-walled Carbon Nanotubes. *Chem. Lett.* **2011,** *40*, 730-732.
14. Roxbury, D.; Tu, X.; Zheng, M.; Jagota, A. Recognition Ability of DNA for Carbon Nanotubes Correlates with Their Binding Affinity. *Langmuir* **2011,** *27*, 8282-8293.
15. Oh, H.; Sim, J.; Ju, S. Y. Binding Affinities and Thermodynamics of Noncovalent Functionalization of Carbon Nanotubes with Surfactants. *Langmuir* **2013,** *29*, 11154-11162.

16. Kato, Y.; Inoue, A.; Niidome, Y.; Nakashima, N. Thermodynamics on Soluble Carbon Nanotubes: How Do DNA Molecules Replace Surfactants on Carbon Nanotubes? *Sci. Rep.* **2012,** *2*.
17. Zhong, W.; Claverie, J. P. Probing the carbon nanotube-surfactant interaction for the preparation of composites. *Carbon* **2013,** *51*, 72-84.
18. Sa, V.; Kornev, K. G. Analysis of Stability of Nanotube Dispersions Using Surface Tension Isotherms. *Langmuir* **2011,** *27*, 13451-13460.
19. Arnold, M. S.; Green, A. A.; Hulvat, J. F.; Stupp, S. I.; Hersam, M. C. Sorting Carbon Nanotubes by Electronic Structure using Density Differentiation. *Nature Nanotechnology* **2006,** *1*, 60-65.
20. Backes, C.; Mundloch, U.; Schmidt, C. D.; Coleman, J. N.; Wohlleben, W.; Hauke, F.; Hirsch, A. Enhanced Adsorption Affinity of Anionic Perylene-Based Surfactants towards Smaller-Diameter SWCNTs. *Chem. Eur. J.* **2010,** *16*, 13185-13192.
21. Subbaiyan, N. K.; Cambre, S.; Parra-Vasquez, A. N. G.; Haroz, E. H.; Doorn, S. K.; Duque, J. G. Role of Surfactants and Salt in Aqueous Two-Phase Separation of Carbon Nanotubes toward Simple Chirality Isolation. *Acs Nano* **2014,** *8*, 1619-1628.
22. Cheng, Y.; Pei, Q. X.; Gao, H. Molecular-Dynamics Studies of Competitive Replacement in Peptide-Nanotube Assembly for Control of Drug Release. *Nanotechnology* **2009,** *20*.
23. Capelo, J. L.; Galesio, M. M.; Felisberto, G. M.; Vaz, C.; Pessoa, J. C. Micro-Focused Ultrasonic Solid-Liquid Extraction (mu FUSLE) Combined with HPLC and Fluorescence Detection for PAHs Determination in Sediments: Optimization and Linking with the Analytical Minimalism Concept. *Talanta* **2005,** *66*, 1272-1280.
24. Shtein, M.; Pri Bar, I.; Regev, O. A Simple Solution for the Determination of Pristine Carbon Nanotube Concentration. *Analyst* **2013,** *138*, 1490-1496.
25. Dror, Y.; Pyckhout-Hintzen, W.; Cohen, Y. Conformation of Polymers Dispersing Single-Walled Carbon Nanotubes in Water: A Small-Angle Neutron Scattering Study. *Macromolecules* **2005,** *38*, 7828-7836.
26. Price, W. S., *NMR Studies of Translational Motion: Principles and Applications*. Cambridge University Press: 2009.
27. Mills, R. Self-Diffusion in Normal and Heavy Water in the Range 1-45°. *J. Phys. Chem.* **1973,** *77*, 685-688.
28. Masel, R. I., *Principles of Adsorption and Reaction on Solid Surfaces*. Wiley: New York, 1996.
29. Granite, M.; Radulescu, A.; Pyckhout-Hintzen, W.; Cohen, Y. Interactions between Block Copolymers and Single-Walled Carbon Nanotubes in Aqueous Solutions: A Small-Angle Neutron Scattering Study. *Langmuir* **2011,** *27*, 751-759.
30. Sarukhanyan, E.; Milano, G.; Roccatano, D. Coating Mechanisms of Single-Walled Carbon Nanotube by Linear Polyether Surfactants: Insights from Computer Simulations. *J. Phys. Chem. C* **2014,** *118*, 18069-18078.
31. Tummala, N. R.; Morrow, B. H.; Resasco, D. E.; Striolo, A. Stabilization of Aqueous Carbon Nanotube Dispersions Using Surfactants: Insights from Molecular Dynamics Simulations. *Acs Nano* **2010,** *4*, 7193-7204.
32. Zana, R., *Dynamics of Surfactant Self-Assemblies*. Taylor&Francis: Boca Raton, 2005.
33. Furó, I.; Iliopoulos, I.; Stilbs, P. Structure and Dynamics of Associative Water-Soluble Polymer Aggregates as seen by ^{19}F NMR Spectroscopy. *J. Phys. Chem. B* **2000,** *104*, 485-494.
34. Kato, Y.; Niidome, Y.; Nakashima, N. Spectroscopic Analysis of Two Distinct Equilibrium States for the Exchange Reaction of Sodium Cholate and Oligo-DNA on Single-Walled Carbon Nanotubes. *ChemPhysChem* **2013,** *14*, 1652-1655.

Supporting information

for

Assessing Surfactant Binding to Carbon Nanotubes via Competitive Adsorption: Binding strength and critical coverage

Ricardo M.F. Fernandes,[1,3] Jing Dai,[1] Oren Regev,[2] Eduardo F. Marques,[3] and István Furó[1] *

Note 1. The supernatant characterization

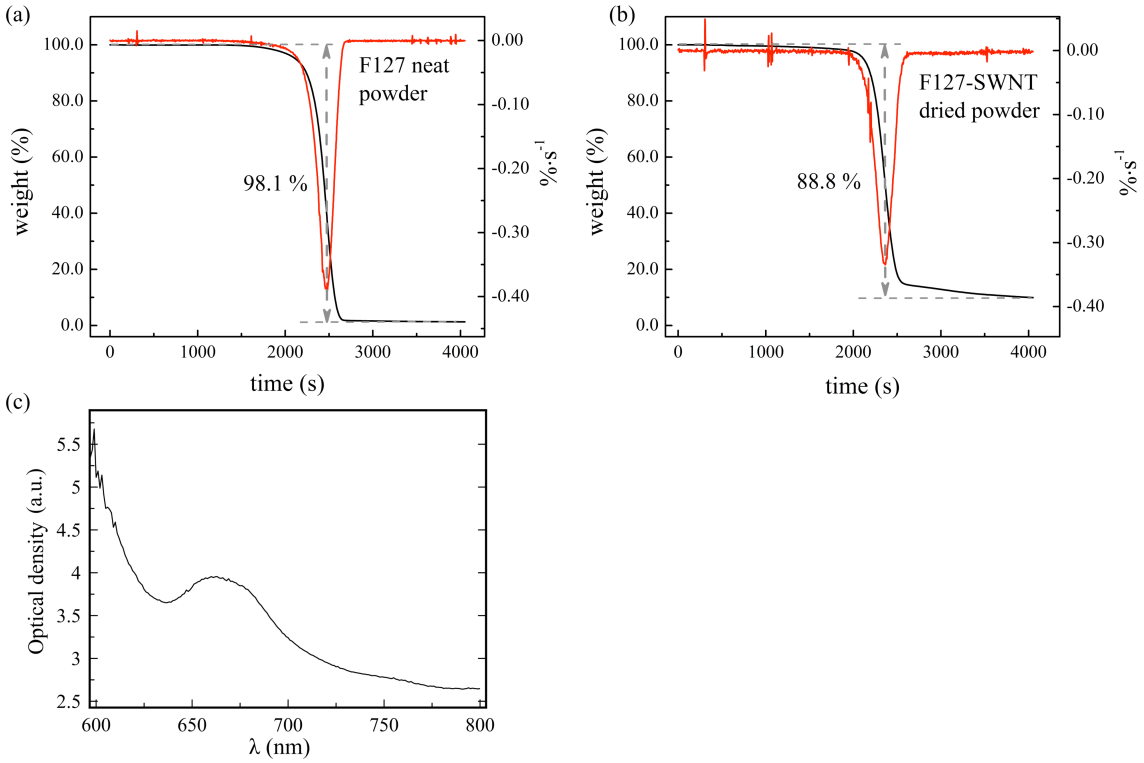

Figure S1. TGA result in neat F127 powder (a) and in F127-SWNT dispersion dried to powder (b); UV-Vis spectrum of a non-diluted F127-SWNT dispersion (c). Optical path = 0.4 cm. The optical density at 660 nm was used to determine the apparent extinction coefficient (Table S1).

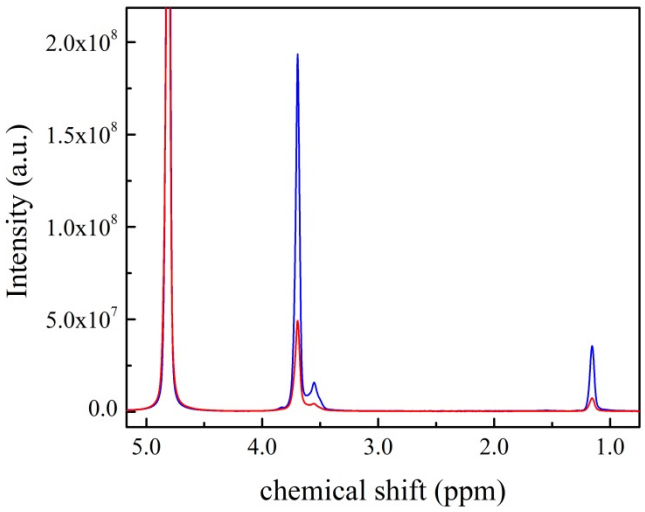

Figure S2. ^{1}H NMR spectrum of a neat F127 solution c=3.0 mg·mL^{-1} (blue) and of an F127-SWNT dispersion (red). The integration of the region between 3.1 and 4.2 ppm was used to estimate the F127 concentration (2.1 mg·mL^{-1}) in the SWNT dispersion. The integration of the methyl peak gives a lower concentration (1.7 mg·mL^{-1}) plausibly because some part of the signal is lost (line broadening) due of the stronger adsorption of the PPO block (that is, as compared to that of the PEO block) onto the SWNT.

Table S1. Parameters for supernatant characterization: V_s, m_s, ϕ_s, ϕ_d, c_{SWNT}, concentration of F127 in the supernatant (determined by NMR and TGA, referred to as $c_{F127\text{-}NMR}$ and $c_{F127\text{-}TGA}$ in the main text, respectively), the optical density and the apparent extinction coefficient**.**

m_s/ mg	V_s / mL	ϕ_s	ϕ_d	c_{SWNT} / mg.mL^{-1}	Final conc. of F127 (TGA) / mg.mL^{-1}	Final conc. of F127 (NMR) / mg.mL^{-1}	Optical density 660 nm	ε_{660} / mL·mg^{-1}·cm^{-1}
3.81	1.50	0.888	0.981	0.24	2.29	2.1	3.96	41.2

Note 2. Two-site diffusion model

The self-diffusion coefficient, D, of the F127 polymer molecules is obtained by fitting the Stejskal-Tanner equation[1]

$$I/I_o=\exp(-(\gamma g\delta)^2(\Delta-\delta/3)D) \qquad \text{(s 1)}$$

to the signal intensity I, normalized by the signal intensity in the absence of gradient I_o; where γ is the magnetogyric ratio of the nucleus, δ is the duration of the gradient pulse of magnitude g, and Δ is the diffusion time. The self-diffusion coefficient D is measured by recording the diffusional signal decay I as function of the gradient strength g steps. All the others parameters are kept constant.

In a system with molecules exchanging between two pools with different self-diffusion coefficients (D), when the residence time of molecules in the pools is longer than the set experimental diffusion time (Δ), the diffusional decay is characterized by the weighted sum of the decay of each population fraction in each pool

$$I/I_o = p_1 \exp(-bD_1) + p_2 \exp(-bD_2) \qquad \text{(s 2)}$$

where $b=(\gamma g \delta)^2 (\Delta - \delta/3)$, p_1 and p_2 are the population fractions and D_1 and D_2 the self-diffusion coefficients of the molecules in each pool. For the SWNT-F127 system, p_1 and D_1 are associated with the F127 molecules free in the bulk, respectively; and p_2 and D_2 assigned with the F127 molecules adsorbed in the SWNT surface. We assume an isotropic three-dimensional diffusion, neglecting the 1-D diffusion of F127 molecules on individual or nanotube thin bundles.[2, 3]

Using the Levenberg-Marquardt curve-fitting method to the diffusional raw data to fit equation 2, the fitted parameters p_1, p_2 and D_2 are extracted. Note that the parameter D_1, the self-diffusion coefficient of F127 free in the bulk was fixed to the value $D_1 = 5.0\times10^{-11}$, obtained independently from the diffusional decay of a neat F127 solution. The relative population of F127 molecules adsorbed in the nanotube surface was calculated by [4]

$$f_{\mathrm{F127}} = \frac{p2}{p1+p2} \qquad \text{(s 3)}$$

Note 3. The composition of the different starting F127-SWNT dispersions

Table S2. Characterization of the various F127-SWNT dispersions to which particular surfactants were added: the final concentration of F127 in the supernatant was measured by NMR, the concentration of SWNT suspended, the fraction of f_{F127} adsorbed in the SWNT surface, and the corresponding surface coverage σ.

Sample	$c_{F127\text{-}NMR}$ / mg·mL^{-1}	c_{SWNT} / mg·mL^{-1}	f_{F127} / %	σ_{F127} / (mg/mg$_{SWNT}$)
A	2.2	0.27	5.2	0.42
B	2.2	0.26	5.5	0.47
C	2.2	0.25	4.8	0.42
D	2.0	0.30	5.8	0.40
E	2.3	0.30	6.7	0.51
F	2.3	0.29	5.8	0.44

Note 4. Surfactant addition to SWNT-F127 samples

A volume of approximately 2—7 µL of concentrated (≈30 mg·mL^{-1}) surfactant solution was added to 100 µL of F127-SWNT dispersion (dispersions A—F in Table S2). The mixture was gently shaken by hand (10—20 sec.) and left for equilibration for a minimum time of 2 min. 100 µL of the final mixture were transferred to an NMR Shigemi tube 5 mm to perform the NMR experiments.

Note 5. Fitting results and the derived parameters (f_{F127} and surface coverage σ) obtained upon addition of surfactants to the initial F127-SWNT dispersions (from table S2).

Table S3. Fraction and surface coverage by F127 upon addition of DTAB to starting dispersion A.

C_{DTAB} / mg.mL^{-1}	f_{F127} / %	σ_{F127} / (mg/mg$_{SWNT}$)	$\sigma/\sigma_{initial}$
0.0	5.2	0.42	1.00
0.5	4.4	0.35	0.84
1.0	4.6	0.37	0.88
1.5	4.6	0.37	0.88
2.0	4.4	0.35	0.84

Table S4. Same as Table S3, but with TTAB added to starting dispersion B.

C_{TTAB} / mg.mL^{-1}	f_{F127} / %	σ_{F127} / (mg/mg$_{SWNT}$)	$\sigma/\sigma_{initial}$
0.0	5.5	0.47	1.00
0.5	4.2	0.36	0.76
1.0	3.6	0.31	0.66
1.5	3.1	0.26	0.57
2.0	2.5	0.21	0.45

Table S5. Same as Table S3, but with Sodium Cholate added to starting dispersion C.

$C_{S.Cholate}$ / mg.mL^{-1}	f_{F127} / %	σ_{F127} / (mg/mg$_{SWNT}$)	$\sigma/\sigma_{initial}$
0.0	4.8	0.42	1.00
0.5	3.2	0.29	0.67
1.0	3.1	0.28	0.64
1.5	2.8	0.25	0.58
2.0	2.5	0.22	0.51

Table S6. Same as Table S3, but with CTAB added to starting dispersion D.

C_{CTAB} / mg.mL^{-1}	f_{F127} / %	σ_{F127} / (mg/mg$_{SWNT}$)	$\sigma/\sigma_{initial}$
0.0	5.8	0.40	1.00
0.5	4.5	0.31	0.77
1.0	3.4	0.23	0.59
1.5	3.4	0.23	0.59
2.0	3.0	0.20	0.52

Table S7. Same as Table S3, but with CPyCl added to starting dispersion D.

C_{CPyCl} / mg.mL^{-1}	f_{F127} / %	σ_{F127} / (mg/mg$_{SWNT}$)	$\sigma/\sigma_{initial}$
0.0	5.8	0.40	1.00
0.5	4.0	0.26	0.65
1.0	3.0	0.19	0.48
1.5	2.9	0.19	0.48
2.0	2.4	0.16	0.41

Table S8. Same as Table S3, but with SDS added to starting dispersion E.

C_{SDS} / mg.mL^{-1}	f_{F127} / %	σ_{F127} / (mg/mg$_{SWNT}$)	$\sigma/\sigma_{initial}$
0.0	6.7	0.51	1.00
0.5	5.4	0.41	0.80
1.0	3.7	0.28	0.55
1.5	2.6	0.20	0.39
2.0	1.8	0.14	0.27

Table S9. Same as Table S3, but with SDBS added to starting dispersion F.

C_{SDBS} / mg.mL^{-1}	f_{F127} / %	σ_{F127} / (mg/mg$_{SWNT}$)	$\sigma/\sigma_{initial}$
0.0	5.8	0.44	1.00
0.5	4.4	0.34	0.77
*1.0	3.3	0.23	0.57
1.5	2.0	0.15	0.34
2.0	1.2	0.094	0.21

*addition of SDBS in sample D

Note 5. Presentation of the data in Figure 3 on a mole concentration basis

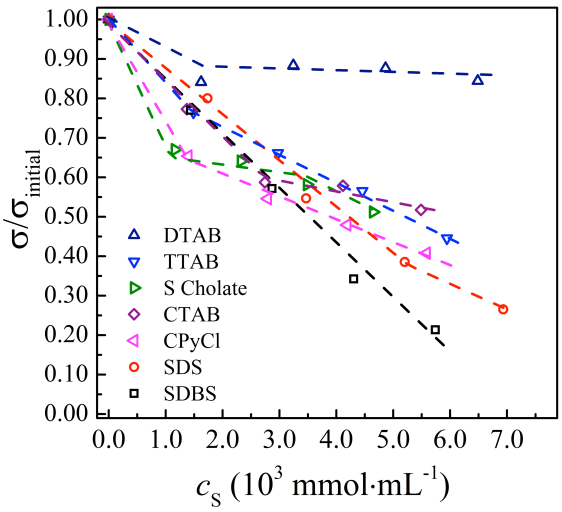

Figure S3. The change in surface coverage by F127 molecules as a result of addition of different surfactant sorts to the initial F127-SWNT dispersion. The dashed lines are guides for the eye.

Note 6. Critical dispersability concentration (*cdc*) values obtained from the reference [5].

Table S10. *cdc* values obtained from the SWNT/surfactant dispersion curves.

Surfactant	*cdc*[a]
SDBS	3.8 ± 2.2 1.3
SDS	5.5 ± 1.0 1.6
DTAB	14 ± 1 4.32
TTAB	5.4 ± 0.2 1.82
CTAB	4.8 ± 1.8 1.75
CPyCl	4.0 ± 0.6 1.36

[a]Values in $mmol \cdot kg^{-1}$ and $mg \cdot mL^{-1}$, respectively.

References

1. Stejskal, E. O.; Tanner, J. E., Spin Diffusion Measurements: Spin Echoes in the Presence of a Time-Dependent Field Gradient. *J Chem Phys* **1965**, 42, 288-292.

2. Fernandes, R. M. F.; Buzaglo, M.; Shtein, M.; Pri Bar, I.; Regev, O.; Marques, E. F.; Furó, I., Lateral Diffusion of Dispersing Molecules on Nanotubes As Probed by NMR. *J Phys Chem C* **2014**, 118, 582-589.

3. Frise, A. E.; Pages, G.; Shtein, M.; Pri Bar, I.; Regev, O.; Furo, I., Polymer binding to carbon nanotubes in aqueous dispersions: residence time on the nanotube surface as obtained by NMR diffusometry. *J Phys Chem B* **2012**, 116, 2635-2642.

4. Fernandes, R. M. F.; Buzaglo, M.; Regev, O.; Marques, E. F.; Furó, I., Surface Coverage and Competitive Adsorption on Carbon Nanotubes. *J Phys Chem C* **2015**, 119, 22190-22197.

5. Fernandes, R. M. F.; Abreu, B.; Claro, B.; Buzaglo, M.; Regev, O.; Furó, I.; Marques, E. F., Dispersing Carbon Nanotubes with Ionic Surfactants under Controlled Conditions: Comparisons and Insight. *Langmuir* **2015** 31, 10955−10965.

V

Mechanical agitation induces aggregation of pre-dispersed carbon nanotubes

Ricardo M.F. Fernandes, Matat Buzaglo, Oren Regev, István Furó and Eduardo F. Marques

Manuscript

Mechanical Agitation Induces Aggregation of Pre-Dispersed Carbon Nanotubes

Ricardo M.F. Fernandes,[1,2] Matat Buzaglo,[3] Oren Regev[3,4], István Furó[2], and Eduardo F. Marques[1]*

[1]Centro de Investigação em Química, Department of Chemistry and Biochemistry, Faculty of Science, University of Porto, Rua do Campo Alegre, s/n, P-4169-007 Porto, Portugal.

[2]Division of Applied Physical Chemistry, Department of Chemistry, KTH Royal Institute of Technology, SE-10044 Stockholm, Sweden.

[3]Department of Chemical Engineering and [4]Ilse Katz Institute for Nanotechnology, Ben-Gurion University of the Negev, 84105 Beer-Sheva, Israel.

ABSTRACT. Mechanical agitation is typically used to fragment and disperse insoluble materials in a solvent. We report here an aggregation process that, contrary to expectation, is induced by mechanical agitation: when aqueous dispersions of single-walled carbon nanotubes (SWNTs) are subject to vortex-shaking, weakly bound micron-sized aggregates are formed. The SWNT dispersions are prepared by adding various dispersants employing a sonication followed by centrifugation approach. While surfactant adsorption to the SWNTs during sonication results in stabilized exfoliated tubes and thin bundles, we find that vortex-shaking the fresh dispersions for short periods (10-60 s) results in re-aggregation into flocs in the 1-10^2 μm range. The aggregation is reversible: if the vortexed dispersions are mildly sonicated, the flocs break down and re-dispersal occurs. Imaging at different resolutions shows that the aggregates consist of loose networks of intertwined tubes and bundles. The data further indicate that the average aggregate size increases logarithmically with vortex time and is critically influenced by dispersant type (ionic or nonionic), centrifugation time (prior to vortexing) and initial concentration of dispersed SWNTs. These results are relevant if stabilization or destabilization of dispersions is sought for, i.e., in drug delivery or sensing applications, and could also be of interest for chiral sorting of SWNTs and percolation conductivity.

TOC GRAPHICS

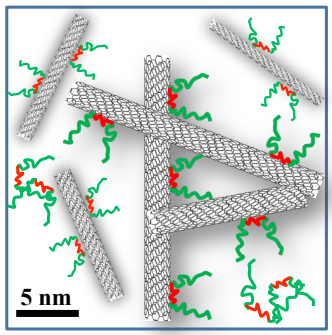

KEYWORDS

Single-walled carbon nanotubes; dispersibility; vortex-shaking; percolated networks; reversible

Separation of highly entangled carbon nanotube (CNT) powders into isolated tubes or small bundles is a pre-requisite for most practical exploitations of the distinctive thermal, mechanical electrical and optical properties of this nanomaterial, such as in the reinforcement of composites[1,2] and advanced molecular electronics.[3,4] Dispersing the powders in an aqueous solvent through non-covalent binding[5,6] of amphiphiles—surfactants[7,8], polymers[9,10] or proteins[11,12]—has become a widely used strategy for that purpose. Besides playing active role in the exfoliation process[13,14], the dispersant also stabilizes the CNTs against re-bundling and precipitation, by imparting electrostatic or steric repulsions between the coated tubes.[15] The dispersion process usually involves sonication of the powder in the dispersant solution followed by centrifugation to remove larger agglomerates and catalyst impurities. The experimental parameters used both in sonication (delivered power density) and centrifugation (acceleration grade and time) are critical[16-18] for the "quality" of the final dispersion obtained[19], that is, for the distribution of individual tubes, whose concentration should be maximized, and bundles, which should be few and as thin as possible.

These dispersions possess only kinetic and not thermodynamic stability.[15] Consequently, flocculation (reversible aggregation) or coagulation (irreversible one) of the CNT species typically occur within hours to weeks (depending on the dispersants and processing conditions used)[7,15], and are usually an undesired effect. It might be thought that if a short but vigorous energy boost were imparted to a dispersion, e.g. by vortex-shaking, any flocculated material that could have been built would redisperse. In fact, vortex-shaking is a well-known method for dispersing materials, either soft colloids[20-23] or hard materials.[24-26] The type of vortex mixer used in colloidal dispersions consists essentially of an electric motor axially connected to a cupped rubber holder of vials and, with the motor on, the holder oscillates circularly (with a few thousand rpm), ultimately creating a turbulent vortex in the liquid inside the vial. Counterintuitively, here we found the opposite effect in nanotube dispersions: vortex-shaking leads to instability and re-aggregation of the dispersed particles (tubes or bundles), inducing discrete weakly bound aggregates in the 1-10^2 μm size range, that is, in the colloidal-to-macroscopic transition.

These observations prompted us to investigate the phenomenon further, and that is the main motivation behind this report. Thus, dispersions prepared by a range of dispersants under rigorously identical conditions were further subject to increasing vortex time. We also investigated the effects on the aggregate size upon varying the centrifugation time (prior to vortexing), and the suspended CNT concentration. In all cases, the aggregates induced by

vortex (Figure 1) are monitored by video-enhanced light microscopy and the average size (longest linear length, $<L_a>$) statistically sampled. Two important points should be hitherto noted. First, the dispersant concentration, c_s, in the CNT dispersions is always sufficiently low so that the known attractive depletion interactions[27-30] originated by free micelles (and typically observed for c_s > 10 x cmc) are absent. Second, the SWNT concentrations are within the dilute dispersion regime, about one order of magnitude lower than the percolation threshold associated with the transition to semidilute dispersions, 0.3 wt% CNT.[31]

The presence of solid-like aggregates built-up of cross-linked tubes in concentrated systems of SWNTs, namely semidilute dispersions and gels, has been previously reported.[31] In dilute, less well-dispersed suspensions of SWNTs, fractal-like aggregates with varying degree of compactness have also been found.[32-34] These structures are intrinsic to the as-produced dispersions and gels, however, there are only very few reports on aggregates resulting from energy-driven (e.g. shear flow) flocculation/percolation of pre-dispersed NTs.[35] On the other hand, Tae-Hwan et al reported that SWNT powders pre-covered by a polymerized layer of surfactant could be easily and well dispersed in several alcohols by means of vortex-mixing.[36] To our knowledge, however, aggregation induced by mechanical agitation in dilute surfactant-assisted dispersions of CNTs (and redispersion effects by mild sonication) has not been recognized and explored before. Herein, we will first present the effect of different factors on SWNT aggregation—vortex time, centrifugation time before vortexing and dispersed SWNT concentration—followed by a microscopic view of the networks formed, and thereafter attempt an interpretation of the data based on that picture.

The dispersions were prepared using single-walled nanotubes (SWCNT/HDPlas, CheapTubes), specified by the supplier as mixed single- and double-walled tubes with outer diameter d = 1 - 4 nm and length L = 3 - 30 μm. Three classes of surfactants were used: the anionic surfactants sodium dodecylbenzenesulfonate (SDBS) and sodium dodecyl sulfate (SDS); the cationic surfactants dodecyltrimethylammonium bromide (DTAB) and cetyltrimethylammonium bromide (CTAB); and the nonionic triblock copolymers F127, $(PEO)_{97}$-$(PPO)_{69}$-$(PEO)_{97}$, and F68, $(PEO)_{76}$-$(PPO)_{29}$-(PEO)76, and surfactant Triton™ X-100 (TX-100). These surfactants cover a range of molecular properties, with ionic surfactants encompassing CNT stabilization based on charge repulsions and nonionic ones providing steric hindrance.

Noteworthy, the dispersions were prepared with the same initial c_{SWNT}, 0.30 mg $mL^{-1,}$ which corresponds to a 0.03 wt% CNT (an order of magnitude below the assumed

percolation threshold) and to about 10% of the initial CNT loading (9 mg). Fixed sonication (tip; t = 8.5 min and average power density ~ 1.0 W·mL^{-1}) and centrifugation (20 min, a = 4 x 10^3 g) conditions were used. It should be also noted that the concentration of dispersant, c_s, differs between the dispersions in Figures 1 and 2 and this is because different surfactants have different dispersing ability (cf. Figure S1 in Supporting Information). The dispersant concentrations used are provided in Table S1 (S.I.), both on mass and molar basis.

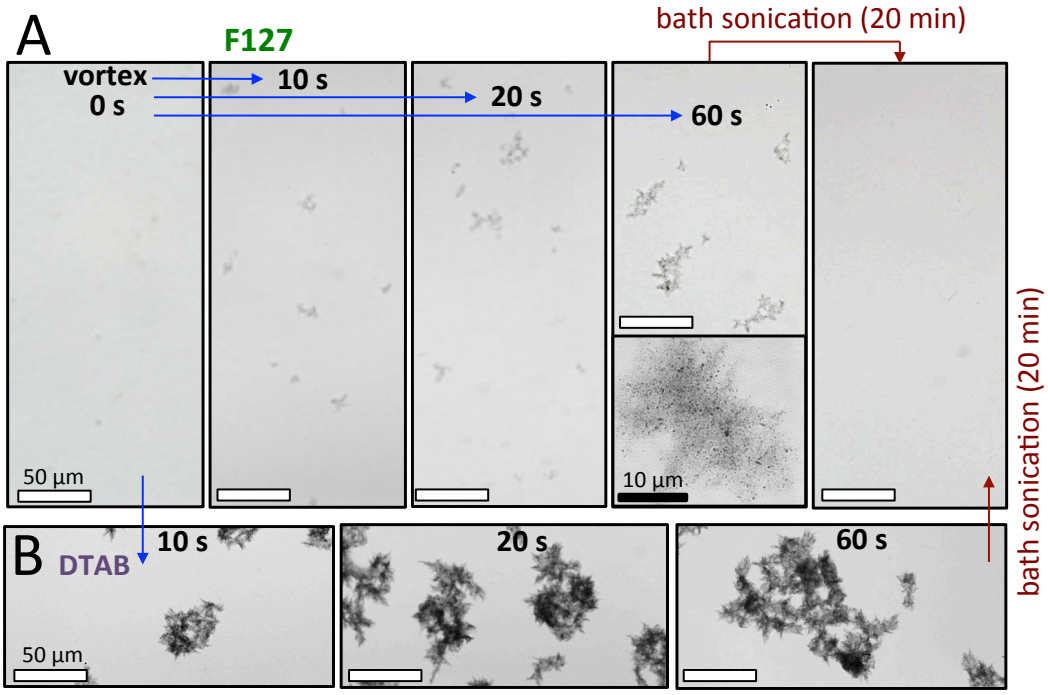

Figure 1. Effect of mechanical agitation by vortex on aqueous dispersion of SWNTs with c_{SWNT}= 0.30 mg·mL^{-1}, (0.03 wt% dispersion) using as dispersant: A) Pluronic F127, c_s = 3.0 mg mL^{-1}; B) DTAB, c_s = 12.5 mg mL^{-1}. When the as-produced dispersion are subject to vortex-shaking, weakly bound dark aggregates appear, with their apparent length increasing with vortex time for both dispersants; the aggregates are visibly bigger for DTAB. Upon mild bath sonication 8for 20 min), the aggregates redisperse.

Under the sonication-centrifugation conditions used here, previous studies have shown that the dispersions contain a mixture of individual tubes and thin bundles[10,37,38], isotropically distributed in the sample. Irrespective of the dispersant used, we find here that if the fresh dispersions are subject to short periods of vortex shaking (up to one minute), micron-sized aggregates build up from otherwise aggregate-free dispersions. Figure 1

illustrates the type of behavior observed, in this case for F127 (Figure 1A), a highly effective dispersant, and DTAB (Figure 1B), a poorly effective one. In both cases, 10 s of vortex shaking are enough to produce dark flocs with an irregular shape, as clearly visible in a light microscope (Olympus BX51 with DIC lenses, and either 100x or 400x magnification; cf. further experimental details below). For F127, one sees qualitatively that the average size of the gray aggregates gradually increases with the vortexing time (10, 20 and 60 s). At 60 s (lower panel in Figure 1A), higher magnification shows in more detail the opened inner structure of the aggregates. A core observation is that after 20 min of bath sonication (a relatively mild treatment in terms of transferred power density), the flocs redisperse and are no longer visible in the microscope (far right panel, Figure 1A). Figure 1B shows that the aggregates formed for DTAB in identical conditions are considerably bigger than for F127 and have a denser (darker) structure (bath sonication has however identical effects as the F127 case). It is obvious that under similar preparation conditions used, differences arise between different dispersants.

Effect of Dispersant Type, Centrifugation and Nanotube Concentration on Aggregate Size. The average major length of the aggregates, $\langle L_a \rangle$, and respective standard deviation, was measured using light microscopy with a minimum of 50 aggregates counted per sample. Figure 2 shows that under identical conditions, vortex-shaking induces aggregation for all surfactants, with $\langle L_a \rangle$ increasing with vortex time. The data also show considerably scattering in $\langle L_a \rangle$ (cf. Table S1, S.I.), but nevertheless trends are evident. It is apparent that significant differences in average size exist for the different surfactants. Logarithm fits can be reasonably adjusted to the size vs. time plots (in an curious similarity to the flocculation behavior of charged colloids[39]). SDBS and F127, in one extreme, form the smallest aggregates attaining an upper $\langle L_a \rangle$ limit of ~ 40 μm and experience a slower rate of growth. F68, SDS and DTAB, on the other extreme, form the largest aggregates (upper $\langle L_a \rangle$ ~ 120 μm) and undergo a steeper growth rate. TX100 and CTAB are in an intermediate case.

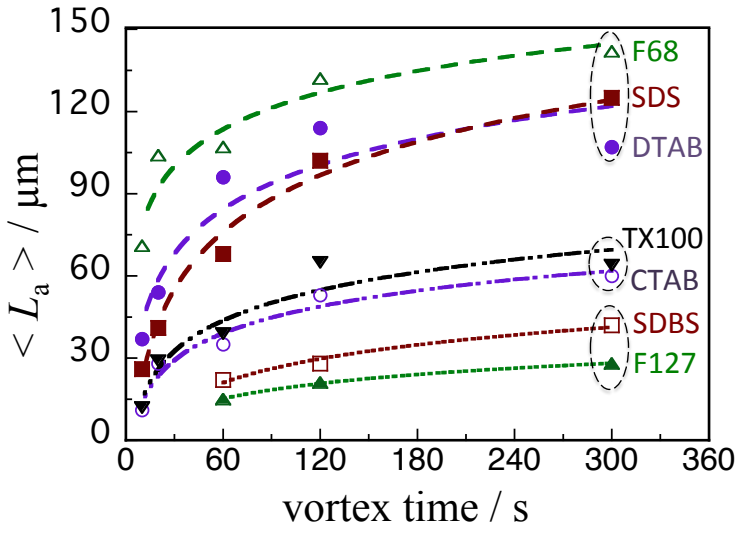

Figure 2. Evolution of average aggregate size with vortex time for different surfactants; lines are log fits. For all dispersions, c_{SWNT} = 0.30 mg·mL^{-1} and the centrifugation acceleration grade used (before vortexing) was constant at 4,000 *g*; the dispersant concentrations are different and can be found in Table S1, S.I.).

Figure 3a) now shows the effect of varying the *g*-grade (keeping 20 min) in the centrifugation step of the preparation of the dispersion, hence prior to vortex-shaking of the supernatants. In order to ensure identical c_{SWNT} dispersed, 0.3 mg·mL^{-1}, c_s = 3.51 mg·mL^{-1} was used in the four samples that then underwent different centrifugation acceleration values, in the range 2,000 - 30,000 *g*.

As expected, lower *a* values (2,000 and 4,000 *g*) results in markedly longer < L_a>, by a 5-fold factor, than obtained at higher ones (10,000 and 30,000 g), for 60 s of vortexing. This difference in aggregate size between *g* values is attenuated as the vortex time increases to 120 and 300 s. The effect of the pre-dispersed nanotube concentration on <L_a> was also tested, Figure 3b), using constant 4,000 g and vortex time, 60 s, in SDS-assisted dispersions (constant 3.51 mmol·kg^{-1}; see also S.I. for further details). Note that the three SWNT concentrations are relatively small—5, 10 and 15 % of the initial powder loading. As c_{SWNT} increases from 0.15 to 0.30-0.60 mg·mL^{-1}, <L_a> increases markedly.

Before attempting an interpretation of these effects, we need to investigate further the structure of the aggregates and capture a microscopic picture.

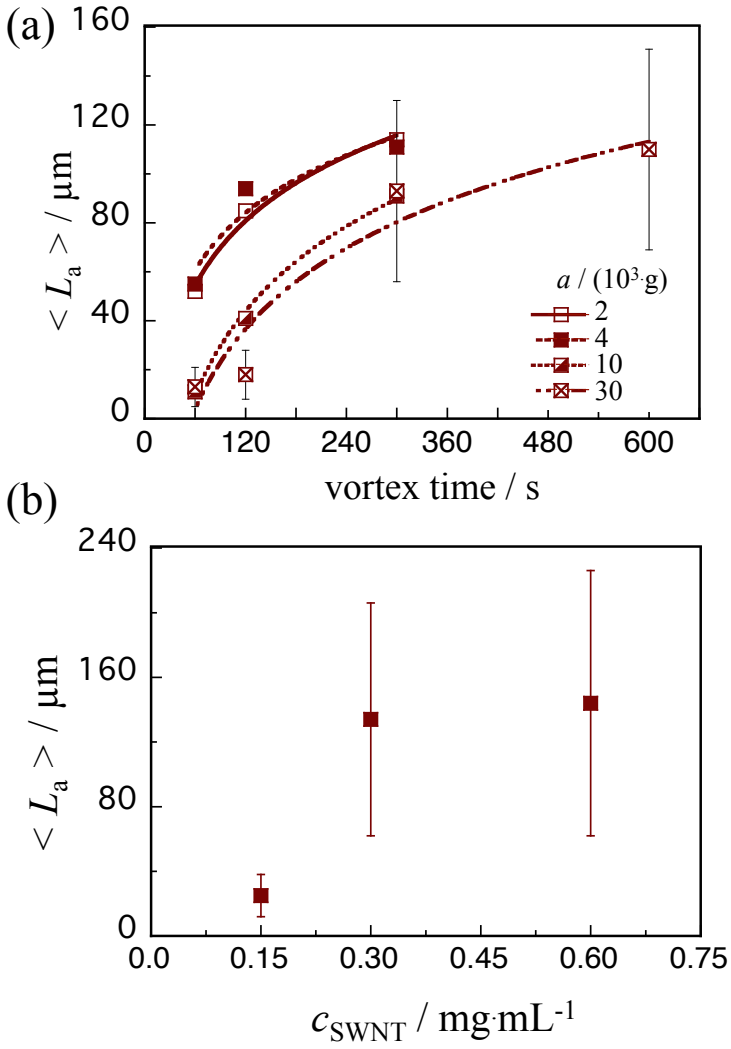

Figure 3. Variation of <L_a> in SDS-assisted dispersions with: (a) vortex time, for dispersions previously centrifuged at different a values, ranging from 2,000 to 30,000 g (c_{SWNT} = 0.3 mg·mL^{-1} and c_s = 3.51 mg·mL^{-1}; typical uncertainty bars shown for one of the data sets); (b) concentration of pre-dispersed SWNTs, using set values of 60 s of vortexing, a = 4,000 g and c_s= 3.51 mmol·kg^{-1}.

Microstructure of the Aggregates at Different Resolutions. The microstructure of the aggregates was investigated resorting to different types of microscopy and corresponding resolutions, as depicted in Figure 4, for F127 dispersions. Light micrographs in Figure 4a) indicate the opened ("loose") and irregular morphology of the aggregates (in this case, formed upon 60 s of vortexing). Cryo-SEM reveals a dense network of entangled rod-like structures that are consistent with individual SWNTs or bundles, Figure 4b). A higher resolution of the network obtained by cryo-TEM, Figure 4(c), shows regions consisting of

cross-linked individualized tubes (dashed circle) and darker regions with more densely compacted material (full circle). Note the reverse contrast from SEM to TEM.

In Figure 4(d), a schematic view of the structure of the mesh-like network is proposed. The picture proposed is that of a percolated network of tubes formed due to sticky tube-tube contacts induced by vorticity. Previous studies have indicated that the degree of surface coverage in dispersed CNTs is low and also that the fraction of adsorbed surfactant amounts to only a few percent of the total surfactant present.[10,40,41]

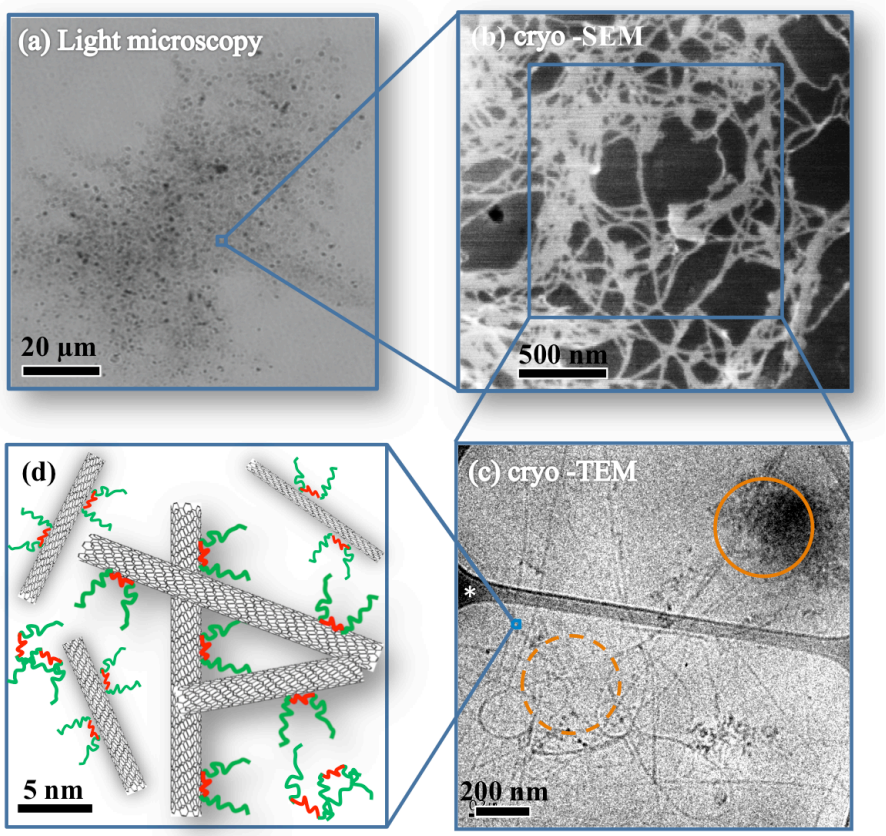

Figure 4. Imaging of the vortex-induced aggregates in F127-assisted dispersions at different size scales: a) light microscopy showing the loose structure of the SWNT flocs, also with denser (darker) regions; b) cryo-SEM showing a network of entangled tubes and/or bundles; c) cryo-TEM showing individual SWNTs, but also the denser regions indicating the lacey substrate on which the sample is suspended; d) schematic view of the SWNT cross-linking.

The dispersions are stabilized by repulsive interactions, either electrostatic or steric, between the dispersant-covered tubes. It is however likely that, when tubes or bundles collide under the turbulent flow induced by vorticity, bare regions of the nanotube surface will act as sites for re-sticking owing to van der Waals and hydrophobic interactions. It is also conceivable

that the shear stress will not be locally so strong so as to dislodge bound surfactant into the bulk; hence, contacts between two dispersant-covered tubes at angles close to 0º, that could leading to parallel rebundling, will be rare due to highest repulsive interactions. On the other hand, collisions at 90º will have the lowest repulsive barrier. Moreover, molecular dynamics simulations have suggested that the dispersant coating is more vulnerable for a pair of perpendicular tubes – i.e. the dispersant shielding that prevents nanotube aggregation is less effective if nanotubes collide at 90º due to clustering of bridging surfactant aggregates.[8] One can then envisage two consequences from these effects: (i) formation of a weakly bound percolated network; (ii) reversibility of the percolated state owing to relatively weak NT-to-NT contacts.

Under this microscopic picture, we now turn to possible explanations for the results in Figures 2 and 3. A key point is that the SWNT concentration in Figure 2 is identical for all surfactants, but not the dispersant concentration, as mentioned above. (1) One possible explanation for the different size of the aggregates could be differences in the degree of surface coverage between the various surfactants. More extensively covered tubes would be less likely to aggregate upon vortexing. If so, for instance, tubes stabilized by F127 or SDBS would be more densely covered than those by F68 or SDS. However, as mentioned above, low coverage seems to be a general feature in this type of dispersants. It may thus be unlikely that the large differences in $\langle L_a \rangle$ between surfactants (amounting to a 5-fold factor) could be assigned principally to this factor. (2) An alternative explanation is related to differences in binding strength of the dispersants with respect to the NT surface. One can conceive that surfactants that bind more strongly would have less lateral mobility. When two tubes approach, slower rate of fluctuations in mobility/coverage would be less favorable for sticky interactions between the tubes. Our recent work on competitive adsorption on SWNTs has shown significant different in binding strength between surfactants, for concentrations similar to those used here.[42] Although a detailed correlation is not at hand for all the dispersants, we note for instance that DTAB, a much weaker binder that SDBS, gives rise to fairly larger vortex-induced aggregates, while CTAB lies in an intermediate position in binding strength and vortex-produced $\langle L_a \rangle$. Comparing triblock copolymers F127 and F68, one can see that the former, with a longer and hence more hydrophobic (stickier) PPO block (69 units compared to 29 in F68), originates much smaller $\langle L_a \rangle$, as expected according to this reasoning. (3) Another hypothesis is related to the differences in dispersant concentration in Figure 2, as highlighted above. Table S1 shows that SDS and DTAB concentrations are

somewhat higher than SDBS and CTAB, in dispersions where the SWNT concentration is equal for all. If the surfactant adsorption is particularly favored at orthogonal tube-tube contacts, as suggested by molecular simulations, then dispersions where more surfactant is available could lead to a higher frequency of sticky collisions upon vigorous agitation. This could lead to more extensive percolation and hence larger aggregates. At this point, we note that due to the complex nature of the interactions at play in these dispersions, more than one effect could be responsible for the differences in behavior observed. Further studies will be needed to complement our main findings.

As concerning the centrifugation effects in Figure 3a), previous studies on varying centrifugation indicated that the as-produced dispersions contain a distribution of isolated tubes and thin bundles, and that these bundles tend to sediment according to their diameter as g increases.[37] This would result in a decrease in the number density of suspended species and an increasing fraction of even thinner bundles and individual tubes left in solution. Consequently, higher g would result in smaller vortex-induced aggregates, for identical vortex time, because of the mass loss. Analysis of the c_{SWNT} influence on $<L_a>$, in Figure 3b), is consistent with this simple interpretation. Higher concentration of CNT species imply higher frequency of collisions between them and hence, as reasonably expected, bigger aggregates form for identical vortex time.

In summary, we have shown that surfactant-assisted dispersions of carbon nanotubes that undergo short vortexing periods (seconds to few minutes) become unstable, forming micron-scale percolated networks (~ 30 - 100 μm). It is proposed here that the tube (or thin bundle) re-aggregation occurs mainly through uncovered contact points. Several hypotheses were put forth for the molecular mechanism behind this aggregation phenomenon, but more studies are required to further elucidate it. Finally, we highlight two instances to which these results relate to and where vortex-assisted aggregation could prove to be instrumental. One is the chiral sorting of tubes based on differential binding affinity of dispersants[43] that could benefit from facile methods of extraction. The other is applications involving conductivity, where partially aggregated states have been found to perform better (due to lower conductivity percolation thresholds).[44]

EXPERIMENTAL SECTION

Preparation of dispersions, quantification of dispersed CNT and vortex shaking. All dispersions were prepared by weighing 9 mg of carbon powder (routine mass, except where otherwise implicit) into a vial followed by addition of 3 mL of the desired surfactant solution. The concentration of dispersants used can be found in Table S1. The mixtures were then subject to tip sonication for 8.5 min (Bandelin Sonoplus Vb 2070 probe set to a vibration amplitude of 30 % and estimated power density of 1.0 $W \cdot mL^{-1}$), followed by 20 min centrifugation (Breda Scientific centrifuge) at 4000 g (typical *g*-grade, except in the *g* variation study). The concentration of dispersed SWNT in the supernatants, c_{SWNT}, was determined using a previously published methodology, combining TGA and UV-Vis absorbance measurements.[45] The apparent absorbance of the dispersions was measured at 660 nm and by using the apparent extinction coefficient e_{660} previously obtained for each of the surfactants, one could accurately estimate c_{SWNT}. A Breda Scientific vortex mixer (max. 3,000 rpm) with a rubber single cup head was used.

Microscopy imaging. Imaging of the vortexed CNT dispersions was carried out with an Olympus BX51 light microscope, with differential interference contrast (DIC) lenses, and 100 x and 400 x magnifications. Images were acquired with an Olympus C5060 videocamera and software CellA. Some of the vortexed samples containing micron-sized loose aggregates were also imaged by cryogenic scanning electron microscopy, using a JEOL JSM 6301F SEM microscope equipped with a Gatan Alto 2500 cryo-preparation chamber. Each sample was vitrified by plunging it into nitrogen slush (-200 ˚C), followed by freeze-fracture at -140 ˚C. The subsequent sublimation of water (solvent) was done at -95 ˚C for 2 min. The specimen was finally sputtered with an Au-Pd alloy, during 30 s in Ar atmosphere, in the cryo-preparation chamber, before transfer into the microscope. Specimens for cryo-TEM were prepared using Leica EM GP cryo-preparation station operated at 100% relative humidity. A drop of 4 μl of solution was applied on a holey carbon TEM grid (Lacey substrate, 300 mesh, Ted Pella, Inc.) automatically blotted with a filter paper, and plunged into liquid ethane at its freezing point. The vitrified samples were stored under liquid nitrogen before being transferred to a TEM (Tecnai 12, FEI) using a Gatan workstation and cryo-holder for imaging at 98K. The microscope was operated at 120 kV in low electron dose mode (to reduce radiation damage) and with a few micrometers under-focus to increase phase contrast. Images were recorded on a Gatan 794 CCD camera.

SUPPORTING INFORMATION AVAILABLE. SWNT dispersibility curves for surfactants SDBS, SDS, DTAB and CTAB (Figure S1); Tables S1-3 with data for average aggregate size and concentrations used in Figures 2 and 3.

AUTHOR INFORMATION

Corresponding Author:

*Email: efmarque@fc.up.pt

ACKNOWLEDGEMENTS. We kindly acknowledge support from Fundação para a Ciência e Tecnologia (FCT, Portugal) through PEst-C/QUI/UI0081/2013 (CIQ-UP) and the Ph.D. grant SFRH/BD/72612/2010. Thanks are also due to FEDER and FCT/MES through NORTE-07-0124-FEDER-000065. The Swedish Research Council VR is also gratefully acknowledged.

REFERENCES

(1) Breuer, O.; Sundararaj, U. Big returns from small fibers: A review of polymer/carbon nanotube composites. *Polym Composite* **2004,** *25*, 630-645.
(2) Moniruzzaman, M.; Winey, K. I. Polymer nanocomposites containing carbon nanotubes. *Macromolecules* **2006,** *39*, 5194-5205.
(3) Grossiord, N.; Loos, J.; Regev, O.; Koning, C. E. Toolbox for dispersing carbon nanotubes into polymers to get conductive nanocomposites. *Chem. Mater.* **2006,** *18*, 1089-1099.
(4) Hecht, D. S.; Hu, L.; Irvin, G. Emerging Transparent Electrodes Based on Thin Films of Carbon Nanotubes, Graphene, and Metallic Nanostructures. *Adv Mater* **2011,** *23*, 1482-1513.
(5) Kharissova, O. V.; Kharisov, B. I.; de Casas Ortiz, E. G. Dispersion of carbon nanotubes in water and non-aqueous solvents. *RSC Adv.* **2013,** *3*, 24812-24852.
(6) Becker, D.; Coelho, L. A. F. Use of Block Copolymers and Surfactants for the Dispersion of CNTs. *Current Organic Chemistry* **2013,** *17*, 1844-1857.
(7) Wang, H. Dispersing carbon nanotubes using surfactants. *Curr. Opin. Colloid Interface Sci.* **2009,** *14*, 364-371.
(8) Angelikopoulos, P.; Bock, H. The science of dispersing carbon nanotubes with surfactants. *PCCP* **2012,** *14*, 9546-9557.
(9) Antaris, A. L.; Seo, J.-W. T.; Green, A. A.; Hersam, M. C. Sorting Single-Walled Carbon Nanotubes by Electronic Type Using Nonionic, Biocompatible Block Copolymers. *ACS Nano* **2010,** *4*, 4725-4732.

(10) Fernandes, R. M. F.; Buzaglo, M.; Shtein, M.; Pri Bar, I.; Regev, O.; Marques, E. F.; Furó, I. Lateral Diffusion of Dispersing Molecules on Nanotubes As Probed by NMR. *J. Phys. Chem. C* **2014,** *118*, 582-589.
(11) Edri, E.; Regev, O. "Shaken, Not Stable": Dispersion Mechanism and Dynamics of Protein-Dispersed Nanotubes Studied via Spectroscopy. *Langmuir* **2009,** *25*, 10459-10465.
(12) Horn, D. W.; Tracy, K.; Easley, C. J.; Davis, V. A. Lysozyme Dispersed Single-Walled Carbon Nanotubes: Interaction and Activity. *J. Phys. Chem. C* **2012,** *116*, 10341-10348.
(13) Strano, M. S.; Moore, V. C.; Miller, M. K.; Allen, M. J.; Haroz, E. H.; Kittrell, C.; Hauge, R. H.; Smalley, R. E. The role of surfactant adsorption during ultrasonication in the dispersion of single-walled carbon nanotubes. *J. Nanosci. Nanotechnol.* **2003,** *3*, 81-86.
(14) Duan, W. H.; Wang, Q.; Collins, F. Dispersion of carbon nanotubes with SDS surfactants: a study from a binding energy perspective. *Chem Sci* **2011,** *2*, 1407-1413.
(15) Premkumar, T.; Mezzenga, R.; Geckeler, K. E. Carbon Nanotubes in the Liquid Phase: Addressing the Issue of Dispersion. *Small* **2012,** *8*, 1299-1313.
(16) Huang, Y. Y.; Terentjev, E. M. Dispersion of Carbon Nanotubes: Mixing, Sonication, Stabilization, and Composite Properties. *Polymers* **2012,** *4*, 275-295.
(17) Blanch, A. J.; Lenehan, C. E.; Quinton, J. S. Parametric analysis of sonication and centrifugation variables for dispersion of single walled carbon nanotubes in aqueous solutions of sodium dodecylbenzene sulfonate. *Carbon* **2011,** *49*, 5213-5228.
(18) Badaire, S.; Poulin, P.; Maugey, M.; Zakri, C. In situ measurements of nanotube dimensions in suspensions by depolarized dynamic light scattering. *Langmuir* **2004,** *20*, 10367-10370.
(19) Green, M. J. Analysis and measurement of carbon nanotube dispersions: nanodispersion versus macrodispersion. *Polymer International* **2010,** *59*, 1319-1322.
(20) Hashizaki, K.; Kageyama, T.; Inoue, M.; Taguchi, H.; Ueda, H.; Saito, Y. Study on preparation and formation mechanism of n-alkanol/water emulsion using alpha-cyclodextrin. *Chemical & Pharmaceutical Bulletin* **2007,** *55*, 1620-1625.
(21) Ruan, G.; Ng, J. K.; Feng, S. S. Effects of polymer, organic solvent and mixing strength on integrity of proteins and liposomes encapsulated in polymeric microspheres fabricated by the double emulsion process. *Journal of Microencapsulation* **2004,** *21*, 399-412.
(22) Muir, B. W.; Zhen, G. L.; Gunatillake, P.; Hartley, P. G. Salt Induced Lamellar to Bicontinuous Cubic Phase Transitions in Cationic Nanoparticles. *J Phys Chem B* **2012,** *116*, 3551-3556.
(23) Dams, R.; Lambert, W. E.; Comhaire, F.; De Leenheer, A. P. Production and characterization of sulforhodamine B containing large unilamellar vesicles labeled with atrazine. *Analytica Chimica Acta* **1999,** *399*, 185-191.
(24) Chekli, L.; Phuntsho, S.; Roy, M.; Shon, H. K. Characterisation of Fe-oxide nanoparticles coated with humic acid and Suwannee River natural organic matter. *Science of the Total Environment* **2013,** *461*, 19-27.

(25) Stojakovic, J.; Farris, B. S.; MacGillivray, L. R. Vortex grinding for mechanochemistry: application for automated supramolecular catalysis and preparation of a metal-organic framework. *Chem Commun* **2012,** *48*, 7958-7960.
(26) Le Bihan, O. L. C.; Ustache, A.; Bernard, D.; Aguerre-Chariol, O.; Morgeneyer, M. Experimental Study of the Aerosolization from a Carbon Nanotube Bulk by a Vortex Shaker. *J Nanomater* **2014**.
(27) Wang, H.; Zhou, W.; Ho, D. L.; Winey, K. I.; Fischer, J. E.; Glinka, C. J.; Hobbie, E. K. Dispersing single-walled carbon nanotubes with surfactants: A small angle neutron scattering study. *Nano Letters* **2004,** *4*, 1789-1793.
(28) Schilling, T.; Jungblut, S.; Miller, M. A. Depletion-Induced Percolation in Networks of Nanorods. *Phys Rev Lett* **2007,** *98*, 108303.
(29) Regev, O.; ElKati, P. N. B.; Loos, J.; Koning, C. E. Preparation of conductive nanotube-polymer composites using latex technology. *Adv Mater* **2004,** *16*, 248-251.
(30) Zakri, C.; Poulin, P. Phase behavior of nanotube suspensions: from attraction induced percolation to liquid crystalline phases. *J Mater Chem* **2006,** *16*, 4095-4098.
(31) Hough, L. A.; Islam, M. F.; Hammouda, B.; Yodh, A. G.; Heiney, P. A. Structure of semidilute single-wall carbon nanotube suspensions and gels. *Nano Letters* **2006,** *6*, 313-317.
(32) Zhou, W.; Islam, M. F.; Wang, H.; Ho, D. L.; Yodh, A. G.; Winey, K. I.; Fischer, J. E. Small angle neutron scattering from single-wall carbon nanotube suspensions: evidence for isolated rigid rods and rod networks. *Chemical Physics Letters* **2004,** *384*, 185-189.
(33) Chen, Q.; Saltiel, C.; Manickavasagam, S.; Schadler, L. S.; Siegel, R. W.; Yang, H. C. Aggregation behavior of single-walled carbon nanotubes in dilute aqueous suspension. *J Colloid Interf Sci* **2004,** *280*, 91-97.
(34) Schaefer, D. W.; Zhao, J.; Brown, J. M.; Anderson, D. P.; Tomlin, D. W. Morphology of dispersed carbon single-walled nanotubes. *Chemical Physics Letters* **2003,** *375*, 369-375.
(35) Lin-Gibson, S.; Pathak, J. A.; Grulke, E. A.; Wang, H.; Hobbie, E. K. Elastic flow instability in nanotube suspensions. *Phys Rev Lett* **2004,** *92*.
(36) Kim, T.-H.; Doe, C.; Kline, S. R.; Choi, S.-M. Organic solvent-redispersible isolated single wall carbon nanotubes coated by in-situ polymerized surfactant monolayer. *Macromolecules* **2008,** *41*, 3261-3266.
(37) Fernandes, R. M. F.; Abreu, B.; Claro, B.; Buzaglo, M.; Regev, O.; Furó, I.; Marques, E. F. Dispersing carbon nanotubes with ionic surfactants under controlled conditions: comparisons and insights. *Langmuir* **2015,** *31*, 10955−10965.
(38) Bandyopadhyaya, R.; Nativ-Roth, E.; Regev, O.; Yerushalmi-Rozen, R. Stabilization of individual carbon nanotubes in aqueous solutions. *Nano Letters* **2002,** *2*, 25-28.
(39) Nguyen, T. T.; Shklovskii, B. I. Kinetics of macroion coagulation induced by multivalent counterions. *Physical Review E* **2002,** *65*.
(40) Frise, A. E.; Pages, G.; Shtein, M.; Pri Bar, I.; Regev, O.; Furó, I. Polymer binding to carbon nanotubes in aqueous dispersions: Residence time on the nanotube surface As Obtained by NMR diffusometry. *J. Phys. Chem. B* **2012,** *116*, 2635-2642.
(41) Frise, A. E.; Edri, E.; Furo, I.; Regev, O. Protein Dispersant Binding on Nanotubes Studied by NMR Self-Diffusion and Cryo-TEM Techniques. *J. Phys. Chem. Lett.* **2010,** *1*, 1414-1419.

(42) Rocha, J.; Fernandes, R. M. F.; Regev, O.; Furó, I.; Marques, E. F. Assessing surfactant binding to carbon nanotubes via competitive adsorption: binding strength and critical coverage. *Manuscript* **2015**.
(43) Oh, H.; Sim, J.; Ju, S. Y. Binding Affinities and Thermodynamics of Noncovalent Functionalization of Carbon Nanotubes with Surfactants. *Langmuir* **2013,** *29*, 11154-11162.
(44) Bryning, M. B.; Islam, M. F.; Kikkawa, J. M.; Yodh, A. G. Very low conductivity threshold in bulk isotropic single-walled carbon nanotube-epoxy composites. *Adv Mater* **2005,** *17*, 1186-1191.
(45) Shtein, M.; Pri-bar, I.; Regev, O. A simple solution for the determination of pristine carbon nanotube concentration. *Analyst* **2013,** *138*, 1490-1496.

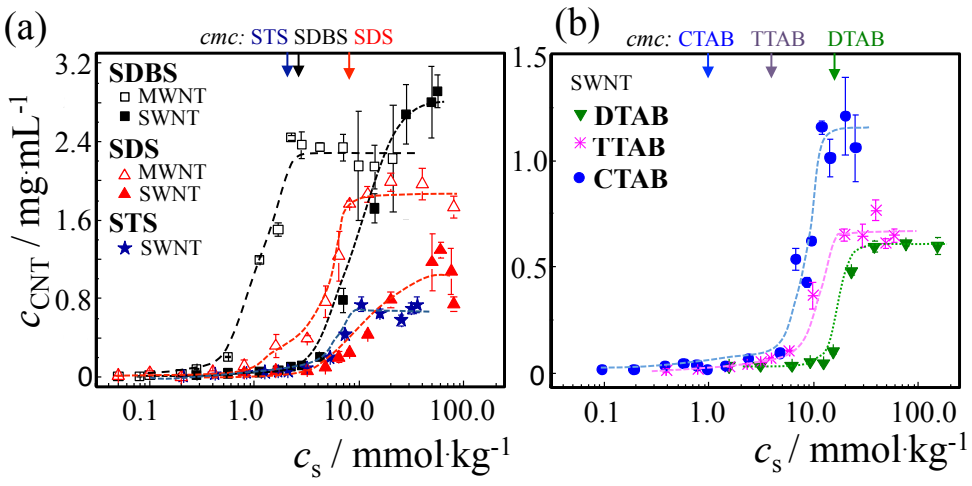

Figure S1. SWNT dispersibility curves for SDBS, SDS, DTAB and CTAB (from ref.[36]).

Table S1. Average aggregate size $\langle L_a \rangle$ (as obtained by light microscopy) for the different surfactant-assisted dispersions as function of vortexing time (c_{SWNT} = 0.3 mg·mL^{-1}).

Vortex time		$\langle L_a \rangle$ / μm						
/ s		**SDBS**	**SDS**	**DTAB**	**CTAB**	**F127**	**F68**	**TX100**
10		---	26±14	37±27	11±4	---	71±35	12±12
20		---	41±23	54±34	28±15	---	104±79	29±18
60		22±14	68±33	96±53	35±19	15±7	107±68	39±23
120		28±12	102±91	114±65	53±23	21±10	132±81 142±12	65±35
300		42±19	125±60	107±63	60±35	28±13	7	64±36
Concentration	/ mg·mL^{-1}	2.51	3.51	12.5	3.18	3.04	3.00	3.02
of dispersant	/ mmol·kg^{-1}	7.2	12.2	40	8.7	-	-	4.7

Table S2. Effect of varying g (before vortexing) on average aggregate size $<L_a>$ for SDS-assisted dispersions (c_s = 3.51 mg.mL^{-1}; c_{SWNT} = 0.3 mg·mL^{-1}).

	$<L_a>$ / μm			
vortex time / s	2,000 g	4,000 g	10,000 g	30,000 g
60	52±28	55±34	11±9	13±8
120	85±42	94±47	41±37	18±10
300	114±42	111±56	91±44	93±37
600	---	---	---	110±41

Table 3. Effect of dispersed SWNT concentration on average aggregate size $<L_a>$ for SDS-assisted (c_s = 3.51 mg.mL^{-1}) and DTAB-assisted (12.5 mg.mL^{-1}) dispersions.[a]

	$<L_a>$ / μm	
c_{SWNT} / mg·mL^{-1}	SDS	DTAB
0.15	25±13	89±38
0.30	134±72	202±87
0.60	144±82	155±116

[a]For the preparation of the dispersions with fixed c_s = 3.51 mg.mL^{-1}, an initial SWNT dispersion at c_{SWNT} = 0.60 mg·mL^{-1} was prepared and then diluted to the other SWNT concentrations with the surfactant solution at 3.51 mg·mL^{-1}. For the DTAB dispersions, a correspondingly similar procedure was used.

VI

Gemini surfactants as dispersants of multiwalled carbon nanotubes: a systematic study on the role of molecular structure

Jessica Rocha, Ricardo M.F. Fernandes, Oren Regev, István Furó and Eduardo F. Marques

Submitted for publication

Gemini Surfactants as Dispersants of Multiwalled Carbon Nanotubes: a Systematic Study on the Role of Molecular Structure

Jessica Rocha[1], Ricardo M.F. Fernandes,[1,2] Oren Regev[3,4], István Furó[2] and Eduardo F. Marques[1*]

[1]*Centro de Investigação em Química, Department of Chemistry and Biochemistry, Faculty of Science, University of Porto, Rua do Campo Alegre, s/n, P-4169-007 Porto, Portugal.*

[2]*Division of Applied Physical Chemistry, Department of Chemistry, KTH Royal Institute of Technology, SE-10044 Stockholm, Sweden.*

[3]*Department of Chemical Engineering and* [4]*Ilse Katz Institute for Nanotechnology, Ben-Gurion University of the Negev, 84105 Beer-Sheva, Israel.*

*email: efmarque@fc.up.pt

Abstract

Surfactants have been widely used as non-covalent dispersants of carbon nanotubes and yet a deeper and systematic understanding of the role of their molecular properties on dispersibility still awaits consensus. Herein, we report on the dispersibility of multiwalled carbon nanotubes (MWNTs) using a set of dicationic gemini surfactants of the *n*-s-*n* type, where both the length of the covalent spacer (*s*) that bridges the two cationic headgroups and the length of the tails (*n*) are systematically varied. Thus, 12-s-12 gemini with *s* = 2, 6, and 12 are studied together with 16-s-16 (*s* = 2 and 12). In addition, the single-tailed homologues dodecyltrimethylammonium bromide, DTAB (*n* = 12), and cetyltrimethylammonium bromide, CTAB (*n* = 16), are employed for comparisons. High precision dispersion curves (dispersed NT vs. surfactant concentration) are presented, obtained through a well-controlled sonication/centrifugation procedure combined with an accurate determination of MWNT concentration. The gemini amphiphiles, despite being double-tailed and double-charged, are found to be less effective dispersants than CTAB and roughly as effective as DTAB. Among the gemini, the following pattern emerges as concerning dispersion behavior. (i) The tail length, *n*, is less influential than spacer length, *s,* in dispersing ability, implying that the spacer hydrophobicity rather than that of the tail may govern the affinity for the nanotube surface. (ii) In the 12-s-12 series, the surfactant concentration needed for maximum MWNT dispersibility depends linearly on *s*, while it is known that the neat *cmc* depends non-monotonically on *s*. (iii) Similarly to single-tailed ionic surfactants, the presence of micelles has no direct effect on the dispersion behavior. In combination, these observations also point to an adsorption mechanism that does not involve the formation of micelle-like aggregates on the nanotube surface but rather coverage by individual dispersant molecules.

1. Introduction

Carbon nanotubes (CNTs) are extremely long and extremely narrow cylinders of graphene sheets. What gives them a combined set of unique mechanical, thermal, optical and electrical properties[1,2] comes also with a heavy price: the high aspect ratio and strong van der Waals (vdW) cohesive forces results in agglomeration into bundles. Since many applications rely on isolated tubes, where the properties (e.g. strength) are optimized, this is a major hurdle for the applicability of CNTs. Hence significant efforts have been made over the years to produce well-dispersed nanotubes from powders made up by large grains of tightly agglomerated tubes.[3,4] One of the most common approaches in aqueous media is to employ amphiphilic dispersants—namely surfactants[5-14], synthetic polymers[15-20], DNA[21,22] and proteins[23-27]—which not only bind to the CNT surface via hydrophobic moieties but also provide hydrophilicity and colloidal stabilization through the polar regions. The obtained dispersions (which are not true solutions)[4] are kinetically stabilized by charge repulsions for ionic dispersants or steric hindrance for nonionic ones.

A large number of low molecular-weight dispersants, ranging from ionic to nonionic and covering a wide scope of molecular properties, has been reported in the literature.[7-14,28-32] The variety of molecular features of the surfactants (e.g. chain length, headgroup polarity, presence of aromatic moieties), together with variation among carbon nanotube batches and processing conditions, often makes comparisons very difficult and obscures a fundamental understanding of the dispersion process. Thus, studies where molecular features are systematically varied and the dispersibility data are accurate and precise, are required.[9-13,33] One of the key issues still awaiting clarification is the type of arrangement of the surfactant molecules on the curved surface of the CNTs. Randomly adsorbed molecules, monolayers or aggregates like spherical micelles and hemimicelles, or even fully wrapping coverage, have been proposed, even though there is relatively scarce experimental evidence.[34,35] Molecular simulations have also provided somewhat disparate views.[12,36] Another relevant question pertains to adsorption and equilibrium aspects, namely the surfactant fraction and surface coverage that are needed to achieve maximal dispersibility (i.e. CNT saturation in the dispersion).

The dispersion of MWNTs using various types of ionic and nonionic single-tailed surfactants has been extensively reported (cf. reviews[3,4,9,37]). In the current work, we resort, alternatively, to a series of dicationic gemini surfactants of the general structure $[C_nH_{2n+1}(CH_3)_2N^+(CH_2)_sN^+(CH_3)_2C_nH_{2n+1}]2Br^-$, conveniently abbreviated here by *n-s-n*

(Figure 1), where the length of the alkyl tail, *n*, and that of the spacer chain linking the two headgroups, *s*, are varied. Thus, 12-*s*-12 gemini with *s* = 2, 6, and 12 are studied together with 16-*s*-16, with *s* = 2 and 12; the single-tailed homologues dodecyltrimethylammonium bromide, DTAB (*n* = 12), and cetyltrimethylammonium bromide, CTAB (*n* = 16), are also employed for direct comparison. Besides assessing the ability of these surfactants as dispersants, our aims are to explore in a systematic way how charge, its separation, and the hydrophobicity affect the ability to disperse MWNTs for molecules that are very different from conventional single-tailed surfactants. In fact, dimeric gemini surfactants are peculiar on two accounts: they possess two polar headgroups (and if they are charged, this means potentially stronger electrostatic effects) and the covalent spacer between them can be made flexible or rigid, short or long.[38-41] Hydrophobicity can thus be controlled through *n* and *s*, and in parallel, the charge-to-charge distance also controlled by *s*. These compounds present superior colloidal properties (lower *cmc*s, higher surface activity and more versatile self-assembly) when compared to their conventional single-tailed (monomeric) homologues.[38-44] Owing to their enhanced performance, they find applications as emulsifiers, detergents, dispersants, gelators, wetting agents, antimicrobial and gene transfection agents.[38-50]

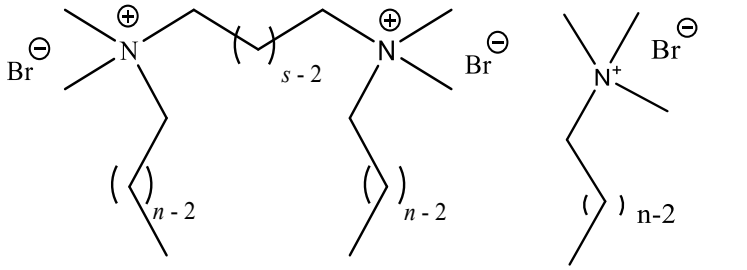

12-2-12 *n* = 12 *s* = 2
12-6-12 6
12-12-12 12

16-2-16 *n* = 16 *s* = 2
16-12-16 12

DTAB *n* = 12
CTAB *n* = 16

Figure 1. Chemical structure of the surfactants herein used: gemini bis(quaternary ammonium) surfactants, 12-*s*-12 and 16-*s*-16; DTAB, dodecyltrimethylammonium bromide; CTAB, cetyltrimethylammonium bromide.

The *cmc* of bis-quat gemini surfactants of the type used here varies with tail length, *n*, in the same trend as for single-tailed surfactants, i.e., it decreases exponentially with *n*. However, the dependence of *cmc* on the hydrophobic spacer length *s* is more complex,

showing to be non-monotonic: at constant n, the *cmc* first increases with s to a maximum at about s = 5 or 6 and then decreases until s = 10-12.[39] This has been interpreted that for $s \leq 6$ the spacer is exposed to the aqueous environment with a resulting interfacial Gibbs energy penalty, whereas for $s > 10$ the spacer bends inside into the micellar hydrophobic core thus strengthening the hydrophobic effect. Moreover, short spacers (s = 2, 3 or 4) originate long threadlike micelles while long ones lead to small rodlike micelles.[39,42,51] In addition, the spacer length of bis-quat and other families of gemini surfactants has been found to have critical influence on several physicochemical features of mixed systems, e.g. melting behavior of bilayers[52,53], binding onto polyelectrolytes[54], nanocrystal synthesis[55], stabilization of silver nanoparticles[56] and transfection efficiency of genetic materials into cells.[47]

With respect to gemini surfactants as dispersants for carbon nanotubes, there are only a few reports. Some encompass the dispersibility of MWNTs in water by *bis*-quat gemini of the type investigated here[57,58], thermal conductivity enhancement studies[59] and molecular dynamics simulations of their adsorption on SWNTs[60], looking for spacer effects. Other studies have reported on the dispersibility of MWNTs with novel ionic liquid-based gemini amphiphiles in water[30,61-64] or sulfonate-based gemini in organic solvents.[65] However, a systematic and comprehensive investigation of the dispersion behavior with varying spacer and tail lengths is not available, and it could greatly influence future applications. As will be shown in what follows, we have observations and conclusions that differ from some of those previous studies.

As in a recent work[13], we follow a stringent experimental protocol to prepare the dispersions. Sonication and centrifugation parameters are known to have considerable influence on the concentration of dispersed CNTs, and on the bundle length and width distributions.[11,31,37,66] A strict control of the processing parameters, suitable statistics, and a method for accurate MWNT quantification (that combines TGA and UV-vis absorption spectroscopy) are relied upon to obtain high-quality dispersion curves, sufficient to extract comparative metrics. The latter include the critical surfactant concentration for dispersibility (*cdc*), the maximum dispersed CNT concentration ($c_{\mathrm{MWNT,max}}$), and respective surfactant concentration at that point ($c_{\mathrm{s,max}}$). The results will be interpreted and critically compared to those obtained in previous studies with gemini and more conventional single-tailed surfactants.

2. Experimental Section

2.1 Materials. MWNTs (d = 8 – 15 nm and L = 10 – 50 μm) were used as received from CheapTubes. All the alkanediyl-α,ω-bis(alkyldimethylammonium bromide) dimeric surfactants used here, and abbreviated as 12-s-12 (s = 2, 6, and 12) and 16-s-16 (s = 2 and 12), were synthesized according to the method described by Menger and Littau[41] and purified by recrystallization. The purity of the compounds was evaluated by NMR and mass spectrometry and further confirmed by the *cmc* values, obtained by conductivity measurements (cf. also Fig. S1 and Table S2 in Supporting Information), and in good agreement with previous reports.[39] DTAB and CTAB were acquired from Sigma Aldrich (purities ≥ 99 %) and used as received, with *cmc* values in line with those typically reported.[67]

2.2 Preparation of CNT dispersions. The CNT-surfactant mixtures were initially prepared by weighing the carbon material, 9 mg, followed by addition of the desired surfactant solution, 3 mL, resulting in a 0.3 wt% CNT mixture. All stock surfactant solutions were prepared in ultrapure water above Krafft temperature to ensure full dissolution. For sonication, a Bandelin Sonoplus Vb 2070 probe with a freshly polished 3 mm microtip was used, with a vibration amplitude set to 30 % and a sonication time to 8.5 min. In order to ensure identical sample treatment, a rigorous procedure, previously established[13], was followed: 1) the sonication energy density transferred to the sample was kept constant and estimated as 5.3 x 10^2 J·mL^{-1} from calorimetric measurements resulting in an average power density of 1.0 W·mL^{-1}; 2) the tip was always placed in the same position inside the same type of vial (1 cm from the bottom); 3) temperature was controlled with an external thermostated bath and set above the Krafft temperature of the surfactants (*viz*. set to 25 ºC, except for CTAB, 30 ºC, and 16-2-16, 45 ºC). After sonication, the samples were centrifuged during 20 min at 4,000 g. After centrifugation, the top 2 mL of the supernatant were separated from the precipitate by decantation for the measurement of MWNT concentration.

2.3 Quantification of CNT concentration. Absolute carbon nanotube concentration in the supernatant was determined using a previously published method.[68] An accurately measured aliquot of each dispersion was lyophilized during 24-48 h. In order to quantify the mass fraction of surfactant present on the solid, thermogravimetric analysis (TGA) was performed using a Mettler Toledo Star System under N_2 atmosphere (flow rate of 50 mL·min^{-1}). Simple mass balance allows the quantification of MWNT concentration in the supernatant.[68] Calibration curves (TGA-UV-vis) were then obtained for each surfactant, by measuring absorbance versus c_{CNT} at λ = 660 nm (ensuring null absorption from surfactant),

using dilutions from a stock dispersion with known MWNT mass concentration. A double-beam Spectrophotometer U-2001 was used, with a plastic cuvette with optical path of 1 cm. For each dispersion composition, 3-5 independent preparations were made and 3 sampling spectrophotometric measurements done.

On the basis of Beer-Lambert law and the linear regimes observed, the apparent extinction coefficients, ε_{660}, were determined (Fig. 2; cf. also Table S1, S. I.), yielding a mass-apparent absorbance calibration curve that clusters for the different surfactants around 40 ± 2 $mL \cdot mg^{-1} \cdot cm^{-1}$, in line with previous reports.[11,13] The MWNT concentrations were then determined from their apparent absorbance.

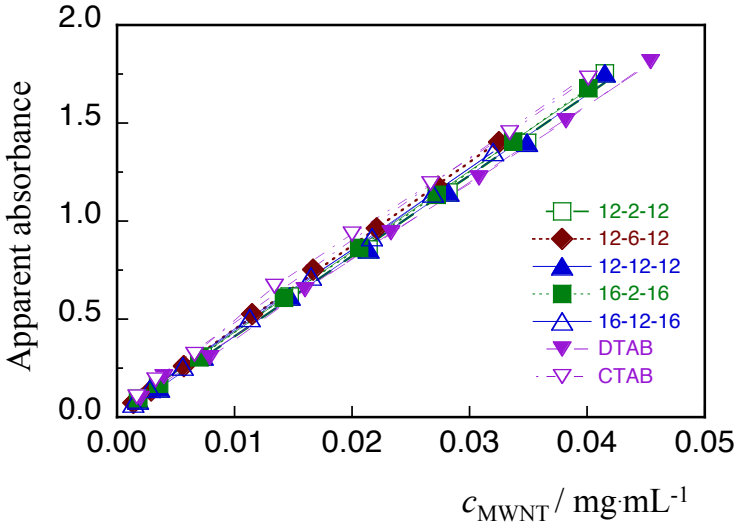

Figure 2. Apparent absorbance (λ = 660 nm) vs. MWNT nanotube concentration for the different surfactant-assisted dispersions.

2.4 Zeta potential. The zeta potential, ζ, of the dispersed particles was measured at 25 ºC using a zeta sizer Nano ZS, ZN 3500, with a 4 mW He-Ne laser (633 nm) and DTS 1060C disposable zeta cells. The electrophoretic mobility, μ, was measured using a combination of electrophoresis and laser Doppler velocimetry techniques and ζ was calculated from μ using the known Henry equation.[8,69] A dielectric constant of 78.5, a medium viscosity of 0.89 cP and a $f(\kappa a)$ function value of 1.5 were used, following previously reported assumptions.[8,69] All ζ values are average values based on at least 2 independent dispersions.

3. Results and Discussion

3.1. Dispersibility curves and extracted parameters. The effect of increasing surfactant concentration, c_s, on the dispersed MWNT concentration, c_{CNT} was monitored. The obtained curves are shown in Fig. 3(a)-(c), where c_s, varied typically in the range (0.1-10) x *cmc* for each surfactant, is given on log scale (in order to enhance features at low c_s). Prior to a detailed analysis of these curves, a few points must be taken into consideration. The initial undispersed CNT mass is constant in all systems, 3 mg·mL^{-1} and c_s (expressed in molality, surfactant amount per mass of solvent in kg) is the surfactant concentration in the *initial* mixture, not the final one in the supernatant. For comparisons, the *cmc* of each neat surfactant is indicated by an arrow at the top of the graph and it is expected to be some 10-30 % lower than cmc_d, the surfactant concentration above which free micelles exist in the dispersion. This difference is due to the uptake of surfactants by the dispersed tubes.[70]

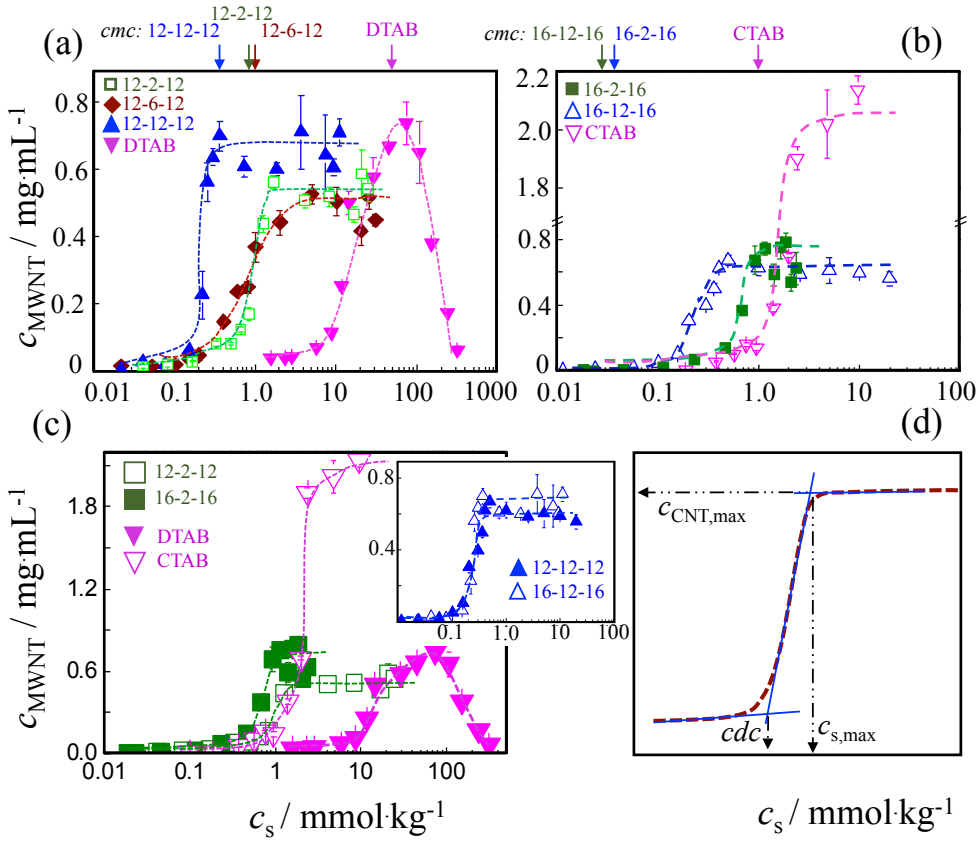

Figure 3. Concentration of dispersed MWNTs vs. surfactant concentration (log scale): (a) for the 12-*s*-12 gemini, including DTAB for comparison; (b) for the 16-*s*-16 gemini, including CTAB for comparison; (c) comparison of chain length effects for homologues 12-2-12/16-2-12, 12-12-12/16-12-16 (shown as an inset) and DTAB/CTAB; (d) representative curve with the graphical definition of the dispersion parameters. Lines are for visual guidance.

All the dispersion curves in Fig. 3a-3c show a sigmoidal profile, in line with previous results for various single-tailed surfactants,[13] and similar to the cooperative binding isotherms of surfactants on various surfaces.[67] Following the schematic curve in Fig. 3d, beyond a given surfactant concentration—*cdc,* the critical dispersibility concentration—the concentration of dispersed MWNT rises more or less steeply and then tends to a plateau (saturation) value, $c_{CNT,max}$, at a surfactant concentration of $c_{s,max}$.

These characteristic parameters can be extracted using appropriate linear regression statistics (cf. also Tables S2-S3, S.I.). For some surfactants, in particular for DTAB (Fig. 3a), the dispersibility drops visibly owing to depletion flocculation effects (an effect that we could reproduce at typically c_s > 10 x *cmc*).[9] In those cases, we chose to represent $c_{CNT,max}$ not as an average value for the apparent plateau but as the maximum reached value. We note also that under the sonication/centrifugation conditions used, the dispersions are expected to consist of a distribution of isolated tubes and thin bundles.[18]

For comparative purposes, the dispersion effectiveness, η, and the dispersion efficiency, η^* are also introduced. The effectiveness is a measure of the capability of a surfactant to disperse a certain mass of MWNT with the relation to the initial loading, and is simply defined as:

$$\eta = \frac{c_{MWNT,max}}{c_{MWNT,in}} \times 100 \quad (1)$$

where $c_{CNT,in}$ is the initial powder MWNT mass per volume of solution (herein, 3 mg·mL^{-1}). The dispersion efficiency, η^*, is defined as:

$$\eta^* = \frac{\eta}{c_{s,max}} \quad (2)$$

and expressed in units of %·kg·mmol^{-1}. For an ideal dispersant, maximal dispersibility (high η) should be attained at the lowest possible $c_{s,max}$ and hence η^* not only has practical relevance but also carries a molecular meaning. Higher η^* could imply e.g. a comparatively higher binding fraction of surfactant, stronger repulsive forces leading to stabilization, or a combination of molecular factors that turn the surfactant efficient as a dispersant.[9,12]

3.2. Role of surfactant concentration and structure on dispersibility. Since the *cmc* allows one to gauge the role of the surfactant state (unimer vs. micelle) in the dispersibility, the ratios *cdc*/*cmc* and $c_{s,max}$/*cmc* are used against *s* in Fig. 4(a), for both the 12-s-12 series, upper graph, and 16-s-16 series, lower graph (cf. also Table S2, S.I.). The dashed lines marking unity ratios

serve to assess the relative importance of *cmc* on dispersibility. For the 12-s-12 series in Fig 3(a), there is a continuous shift toward a steeper rise with increasing *s* of the dispersibility above *cdc*, meaning higher cooperativity in binding. The DTAB curve is shifted to much higher concentrations, by about two decades compared to the gemini. With respect to the 16-s-16 series, Fig. 3(b), the pattern with gemini is essentially similar, but the most striking aspect is that CTAB is able to attain a much higher $c_{CNT,max}$ (Table 1). If we now compare tail length effects, in Fig 3(c), the most notable effect is the sharp difference between DTAB and CTAB in all dispersibility parameters. Within corresponding gemini pairs, the differences are much weaker: 16-2-16 attains a slightly higher plateau than 12-2-12 and for slightly lower $c_{s,max}$, but for the longer spacer, it is 12-12-12 that disperses slightly more than 16-12-16 (Table 1).

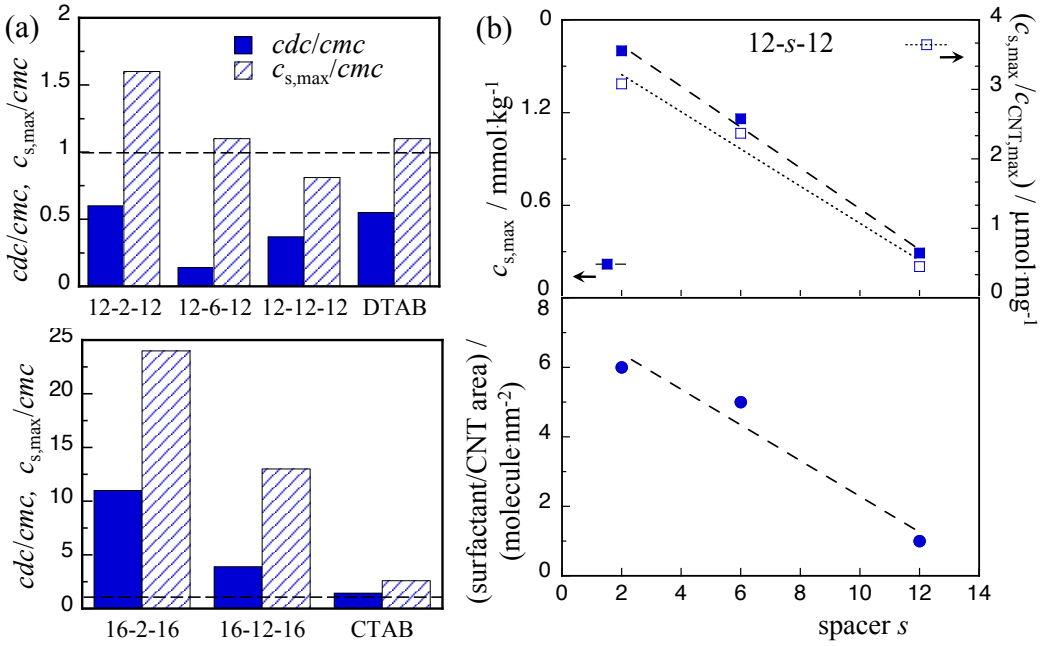

Figure 4. Dispersion parameters for the 12-s-12 and 16-s-16 gemini surfactants and their single-tailed homologues DTAB and CTAB: (a) *cdc* and $c_{s,max}$ relative to *cmc*; the dashed horizontal lines mark the unity value.

From the data in Fig 4(a), it is obvious that for all C12 surfactants (gemini and DTAB), the take off of dispersibility does not depend on micelles being present (that is, *cdc* < *cmc*). With respect to maximal dispersibility, one can observe that 12-12-12, the most effective gemini surfactant (as detailed below) attains it well below *cmc*, whereas for all others that occurs just about *cmc*. In contrast, Fig. 4(a) also shows that any meaningful dispersibility of the C16 surfactants requires concentrations well above *cmc*. However, here

we must bear in mind that the *cmc* of 16-2-16 and 16-12-12 are in the range of 30-40 $\mu mol \cdot kg^{-1}$ and hence much lower than that of all other surfactants by about 2 orders of magnitude (cf. Table S2, S.I.); consequently, any effective concentrations for dispersibility must lie necessarily well above their *cmc*.

Table 1. Surfactant concentration ($c_{s,max}$) and CNT concentration ($c_{CNT,max}$) at maximal dispersibility (saturation) and respective surfactant available per unit CNT area, using a specific surface area of 3 x 10^2 $m^2 \cdot g^{-1}$ for the MWNTs (statistical analysis is found in Table S2, S.I.)

Surf.	$c_{s,max}$ /($\mu mol \cdot mL^{-1}$)	$C_{CNT,max}$ /($mg \cdot mL^{-1}$)	surfactant amount per CNT area / ($\mu mol \cdot m^{-2}$)	surfactant molecules per CNT area / ($molec \cdot nm^{-2}$)
12-2-12	1.6	0.52	10.3	6
12-6-12	1.2	0.49	7.9	5
12-12-12	0.29	0.64	1.5	1
16-2-16	0.95	0.70	4.5	3
16-12-16	0.41	0.61	2.2	1
DTAB	15.9	0.58	91.6	55
CTAB	2.5	2.0	4.2	3

A global analysis of these data strongly suggest that micelles do not have any particular role on dispersibility, but rather that it is surfactant concentration, irrespective of the surfactant being in unimer or micelle form, that matters for exfoliation. This is particularly evident for 12-12-12, clearly the most efficient of the 5 gemini investigated (see also below). These observations are in agreement with those reported for dispersions of MWNTs and SWNTs by various single-tailed surfactants, including the anionic surfactants sodium dodecylbenzenesulfonate (SDBS) and sodium dodecyl sulfate (SDS), where no correlation was found between the surfactant dispersing ability and its *cmc*.[13]

Interestingly, for the 12-s-12, there is an apparent linear dependence of $c_{s,max}$ and the ratio $c_{s,max}/c_{CNT,max}$ versus *s*, as shown in Fig 4(b), upper graph. By choosing a specific surface area of 3 x 10^2 $m^2 \cdot g^{-1}$ for the MWNTs[71], we can estimate the surfactant amount per nanotube surface area for all surfactants at saturation (Table 1). A word of caution here: this indicator does not yield the number of *bound* molecules but the number of molecules *available* in the

dispersion per nm^2 of MWNT. Table 1 then shows that this indicator decreases with spacer at constant *n* (both for the 12 and 16 series), while the effect of tail at constant *s* is not evident (a decrease for the pair 12-2-12/16-2-16 but constant values within 12-12-12/16-12-16). Our conclusion is that spacer rather than tail length is the most determining factor affecting the ability of gemini as dispersants.

3.3. In-depth analysis of dispersibility per surface area and comparative adsorption. The surface area analysis of dispersibility in Table 1 is based on the assumption that only individual MWNTs are present and that their specific surface area is ca 3 x 10^2 $m^2.g^{-1}$, a reasonable value considering the average dimensions of the used tubes.[71] The results in Table 1 seem to be essentially consistent with a surface coverage of 3 molecule·nm^{-2} at saturation previously reported for SDBS on multiwalled tubes.[72] The rather discrepant value is that of DTAB. If we assume that similarly few molecules of this surfactant (about 3-5 per nm^2) are needed for saturation, the conclusion is that most DTAB molecules remain in the bulk (either as unimers or in micelles). This illustrates how inefficient a surfactant DTAB is, compared to all the other compounds tested here. The value of 1 molecule·nm^{-2} obtained for 12-12-12 and 16-12-16 is noteworthy and allows for some speculation: under the assumption of a perpendicular type binding of the molecules onto the NT surface (with reference to the tails), this value does not seem to convey a picture of dense coverage of dispersant around the nanotubes.

For the 12-s-12 series, a linear decrease with *s* is found for the number of surfactant molecules per unit area at maximum dispersibility, as shown in Fig. 4(b), lower graph. Two explanations can be envisaged for this effect. (1) If we assume that identical surface coverage is needed at saturation for the three 12-*s*-12 surfactants, then a surfactant with a more hydrophobic spacer (and hence, presumably, stickier) would achieve this value at lower concentration because the fraction of adsorbed surfactant would rise with surfactant hydrophobicity. (2) Alternatively, we could assume that it is the degree of surface coverage that increases with spacer length. While it is not easy to discern between the two mechanisms with the data available, some support for mechanism (2) comes from zeta potential studies described below.

Fig. 5 shows the zeta potential of several dispersions as a function of surfactant concentration, for values below *cmc* (hence measuring ζ of the surfactant-coated CNTs and not of micelles) corresponding to the regions of MWNT dispersibility (< 0.1 mg·mL^{-1}, Fig. 3), close to *cdc*. One sees that as c_s increases for 12-2-12, 12-12-12 and CTAB, ζ increases. In

addition, and significantly, 12-12-12-coated MWNTs show the highest ζ, followed by 12-2-12, whereas DTAB-coated MWNTs show the lowest.

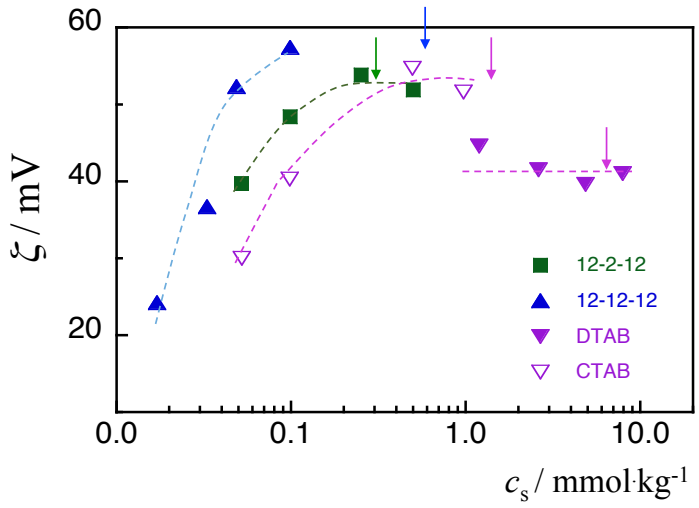

Figure 5. Zeta potential for MWNT dispersions vs. surfactant concentration for 12-2-12, 12-12-12, DTAB and CTAB; the *cmc* of the surfactants are marked. The corresponding concentration of suspended MWNT can be followed by reporting to the dispersibility curves in Fig. 3.

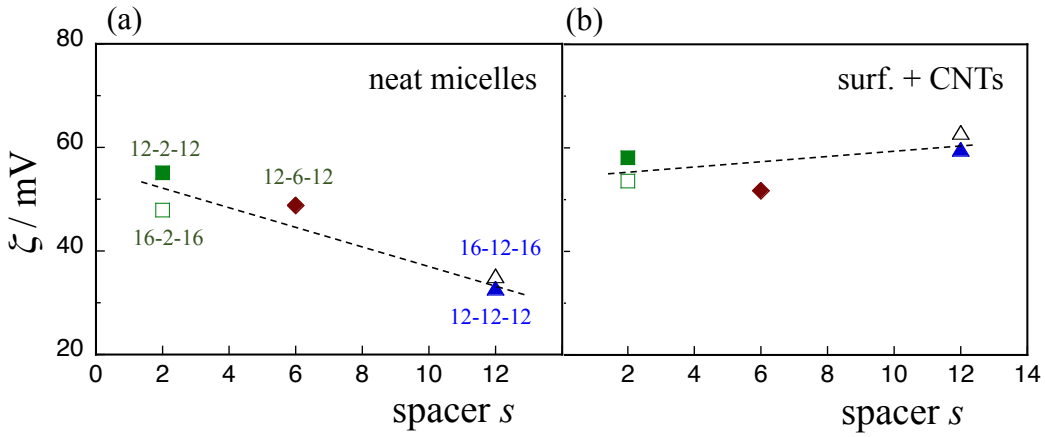

Figure 6. Zeta potential vs. the number of carbons in the spacer, *s,* for: (a) neat gemini micelles, $c_s = 2$ mmol·kg^{-1}; (b) MWNT dispersions, $c_s = 2$ mmol·kg^{-1} and $c_{CNT} = 0.1$ mg·mL^{-1}.

Experiments on dispersions with identical surfactant concentration and identical mass of dispersed MWNTs, as shown in Fig. 6 (such dispersions require special preparation; cf. S.I. and Table S4 for details), provide additional support together with the ζ values for the neat gemini micelles. We observe that in the case of neat micelles, ζ decreases with *s* (likely due to

changes in micellar shape), for both the C12 and C16 series. In striking contrast, when nanotubes are present, ζ, if any, increases with *s*. Since the same mass of MWNT and the same amount of surfactant are present in these dispersions, the conclusion is that there is slightly increasing coverage with increasing *s* (that is, under the assumptions of higher coverage/higher surface charge density and a similar degree of debundling).

Another important aspect is unveiled by the results in Fig. 4(b) and Fig. (6). It is known that for a family of gemini with similar *n*, the *cmc* varies non-monotonically with *s*, as we pointed above. The *cmc* first rises (rather counterintuitively) with the increase in the number of hydrophobic methylene groups, attains a maximum at *s* = 4-6 (depending on *n*) and then decreases as normally expected.[39] Clearly, we do not see such effects in the trends of $c_{s,max}$, $c_{s,max}/c_{CNT,max}$ and zeta potential. Instead, monotonic patterns emerge, in particular the linearities in Fig. 4(b). Consequently, one can reasonably infer that the dispersion mechanism does not entail formation of micellar or micelle-like aggregates at the surface of the MWNT. The surfactant molecules likely bind in an isolated manner along the surface and simply the more hydrophobic the spacer is, the more extensively the molecules bind.

3.4. Dispersion efficiency and effectiveness. We now detail the trends in effectiveness, η, and efficiency, η^* (using a surfactant mole basis as implicit in eqn. (1) and (2)) with both *s* and *n*, as can be followed in Fig. 7. These metrics are more technical and utilitarian in nature. For the 12-s-12 gemini, Fig. 7(a), the dispersion effectiveness is similar between all surfactants including DTAB, lying at about 20%. However, the efficiency increases with *s*, being especially high for the long spacer, 12-12-12 (3-fold as high as for spacer 2). With respect to the 16-s-16 series, Fig. 7(b), the dispersion effectiveness also remains at about 20% and the efficiency increases by a 2-fold factor from 16-2-16 to 16-12-16. However, comparison with CTAB, shows that this surfactant is by far the most effective of the lot, with a maximum relative dispersibility of 67%, ca. 3 times more than the two other surfactants. Nevertheless, 16-12-16 is the most efficient of the C16 surfactants.

In Fig. 7(c), where both are η and η^* are depicted vs. *s* for all gemini, two main trends are evident: (i) the effectiveness in dispersing MWNTs does not vary much with gemini structure, neither with spacer for fixed tail, nor with tail for fixed spacer; (ii) in contrast, the efficiency changes dramatically when a longer spacer is used (*s* = 12), and somewhat surprisingly 12-12-12 is more efficient than 16-12-16, despite the fact that the latter is much more hydrophobic.

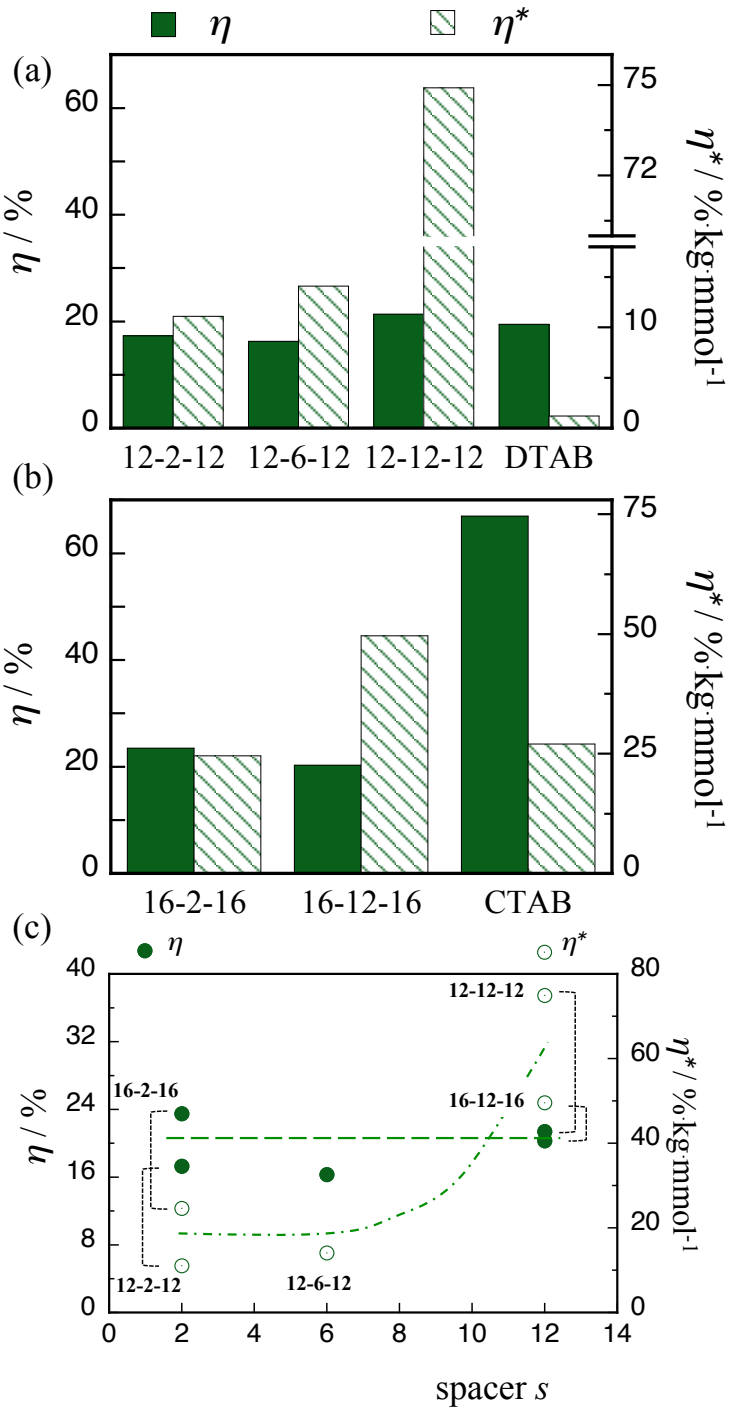

Fig. 7. Dispersion effectiveness η and efficiency η^* for (a) the 12-s-12 gemini and DTAB; (b) 16-s-16 gemini and CTAB; (c) all gemini versus *s*, the number of carbon atoms in the spacer.

Hence, once again it becomes obvious that the spacer length is the dominating structural parameter for the behavior of gemini surfactants as dispersants. One could therefore assume that the spacer portion of the gemini has a more intimate contact with the tubes, compared to the dangling hydrocarbon tails. In that sense, the spacer resembles the hydrophobic portion in

a triblock copolymer earlier studied[20], however there the tails were less hydrophobic in nature.

3.5. Comparisons with previous works. Our results can now be compared with the few previous studies available on the dispersion of CNTs by gemini surfactants. There are some similarities, but also striking contrasts. Wang et al. have used 12-6-12 and DTAB to disperse MWNTs[57], starting with a NT load of 2.0 $mg \cdot mL^{-1}$, and found that 12-6-12 disperses twice as much as DTAB for concentrations well below *cmc*. In sharp contrast, here (i) we do not find significant differences in effectiveness between DTAB and all the other gemini surfactants, and in fact 12-6-12 is found to disperse slightly worse than DTAB (only 16-2-16 performs a little better); (ii) 12-6-12, similarly to DTAB, attains saturation not below but just about *cmc* (Fig. 4(a)). In another study, Chen et al. investigated the thermal conductivity of MWNTs stabilized by 12-s-12, with s = 3, 4 and 6 and concluded that both dispersibility and conductivity were better for short spacers.[58] Herein, and even though their range of s differs from ours, we find that the effectiveness of spacer 6 (16 %) is within error similar to 2 (17%), but a longer spacer like 12 disperses a bit more (21%). Besides, the higher efficiency of a longer spacer is rather evident (Fig. 7). Zheng and co-workers used somewhat unusual ionic-liquid-type (imidazolium)-based gemini to investigate the effect of tail length, concluding that [14-4-14im]Br_2 dispersed much more than [12-4-12im]Br_2;[61] similar results were obtained using pyrrolidinium-based homologues.[64] However, we did not find such tail length effects on dispersibility.

Interestingly, recent molecular dynamics simulation studies on the binding of DTAB, 12-2-12 and 12-6-12 to SWNTs—where obviously curvature is much higher than for MWNTs—show that all these surfactants tend in fact to adsorb aligned to the surface at low coverage (1 $molecule \cdot nm^{-2}$).[60] However, the authors also noted that at higher coverage (2.3 $molecule \cdot nm^{-2}$), the two gemini bind in a more tilted manner and with the headgroups more exposed to the surface. In all cases, there was no indication of micelle-like aggregates on the nanotube surface[60] and our experimental results (namely the trends in $c_{s,max}$, $c_{s,max}/c_{CNT}$ and zeta potential) clearly point in the same direction.

4. Conclusions

In this work, we obtained high-precision dispersibility curves of MWNTs in water for a series of 12-*s*-12 and 16-*s*-16 gemini surfactants and their two monomeric homologues DTAB and CTAB, using a carefully controlled experimental procedure and statistical sampling. This allowed us to extract some reliable metrics for each surfactant, for proper comparisons, namely the critical dispersibility concentration (*cdc*), the maximum dispersed CNT concentration ($c_{CNT,max}$) and respective surfactant concentration at that point ($c_{s,max}$), and the dispersion effectiveness (η) and efficiency (η^*).

In general, *bis*-quat gemini exhibit a relatively modest performance as MWNT dispersants, especially compared to CTAB, which is a bit unexpected. If we compare for instance 16-12-16 and CTAB, both soluble at around room temperature, the dimeric surfactant has almost 3 times as many hydrophobic CH_2 groups as the monomeric one (and hence presumably should show more affinity for the CNT surface); yet, strikingly, 16-12-16 disperses less than CTAB by a 3-fold factor. It seems that the hydrophobicity provided by the two tails is largely counterweighted by the two hydrophilic charges. Hence, the high charge capacity of the gemini structure may presumably aid stability (given the high zeta potentials observed in Fig. 6) but dispersibility is not especially enhanced. It is not negligible, however, that the gemini are found to be much more efficient than the two single-tailed cationic surfactants (and in fact than other common dispersants such as F127, SDBS and SDS) and provided that the binding affinity is suitably tailored—e.g. by covalently linking aromatic moieties to the gemini structure—the overall performance (η and η^*) can then be largely improved.

Comparing only the gemini compounds, we found that spacer length has a more significant influence than tail length on the ability to disperse MWNTs. In fact, while the effectiveness remains basically insensitive to both spacer and tail variation, the efficiency is clearly increased as the spacer length increases. Moreover, and this is one of the most important observations, we have observed that $c_{s,max}$, the ratio $c_{s,max}/c_{CNT,max}$ and the surfactant amount per CNT area at $c_{s,max}$ all decrease linearly with spacer length. This implies that the adsorption of gemini surfactants to the MWNT surface, although governed essentially by hydrophobicity, is rather different from the bulk micellization process, for which the *cmc* is well known to vary non-monotonically with spacer length. This also points to an adsorption mechanism that does not involve the formation of micelle-like aggregates on the MWNT surface. In view of the results we also suspect that the hydrocarbon tails (in contrast to the

spacer) do not take active part in the adsorption process. In addition, our data also indicate that the presence of bulk surfactant micelles does not play any decisive role in the exfoliation process and in the final dispersibility, and this follows a pattern similar to that found for conventional single-tailed surfactants.

Supporting Information Available. Table S1 (apparent extinction coefficients of MWNTs for the different surfactant dispersions); Table S2 (parameters obtained from the MWNT dispersion curves); Tables S3 (critical concentrations relative to *cmc* and respective fraction of micellized surfactant[)]; Table S4 (zeta potential measurements); Figure S1 (conductimetric curves for the determination of the *cmc* of the surfactants).

Acknowledgements. We kindly acknowledge support from Fundação para a Ciência e Tecnologia (FCT, Portugal) through PEst-C/QUI/UI0081/2013 (CIQ-UP) and the Ph.D. grant SFRH/BD/72612/2010. Thanks are also due to FEDER and FCT/MES through NORTE-07-0124-FEDER-000065. The Swedish Research Council VR is also gratefully acknowledged.

5. References

(1) Hecht, D. S.; Hu, L.; Irvin, G. Emerging Transparent Electrodes Based on Thin Films of Carbon Nanotubes, Graphene, and Metallic Nanostructures. *Adv Mater* **2011,** *23*, 1482-1513.

(2) Breuer, O.; Sundararaj, U. Big returns from small fibers: A review of polymer/carbon nanotube composites. *Polym Composite* **2004,** *25*, 630-645.

(3) Kharissova, O. V.; Kharisov, B. I.; de Casas Ortiz, E. G. Dispersion of carbon nanotubes in water and non-aqueous solvents. *RSC Adv.* **2013,** *3*, 24812-24852.

(4) Premkumar, T.; Mezzenga, R.; Geckeler, K. E. Carbon Nanotubes in the Liquid Phase: Addressing the Issue of Dispersion. *Small* **2012,** *8*, 1299-1313.

(5) Moore, V. C.; Strano, M. S.; Haroz, E. H.; Hauge, R. H.; Smalley, R. E.; Schmidt, J.; Talmon, Y. Individually suspended single-walled carbon nanotubes in various surfactants. *Nano Lett.* **2003,** *3*, 1379-1382.

(6) Islam, M. F.; Rojas, E.; Bergey, D. M.; Johnson, A. T.; Yodh, A. G. High weight fraction surfactant solubilization of single-wall carbon nanotubes in water. *Nano Lett.* **2003,** *3*, 269-273.

(7) Vaisman, L.; Wagner, H. D.; Marom, G. The role of surfactants in dispersion of carbon nanotubes. *Adv. Colloid Interface Sci.* **2006,** *128*, 37-46.

(8) Sun, Z.; Nicolosi, V.; Rickard, D.; Bergin, S. D.; Aherne, D.; Coleman, J. N. Quantitative evaluation of surfactant-stabilized single-walled carbon nanotubes: Dispersion quality and its correlation with zeta potential. *J. Phys. Chem. C* **2008,** *112*, 10692-10699.

(9) Wang, H. Dispersing carbon nanotubes using surfactants. *Curr. Opin. Colloid Interface Sci.* **2009,** *14*, 364-371.
(10) Clark, M. D.; Subramanian, S.; Krishnamoorti, R. Understanding surfactant aided aqueous dispersion of multi-walled carbon nanotubes. *J. Colloid Interface Sci.* **2011,** *354*, 144-151.
(11) Blanch, A. J.; Lenehan, C. E.; Quinton, J. S. Parametric analysis of sonication and centrifugation variables for dispersion of single walled carbon nanotubes in aqueous solutions of sodium dodecylbenzene sulfonate. *Carbon* **2011,** *49*, 5213-5228.
(12) Angelikopoulos, P.; Bock, H. The science of dispersing carbon nanotubes with surfactants. *PCCP* **2012,** *14*, 9546-9557.
(13) Fernandes, R. M. F.; Abreu, B.; Claro, B.; Buzaglo, M.; Regev, O.; Furó, I.; Marques, E. F. Dispersing carbon nanotubes with ionic surfactants under controlled conditions: comparisons and insights. *Langmuir* **2015,** *31*, 10955−10965.
(14) Fernandes, R. M. F.; Buzaglo, M.; Regev, O.; Marques, E. F.; Furo, I. Surface Coverage and Competitive Adsorption on Carbon Nanotubes. *J Phys Chem C* **2015,** *119*, 22190-22197.
(15) Grossiord, N.; Loos, J.; Regev, O.; Koning, C. E. Toolbox for dispersing carbon nanotubes into polymers to get conductive nanocomposites. *Chem. Mater.* **2006,** *18*, 1089-1099.
(16) Shvartzman-Cohen, R.; Florent, M.; Goldfarb, D.; Szleifer, I.; Yerushalmi-Rozen, R. Aggregation and self-assembly of amphiphilic block copolymers in aqueous dispersions of carbon nanotubes. *Langmuir* **2008,** *24*, 4625-4632.
(17) Frise, A. E.; Pages, G.; Shtein, M.; Pri Bar, I.; Regev, O.; Furó, I. Polymer binding to carbon nanotubes in aqueous dispersions: Residence time on the nanotube surface As Obtained by NMR diffusometry. *J. Phys. Chem. B* **2012,** *116*, 2635-2642.
(18) Dror, Y.; Pyckhout-Hintzen, W.; Cohen, Y. Conformation of polymers dispersing single-walled carbon nanotubes in water: A small-angle neutron scattering study. *Macromolecules* **2005,** *38*, 7828-7836.
(19) Saint-Aubin, K.; Poulin, P.; Saadaoui, H.; Maugey, M.; Zakri, C. Dispersion and Film-Forming Properties of Poly(acrylic acid)-Stabilized Carbon Nanotubes. *Langmuir* **2009,** *25*, 13206-13211.
(20) Fernandes, R. M. F.; Buzaglo, M.; Shtein, M.; Pri Bar, I.; Regev, O.; Marques, E. F.; Furó, I. Lateral Diffusion of Dispersing Molecules on Nanotubes As Probed by NMR. *J. Phys. Chem. C* **2014,** *118*, 582-589.
(21) Badaire, S.; Zakri, C.; Maugey, M.; Derre, A.; Barisci, J. N.; Wallace, G.; Poulin, P. Liquid crystals of DNA-stabilized carbon nanotubes. *Adv Mater* **2005,** *17*, 1673-+.
(22) Tardani, F.; La Mesa, C.; Poulin, P.; Maugey, M. Phase Behavior of DNA-Based Dispersions containing Carbon Nanotubes: Effects of Added Polymers and Ionic Strength on Excluded Volume. *J Phys Chem C* **2012,** *116*, 9888-9894.
(23) Karajanagi, S. S.; Yang, H. C.; Asuri, P.; Sellitto, E.; Dordick, J. S.; Kane, R. S. Protein-assisted solubilization of single-walled carbon nanotubes. *Langmuir* **2006,** *22*, 1392-1395.
(24) Edri, E.; Regev, O. "Shaken, Not Stable": Dispersion Mechanism and Dynamics of Protein-Dispersed Nanotubes Studied via Spectroscopy. *Langmuir* **2009,** *25*, 10459-10465.

(25) Frise, A. E.; Edri, E.; Furo, I.; Regev, O. Protein Dispersant Binding on Nanotubes Studied by NMR Self-Diffusion and Cryo-TEM Techniques. *J. Phys. Chem. Lett.* **2010,** *1*, 1414-1419.
(26) Horn, D. W.; Tracy, K.; Easley, C. J.; Davis, V. A. Lysozyme Dispersed Single-Walled Carbon Nanotubes: Interaction and Activity. *J. Phys. Chem. C* **2012,** *116*, 10341-10348.
(27) Karchemsky, F.; Drug, E.; Mashiach-Farkash, E.; Fadeev, L.; Wolfson, H. J.; Gozin, M.; Regev, O. Diameter-selective dispersion of carbon nanotubes by beta-lactoglobulin whey protein. *Colloids Surf. B* **2013,** *112*, 16-22.
(28) Oh, H.; Sim, J.; Ju, S. Y. Binding Affinities and Thermodynamics of Noncovalent Functionalization of Carbon Nanotubes with Surfactants. *Langmuir* **2013,** *29*, 11154-11162.
(29) Ernst, F.; Heek, T.; Setaro, A.; Haag, R.; Reich, S. Functional Surfactants for Carbon Nanotubes: Effects of Design. *J. Phys. Chem. C* **2013,** *117*, 1157-1162.
(30) Di Crescenzo, A.; Cambre, S.; Germani, R.; Di Profio, P.; Fontana, A. Dispersion of SWCNTs with Imidazolium-Rich Surfactants. *Langmuir* **2014,** *30*, 3979-3987.
(31) Dassios, K. G.; Alafogianni, P.; Antiohos, S. K.; Leptokaridis, C.; Barkoula, N.-M.; Matikas, T. E. Optimization of Sonication Parameters for Homogeneous Surfactant-Assisted Dispersion of Multiwalled Carbon Nanotubes in Aqueous Solutions. *J Phys Chem C* **2015,** *119*, 7506-7516.
(32) Grossiord, N.; Regev, O.; Loos, J.; Meuldijk, J.; Koning, C. E. Time-dependent study of the exfoliation process of carbon nanotubes in aqueous dispersions by using UV-visible spectroscopy. *Anal. Chem.* **2005,** *77*, 5135-5139.
(33) Duan, W. H.; Wang, Q.; Collins, F. Dispersion of carbon nanotubes with SDS surfactants: a study from a binding energy perspective. *Chem Sci* **2011,** *2*, 1407-1413.
(34) Richard, C.; Balavoine, F.; Schultz, P.; Ebbesen, T. W.; Mioskowski, C. Supramolecular self-assembly of lipid derivatives on carbon nanotubes. *Science* **2003,** *300*, 775-778.
(35) Nativ-Roth, E.; Nap, R. J.; Szleifer, I.; Yerushalmi-Rozen, R. Order-disorder transition induced by surfactant micelles in single-walled carbon nanotubes dispersions. *Soft Matter* **2010,** *6*, 5289-5292.
(36) Poorgholami-Bejarpasi, N.; Sohrabi, B. Self-assembly of cationic surfactants on the carbon nanotube surface: insights from molecular dynamics simulations. *J. Mol. Model.* **2013,** *19*, 4319-4335.
(37) Huang, Y. Y.; Terentjev, E. M. Dispersion of Carbon Nanotubes: Mixing, Sonication, Stabilization, and Composite Properties. *Polymers* **2012,** *4*, 275-295.
(38) Menger, F. M.; Keiper, J. S. Gemini surfactants. *Angewandte Chemie - International Edition* **2000,** *39*, 1906-1920.
(39) Zana, R. Dimeric and oligomeric surfactants. Behavior at interfaces and in aqueous solution: A review. *Advances in Colloid and Interface Science* **2002,** *97*, 205-253.
(40) Alami, E. O.; Holmberg, K. Heterogemini surfactants. *Advances in Colloid and Interface Science* **2003,** *100*, 13-46.
(41) Menger, F. M.; Littau, C. A. Gemini surfactants - synthesis and properties. *J Am Chem Soc* **1991,** *113*, 1451-1452.

(42) Danino, D.; Talmon, Y.; Zana, R. Alkanediyl-alpha,omega-bis(dimethylalkylammonium bromide) surfactants (dimeric surfactants). 5. Aggregation and microstructure in aqueous-solutions. *Langmuir* **1995,** *11*, 1448-1456.
(43) Berthier, D.; Buffeteau, T.; Leger, J. M.; Oda, R.; Huc, I. From chiral counterions to twisted membranes. *J Am Chem Soc* **2002,** *124*, 13486-13494.
(44) Silva, S. G.; Alves, C.; Cardoso, A. M. S.; Jurado, A. S.; Pedroso De Lima, M. C.; Vale, M. L. C.; Marques, E. F. Synthesis of gemini surfactants and evaluation of their interfacial and cytotoxic properties: Exploring the multifunctionality of serine as headgroup. *European Journal of Organic Chemistry* **2013**, 1758-1769.
(45) Wettig, S. D.; Verrall, R. E.; Foldvari, M. Gemini surfactants: A new family of building blocks for non-viral gene delivery systems. *Current Gene Therapy* **2008,** *8*, 9-23.
(46) Tehrani-Bagha, A. R.; Holmberg, K.; van Ginkel, C. G.; Kean, M. Cationic gemini surfactants with cleavable spacer: Chemical hydrolysis, biodegradation, and toxicity. *J Colloid Interf Sci* **2015,** *449*, 72-79.
(47) Cardoso, A. M.; Morais, C. M.; Silva, S. G.; Marques, E. F.; Pedroso de Lima, M. C.; Jurado, M. A. S. Bis-quaternary gemini surfactants as components of nonviral gene delivery systems: A comprehensive study from physicochemical properties to membrane interactions. *International Journal of Pharmaceutics* **2014,** *474*, 57-69.
(48) Mivehi, L.; Bordes, R.; Holmberg, K. Adsorption of Cationic Gemini Surfactants at Solid Surfaces Studied by QCM-D and SPR: Effect of the Rigidity of the Spacer. *Langmuir* **2011,** *27*, 7549-7557.
(49) Magdassi, S.; Ben Moshe, M.; Talmon, Y.; Danino, D. Microemulsions based on anionic gemini surfactant. *Colloid Surface A* **2003,** *212*, 1-7.
(50) Oda, R.; Huc, I.; Candau, S. J. Gemini surfactants as new, low molecular weight gelators of organic solvents and water. *Angewandte Chemie-International Edition* **1998,** *37*, 2689-2691.
(51) Bernheim-Groswasser, A.; Zana, R.; Talmon, Y. Sphere-to-cylinder transition in aqueous micellar solution of a dimeric (gemini) surfactant. *J Phys Chem B* **2000,** *104*, 4005-4009.
(52) Almeida, J. A. S.; Pinto, S. P. R.; Wang, Y.; Marques, E. F.; Pais, A. A. C. C. Structure and order of DODAB bilayers modulated by dicationic gemini surfactants. *Physical Chemistry Chemical Physics* **2011,** *13*, 13772-13782.
(53) Almeida, J. A. S.; Marques, E. F.; Jurado, A. S.; Pais, A. A. C. C. The effect of cationic gemini surfactants upon lipid membranes. An experimental and molecular dynamics simulation study. *Physical Chemistry Chemical Physics* **2010,** *12*, 14462-14476.
(54) Burrows, H. D.; Tapia, M. J.; Silva, C. L.; Pais, A. A. C. C.; Fonseca, S. M.; Pina, J.; de Melo, J. S.; Wang, Y.; Marques, E. F.; Knaapila, M.; Monkman, A. P.; Garamus, V. M.; Pradhan, S.; Scherf, U. Interplay of electrostatic and hydrophobic effects with binding of cationic gemini surfactants and a conjugated polyanion: Experimental and molecular modeling studies. *J Phys Chem B* **2007,** *111*, 4401-4410.
(55) Singh, K.; McLachlan, A. A.; Marangoni, D. G. Effect of morphology and concentration on capping ability of surfactant in shape controlled synthesis of PbS nano- and micro-crystals. *Colloid Surface A* **2009,** *345*, 82-87.

(56) Datta, S.; Biswas, J.; Bhattacharya, S. How does spacer length of imidazolium gemini surfactants control the fabrication of 2D-Langmuir films of silver-nanoparticles at the air-water interface? *J Colloid Interf Sci* **2014,** *430*, 85-92.
(57) Wang, Q.; Han, Y.; Wang, Y.; Qin, Y.; Guo, Z.-X. Effect of surfactant structure on the stability of carbon nanotubes in aqueous solution. *J Phys Chem B* **2008,** *112*, 7227-7233.
(58) Chen, L.; Xie, H.; Li, Y.; Yu, W. Applications of cationic gemini surfactant in preparing multi-walled carbon nanotube contained nanofluids. *Colloid Surface A* **2008,** *330*, 176-179.
(59) Chen, L.; Xie, H. Properties of carbon nanotube nanofluids stabilized by cationic gemini surfactant. *Thermochim. Acta* **2010,** *506*, 62-66.
(60) Poorgholami-Bejarpasi, N.; Sohrabi, B. Role of surfactant structure in aqueous dispersions of carbon nanotubes. *Fluid Phase Equilibria* **2015,** *394*, 19-28.
(61) Liu, Y.; Yu, L.; Zhang, S.; Yuan, J.; Shi, L.; Zheng, L. Dispersion of multiwalled carbon nanotubes by ionic liquid-type Gemini imidazolium surfactants in aqueous solution. *Colloid Surface A* **2010,** *359*, 66-70.
(62) Di Crescenzo, A.; Germani, R.; Del Canto, E.; Giordani, S.; Savelli, G.; Fontana, A. Effect of Surfactant Structure on Carbon Nanotube Sidewall Adsorption. *European Journal of Organic Chemistry* **2011**, 5641-5648.
(63) Xie, H.; Chen, L. Review on the Preparation and Thermal Performances of Carbon Nanotube Contained Nanofluids. *Journal of Chemical and Engineering Data* **2011,** *56*, 1030-1041.
(64) Zhang, S.; Lu, F.; Zheng, L. Dispersion of multiwalled carbon nanotubes (MWCNTs) by ionic liquid-based Gemini pyrrolidinium surfactants in aqueous solution. *Colloid and Polymer Science* **2011,** *289*, 1815-1819.
(65) Sun, G.; Chen, G.; Liu, J.; Yang, J.; Xie, J.; Liu, Z.; Li, R.; Li, X. A facile gemini surfactant-improved dispersion of carbon nanotubes in polystyrene. *Polymer* **2009,** *50*, 5787-5793.
(66) Badaire, S.; Poulin, P.; Maugey, M.; Zakri, C. In situ measurements of nanotube dimensions in suspensions by depolarized dynamic light scattering. *Langmuir* **2004,** *20*, 10367-10370.
(67) Holmberg, K.; Jönsson, B.; Kronberg, B.; Lindman, B. *Surfactant and Polymers in Aqueous Solution*; John Wiley & Sons: Chichester, 2002.
(68) Shtein, M.; Pri-bar, I.; Regev, O. A simple solution for the determination of pristine carbon nanotube concentration. *Analyst* **2013,** *138*, 1490-1496.
(69) White, B.; Banerjee, S.; O'Brien, S.; Turro, N. J.; Herman, I. P. Zeta-potential measurements of surfactant-wrapped individual single-walled carbon nanotubes. *J. Phys. Chem. C* **2007,** *111*, 13684-13690.
(70) Sa, V.; Kornev, K. G. Analysis of Stability of Nanotube Dispersions Using Surface Tension Isotherms. *Langmuir* **2011,** *27*, 13451-13460.
(71) Peigney, A.; Laurent, C.; Flahaut, E.; Bacsa, R. R.; Rousset, A. Specific surface area of carbon nanotubes and bundles of carbon nanotubes. *Carbon* **2001,** *39*, 507-514.
(72) Zhong, W.; Claverie, J. P. Probing the carbon nanotube-surfactant interaction for the preparation of composites. *Carbon* **2013,** *51*, 72-84.

Supporting Information

Table S1. Apparent extinction coefficients of MWNTs for the different surfactants as obtained from the linear dependence of the apparent absorbance on MWNT concentration.

Surfactant	ε_{660} / mL·mg^{-1}·cm^{-1}
12-2-12	38.7 ± 0.2
12-6-12	42.6 ± 0.4
12-12-12	41.1 ± 0.7
16-2-16	41.2 ± 0.2
16-12-16	41.6 ± 0.3
DTAB	39.3 ± 0.4
CTAB	42.2 ± 0.7

Table S2. Dispersability parameters obtained from the MWNT/surfactant curves.

Surf.	*cmc*[a,b]	*cdc*[a]	$c_{s,max}$[a]	$c_{CNT,max}$[c]	η / %	η^* / % kg·mmol^{-1}
12-2-12	0.95±0.01 0.58 0.058	0.57 ± 0.31 0.35 0.035	1.6 ± 0.3 0.98 0.098	0.52 ± 0.03 0.052	17.3	11.1
12-6-12	1.03 ± 0.01 0.691 0.0691	0.15 ± 0.01 0.101 0.0101	1.16 ± 0.07 0.778 0.0778	0.49 ± 0.03 0.049	16.3	14.1
12-12-12	0.35 ± 0.01 0.26 0.026	0.13 ± 0.06 0.098 0.0098	0.29 ± 0.07 0.219 0.0219	0.64 ± 0.03 0.064	21.4	74.9
16-2-16	0.040 ± 0.002 0.035 0.0035	0.44 ± 0.08 0.27 0.027	0.95 ± 0.19 0.58 0.058	0.70 ± 0.22 0.070	23.5	24.6
16-12-16	0.032 ± 0.001 0.029 0.0029	0.12 ± 0.02 0.091 0.0091	0.41 ± 0.03 0.31 0.031	0.61 ± 0.01 0.061	20.3	49.6
DTAB	14.0 4.32 0.432	7.9 ± 3.2 4.9 0.49	15.9 ± 3.9 9.8 0.98	0.58 ± 0.08 0.058	19.5	1.2
CTAB	0.97 ± 0.01 0.35 0.035	1.4 ± 0.1 0.51 0.051	2.5 ± 0.6 0.91 0.091	2.0 ± 0.1 0.20	67	27

[a]Values in units of mmol·kg^{-1}, mg·mL^{-1} and wt%, respectively.
[b]Krafft temperatures: 12-2-12, 14.4 ºC; 12-6-12, < 0 ºC; 12-12-12, 13.6 ºC; 16-2-16, 45 ºC; 16-12-16, 13.5 ºC; DTAB, < 0 ºC; CTAB, 26 ºC.
[c]Values in mg·mL^{-1} and wt%.

Table S3. Critical concentrations relative to *cmc* and respective fraction of micellized surfactant[a].

Surf.	*cdc*/*cmc*	f_{mic}[a]	$c_{s,max}$ /*cmc*	$f_{mic,\ max}$[a]
12-2-12	0.60	0	1.6	0.39
12-6-12	0.14	0	1.1	0.11
12-12-12	0.37	0	0.81	0
16-2-16	11	0.91	24	0.96
16-12-16	3.9	0.74	13	0.92
DTAB	0.55	0	1.1	0.10
CTAB	1.4	0.30	2.6	0.61

[a]Calculated as $f = (c_s - cmc) / c_s$, where c_s is the specified surfactant concentration.

Table S3. ζ for neat surfactant micelles and for surfactant-assisted MWNT dispersions with $c_{MWNT} = 0.1$ mg·mL^{-1} and $c_s = 2$ mmol·kg^{-1} for all gemini surfactants.

surfactant	ζ / mV	
	neat micelles	MWNT-surfactant dispersion
F-127	not measurable	– 11.0[b]
12-2-12	+47.9	+53.6
12-6-12	+48.8	+51.7
12-12-12	+32.8	+59.7
16-2-16	+55.1	+58.1
16-12-16	+35.2	+63.0
DTAB	not measurable	+44.6[c]
CTAB	not measurable	+51.6[c]

[a]Observed distributions are unimodal and meet quality criteria. Typical uncertainties in ζ potential are ±5 % (5 runs on average).
[b]$c_{F127} = 3$ mg·mL^{-1}.
[c]$c_s = 1$ mg·mL^{-1}.

Note on zeta potential measurements:

For these measurements, since the curves in Fig. 3 show that the dispersed c_{MWNT} varies differently with c_s for different surfactants, a careful procedure was followed. All dispersions were prepared in the usual manner using $c_s = 2$ mmol·kg^{-1} which yielded different c_{MWNT} values between surfactants, but all above 0.1 mg·mL^{-1} (Fig. 3); then, the samples were diluted with its respective neat surfactant solution ($c_s = 2$ mmol·kg^{-1}) to the final desired c_{MWNT} (0.1 mg·mL^{-1}). The zeta potential for F127-coated MWNTs was also measured as a baseline value (yielding – 11 mV).

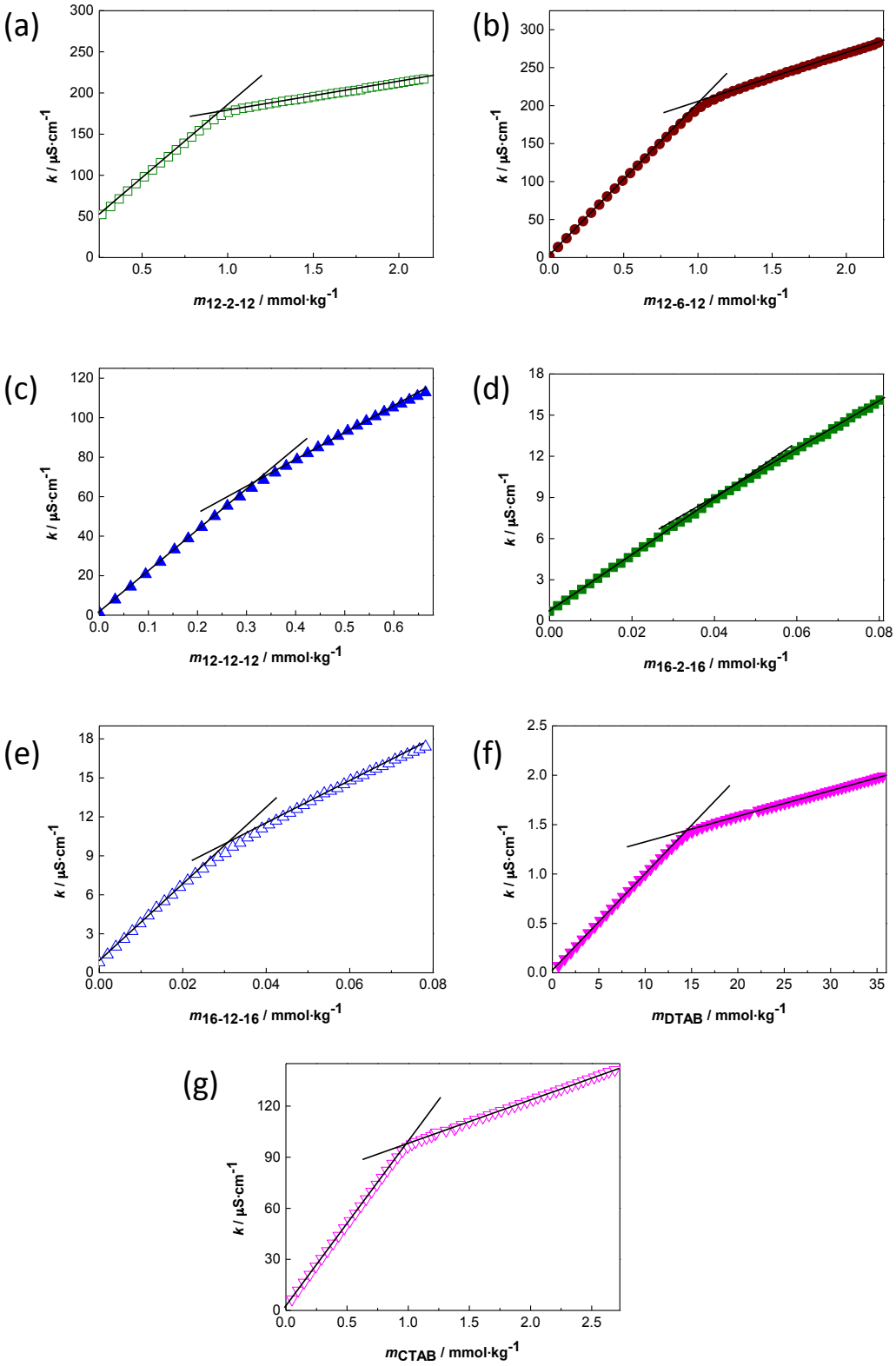

Figure S1 – Conductivity plots for *cmc* measurements: (a) 12-2-12; (b) 12-6-12; (c) 12-12-12; (d) 16-2-16; (e) 16-12-16; (f) DTAB; (g) CTAB. The calculated *cmc* values are presented in Table S2.

VII

Strong spacer length effects on the thermal behavior and mesophase formation by gemini surfactants

Ricardo M.F. Fernandes, Yujie Wang, Pedro B. Tavares, Sandra C.C. Nunes, Alberto A.C.C. Pais and Eduardo F. Marques

Manuscript

Strong Spacer Length Effects on The Thermal Behavior and Mesophase Formation By Gemini Surfactants

Ricardo M.F. Fernandes,[1,2] Yujie Wang,[1] Pedro B. Tavares[3], Sandra C.C. Nunes[4], Alberto A.C.C. Pais[4], and Eduardo F. Marques[1*]

[1]*Centro de Investigação em Química, Department of Chemistry and Biochemistry, Faculty of Science, University of Porto, Rua do Campo Alegre, s/n, P-4169-007 Porto, Portugal.*

[2]*Division of Applied Physical Chemistry, Department of Chemistry, KTH Royal Institute of Technology, SE-10044 Stockholm, Sweden.*

[3]*CQVR Centro de Química – Vila Real, Departamento de Química, Universidade de Trás-os-Montes e Alto Douro, 5000-801 Vila Real, Portugal.*

[4]*CQC Centro de Química de Coimbra, Department of Chemistry, University of Coimbra, Rua Larga 3004-535, Coimbra, Portugal.*

*email: efmarque@fc.up.pt

Abstract

The self-aggregation properties in aqueous solution of gemini surfactants of the type alkanediyl-α,ω-bis(dodecyldimethylammonium bromides), 12-*s*-12, have been extensively reported and are known to be significantly influenced by the number of methylene groups, *s*, of the covalent spacer. In contrast, the thermal behavior of the anhydrous compounds as a function of varying *s* has not been investigated in a similarly systematic way. Herein, we present the thermal phase behavior of eight compounds of the 12-*s*-12 family (with *s* = 2-6, 8, 10 and 12), resorting to differential scanning calorimetry (DSC), polarized light microscopy (PLM) and X-ray diffraction (XRD). We find that compounds with either the shortest spacer, *s* = 2, or the longest ones—8, 10 and 12—form several smectic liquid-crystalline phases prior to isotropization to the liquid phase, with appearance of oily streaks, focal conics, mosaic and fan-shaped birefringent textures. In sharp contrast, gemini compounds with intermediate spacers, *s* = 3-6, decompose and do not form any disordered, fluid mesophases. Both the DSC thermodynamic parameters for the phase transitions and d_{001} spacings obtained from XRD show non-monotonic trends with spacer variation, indicating that there are significant differences in solid-state packing and melting process. Plausible molecular packing arrangements in the solid-state are presented, consistent with the XRD information and geometric considerations, and their influence on the phase behavior trends critically discussed.

1. **Introduction**

The gemini or dimeric surfactants known as alkanediyl-α,ω-bis(alkyldimethylammonium bromides), commonly designated by *n-s-n* (where *n* and *s* are the number of carbon atoms of the surfactant alkyl tail and alkyl spacer, respectively), have been extensively investigated in terms of their interfacial properties, thermodynamics of micellization and self-assembled nanostructures in aqueous solution.[1-4] In comparison, the thermal phase behavior of the anhydrous compounds has been much less studied, with only a sparse number of reports available in the literature.[5-8] Yet, it could be anticipated that, in comparison with monomeric surfactants, the new structural degree of freedom provided by spacer length variation imparts the gemini with interesting mesogenic properties.

Thermotropic liquid crystals (TLC), and mesophases in general, are intermediate phases between the solid (crystalline or amorphous) and the (isotropic) liquid phase. For amphiphilic mesogens, any such mesophase always contains some degree of structural order of headgroups and structural disorder of the alkyl chains (positional, orientational, or conformational).[9-11] The type of chain disorder depends *inter alia* on alkyl chain length, headgroup composition, and original crystalline lattice structure. Different models for thermally-induced chain disordering have been proposed on the basis of experimental data[12-21] as well as Monte-Carlo simulations[22], molecular dynamics[23] and thermodynamic considerations.[22-26] TLCs can respond to external stimuli such as mechanical stress or electrical fields, thereby changing their optical properties (e.g. birefringence and color)[27]. Thus, the electro-optical properties of TLCs have had a great impact in technology, aiding in the development of displays, sensors and new devices such as smart phones or tablets.[11,28] Fundamental studies, on the other hand, have focused on the development and characterization of novel molecules. More recently, TLCs have also gained renewed interest as components in the production of functional textile fibers[29] and in nanocomposites with carbon nanotubes, for the enhancement of liquid-crystalline properties or nanotube dispersability.[28,30-33]

For most surfactants, where chain-chain interactions are governed by weak van der Walls dispersion forces, the first thermotropic mesophase is typically associated with chain melting or partial chain melting.[9,15] However, the formation of TLCs also depends on headgroup interactions and rearrangements of headgroup positions, which in turn depend on factors such as headgroup polarity, charge density[34] and hydrogen bonding.[13,15] The influence of headgroup interactions is clearly demonstrated by the fact that in binary surfactant mixtures

with equally or oppositely charged headgroups the thermal range and variety of mesophases is expanded in comparison with the individual compounds.[34-37]

Regarding *n*-*s*-*n* gemini compounds, early work on thermogravimetry showed that they readily decompose upon heating for $\theta \geq 200$ ºC, but they can withstand long periods of heating below 200 ºC with no detectable decomposition.[6] In the 120-180 ºC range, the formation of TLC upon was reported to be absent.[6] Later, Fuller et al. observed for 15-*s*-15 (*s* = 1, 2, 3, and 6), for $\theta > 100$ ºC, a so-called viscous neat mesophase and, specifically for 15-3-15 and 15-6-15 also smectic A mesophases[7], prior to isotropic liquid formation. Asymmetric 12-*s*-14 gemini with *s* = 2, 6, and 10 were found to exhibit a complex solid polymorphism and thermal behavior, on going from crystal to smectic liquid crystalline phases.[8] The number and sequence of phase transitions were markedly affected by spacer length. Here, the authors deemed 12-*s*-12 surfactants not able to form thermotropic mesophases, implying that gemini mesomorphism was a consequence of chain length asymmetry. However, occurrence of smectic phases for *n*-2-*n* gemini surfactants with *n* = 12, 14, 16, and 18 was demonstrated the basis of DSC and PLM data.[35] In a subsequent study for 12-2-12, the phase sequence soft crystal→SmC→SmA→liquid phase/decomposition was found.[38] The gemini 14-2-14 with different counterions was also reported to form thermotropic mesophases.[39] Mesomorphism has also been described for ionic liquids with a gemini architecture: a SmA phase was found for gemini imidazolium salts with 12-6-12 and 14-6-14 architecture.[40] Gemini surfactants *n*-3-*n* (*n* = 10, 12, 14, 16) with a hydroxyl group incorporated in spacer have also been investigated, and SmB and SmC phases were observed.[41]

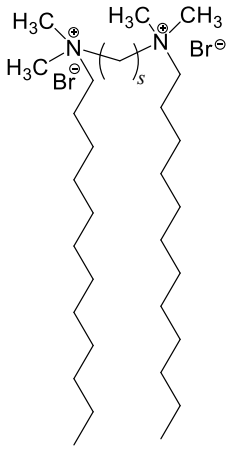

Figure 1. Molecular structure of 12-s-12 gemini surfactants, where *s* in the number of methylene groups in the spacer (*s* = 2, 3, 4, 5, 6, 8, 10 and 12 were herein investigated).

In this work, our goal was to carry out a systematic study on the effect of spacer length variation of 12-*s*-12 surfactants (Figure 1) on the thermal phase behavior and formation of liquid-crystalline phases. The thermodynamic parameters for the observed phase transitions were determined on the basis of DSC data. Further, polarizing light microscopy observations allowed the detection of mesophase textures between crystal and isotropic melt (liquid phases), and in some cases the respective phase assignment. Finally, we assessed the relation between spacer length, molecular packing and observed thermal behavior, based on our data and previous reports from the literature.

2. Experimental Section

2.1 Materials. The 12-*s*-12 gemini surfactants were synthesized according to the method originally described by Menger et al.[42]. For 12-2-12, *N*,*N*,*N*′,*N*′-tetramethylethylenediamine (99 %, Aldrich) and 1-bromododecane (97 %, Aldrich) were used as received. For the remaining compounds, 1-dimethylaminododecane (97 %, Fluka) and the appropriate dibromoalkanes were used, namely 1,3-dibromopropane (99 %, Aldrich), 1,4-dibromobutane (99 %, Aldrich), 1,5-dibromopentane (97 %, Aldrich), 1,6-dibromohexane (96 %, Aldrich), 1,8-dibromooctane (98 %, Aldrich), 1,10-dibromodecane (97 %, Aldrich), 1,12-dibromododecane (98 %, Aldrich). All the surfactants were twice recrystallized with an acetone-methanol mixture. The high purity of the gemini was ascertained by NMR and mass spectrometry. In addition, from conductivity measurements previously reported[36,43,44], it was found that the critical micelle concentrations the surfactants were in good agreement with those found by other authors.[3]

2.2 Differential Scanning Calorimetry (DSC). DSC scans were performed using a Setaram DSC141 differential calorimeter. The equipment was previously calibrated, both for temperature and energy, using benzoic acid, indium and tin as reference compounds.[45] A mass of 6-12 mg of solid compound was weighed to Al crucibles, and an empty crucible was used as a reference. The heating-cooling cycles were performed at a scanning rate of 3 K min^{-1} in a temperature range of 20-250 °C, with nitrogen (p = 0.3 bar) used as sweeping fluid. Five independent essays were typically run for each compound, with at least one heating-cooling scan for each sample.

2.3 Polarizing Light Microscopy (PLM). Characterization of thermal behavior, with assignment of different birefringent textures, was carried out by inspecting glass-cover slip

preparations of each gemini compound on the polarized light microscope. An Olympus BX51 microscope, equipped with a Linkam THMS-600 heating stage with a temperature control of about ±0.1 ºC, was used. The micrographs were obtained with an Olympus C-5060 Wide-Zoom digital camera. Typically, 3-5 independent preparations were analyzed for each compound with heating-cooling cycles, at different heating rates.

2.4 X-ray Diffraction (XRD). The x-ray powder diffraction spectra of the solid state gemini compounds were recorded at room temperature with a PANalytical X'Pert MPD diffractometer using the $\lambda = 0.154$ nm $K\alpha$ line of a Cu anode (Bragg–Brentano geometry) equipped with a X'Celerator detector. The spectra were obtained from 10 to 95° (2θ), using a step of 0.017° and 100 s/step.

3. Results and Discussion

3.1. Phase transitions and thermodynamic parameters. Representative thermograms for the 12-s-12 gemini compounds are shown in Figure 2. The obtained thermodynamic parameters for the phase transitions are presented in Table 1. Peaks are numbered according to increasing temperature for easier identification, and in the case of resolved peaks, an apparent enthalpy for the global transition is presented and no transition entropy is given. As can be seen, all compounds show several phase transitions denoting a gradual and complex isotropization process. Furthermore, it is obvious that the incremental length of the spacer has a marked effect on the thermal behavior.

A common feature is that all compounds show one main endothermic peak. Inspection of the thermograms and enthalpy values allows us to infer that this peak corresponds to partial melting of the surfactant alkyl chains, as observed in similar amphiphilic compounds. [9,46] Hence, the phase formed on heating immediately after the strongest peak, designated by M1 (mesophase 1), is proposed to be a strongly ordered mesophase or even a soft-crystalline phase, most likely with the headgroups positions fixed by the strong ionic interactions and with only partially molten chains. Noteworthy, all the compounds undergo chemical degradation for temperatures for $\theta \geq 200$ ºC, in accordance also with previous reports.[6-8,35,36] Thus, DSC heating traces are not shown for $\theta > 200$ ºC. Microscopy observations that were concomitantly run (described below) show indeed the formation of brownish viscous residues on the slide/coverslip preparations, which form at a particularly fast rate (within minutes) for 12-5-12 and 12-6-12 once this temperature is reached.

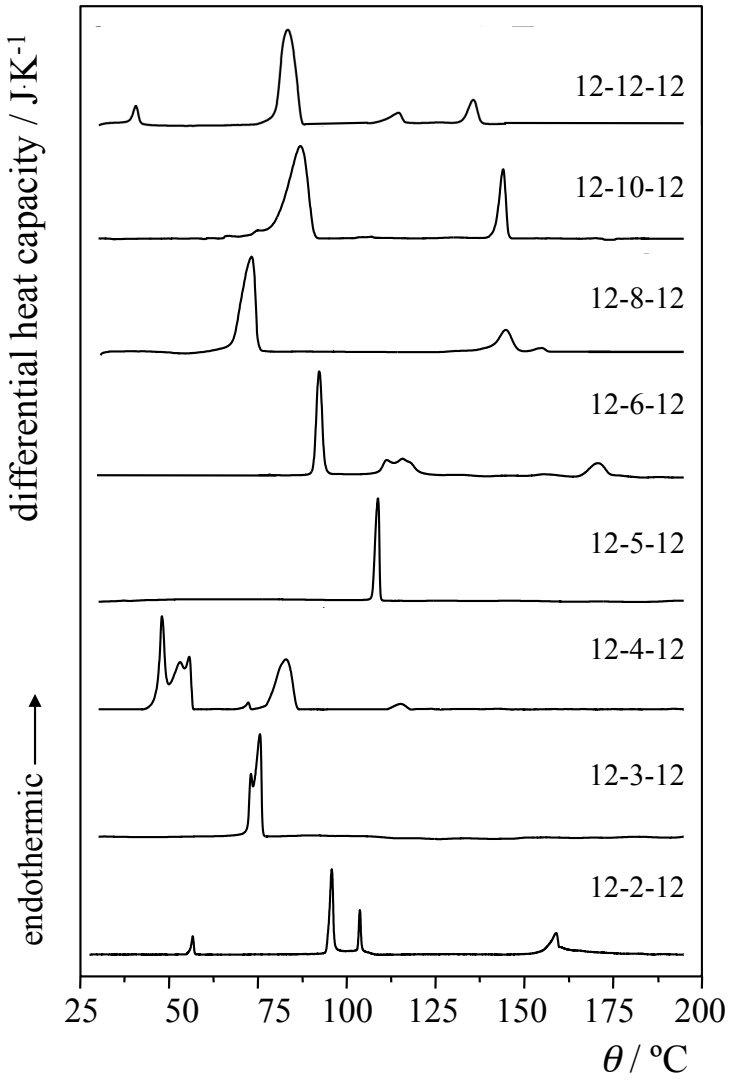

Figure 2. DSC thermograms for the 12-s-12 gemini surfactants.

For s = 2, 3, 4 and 12, one or more peaks appear at lower temperature than the main peak. The 12-4-12 case is particularly significant since a complex peak with three coalesced peaks is observed, implying the occurrence of successive phase transitions in the crystalline region within a narrow temperature range (θ = 47-67 ºC), i.e. the occurrence of solid polymorphism. Compounds 12-3-12 and 12-6-12 also show resolved peaks in their thermograms.

For 12-8-12, 12-10-12, 12-12-12, which are the only compounds that melt to the liquid phase before decomposition, it is possible to plot the total crystal-to-liquid phase transition enthalpy, $\Delta^{\mathrm{I}}_{\mathrm{cr}}H_{\mathrm{m}}$ and entropy $\Delta^{\mathrm{I}}_{\mathrm{cr}}S_{\mathrm{m}}$ as a function of s (Fig. 3). A linear trend is observed for both thermodynamic parameters in this range of s. From linear regression fits, one obtains a slope of 25.5 kJ mol^{-1} for the enthalpy graph and 69.8 J K^{-1} mol^{-1} for the entropy,

which are the contributions to melting per added CH_2 group in the spacer. This linearity reflects a constant contribution per methylene group in the spacer, without further influence from variations in structural arrangements. Nevertheless, the value does not amount to a simple gradual increase in the magnitude of van der Waals dispersion forces.

Table 1. Thermodynamic data for phases transition for 12-s-12 gemini surfactants*

Compound	peak no.	Phase transition	θ / ºC	$\Delta_{trs}H_m$ / kJ·mol^{-1}	$\Delta_{trs}S_m$ / J·K^{1}·mol^{-1}
12-2-12	1	Cr-M1	58.2	4.20	12.7
	2	M1-M2	97.3	43.31	116.9
	3	M2-SmC	105.2	11.96	31.7
	4	SmC-SmA	165.5	23.79	54.3
12-3-12	1-2	Cr-M1$^{(1)}$	75.0, 77.6	43.71	-
12-4-12	1-3	Cr-Cr$^{(1)}$	48.8, 54.3, 56.7	18.9$^{(2)}$	-
	4	Cr-Cr$^{(1)}$	73.3	0.29	0.80
	5	Cr-M1	83.9	15.72	44.0
	6	M1-M2	116.6	0.20	0.50
12-5-12	1	Cr-M1	99.9	58.34	156.4
12-6-12	1	Cr-M1	91.1	31.90	87.6
	2-3	M1-M1', M1'-M2	108.8,113.0	17.5	21.5
	4	M2-M3	163.1	9.39	
12-8-12	1	Cr-M1	75.1	26.50	76.1
	2	M1-M2	146.5	3.74	8.8
	3	M2-SmA (+ SmA-I)	189.8	0.10	0.22
12-10-12	1	Cr-M1	87.7	57.36	157.2
	2	M1-SmA (+ SmA-I)	144.2	15.55	36.8
12-12-12	1	Cr-Cr$^{(1)}$	40.7	10.6	-
	2	Cr-M2	83.0	108.10	303.5
	3	SmC-SmA	114.4	7.60	19.6
	4	SmA-I	134.3	16.89	41.4

*Uncertainties: θ, ± 0.20 ºC; $\Delta_{trs}H_m$, ±5 %; $\Delta_{trs}S_m$, ±5 %.

This is because a value of 3.8 kJ per mole of CH_2 is associated with complete melting of aliphatic chains from their fully crystalline state and here we obtain a 6-fold higher contribution. If one now divides $\Delta^{I}_{cr}H_m$ by the number of total of carbons in the chains (spacer and long chains), values of 0.95, 2.3 and 3.9 kJ per mol of aliphatic CH_2 are obtained. This implies that the $\Delta^{I}_{cr}H_m$ values for spacer 8 and 10 are in fact much lower than expected. The total enthalpy of the Cr→M1 transition for all surfactants, which dominates over the other contributions, can also be plotted as function of *s* for comparisons (Fig. 3). Here, two trends are observed: decreasing enthalpy with *s* from 2 to 8 (apparently linear) excluding 5, followed by increasing enthalpy from 8 to 12. This non-monotonic trend should now reflect the effect of particular structural arrangements present in the solid phase, denoting variation in structure as *s* increases. Such effects outweigh the expected increase in dispersions forces associated with more methylene groups in the spacer.

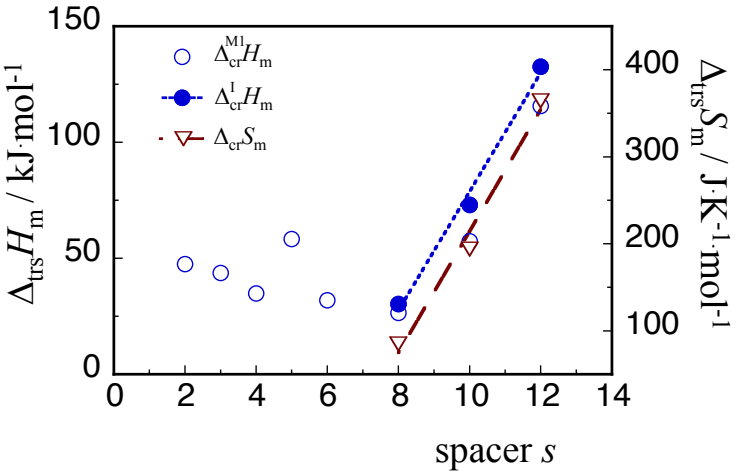

Figure 3. Molar enthalpy for Cr→M1 phase transition (□), molar enthalpy (●) and molar entropy (○) for Cr→I phase transition as function of *s*, number of methylene groups in covalent spacer of 12-*s*-12 gemini.

3.2. Thermal Phase Behavior. The thermal behavior of the compounds was further characterized by combining the DSC data with microscopy observations of the textures under plane-polarized light, in order to attempt an assignment of the different phases present. In Fig. 4, M1, M2 and M3 indicate different mesophases whose features will be further described below, and SmA and SmC indicate smectic A and smectic B liquid-crystalline phases. Cr denotes crystalline phases and I, the isotropic liquid phase. Before the onset of decomposition,

only compounds for *s* = 8, 10 and 12 form an isotropic liquid phase, whereas all others form some type of mesophase without attainment of isotropization.

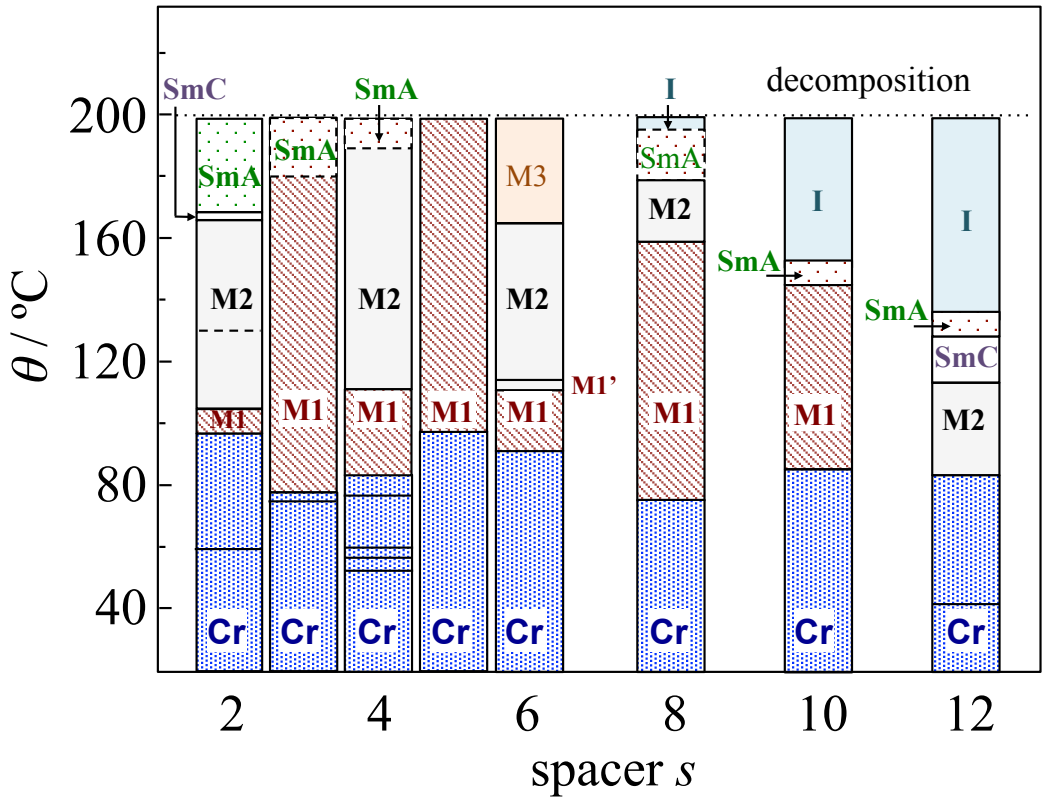

Figure 4. Thermal phase behavior of 12-*s*-12 gemini compounds. Notations are: Cr, crystalline solid phase region; M1, mesophase 1; M2, mesophase 2; M3, mesophase 3; SmA, smectic A liquid crystalline phase; SmB, smectic C liquid crystalline phase; I isotropic liquid phase.

Starting from 20ºC to up to the transition temperature to phase M1, all the 12-*s*-12 compounds exhibit a region of crystalline solid phases (region Cr), which show as birefringent crystallites under the microscope. 12-2-12 and 12-4-12 show transitions between different crystalline phases. When the temperature goes over the main peak into M1, partial loss of birefringence occurs in general, particularly evident up to *s* = 6. The M1 phase is characterized by being a solid-like phase that upon applied shear on the slide-cover slip preparation develops an incipient, low-birefringence marble-like texture. When obtained under cooling, for 12-8-12 and 12-10-12 this phase appears with a better-defined texture with cotton-like domains. Furthermore, for s = 3 and 5, mesophase M1 has a wide thermal stability range and in the case of 12-5-12 it is the only mesophase formed prior to decomposition.

The next mesophase, M2, which occurs for s = 2, 4, 6, 8 and 12 is more birefringent and more fluid (that is, more viscous rather than elastic) than the previous one. This mesophase occurs for s = 8 and 10 with a distinctive tree-branched texture on cooling from the isotropic liquid. For the longest spacer, 12-12-12, an important difference to other compounds is that M2 is the first mesophase to form above the Cr, and no M1 is present.

Above M2, the type of mesophases that forms depends on spacer length. For 12-2-12 and 12-12-12, there is a similar pattern: a SmC liquid crystal appears, with characteristic Schlieren textures, followed by a SmA liquid crystal, appearing either as characteristic "oily streaks" or fan-shaped domains with focal conics, followed by I. For 12-4-12, SmC is absent and there is a direct M2→SmA transition very close to 20 ºC (no peak was detected by DSC). For compound 12-6-12, there is a M2→M3 transition, where the latter shows as an incipient mosaic texture, not fluid-like, appearing not to be SmC or SmA, but instead a still fairly ordered mesophase. For 12-8-12, there is an M2→SmA→I sequence, while 12-10-12 shows an M1→SmA→I sequence.

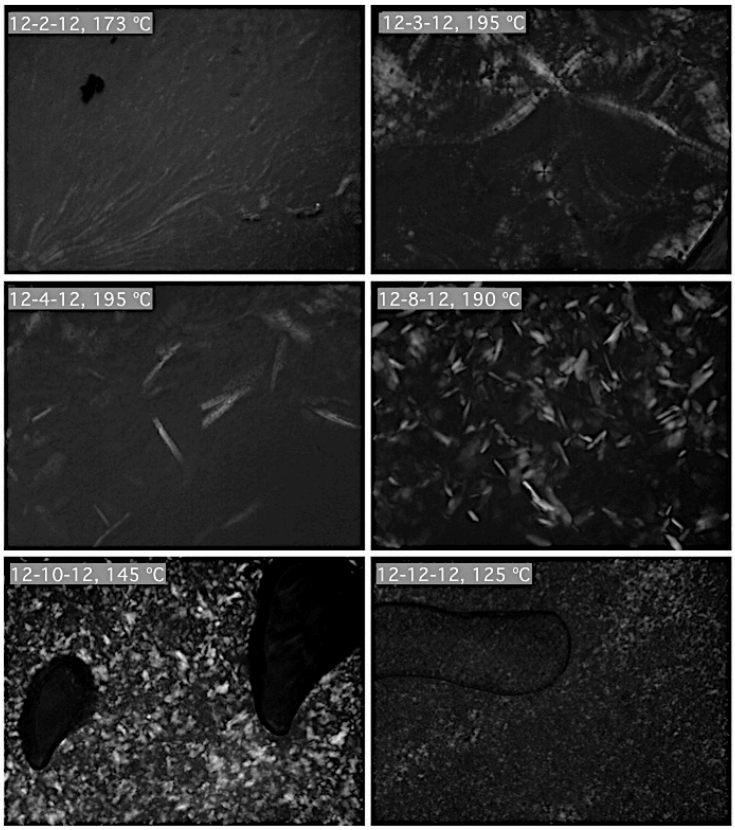

Figure 5. Different textures for the SmA liquid crystal of 12-*s*-12 compounds: *s* = 2, oily streak; *s* = 3, oily streaks and focal conics; *s* = 4, narrow flake; *s*=8, feather-like flake; *s* = 10, mosaics; and *s* = 12, mosaics.

The textures observed for the SmA phase depend on the spacer of gemini surfactants, as shown in Fig. 5: 12-2-12, oily streaks and fan-shape textures; 12-3-12, oily streaks and focal conics; 12-4-12, narrow flakes; 12-8-12, feather-like flakes; 12-10-12, mosaics and fan-shapes; and 12-12-12, mosaics. On cooling the liquid of *s*=2, 8, 10, and 12 compounds, hysteresis effects for the I-LC transition appears. The textures show fan-shapes for 12-2-12, feather-like fan-shapes for 12-8-12, fan-shapes and striated fan-shapes for 12-10-12, and battonets for 12-12-12 (Fig. 6), different from the SmA equilibrium textures on heating. While lowering the temperature until solid appearance, the high-temperature texture is often retained, although the annealing will in most cases eventually lead to phase transformation into M1 or a Cr phase. Small visual changes mark, sometimes, a phase transition between a smectic phase and M1, such as the change from fan-shapes to striated fan-shapes for 12-10-12 (Fig. 6).

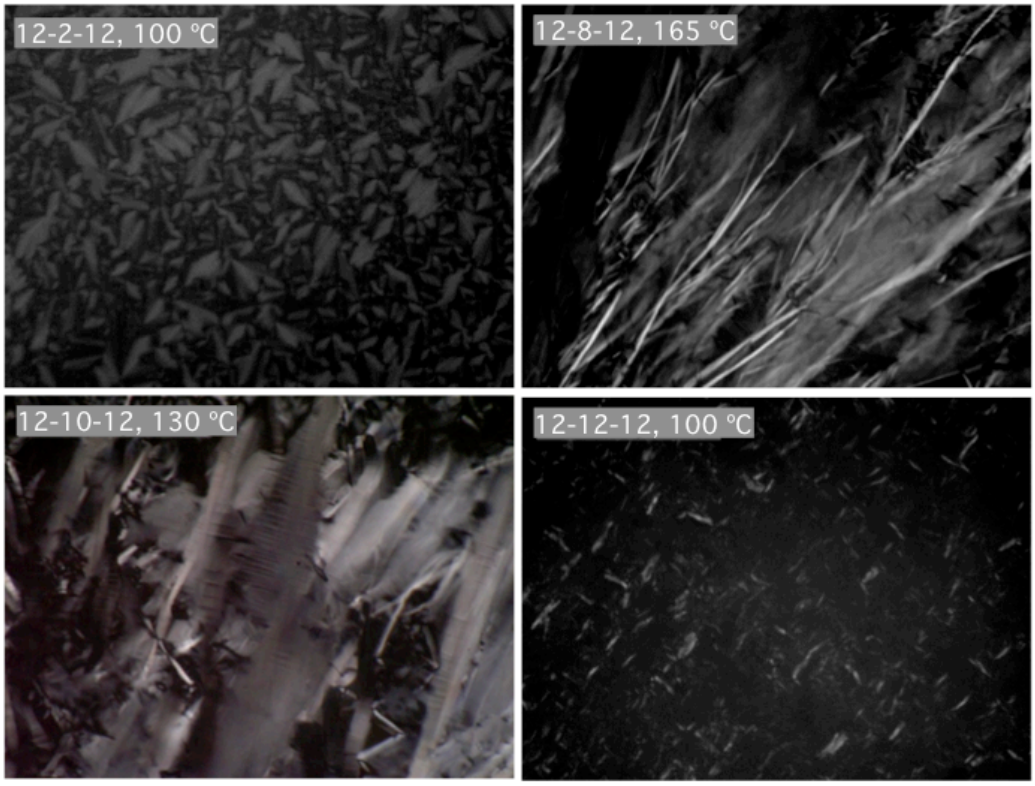

Figure 6. Birefringent textures observed for 12-*s*-12 compounds upon cooling the isotropic liquid: *s* = 2, fan shapes; *s* = 8, feather-like fan shapes; *s* = 10, striated fan-shapes; *s* = 12, battonets.

3.3 X-ray diffraction study of solid state. Structural information for the solid state at room temperature of all the gemini surfactants was obtained from the powder X-ray patterns. Fig. 7 shows some illustrative patterns for a short, middle and long spacer, in this case 12-2-12, 12-6-12 and 12-12-12. Bragg reflection peaks were observed in a q sequence of 1:2:3:4… corresponding to a smectic layering of the molecules. From the (00l) reflections, we could determine the interplanar distances, d_{00l}, and they are plotted vs. spacer length in Fig. 8.

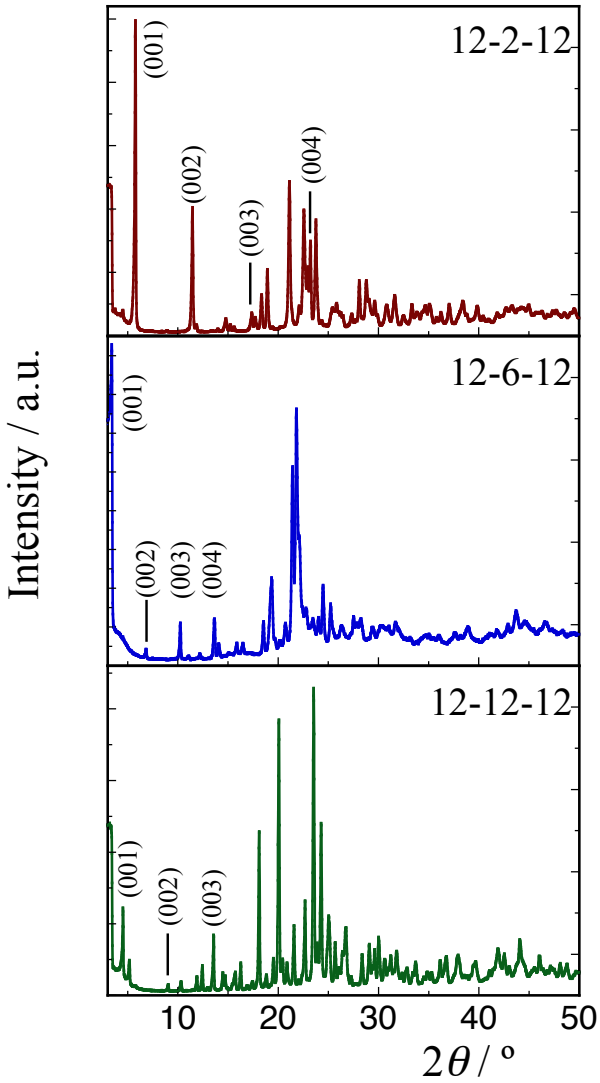

Figure 7. Illustrative X-ray diffraction patterns of gemini surfactants, 12-2-12, 12-6-12 and 12-12-12, showing some of the (00l) peaks from which interplanar distances were calculated.

Clearly, there is a non-monotonic trend of *d*-spacing with spacer length, which is qualitatively in line with our main observations so far, namely with the trends in Fig. 4 and also to some extent with the thermodynamic data in Fig. 3. Thus, the *d*-spacing has a jump from s = 2 to s = 3-6, increasingly only marginally in this region, and then drops for s = 8, remaining essentially constant in the range s = 8-12. If we take into consideration the length of a dodecyl chain (1.67 nm) and the ionic radii of a bromide ion (0.11 nm), an arrangement of bilayers (tail to tail positioning) with tails perpendicular to the headgroup plane and without interdigitation, then we would obtain a *d*-spacing of the order of 3.5 nm.[38] This is a much higher value than any of those shown in Fig. 8 and hence such a structure is ruled out. In fact, several authors have proposed on the basis of XRD data that *n*-2-*n* bis-quat gemini in the crystalline lattice have their alkyl tails in a trans conformation with respect to the spacer plane.[38,47,48] Jurasin et al have also proposed that the tails interdigitate and pack with a tilt angle with respect to the bromide ions planes.[38] It seems obvious from Fig. 8 that there are significant differences in packing according to spacer, and we do not expect the crystal unit cell of 12-2-12 to be reproduced for the following spacers, because no regularity in the smectic periodicities is observed. We return to this point, in more detail, in the next section.

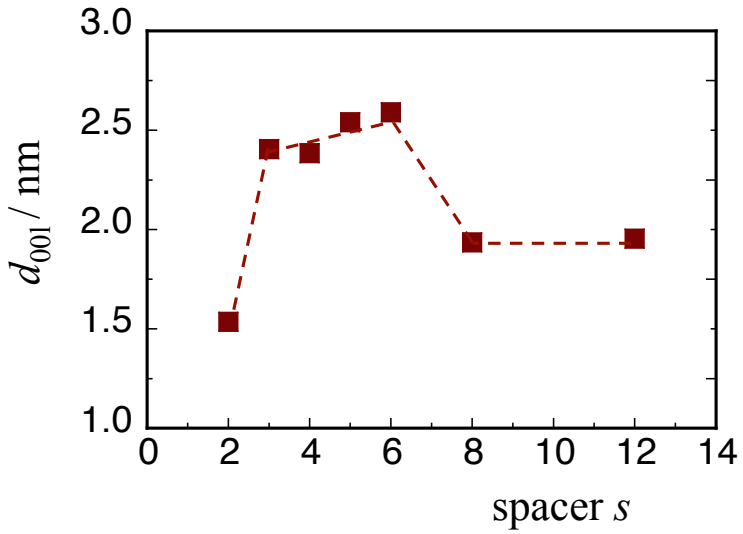

Figure 8. Smectic repeat (interlayer) distance, d00l, as a function of the number of carbons in the spacer alkyl chain.

3.4 Molecular structure, packing and phase behavior trends. We have thus far shown that 12-*s*-12 molecules exhibit smectic liquid crystalline structures. These structures are among the most frequently found TLCs for amphiphiles.[9,49,50] Figure 9 shows possible smectic arrangements for the gemini molecules that will be discussed below. In general, smectic LC structures consist of bilayers either parallel, like those in A1, or tilted with an angle (α) with respect to layer normal (**n)**, like in A2, depending on the possible mismatches between the cross section areas of the hydrophilic headgroups and the hydrophobic chains. In the case of highly interdigitated tail arrangements, A3 and A4, the layers are best described as monolayers. Naturally, intermediate arrangements between A1-A2 and between A3-A4 may exist. Regarding disordered smectic phases, the tails may also be parallel (SmA) or tilted (SmC) with respect to the normal. If the headgroups arrange into some positional ordering within the bilayer plane, in ordered smectic phases, the structures are referred to SmB if the chains are perpendicular to the headgroup plane, SmI if the chains are tilted to the apex of the in-plane hexagon, and SmF if the chains have a tilt to their side.[49] I

In the case of gemini amphiphiles, as pointed out above, the results for the *d*-spacings of the gemini series (Fig. 8) clearly indicate that none of the smectic arrangements from $s = 2$ to $s = 12$ consists of bilayers of cis conformers of the type in A1, which would require $d_{001} \sim$ 3.5 nm. For spacer 2, we found $d_{001} = 1.54$ nm, in good agreement with that reported by Jurasin et al.[38] On the basis of XRD data and geometric considerations, these authors proposed an arrangement of type B4 for 12-2-12, which consists of tilted and interdigitated chains in trans conformation; this seems plausible and would require $\alpha \sim 19^{\circ}$. Analyzing now spacers 3-6, one observes that they have similar *d* values, in the range of 2.4-2.6 nm, and that *d* decreases slightly with increasing *s*, which suggests a common type of packing. Arrangements A3-A4 and B1 are ruled out because the *d* is not compatible, while A2 would imply *d* independent of *s*. We therefore propose that arrangement B2 is the most likely because it is both consistent with the *d* values observed and the *d* dependence on *s*. This arrangement implies tilt angles of the order of 60º. We note that such large values of tilt angles (> 50º) in smectic LC layers, tough not very common, have been previously reported in the literature.[51-55]

As concerning spacers 8-12, taking into account the similarity of their *d* values, as well as the similarity in their thermal behavior with 12-2-12, an arrangement of trans tails with interdigitation as in type B4 seems highly plausible. Since for this sub-set of compounds,

d remains essentially constant, that is compatible with a decreasing tilt angle with increasing s (from $\alpha = 20^{\circ}$ for s = 8 to $\alpha = 13^{\circ}$ for *s* = 12).

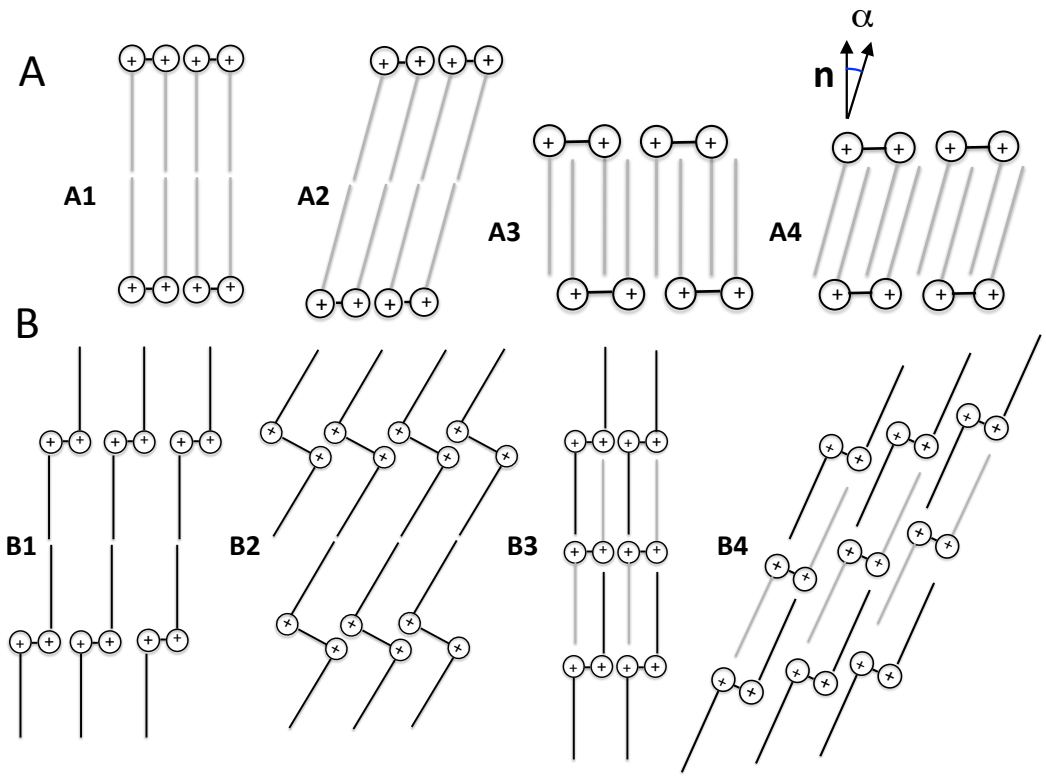

Figure 9. Possible packing configurations for the smectic layers in the 12-s-12 gemini, based on a cis (A) or trans (B) tail conformations. For A arrangements: A1, upright tails with no interdigitation (tail-to-tail); A2; tilted tails with no interdigitation; A3, upright tails with full interdigitation (tail-to-head); A4, tilted tails with full interdigitation. For B arrangements: B1, upright tails with no interdigitation (tail-to-tail); B2, tilted tails with no interdigitation; B3 upright tails with interdigitation (tail to head); B4, tilted tails with interdigitation (tail-to-head). For simplicity, the bromide counterions are omitted.

Figure 10 represents then a summary of the proposed structures, illustrated with those of 12-2-12, 12-5-12 and 12-12-12. To be noted is that in the case of 12-12-12, as shown in Fig. 10c), the spacer is long enough so that two packings are possible: a lower density (left) and a higher density one (right).

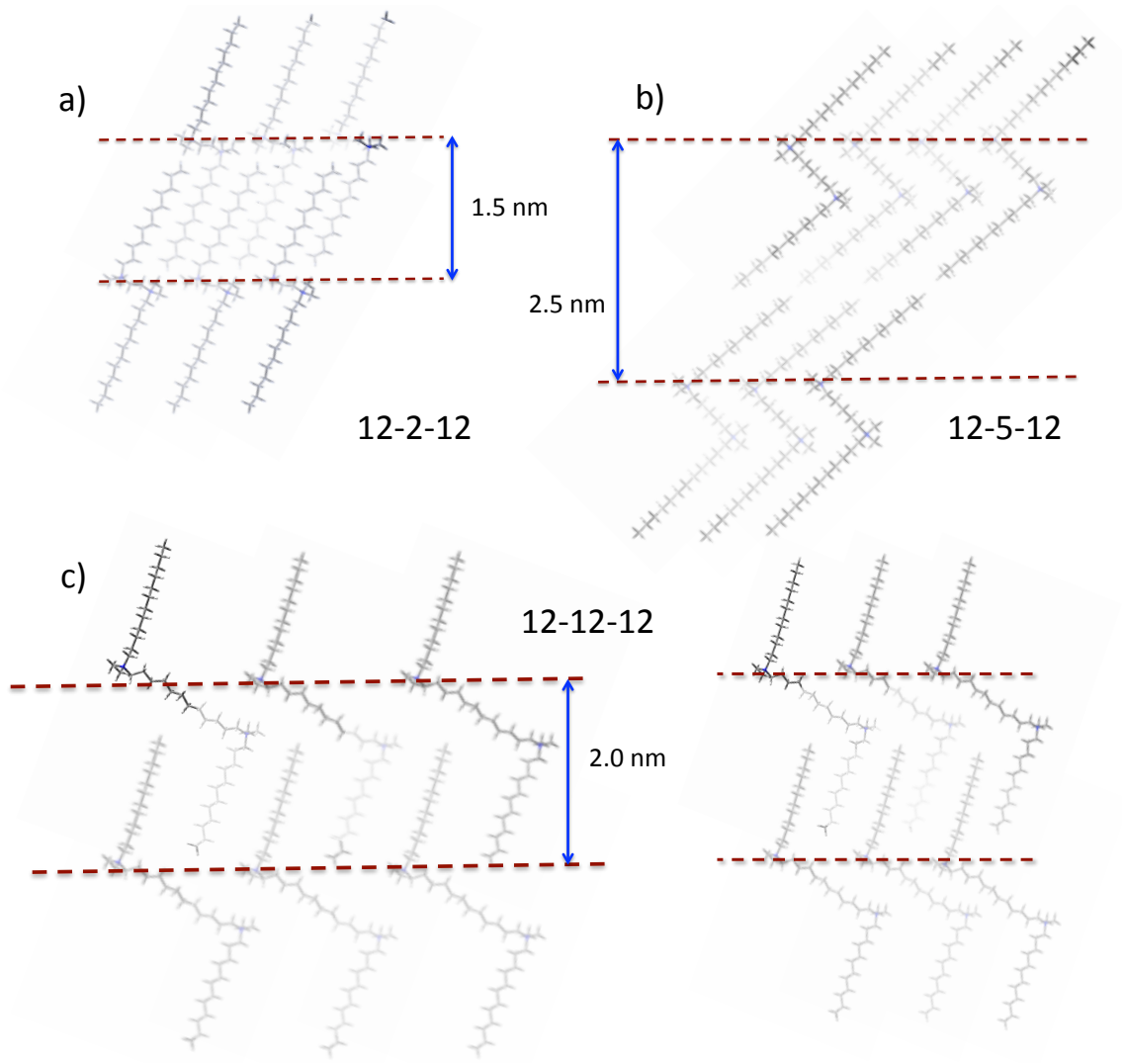

Figure 10. Proposed solid-state arrangements for the different sub-sets of 12-s-12 gemini surfactants: a) 12-2-12; b) 12-5-12 (common to *s* = 3, 4 and 6); c) 12-12-12 (common to *s* = 8 and 10). For simplicity, the bromide counterions are omitted.

If we now go back to Fig. 3, the decreasing trend for the Cr-M1 enthalpy—associated with chain melting—in the range *s* = 2-8 is somewhat unexpected, since longer spacers should in principle imply stronger dispersion forces. One tentative explanation is that for *s* = 3-6, the bilayer arrangement of Fig. 10b) is more resilient to the thermally induced disordered chain conformations (in particular with respect to the spacer) and hence only partial chain melting occurs. This wouldexplain why spacers 4, 5 and 6 show ordered mesophases for a wide temperature range and do not form disordered smectic phases (SmC or SmA) prior to decomposition.

Spacer 8 seems to be the critical length for a shift in trend. This spacer seems to be just about long enough to allow for preferred arrangements of the type in Fig. 10c), with dense interdigitation and low tilt angles. For *s* = 8-12, the isotropization temperature decreases with *s*, but the full melting enthalpy (and entropy) increases sharply with *s*. This is an interesting and apparently paradoxical effect. If the arrangement of Fig. 10c) is valid, the extreme lateral (i.e. in plane) and interlayer cohesiveness caused by this type of interdigitation requires high energy to break, hence the high and increasing enthalpy values observed. Once temperature provides enough thermal fluctuations in the chains, the interdigitated structure easily collapses. This could be due to the fact that the long flexible spacer would then have large conformational disorder and thus would more dramatically disturb the crystalline and liquid-crystalline order. The longer the spacer, the more disturbing this conformational disorder effect. Hence, this set of compounds would melt to the liquid phase at significantly lower temperature than the other gemini and the isotropization temperature would decrease with *s*, as indeed observed.

4. Conclusions

In this work, we have shown that an incremental variation of spacer length in 12-*s*-12 gemini amphiphiles causes rather strong and non-monotonic effects on thermal phase behavior and solid-state packing. All the compounds show several phase transitions and formation of mesophases, denoting a gradual and complex melting process. The strongest endothermic peak observed in the DSC thermograms is associated with partial chain melting and formation of some ordered (smectic) phases. SmA and/or SmC phases form for s = 2, 8, 10 and 12 and these compounds are able to fully melt to the liquid phase before decomposition takes place. Strikingly, for the intermediate spacers investigated (3 - 6), this was not observed: these compounds form highly ordered mesophases until decomposition. XRD data for the solid phases agree qualitatively with the trends observed in thermal behavior. Essentially two different types of packing are proposed. Spacer 2 (with d_{001} ~1.5 nm) and the long spacers 8-10 (with d_{001} ~2.0 nm) are thought to pack as trans conformers in tilted monolayers with high interdigitation. In contrast, spacers 3-6 (with d_{001} ~2.5 nm) are proposed to pack as trans conformers in highly tilted bilayers with no interdigitation; this type of arrangement seemingly promotes stronger cohesiveness in the crystalline and mesophase lattices and is more thermally resilient, lying behind the markedly different thermal behavior observed for these intermediate spacers.

Acknowledgements. We kindly acknowledge support from Fundação para a Ciência e Tecnologia (FCT, Portugal) through PEst-C/QUI/UI0081/2013 (CIQ-UP) and the Ph.D. grant SFRH/BD/72612/2010. Thanks are also due to FEDER and FCT/MES through NORTE-07-0124-FEDER-000065. The Swedish Research Council VR is also gratefully acknowledged.

References

(1) Zana, R.; Talmon, Y. Dependence of Aggregate Morphology on Structure of Dimeric Surfactants. *Nature* **1993,** *362*, 228-230.

(2) Zana, R. Gemini (dimeric) surfactants. *Curr. Opin. Colloid In.* **1996,** *1*, 566-571.

(3) Zana, R. Dimeric and oligomeric surfactants. Behavior at interfaces and in aqueous solution: a review. *Adv. Colloid Interfac.* **2002,** *97*, 205-253

(4) Menger, F. M.; Keiper, J. S. Gemini surfactants. *Angew. Chem. Int. Edit.* **2000,** *39*, 1907-1920.

(5) Zana, R. Alkanediyl-alpha,omega-bis(dimethylalkylammonium bromide) surfactants: II. Krafft temperature and melting temperature. *J. Colloid Interf. Sci.* **2002,** *252*, 259-261.

(6) Alami, E.; Levy, H.; Zana, R.; Skoulios, A. Alkanediyl-Alpha,Omega-Bis(Dimethylalkylammonium Bromide) Surfactants .2. Structure of the Lyotropic Mesophases in the Presence of Water. *Langmuir* **1993,** *9*, 940-944.

(7) Fuller, S.; Shinde, N. N.; Tiddy, G. J. T.; Attard, G. S.; Howell, O. Thermotropic and lyotropic mesophase behavior of amphitropic diammonium surfactants. *Langmuir* **1996,** *12*, 1117-1123.

(8) Sikirić, M.; Šmit, I.; Tušek-Božić, L.; Tomašić, V.; Pucić, I.; Primožič, I.; Filipović-Vinceković, N. Effect of the spacer length on the solid phase transitions of dissymmetric gemini surfactants. *Langmuir* **2003,** *19*, 10044-10053.

(9) Corkery, R. W. Metal organic framework (MOF) liquid crystals. 1D, 2D and 3D ionic coordination polymer structures in the thermotropic mesophases of metal soaps, including alkaline earth, transition metal and lanthanide soaps. *Curr. Opin. Colloid Interface Sci.* **2008,** *13*, 288-302.

(10) Masson, P.; Guillon, D. Molecular design of thermotropic ionic side-chain liquid crystalline polymers. *Molecular Crystals and Liquid Crystals* **2001,** *362*, 313-346.

(11) Collings, P. J.; Hird, M. *Introduction to Liquid Crystals - Chemistry and Physics*; 1st ed.; Taylor & Francis: London, 1997.

(12) Almirante, C.; Minoni, G.; Zerbi, G. Mechanism of Solid to Liquid-Like Phase-Transition of Alkyl Chains in Bilayer Systems - an Infrared Spectroscopic Study of [Ch3(Ch2)13nh3]2mncl4 and [Ch3(Ch2)13nh3]2zncl4. *J. Phys. Chem.* **1986,** *90*, 852-859.

(13) Galema, S. A.; Engberts, J.; vanDoren, H. A. Synthesis, purification and liquid-crystalline behaviour of several alkyl 1-thio-D-glycopyranosides. *Carbohyd. Res.* **1997,** *303*, 423-434.

(14) Van Doren, H. A.; Vandergeest, R.; Kellogg, R. M.; Wynberg, H. Synthesis and Liquid-Crystalline Properties of the Normal-Alkyl 1-Thio-Alpha-D-Glucopyranosides, a New Homologous Series of Carbohydrate Mesogens. *Carbohyd. Res.* **1989,** *194*, 71-77.
(15) Mathevet, F.; Masson, P.; Nicoud, J. F.; Skoulios, A. Smectic liquid crystals from supramolecular guanidinium alkylbenzenesulfonates. *Chem-Eur. J.* **2002,** *8*, 2248-2254.
(16) McClure, D. W. Nature of Rotational Phase Transition in Paraffin Crystals. *J. Chem. Phys.* **1968,** *49*, 1830-&.
(17) Strobl, G.; Ewen, B.; Fischer, E. W.; Piesczek, W. Defect Structure and Molecular-Motion in 4 Modifications of Normal-Tritriacontane .1. Study of Defect Structure in Lamellar Interfaces Using Small-Angle X-Ray-Scattering. *J. Chem. Phys.* **1974,** *61*, 5257-5264.
(18) Ewen, B.; Fischer, E. W.; Piesczek, W.; Strobl, G. Defect Structure and Molecular-Motion in 4 Modifications of Normal-Tritriacontane .2. Study of Molecular-Motion Using Infrared Spectroscopy and Wide-Line Nuclear Magnetic-Resonance Measurements. *J. Chem. Phys.* **1974,** *61*, 5265-5272.
(19) Zerbi, G.; Magni, R.; Gussoni, M.; Moritz, K. H.; Bigotto, A.; Dirlikov, S. Molecular Mechanics for Phase-Transition and Melting of Normal-Alkanes - a Spectroscopic Study of Molecular Mobility of Solid Normal-Nonadecane. *J. Chem. Phys.* **1981,** *75*, 3175-3194.
(20) Doucet, J.; Denicolo, I.; Craievich, A. X-Ray Study of the Rotator Phase of the Odd-Numbered Paraffins C17h36, C19h40, and C21h44. *J. Chem. Phys.* **1981,** *75*, 1523-1529.
(21) Jeffrey, G. A.; Wingert, L. M. Carbohydrate Liquid-Crystals. *Liq. Cryst.* **1992,** *12*, 179-202.
(22) Vacatello, M.; Busico, V.; Corradini, P. The Conformation of Hydrocarbon Chains in Disordered Layer Systems. *J. Chem. Phys.* **1983,** *78*, 590-591.
(23) Van der Ploeg, P.; Berendsen, H. J. C. Molecular-Dynamics Simulation of a Bilayer-Membrane. *J. Chem. Phys.* **1982,** *76*, 3271-3276.
(24) Vacatello, M.; Avitabile, G.; Corradini, P.; Tuzi, A. A Computer-Model of Molecular Arrangement in a N-Paraffinic Liquid. *J. Chem. Phys.* **1980,** *73*, 548-552.
(25) Nagle, J. F. Theory of the Main Lipid Bilayer Phase-Transition. *Annu. Rev. Phys. Chem.* **1980,** *31*, 157-195.
(26) Bell, G. M.; Combs, L. L.; Dunne, L. J. Theory of Cooperative Phenomena in Lipid Systems. *Chem. Rev.* **1981,** *81*, 15-48.
(27) Lin, X. K.; Li, W.; Zhang, J.; Sun, H.; Yan, Y.; Wu, L. X. Thermotropic Liquid Crystals of a Non-Mesogenic Group Bearing Surfactant-Encapsulated Polyoxometalate Complexes. *Langmuir* **2010,** *26*, 13201-13209.
(28) Lagerwall, J. P. F.; Scalia, G. A new era for liquid crystal research: Applications of liquid crystals in soft matter nano-, bio- and microtechnology. *Current Applied Physics* **2012,** *12*, 1387-1412.
(29) Chan, C.; Crawford, G.; Gao, Y. M.; Hurt, R.; Jian, K. Q.; Li, H.; Sheldon, B.; Sousa, M.; Yang, N. Liquid crystal engineering of carbon nanofibers and nanotubes. *Carbon* **2005,** *43*, 2431-2440.
(30) Schymura, S.; Kuehnast, M.; Lutz, V.; Jagiella, S.; Dettlaff-Weglikowska, U.; Roth, S.; Giesselmann, F.; Tschierske, C.; Scalia, G.; Lagerwall, J. Towards Efficient Dispersion of

Carbon Nanotubes in Thermotropic Liquid Crystals. *Advanced Functional Materials* **2010,** *20*, 3350-3357.
(31) Scalia, G. Alignment of Carbon Nanotubes in Thermotropic and Lyotropic Liquid Crystals. *Chemphyschem* **2010,** *11*, 333-340.
(32) Zakri, C.; Blanc, C.; Grelet, E.; Zamora-Ledezma, C.; Puech, N.; Anglaret, E.; Poulin, P. Liquid crystals of carbon nanotubes and graphene. *Philosophical Transactions of the Royal Society a-Mathematical Physical and Engineering Sciences* **2013,** *371*.
(33) Ould-Moussa, N.; Blanc, C.; Zamora-Ledezma, C.; Lavrentovich, O. D.; Smalyukh, I. I.; Islam, M. F.; Yodh, A. G.; Maugey, M.; Poulin, P.; Anglaret, E.; Nobili, M. Dispersion and orientation of single-walled carbon nanotubes in a chromonic liquid crystal. *Liquid Crystals* **2013,** *40*, 1628-1635.
(34) Marques, E. F.; Brito, R. O.; Wang, Y. J.; Silva, B. F. B. Thermotropic phase behavior of triple-chained catanionic surfactants with varying headgroup chemistry. *J. Colloid Interf. Sci.* **2006,** *294*, 240-247.
(35) Wang, Y. J.; Marques, E. F. Thermotropic phase behavior of cationic gemini surfactants and their equicharge mixtures with sodium dodecyl sulfate. *J. Phys. Chem. B* **2006,** *110*, 1151-1157.
(36) Wang, Y.; Marques, E. F. Mesophase formation and thermal behavior of catanionic mixtures of gemini surfactants with sodium alkylsulfates. *Journal of Thermal Analysis and Calorimetry* **2010,** *100*, 501-508.
(37) Al-Ali, F.; Brun, A.; Rodrigues, F.; Etemad-Moghadam, G.; Rico-Lattes, I. New catanionic amphiphiles derived from the associative systems (alpha-hydroxyalkyl)-phosphinic or (alpha-hydroxyalkyl)-phosphonic acid/cetyltrimethylammonium hydroxide. Preparation, characterization, and self-organization properties. *Langmuir* **2003,** *19*, 6678-6684.
(38) Jurasin, D.; Pustak, A.; Habus, I.; Smit, I.; Filipovic-Vincekovic, N. Polymorphism and Mesomorphism of Oligomeric Surfactants: Effect of the Degree of Oligomerization. *Langmuir* **2011,** *27*, 14118-14130.
(39) Manet, S.; Karpichev, Y.; Dedovets, D.; Oda, R. Effect of hofmeister and alkylcarboxylate anionic counterions on the krafft temperature and melting temperature of cationic gemini surfactants. *Langmuir* **2013,** *29*, 3518-3526.
(40) Bara, J. E.; Hatakeyama, E. S.; Wiesenauer, B. R.; Zeng, X.; Noble, R. D.; Gin, D. L. Thermotropic liquid crystal behaviour of gemini imidazolium-based ionic amphiphiles. *Liq. Cryst.* **2010,** *37*, 1587-1599.
(41) Wei, Z.; Wei, X.; Sun, D.; Liu, J.; Tang, X. Crystalline structures and mesomorphic properties of gemini diammonium surfactants with a pendant hydroxyl group. *J. Colloid Interf. Sci.* **2011,** *354*, 677-685.
(42) Menger, F. M.; Littau, C. A. Gemini Surfactants - Synthesis and Properties. *J. Am. Chem. Soc.* **1991,** *113*, 1451-1452.
(43) Wang, Y.; Marques, E. F. Non-ideal behavior of mixed micelles of cationic gemini surfactants with varying spacer length and anionic surfactants: A conductimetric study. *Journal of Molecular Liquids* **2008,** *142*, 136-142.
(44) Burrows, H. D.; Tapia, M. J.; Silva, C. L.; Pais, A. A. C. C.; Fonseca, S. M.; Pina, J.; de Melo, J. S.; Wang, Y.; Marques, E. F.; Knaapila, M.; Monkman, A. P.; Garamus, V. M.;

Pradhan, S.; Scherf, U. Interplay of electrostatic and hydrophobic effects with binding of cationic gemini surfactants and a conjugated polyanion: Experimental and molecular modeling studies. *Journal of Physical Chemistry B* **2007,** *111*, 4401-4410.
(45) Sabbah, R.; An, X. W.; Chickos, J. S.; Leitao, M. L. P.; Roux, M. V.; Torres, L. A. Reference materials for calorimetry and differential thermal analysis. *Thermochim. Acta* **1999,** *331*, 93-204.
(46) Morán, M. C.; Pinazo, A.; Clapes, P.; Perez, L.; Infante, M. R.; Pons, R. Investigation of the thermotropic behavior of isomer mixtures of diacyl arginine-based surfactants. Comparison of polarized light microscopy, DSC, and SAXS observations. *J. Phys. Chem. B* **2004,** *108*, 11080-11088.
(47) Hattori, N.; Masuda, H.; Okabayashi, H.; O'Connor, C. J. Crystal structures of bis(quaternaryammonium bromide) surfactants, ethanediyl-1,2-bis(butyldimethylammonium bromide) dihydrate and propanediyl-1,3-bis(butyldimethylammonium bromide). *Journal of Molecular Structure* **1998,** *471*, 13-18.
(48) Berthier, D.; Buffeteau, T.; Leger, J. M.; Oda, R.; Huc, I. From chiral counterions to twisted membranes. *Journal of the American Chemical Society* **2002,** *124*, 13486-13494.
(49) Dierking, I. *Textures of Liquid Crystals*; WILEY-VCH GmbH & Co. KGaA: Weinheim, 2003.
(50) Demus, D.; Richter, L. *Textures of Liquid Crystals*; Verlag Chemie Weinheim, 1978.
(51) Keith, C.; Reddy, R. A.; Hauser, A.; Baumeister, U.; Tschierske, C. Silicon-containing polyphilic bent-core molecules: The importance of nanosegregation for the development of chirality and polar order in liquid crystalline phases formed by achiral molecules. *Journal of the American Chemical Society* **2006,** *128*, 3051-3066.
(52) Mathis, A.; Galin, M.; Galin, J. C.; Heinrich, B.; Bazuin, C. G. Long alkyl chain dimethylammonioalkoxydicyanoethenolates as new zwitterionic thermotropic liquid crystals. *Liquid Crystals* **1999,** *26*, 973-984.
(53) Bardon, S.; Ober, R.; Valignat, M. P.; Vandenbrouck, F.; Cazabat, A. M.; Daillant, J. Organization of cyanobiphenyl liquid crystal molecules in prewetting films spreading on silicon wafers. *Physical Review E* **1999,** *59*, 6808-6818.
(54) Nguyen, H. T.; Destrade, C.; Allouchi, H.; Bideau, J. P.; Cotrait, M.; Guillon, D.; Weber, P.; Malthete, J. Phasmid and biforked mesogens with thiobenzoate end-groups. *Liquid Crystals* **1993,** *15*, 435-449.
(55) Hori, K.; Ohashi, Y. Structures of 2 crystal forms of chiral smectogenic 4'-hexyloxy-4-biphenylyl p-((s)-2-methylbutyl)benzoate. *Liquid Crystals* **1991,** *9*, 383-396.